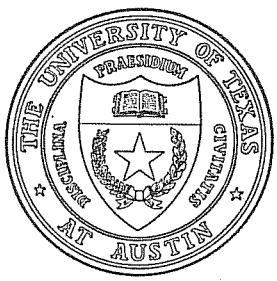

PMFSEL REPORT NO. 82-3
JULY 1982

SHEAR STRENGTH AND DETERIORATION OF SHORT REINFORCED CONCRETE COLUMNS UNDER CYCLIC DEFORMATIONS

By
H. UMEHARA

and
J. O. JIRSA

Report on a Research Project
Sponsored by
National Science Foundation
Directorate for Applied Science and Research Applications
Division of Problem-Focused Research Applications
Grant No. PFR-7720816

DEPARTMENT OF CIVIL ENGINEERING / Phil M. Ferguson Structural Engineering Laboratory
THE UNIVERSITY OF TEXAS AT AUSTIN

SHEAR STRENGTH AND DETERIORATION OF SHORT REINFORCED CONCRETE COLUMNS UNDER CYCLIC DEFORMATIONS

by

H. Umehara

and

J. O. Jirsa

Report on a Research Project

Sponsored by

National Science Foundation

Directorate for Applied Science and Research Applications

Division of Problem-Focused Research Applications

Grant No. PFR-7720816

Phil M. Ferguson Structural Engineering Laboratory
The University of Texas at Austin

July 1982

Any opinions, findings, conclusions, or recommendations expressed in this publication are those of the authors and do not necessarily reflect the views of the National Science Foundation.

A C K N O W L E D G M E N T S

The development of the bidirectional loading facility and the initial testing of short columns were supported by the Division of the Advanced Environmental Research. Funding for a comprehensive test program on columns failing in shear was received (Grant No. PFR-7720816) from the National Science Foundation's Directorate for Applied Science and Research Applications, Division of Problem-Focused Research. The grant provided funding for extensive experimental work, data reduction, and evaluation aimed towards development of design recommendations for frame structures subjected to bidirectional deformations.

The project staff was guided by an Advisory Panel consisting of the following:

Professor V. V. Bertero, University of California, Berkeley
Dr. W. G. Corley, Portland Cement Association, Skokie, Illinois
Mr. James Lefter, Veterans Administration, Washington, D.C.
Mr. C. W. Pinkham, S. B. Barnes & Associates, Los Angeles California
Mr. Loring A. Wyllie, Jr., H. J. Degenkolb Associates, San Francisco, California

The assistance of the Advisory Panel and the National Science Foundation Program Manager, Dr. John B. Scalzi, is gratefully acknowledged.

The project was conducted at the Phil M. Ferguson Structural Engineering Laboratory at the Balcones Research Center of The University of Texas at Austin. The experimental program was aided immeasurably by research assistants K. Maruyama, H. Ramirez, K. Woodward, M. Moore, W. Little, J. Reeder, and J. Ramirez. The assistance of the laboratory staff, G. Moden, R. Marshall, G. Hinckley, D. Perez, M. DeButts, and L. Golding was instrumental in the success of the project.

A B S T R A C T

Short column failures have been observed following many earthquakes. Short columns can generally be limited to cases where the shear span-to-depth or thickness ratio is less than about 3. There has been research conducted on such members but many variables have not been evaluated systematically.

A series of ten short columns with rectangular sections (9×16 in.) were tested in this study and compared with the results of square columns (12×12 in.). Loading history and level of axial load were the main variables. Columns with square sections were tested under cyclic bidirectional lateral loadings and reported previously by other researchers. Based on the tests, it was concluded that the maximum capacities of columns subjected to diagonal unidirectional loading could be estimated by an interaction line (circle or ellipse) connecting the maximum capacities of the column under unidirectional loading along the principal axis. In addition to strength considerations, short columns must be evaluated in terms of their energy dissipating (hysteretic) characteristics.

An empirical equation for the shear strength of columns was derived using data from continuous beams failing in shear. The equation was calibrated using results of short column tests. The equation is a function of the shear span-to-depth ratio, the concrete strength, the core area of the column and the axial load. The effect of transverse reinforcement was not included because the short column tests indicated that increased amounts of transverse reinforcement had a minimal influence on shear capacity. More than 70 percent of the total shear capacity was contributed by the concrete. To prevent rapid strength degradation, the shear capacity of a column must be greater than the capacity corresponding to the

development of flexural hinges at the ends of the columns. Columns evaluated using existing procedures for shear strength did not always exhibit satisfactory strength and energy dissipating characteristics. An evaluation of columns meeting the proposed shear criteria showed that strength and energy dissipating capacities were maintained under severe reversed loading conditions.

TABLE OF CONTENTS

LIST OF TABLES

L I S T O F F I G U R E S

NOTATION

a	shear span, in.
A_c	area of concrete core, out-to-out of ties, $in.^2$
A_g	gross area of cross section, $in.^2$
A_ℓ	cross-sectional area of the lower stringer, $in.^2$
A_s	area of longitudinal tension reinforcement, $in.^2$
$A_{s\ell}$	total area of longitudinal reinforcement, $in.^2$
A_{st}	area of longitudinal extreme tension reinforcement, $in.^2$
A_u	cross-sectional area of the upper stringer, $in.^2$
A_v	area of transverse reinforcement within a distance s_h, $in.^2$
b	section with perpendicular to direction of applied load, $in.^2$
b''	width of confined core, in.
b_w	web width, in.
d	distance from extreme compression fiber to the centroid of the tension reinforcement, in.
d^*	distance from extreme compression fiber to the centroid of the extreme tension reinforcement, in.
D	diagonal resultant of the concrete compression field
E_s	Young's modulus of longitudinal reinforcement
f_c	effective concrete strength
f'_c	concrete compressive strength (6×12 in. cylinder), psi (28 days strength for design. Strength at age of testing for analysis of data)
f_s	stress of longitudinal reinforcement

f_{su} ultimate tensile strength of longitudinal reinforcement, psi

f_t concrete tensile strength, psi

f_y yield strength of longitudinal reinforcement, psi

$f_{y\ell}$ yield stress of the lower stringer

f_{ys} yield strength of transverse reinforcement, psi

f_{yu} yield stress of the upper stringer

F_ℓ force in the lower stringer

F_u force in the upper stringer

$F_{y\ell}$ yield force of the lower stringer

F_{yu} yield force of the upper stringer

h overall depth of section parallel to direction at applied load, in.

h' distance between internal tension and compression resultants resisting the bending moment: can be approximated by 0.9d, in.

I moment of inertia parallel to direction of applied load, $in.^4$

L length of the column, in.

M bending moment

M_n nominal moment strength

M_u factored moment at section, lbs.-in.

M_P plastic bending moment

M_{P0} plastic bending moment if the plastic shear force $V_P = 0$

n number of element

N applied axial compression, lbs.

P_b axial load capacity at balanced strain conditions

R drift ratio, Δ_m/L

s_h spacing of transverse reinforcement, center-to-center, in.

S force of transverse reinforcement

S_y yield force of transverse reinforcement

V shear force at a section

V_a contribution of axial compression to shear capacity, lbs.

V_c nominal shear strength provided by concrete, lbs.

V_f lateral load capacity based on M_n, lbs.

V_m measured maximum lateral load (resultant for diagonal loading), lbs.

V_n nominal shear strength in ACI Code, $V_c + V_s$, lbs.

V_{nr} nominal shear strength of short columns (V_r adjusted to reflect short column data), lbs.

V_r total shear capacity calculated using regression method, lbs.

V_{rc} shear capacity of the member without web reinforcement and axial load calculated using regression method, lbs.

V_{rs} shear capacity carried by transverse reinforcement calculated using regression method, lbs.

V_{rt} shear capacity of the member without axial load calculated using regression method, lbs.

V_s nominal shear strength provided by transverse reinforcement, lbs.

V_u factored shear force at section, lbs.

V_N maximum shear capacity calculated using Nielsen's approach

V_P plastic shear force

V_{PO} plastic shear force if the plastic bending moment $M_P = 0$

V_z maximum shear capacity calculated using Zsutty's equation

V_{zc} calculated shear capacity on cracking of concrete using Zsutty's equation

α angle of inclination of the concrete compression field

Δ deflection, in.

Δ_m peak deflection; deflection corresponding to maximum load, in.

ϵ_c strain of concrete, in./in.

$\epsilon_{\ell y}$ yield strain of longitudinal reinforcement, in./in.

ϵ_{ty} yield strain of transverse reinforcement, in./in.

ϵ_s strain of longitudinal reinforcement, in./in.

ν web effectiveness factor

ρ^* ratio of longitudinal extreme tension reinforcement A_{st}/bd^* percent

ρ_g ratio of total longitudinal reinforcement, $A_{s\ell}/bd$

ρ_h ratio of vertical shear reinforcement area to gross concrete area of horizontal section A_v/bs_h

ρ_w ratio of longitudinal tension reinforcement, $A_s/b_w d$

σ standard deviation

σ_b axial stress at balanced stress conditions

σ_c concrete stress of the compression field

σ_N concrete stress under axial compression

CHAPTER 1

INTRODUCTION

1.1 Background

In Japan the 1968 Tokachi-oki earthquake, and in the U.S. the 1971 San Fernando earthquake caused significant damage to the reinforced concrete buildings designed according to modern codes and representing state-of-the-art construction techniques.[1,2,3] These earthquakes motivated study of the behavior of structures and members under multidirectional load reversals.[4,5,6,7]

Post-earthquake observations have indicated that severe damage to structures was due to instability of columns under large deformation and shear distress in short columns. Columns failing in a shear mode must be avoided if possible because of their unstable hysteretic behavior with degradation of stiffness and strength under seismic loading. However, short columns often result from the placement of nonstructural walls or other appurtenances which reduce the clear height. Columns of this type, called "captive" columns, which fail in shear have been reported following several earthquakes.[2,8,9,10] Figure 1.1 shows an example of a captive column damaged by earthquake.[2] A short column is defined as a column with clear height-to-depth ratio less than 5 for the purposes of this report.

Although ground accelerations are three-dimensional in nature, the study of members under bidirectional loadings has received little attention. There have been several experimental and analytical studies on the behavior of columns under seismic loading, especially long columns in which the flexural mode of

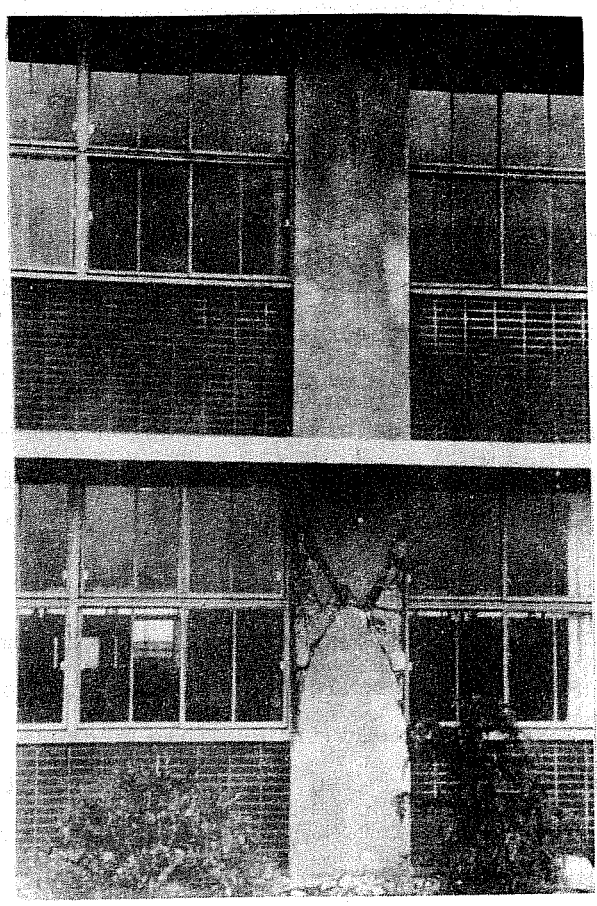

Fig. 1.1 Tokachi-oki earthquake

failure dominated. The use of a "discrete element method"[11] to calculate moment-curvature relationships helped to explain the flexural characteristics of reinforced concrete columns subjected to load reversals in the inelastic range.[12,13] Behavioral models have been developed including one-dimensional bilinear, and trilinear models and models with degrading stiffness. This concept has been extended into two-dimensional models using plastic theory.[14,15] These models appear to correlate well with experimental results of columns subjected to bidirectional bending moments, and whose failure is dominated by flexure.[16,17,18]

On the other hand, very few studies have been conducted on reinforced concrete columns failing in shear. Generally, from empirical studies it is clear that lateral force is transferred by shear and compressive stresses in the concrete, aggregate interlock, dowel action of the longitudinal reinforcement, and transverse reinforcement.[19] However, no effective analytical method has yet been established for treating shear behavior in a manner similar to the moment-curvature concept for flexural behavior.

For short columns, only the Building Research Institute of the Ministry of Construction in Japan has conducted a large and well-organized project concerned with the shear behavior of short reinforced concrete columns under unilateral inelastic load reversals. This project was conducted over a five-year period (1973-1977) and about four-hundred specimens were tested. Many parameters which were considered to influence the behavior of columns were examined.[20,21] However, as mentioned before, ground accelerations are three-dimensional and tests of short columns under bidirectional loadings are needed.

1.2 Outline of Investigation

The current study is part of a large investigation of the shear behavior of reinforced concrete frame elements subjected to

cyclic bidirectional deformations. Studies of short columns and beam-column joints are underway. This report covers short columns only.

The investigation on short columns in The University of Texas at Austin started in 1975 and three series of tests have been previously reported.

The first study was reported by Maruyama.[22] The principal objective was to study the influence of bidirectional lateral deformation histories (shown in Fig. 1.2) on square, symmetric columns without axial load. The conclusion of this study was that previous loading in perpendicular directions did not significantly affect the maximum shear strength of the columns unless the maximum deflection of any previous loading exceeded the deflection at which the maximum shear strength of columns under monotonic loading was reached. Figure 1.3 shows that the maximum shear strength for several different histories was reached at a deflection of about 0.6 in.—the deflection at which the capacity under monotonic loading was reached.

The second study was reported by Ramirez.[23] The principal objective was to study the influence of varying axial load, constant compression, constant tension, and varying compression and tension as shown in Fig. 1.4. The specimen geometry was the same as Maruyama used. The conclusions of this study were:

(1) Constant compressive axial loads ($N = 0.4P_b$) appeared to accelerate shear deterioration as shown in Fig. 1.5.

(2) Constant tension decreased shear deterioration but substantially reduced the shear capacity and stiffness as shown in Fig. 1.6.

(3) The effect of tension alternately with compression was reflected as a reduction in shear and stiffness, but

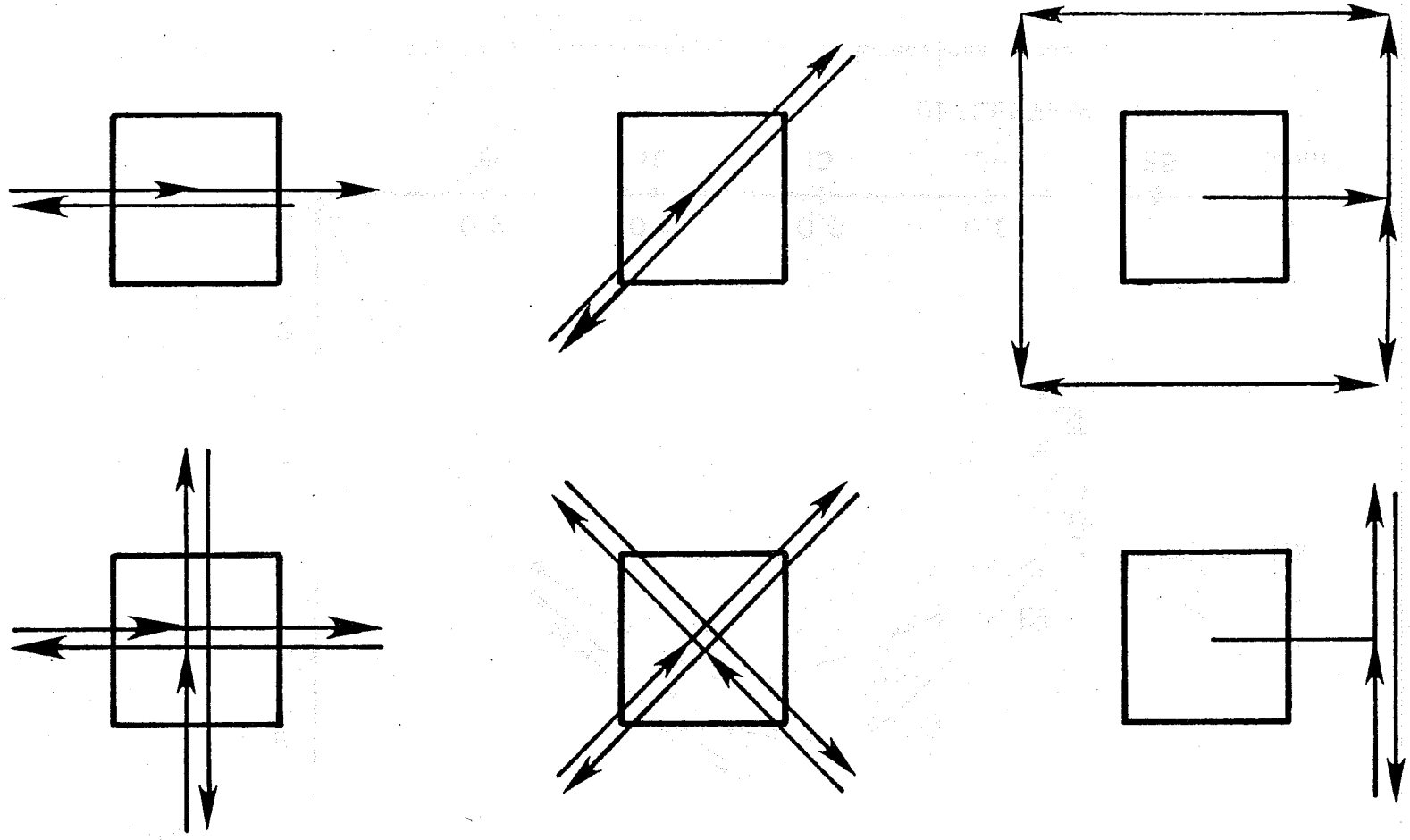

Fig. 1.2 Square columns - lateral loading histories (no axial load)

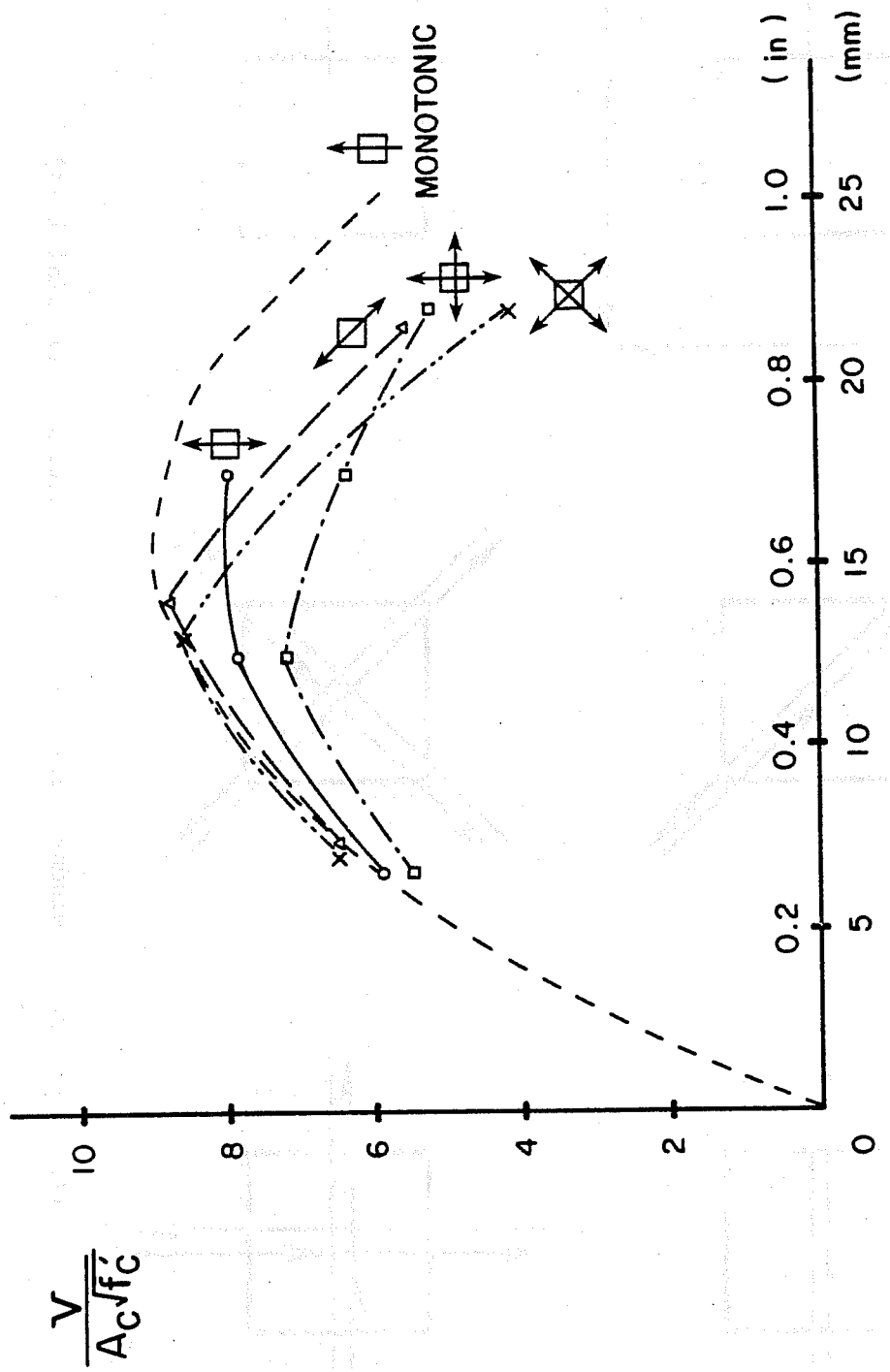

Fig. 1.3 Unidirectional vs. bidirectional loading

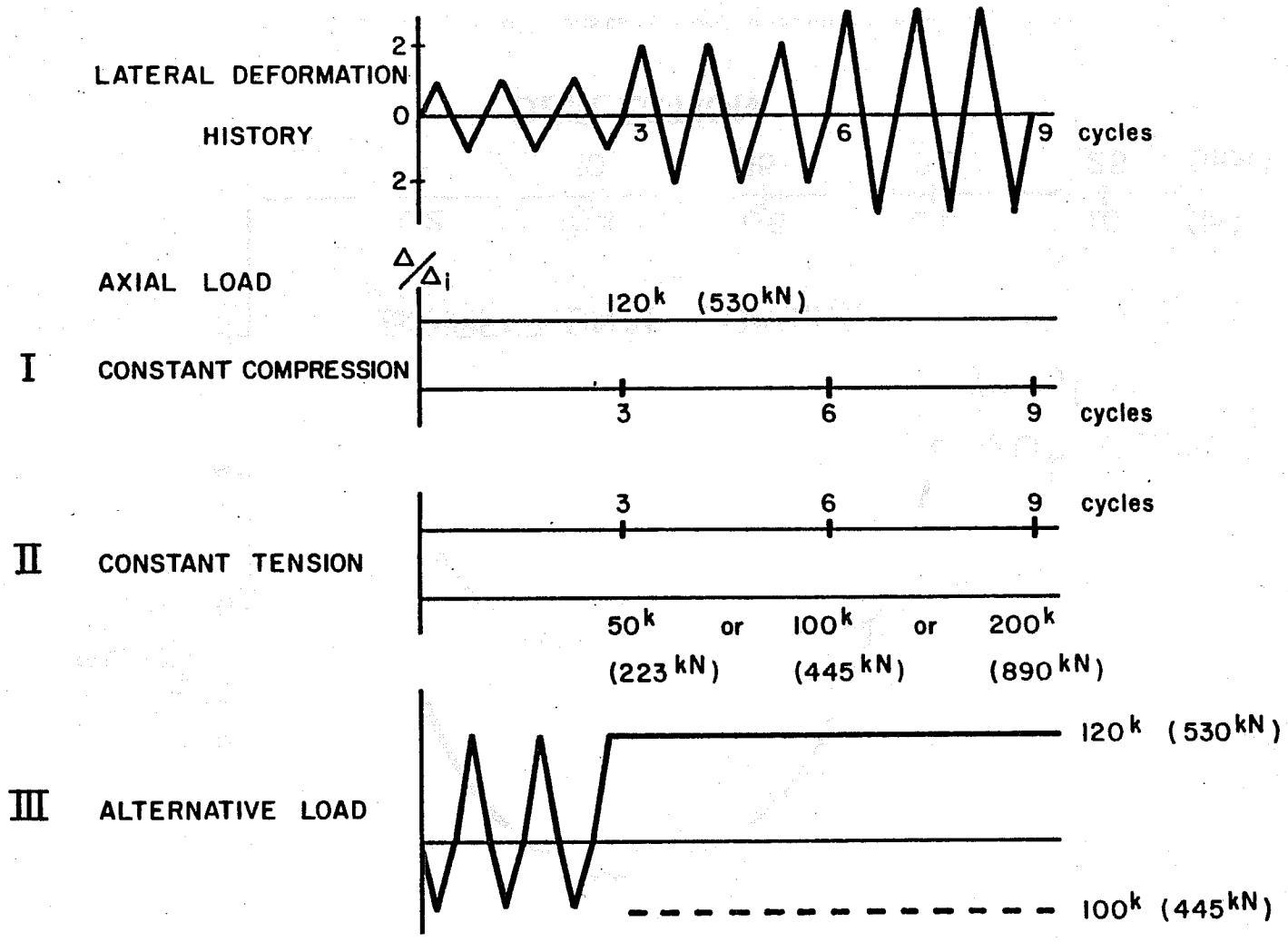

Fig. 1.4 Axial load histories--square columns

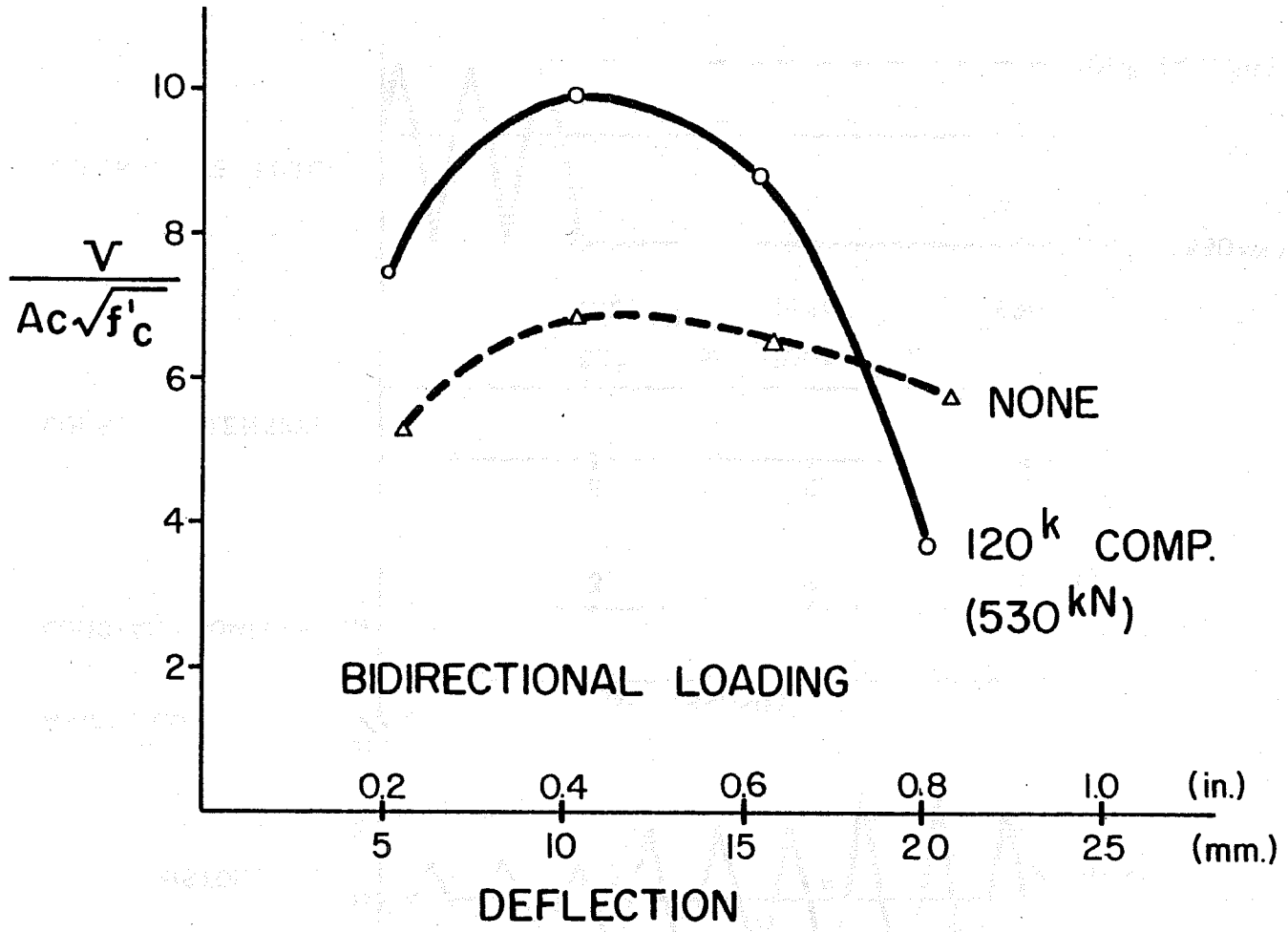

Fig. 1.5 Effect of constant compression — square columns

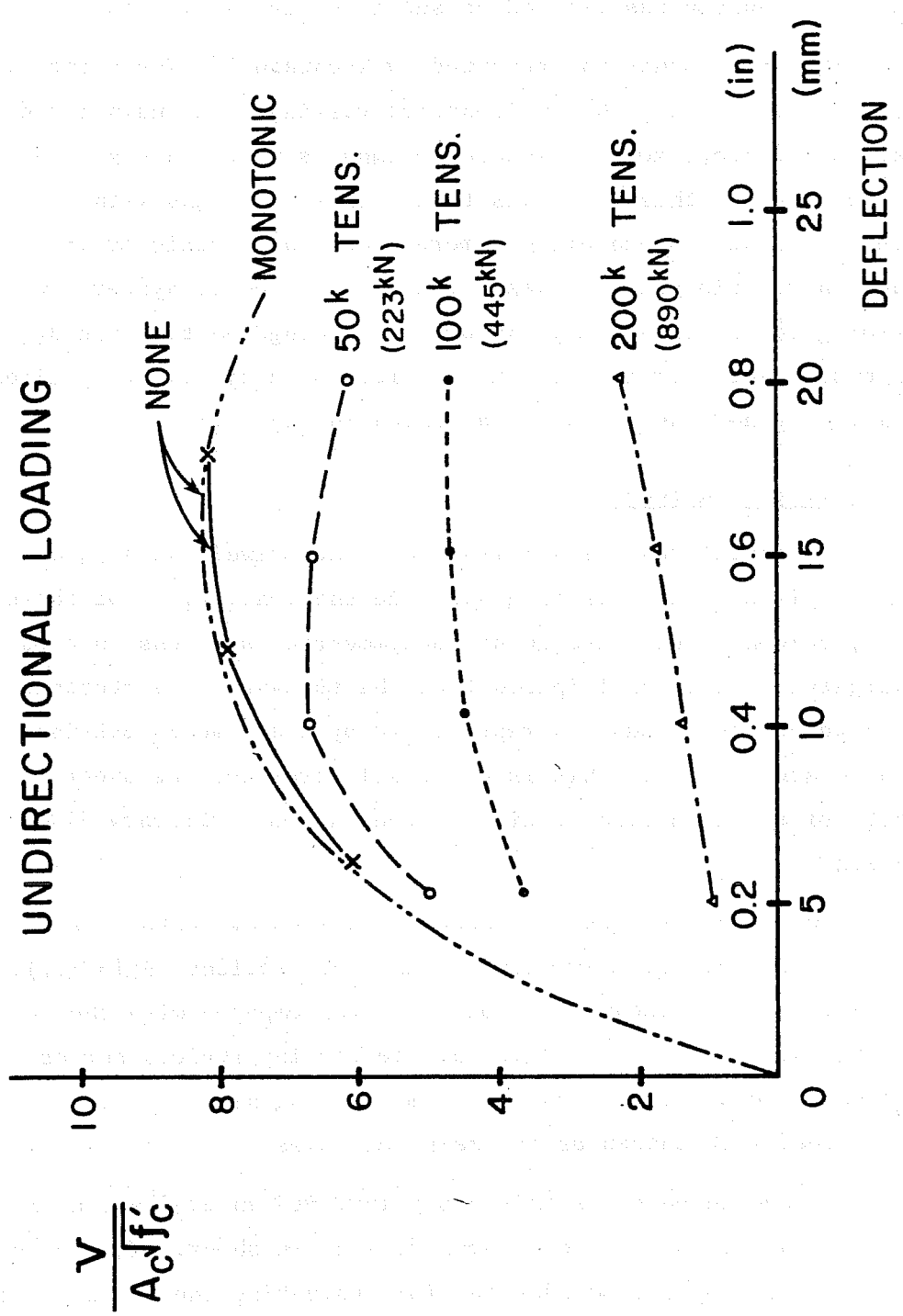

Fig. 1.6 Effect of constant tension - square columns

only during that part of the loading history where tension was imposed as shown in Fig. 1.7.

The third study was reported by Woodward.[24] The principal objective was to study the influence of varying longitudinal and transverse reinforcement in square columns as shown in Fig. 1.8. The conclusion of this study was that although columns with smaller tie spacings exhibited a more stable hysteretic load-deflection relationship, it was difficult to achieve hysteretic behavior governed totally by flexure. Reducing the tie spacing did not substantially improve the lateral capacity of the specimens (low shear span-to-depth ratio) as shown in Fig. 1.9.

1.3 Objective and Scope

All three previous studies dealt exclusively with square column sections. In order to generalize the conclusions of those studies, columns with rectangular (unsymmetric) sections must be investigated. It is anticipated that the behavior of a rectangular section cannot be adequately represented by the results obtained from a square section. This is especially true for the shear capacity of a rectangular section loaded in some arbitrary diagonal direction.

The first phase of this study consisted of tests of a series of ten short columns with rectangular sections (9x16 in.). The results of the rectangular columns were compared with the results of square columns (12x12 in.) tested in previous series. In the rectangular column test program, loading history and level of axial load were chosen as the main variables.

The second phase of this study involved an evaluation of data from tests of beams and columns failing in shear. The objective was to develop recommendations for evaluating the strength of short columns. Based on data from continuous beams with $1 \leq a/d \leq 2.5$ which failed in shear, an equation for shear strength was

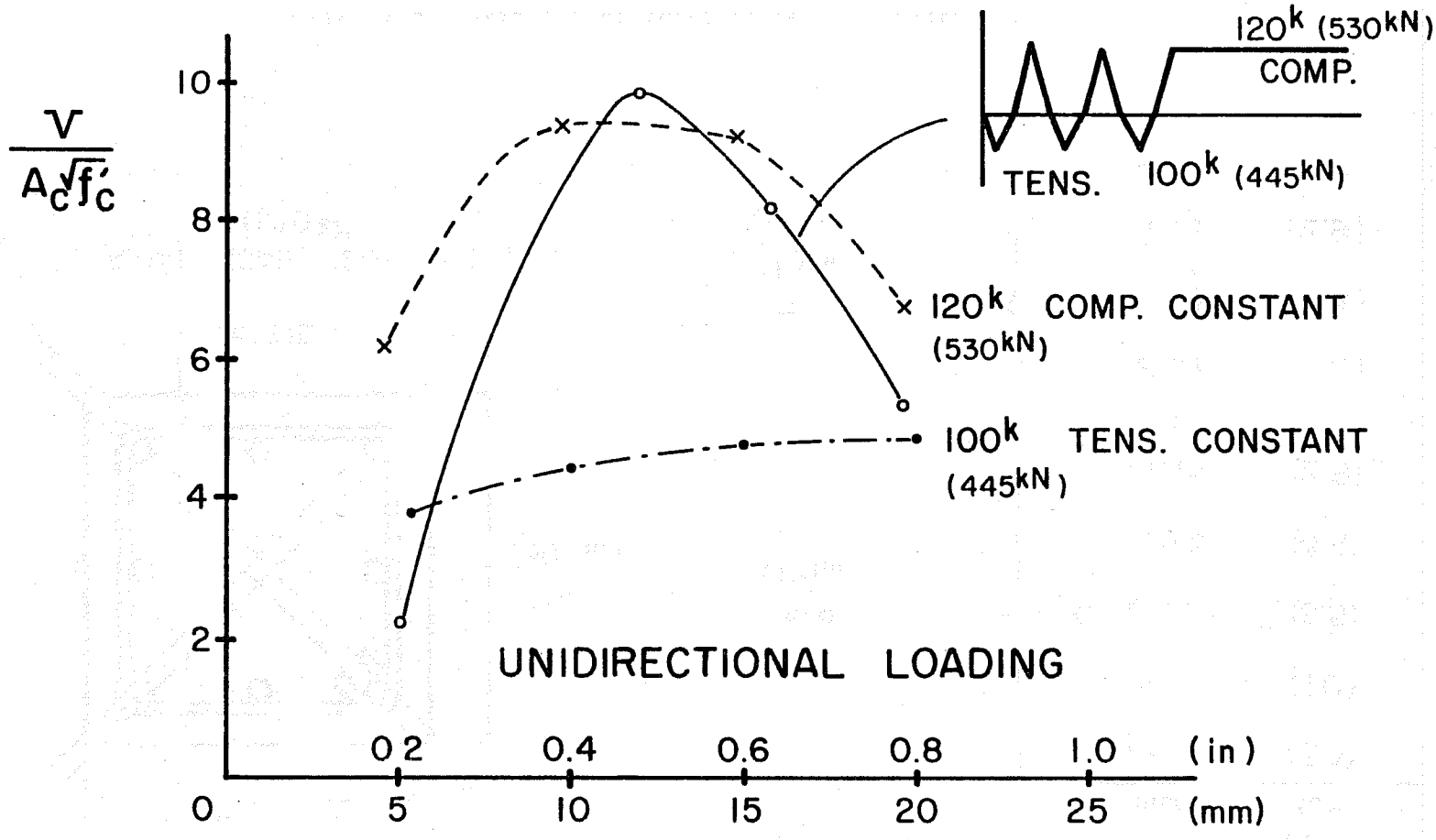

Fig. 1.7 Effect of varying compression and tension - square columns

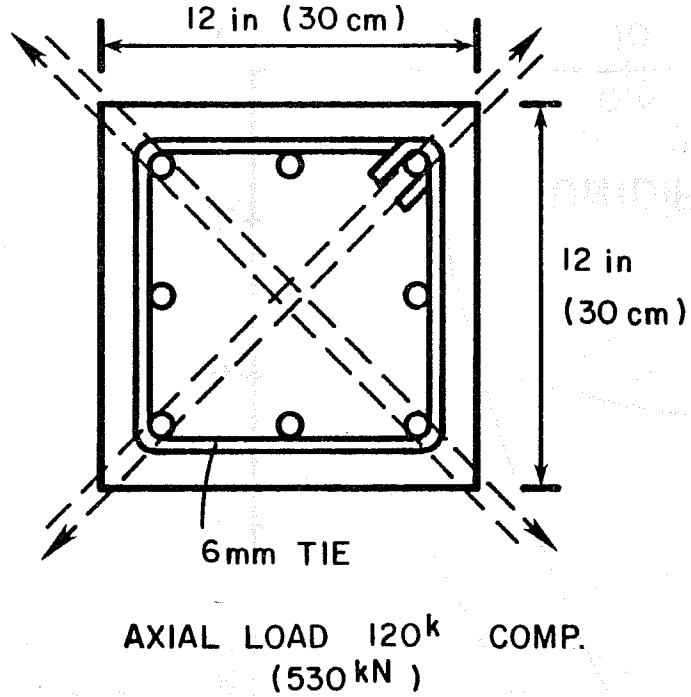

LONGITUDINAL		TRANSVERSE 6mm SPACING	
		inch	(cm)
# 6 (19mm)		12	(30)
		4	(10)
	*	2.57	(6.5)
		1.75	(4.4)
		1.13	(2.9)
# 4 (13mm)		2.57	(6.5)
		1.75	(4.4)
		1.13	(2.9)

Fig. 1.8 Variation of reinforcement - square columns

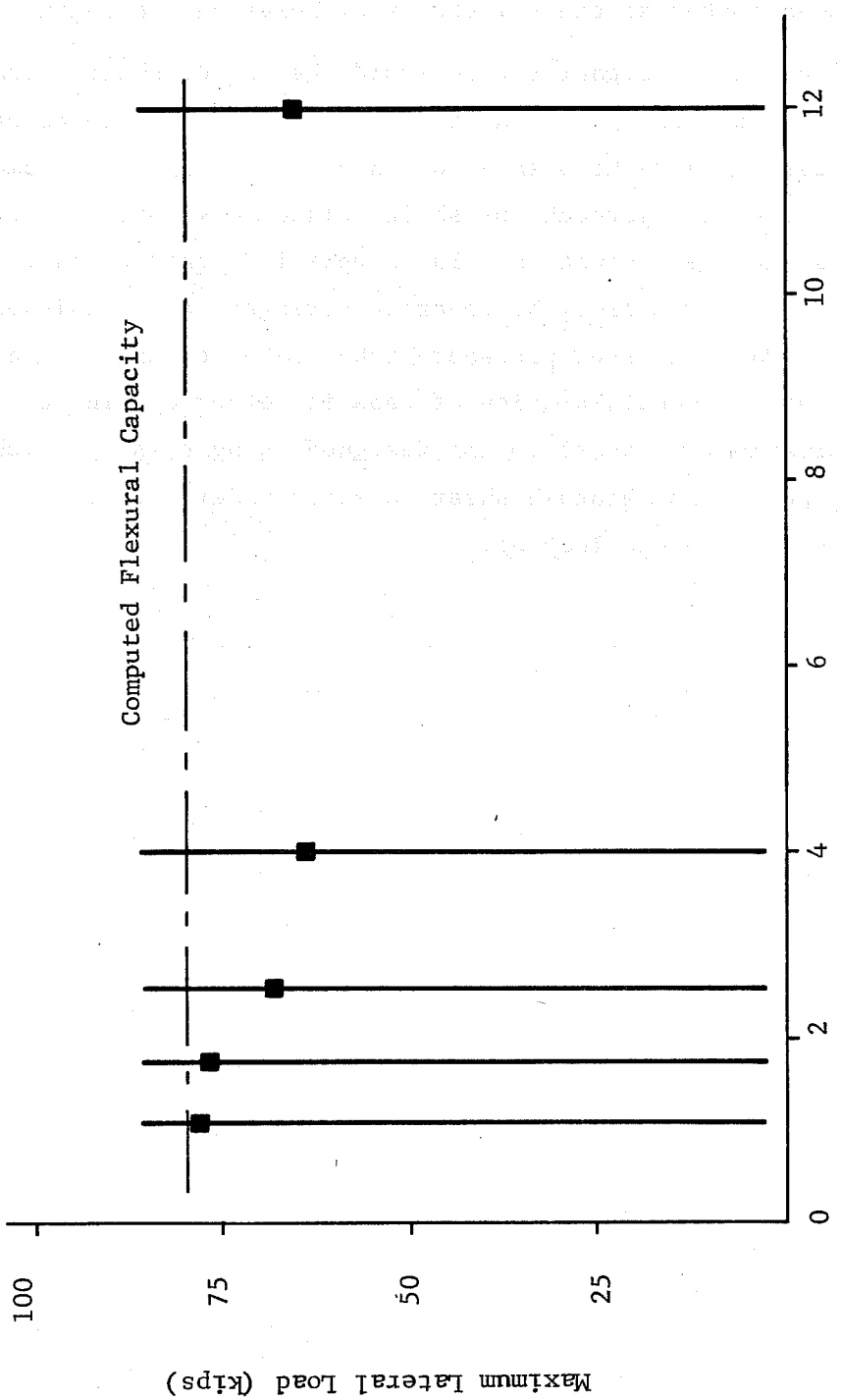

Fig. 1.9 Influence of tie spacing on lateral load capacities - square columns

derived. The equation was used to calculate the shear capacities of short columns tested at the University of Texas and in Japan.

Although a designer should avoid the use of short columns in any structural configuration, there may be cases where no other options exist or where he wishes to evaluate an existing column. Therefore, a design approach for short columns was developed by simplifying the shear equation. The simplified equation is a function of the a/d ratio, the concrete strength, and the level of axial load. The suggested procedure takes into account not only strength, but also deterioration of capacity under cycling to large deformation. A short column designed using this approach would be expected to maintain shear capacity under static or unidirectional reversed loading.

CHAPTER 2

TEST SPECIMEN AND LOADING HISTORY

2.1 Specimen Details

Ten short columns with rectangular cross sections (shown in Fig. 2.1) were tested in this study. The specimens were designed so that the results could be compared with the results of square columns (shown in Fig. 2.2) tested in the previous three investigations by Maruyama,[22] Ramirez,[23] and Woodward.[24] The area (A_g = 144 in^2.) of cross section and the transverse reinforcement ratio (ρ_h = 0.3 percent) were kept almost the same as in the square columns. Ten #6 (19 mm) longitudinal bars were used with the intent being to provide flexural capacity in excess of the shear capacity in both the strong and weak directions of the rectangular column. For calculation of flexural and shear capacities, the 1977 ACI Building Code was used. Details are discussed in Chapter 7.

The cross section of the test specimen was a 2/3-scale model of a prototype column. The prototype column has a 13.5 in. (34 cm) x 24 in. (61 cm) rectangular section with ten #9 (28 mm) longitudinal bars (ρ_g = 0.031) and #3 bars for the transverse reinforcement. Cover in the prototype is 1-1/2 in. (3.8 cm). With the 2/3-scale factor, #6 (19 mm) longitudinal bars were used and cover was reduced to 1 in. (2.5 cm). The column height was reduced to 36 in. (0.9 m). For transverse reinforcement, 6 mm deformed bars were used. The spacing of transverse reinforcement was set at 3.5 in. (8.9 cm) in a 2/3-scale model.

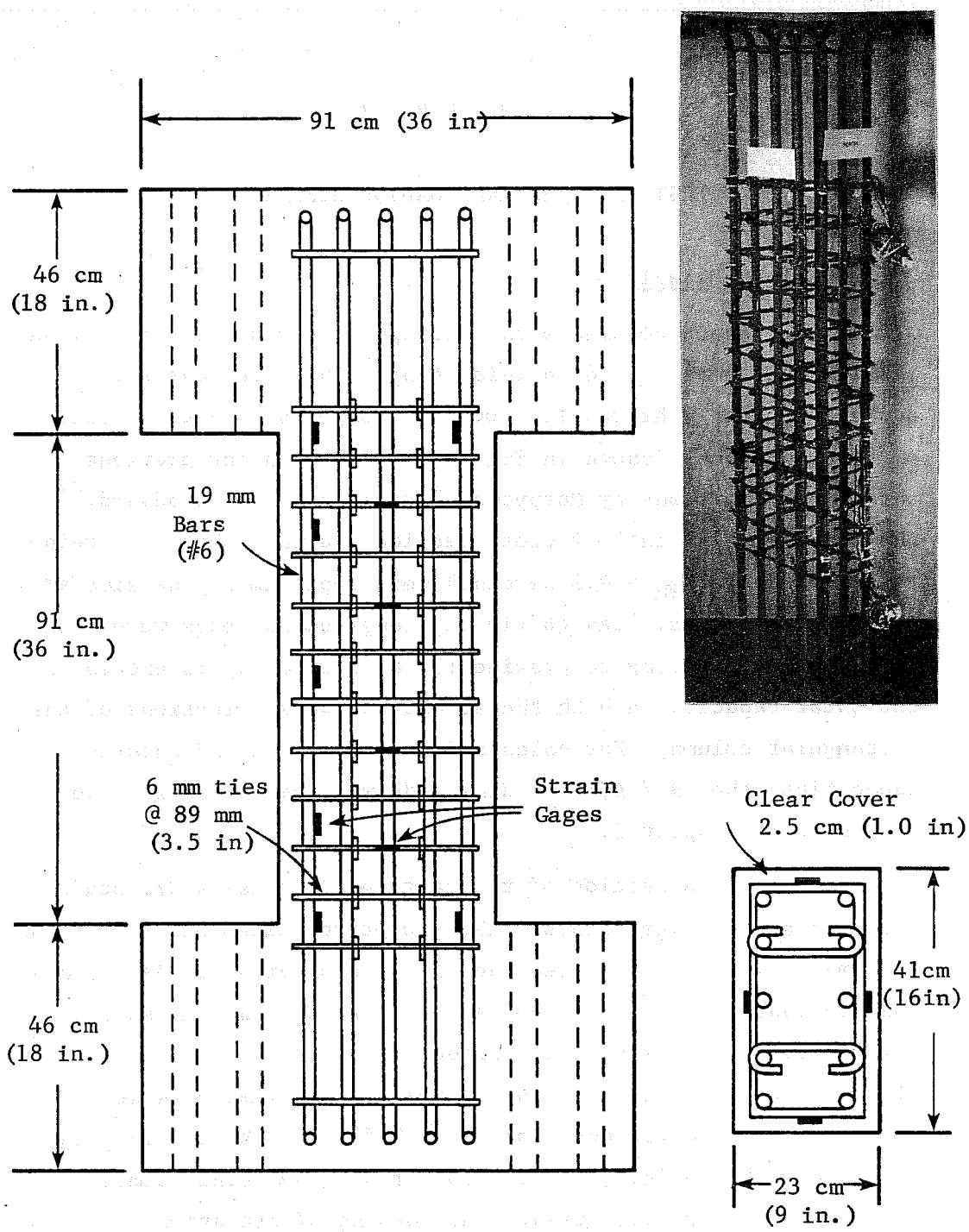

Fig. 2.1 Test specimen

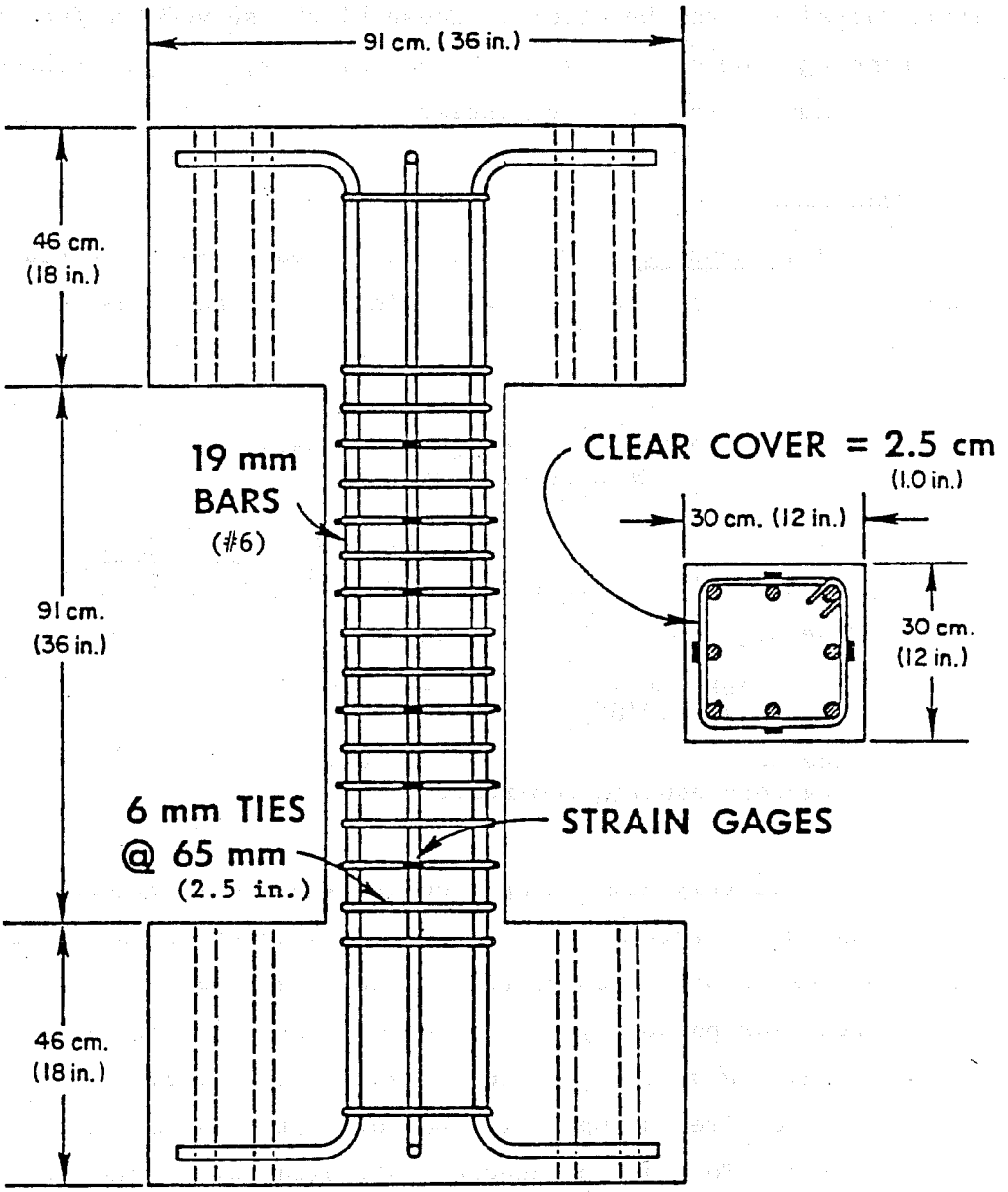

Fig. 2.2 Square column

The column was bounded at each end by large blocks cast monolithically with the column. These blocks served two functions: (1) anchorage for the column longitudinal bars, and (2) attachment of the column to the loading system.

2.2 Materials

2.2.1 Concrete. The concrete for each cast was obtained from the same local readymix plant. The mix proportions were as follows:

Concrete Mix Design (5000 psi)
Proportions for 1 yd^3

Water		220 lb.	w/c = 0.42
Cement	5-1/2 sacks	520 lb.	
Fine aggregate		1500 lb.	
Coarse aggregate (max. size 5/8")		1800 lb.	
Airsene L (water-reducing admixture)		25 oz.	

A relatively high slump concrete was necessary because of congestion of reinforcement in the form and the need to ensure proper placement of the concrete without excessive vibration. The concrete was purposely ordered with a slump less than the desired 7 in. and water was added on site prior to casting to achieve the required slump. Six control cylinders were cast with each specimen. To minimize concrete strength variations, two specimens were cast at a time.

2.2.2 Reinforcement. #6 (19 mm) deformed bars were used for longitudinal reinforcement and 6 mm deformed bars for transverse reinforcement. Samples of the deformed bars were tested to obtain yield stress, ultimate stress and the stress-strain

relationship. Stress-strain curves for the reinforcement are shown in Fig. 2.3. (Instrumentation on 6 mm bars failed at a strain of about 0.005.)

The material properties in each specimen are summarized in Table 2.1.

2.3 Deformation Path and Loading History

The current investigation is the fourth in a series of studies on short columns. Square column sections were used in the previous three investigations. In the first investigation,[22] the effect of deformation path shown in Fig. 1.2 was studied. In the second investigation,[23] the effect of axial load on the hysteretic behavior of the column was studied under unidirectional and bidirectional loading histories. In the third investigation,[24] the effect of longitudinal and transverse reinforcement on the hysteretic behavior of the column was studied, and bidirectional deformation along the diagonals was chosen. In order to make comparisons with the results of the square column tests, the selection of loading history, and level of axial load in the current investigation were limited to cases used in the previous three investigations.

2.3.1 Deformation Path. Deformation paths shown in Fig. 2.4 were chosen. There are seven types of deformation paths which can be divided into two groups. In the first group, deformation paths in Fig. 2.4 (a) to (e), the ultimate shear capacities of rectangular columns under principal and skewed directions were ascertained. In this case, unidirectional loading was used. In the second group, deformation paths in Fig. 2.4 (f) and (g), the influence of previous loading in another direction on the ultimate shear capacity of rectangular columns was studied.

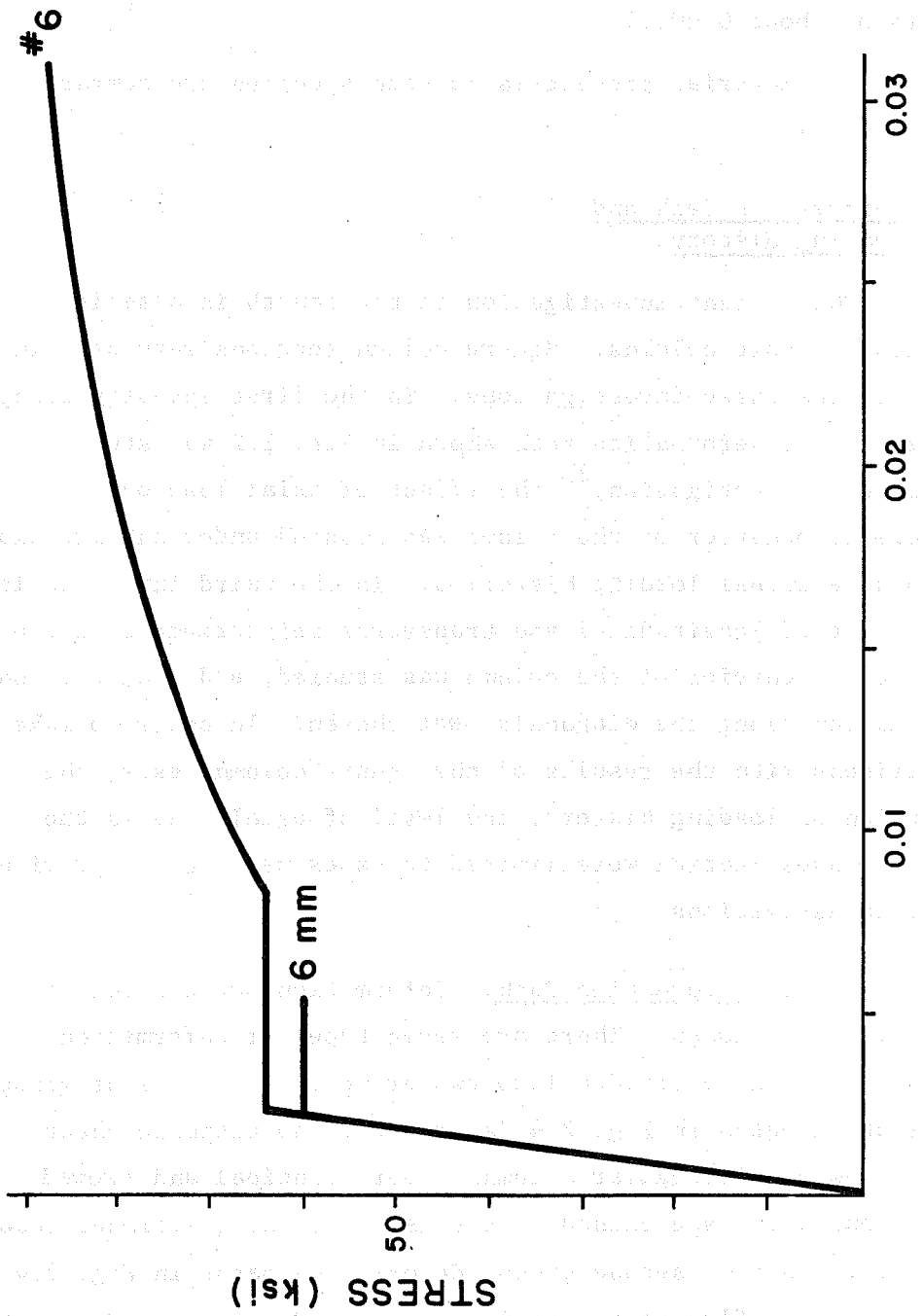

Fig. 2.3 Stress-strain curves for reinforcement

TABLE 2.1 MATERIAL PROPERTIES

REINFORCEMENT

Bar	Nominal Bar Area ($in.^2$)	Yield Stress (ksi)	Ultimate Stress (ksi)
6mm	0.05	60.0	80.0
#6	0.44	64.0	108.0

CONCRETE

Specimen	f'_c (psi)	Age (days)	Slump (in.)
0US	5810	184	5-1/2
0UW	5820	212	5-1/2
CMS	6090	77	8
CUS	5060	55	8
CUW	5060	84	8
2CUS	6090	73	8
CDS30	6180	90	6
CDW30	6120	69	6
CBSW	5090	74	10
CDSW30	5090	81	10

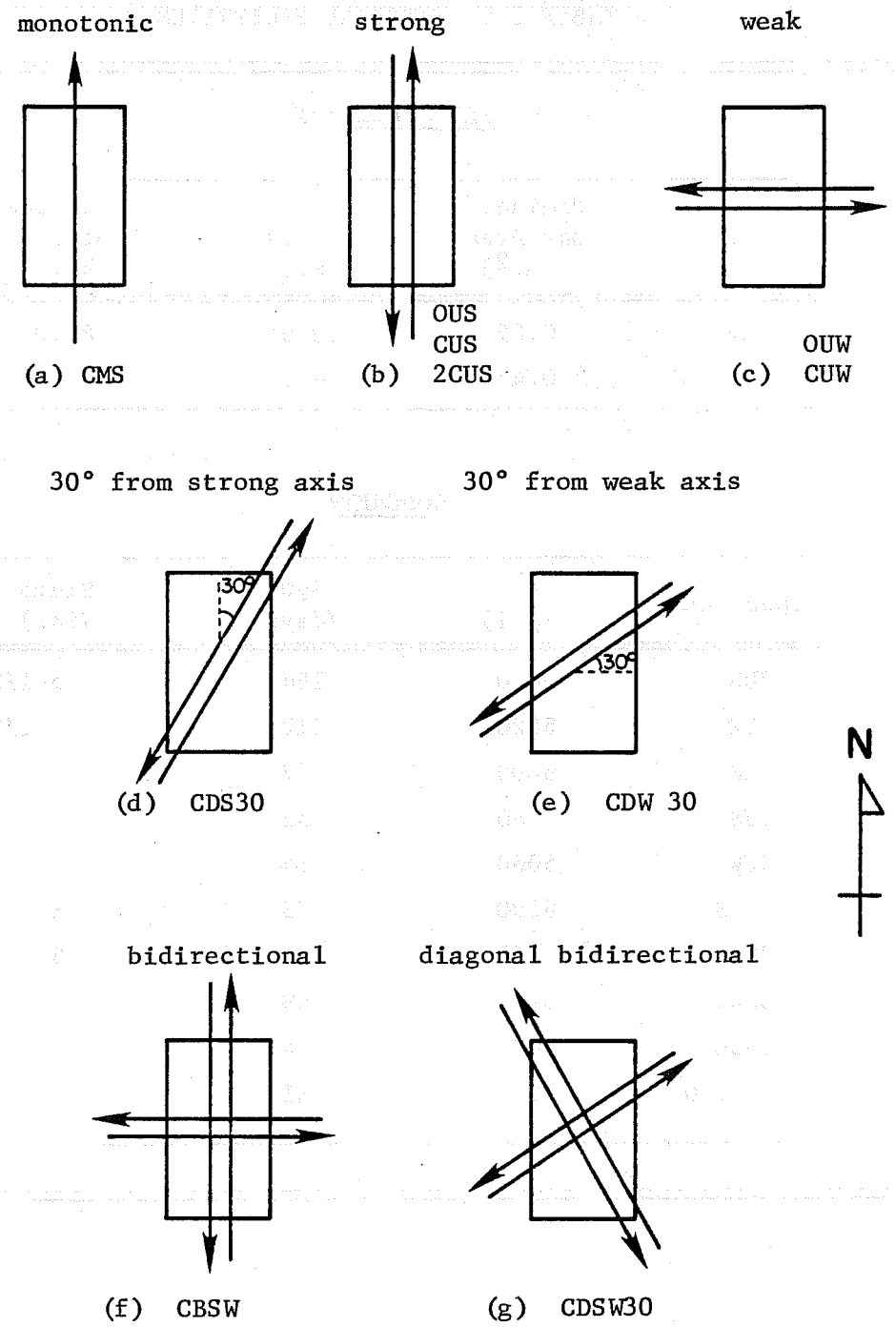

Fig. 2.4 Deformation paths

2.3.2 Loading History. In the previous three investigations, the deformations were cyclically reversed between incrementally increasing deflection limits. Within each deflection limit, the specimen was cycled three times. The first deflection limit (0.2 in.) was set by using observed deflection at the point of yielding in the column longitudinal reinforcement (at the end block-column interface) and the same limit was applied to all square columns. In the current investigation, different deflection limits were set for each loading direction because the section was not symmetric. The first deflection limit was set as the observed deflection at the point where strain reached half of yield in the column longitudinal reinforcement in either direction (strong or weak) of a rectangular column without axial load. Half of yield was selected in case shear failure occurred before the flexural reinforcement started yielding. In the strong direction, 0.2 in. was chosen for the first deflection limit. In the weak direction, 0.16 in. was chosen. Figure 2.5 shows the loading histories in the principal direction. Figure 2.6 shows diagonal loading histories. When the first deflection limit in the diagonal direction is set, the deflection limit in the other principal direction is automatically set because the angle in which the deformation is to be applied is also set. Therefore, in the case of loading 30^{o} from the strong axis, a 0.2 in. deflection limit in the strong direction was used resulting in deflection limit along the diagonal direction of 0.23 in. In the case of loading 30^{o} from the weak axis, a 0.16 in. deflection limit in the weak direction was used resulting in a deflection limit along the diagonal direction of 0.18 in. The number of cycles at each level (three cycles) was not changed in any tests.

2.3.3 Axial Load. Ramirez[23] studied the effect of constant tensile or compressive axial load and alternating tensile and compressive axial load. Only one compressive axial load (120 kips)

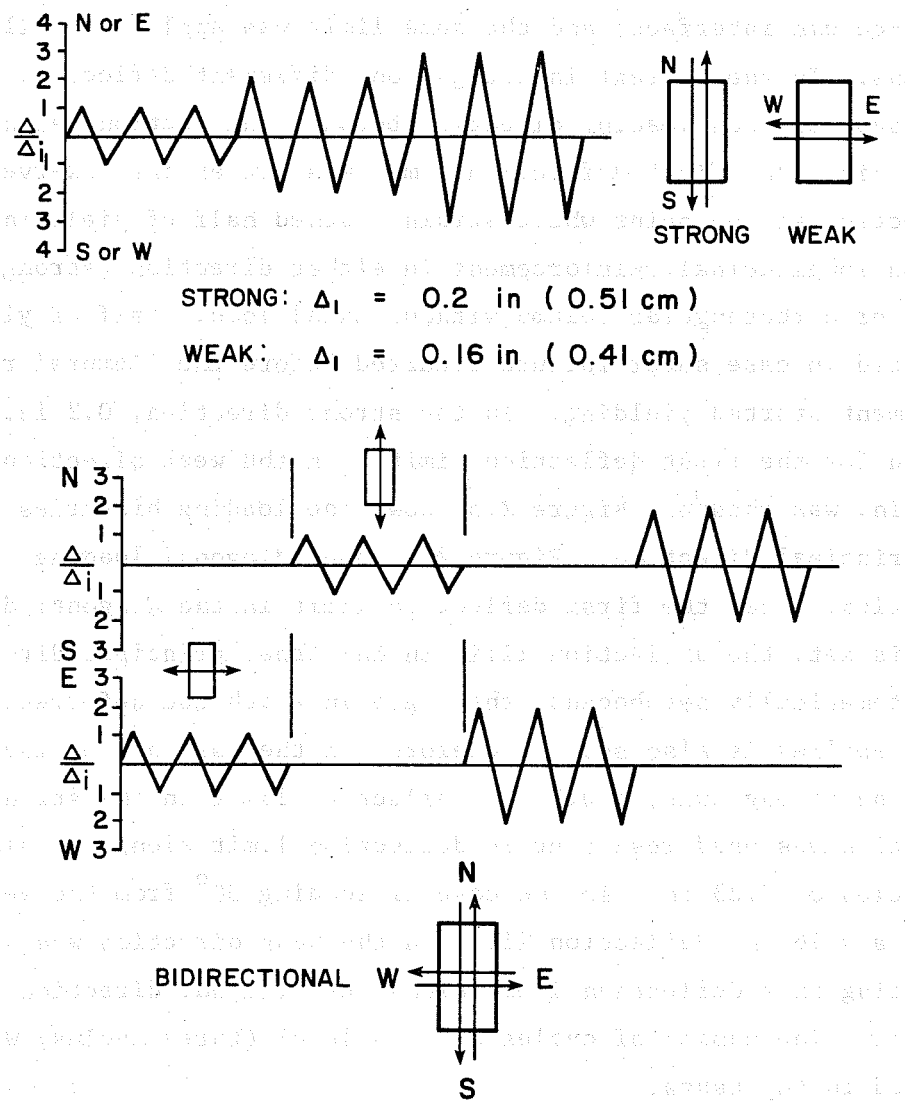

Fig. 2.5 Loading histories in the principal directions

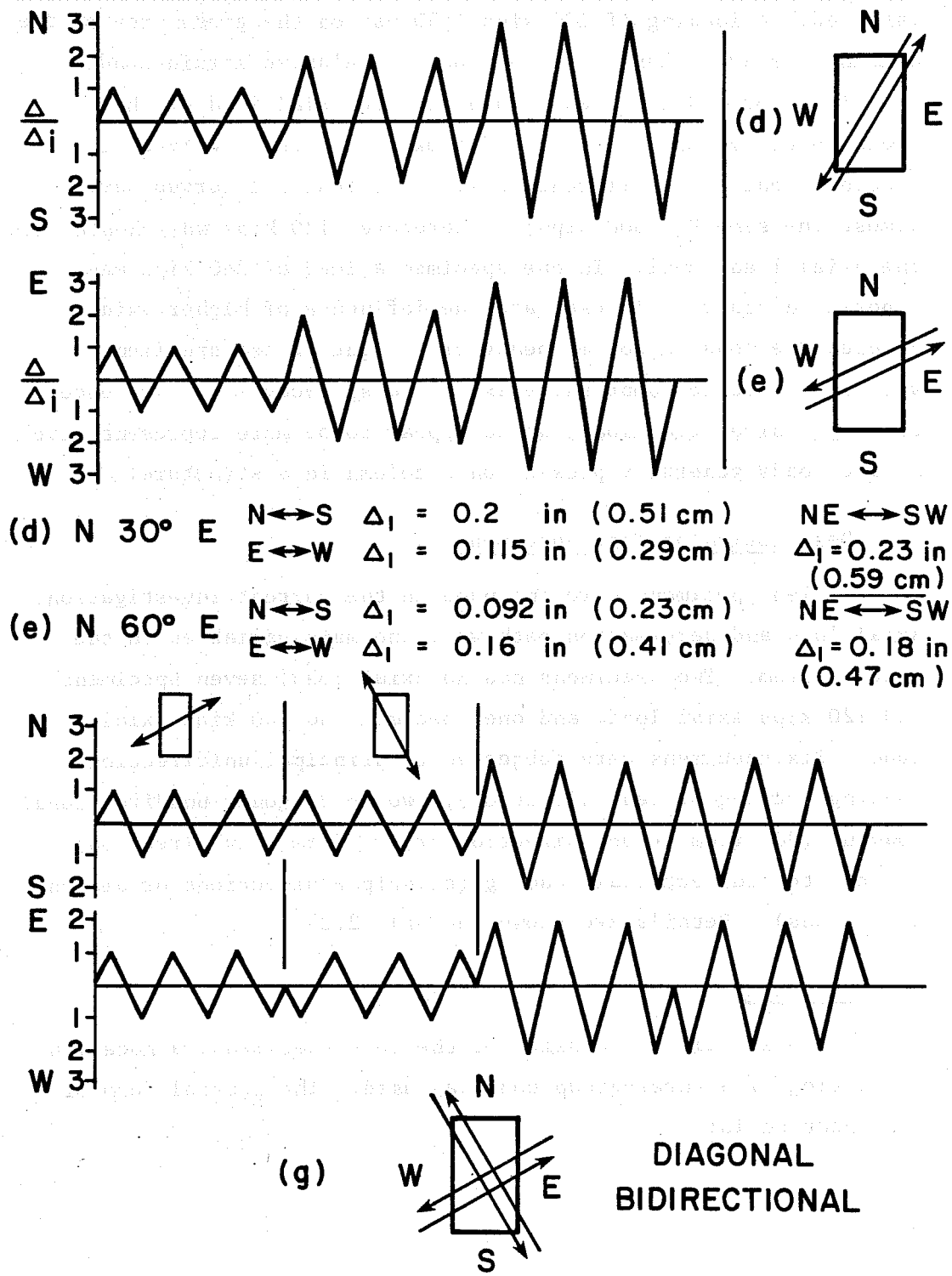

Fig. 2.6 Diagonal loading histories

was used. A loading of 120 kips (830 psi on the gross area of the column) was 40 percent of axial load at balanced strain condition P_b. Therefore, 0.4 P_b was chosen for the axial load on the rectangular columns. Figure 2.7 shows interaction curves for bending about four different axes. Note that all curves have almost the same P_b (300 kips). Therefore, 120 kips was chosen for the axial load level. In one specimen a load of 240 kips was imposed in order to investigate the influence of higher axial compressive load on column behavior. Eight of ten specimens were subjected to compressive axial loads, because the presence of compressive axial loads would appear to be more representative of the loads generally present on a column in a structure.

2.4 Description of Test Specimens

Ten specimens were included in the current investigation. Axial load and deformation path were the main variables in the test program. Two specimens had no axial load, seven specimens had 120 kips axial load, and one specimen had 240 kips axial load. Six specimens were subjected to principal unidirectional loading (strong or weak direction), two to diagonal unidirectional loading (30^o from strong direction or 30^o from weak direction), and two to bidirectional loading (principal directions or diagonal directions). Details are shown in Table 2.2.

2.5 Notation

To simplify discussion of the test specimens, a notation consisting of a three-group code was used. The general form of the notation is:

ALX

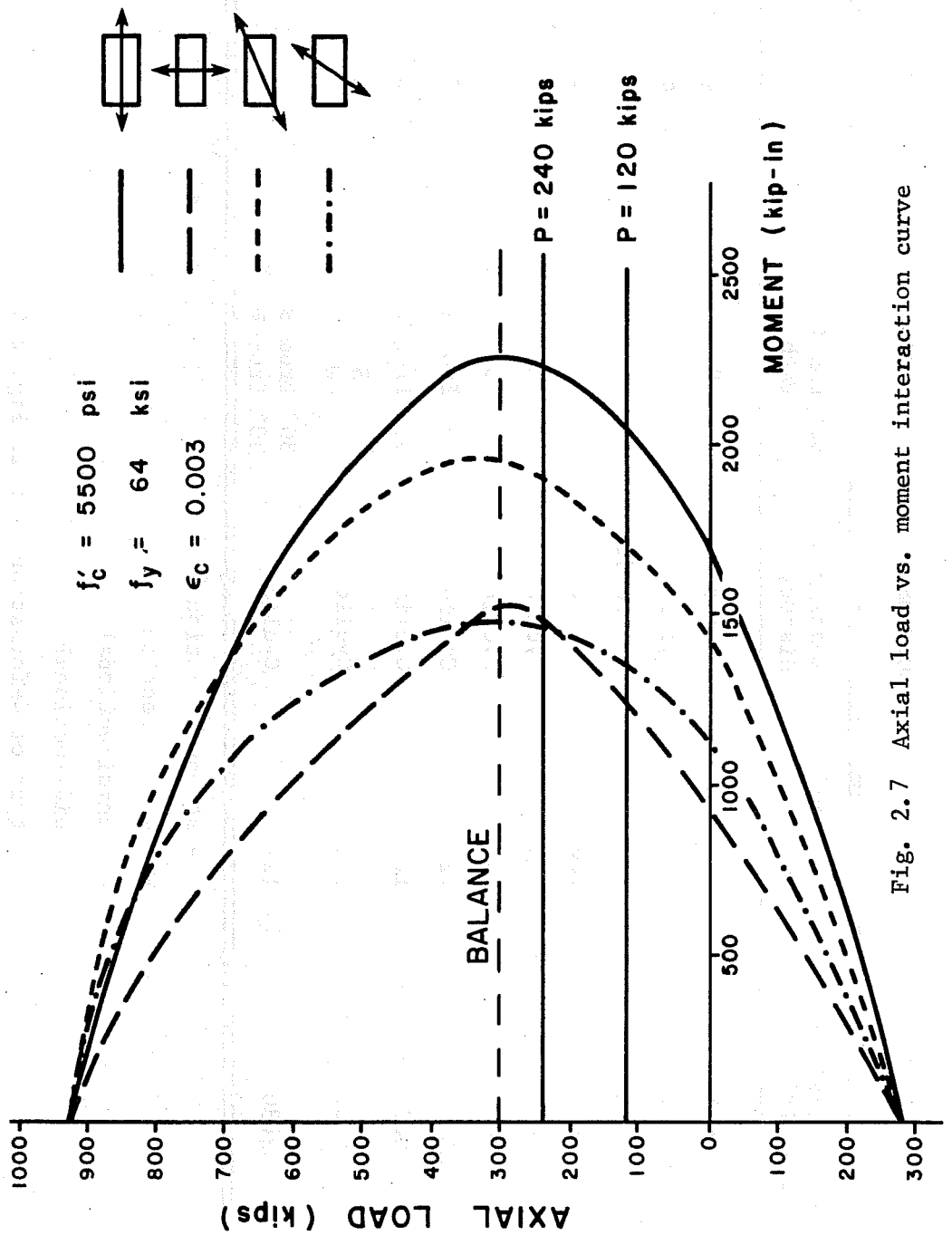

Fig. 2.7 Axial load vs. moment interaction curve

TABLE 2.2 TEST SPECIMENS -- LOADING HISTORY

Specimen Identifier	Axial Load (kips)	Loading History	Deformation Path		Type*
0US	0	Cyclic	S	U	b
0UW	0	Cyclic	W	U	c
CMS	120	Monotonic	S	U	a
CUS	120	Cyclic	S	U	b
CUW	120	Cyclic	W	U	c
2CUS	240	Cyclic	S	U	b
CDS30	120	Cyclic	30° from S	U	d
CDW30	120	Cyclic	30° from W	U	e
CBSW	120	Cyclic	S W	B	f
CDSW30	120	Cyclic	30° from S 30° from W	B	g

S - strong direction

W - weak direction

U - unidirectional

B - bidirectional

* - type of deformation path in Fig. 2.4

A = level of axial load

- 0 = no axial load
- C = 120 kips axial compression
- 2C = 240 kips axial compression

L = loading pattern

- M = monotonic
- U = unidirectional } only principal direction
- B = bidirectional } only principal direction
- D = diagonal (including unidirectional and bidirectional)

X = loading direction

- S = strong direction
- W = weak direction
- S30 = 30^{o} from strong direction
- W30 = 30^{o} from weak direction
- SW = strong and weak directions
- SW30 = 30^{o} from strong direction and 30^{o} from weak direction

The specimens listed in Table 2.2 are identified using this notation.

CHAPTER 3

LOADING SYSTEM AND INSTRUMENTATION

3.1 Loading System

The loading system consists of a reaction frame and a hydraulic system including two lateral loading rams, one axial loading ram, and three pairs of rams to control the rotation of the specimen ends. A picture of the loading system is shown in Fig. 3.1.

3.1.1 Reaction Frame. The loading system is positioned on the reinforced concrete floor-wall reaction system shown in Fig. 3.2. Details of the loading frame are shown in Fig. 3.3. The floor-wall reaction system consists of a structural tie-down floor and two orthogonal buttressed walls. The walls provide a base for rams loading the specimen horizontally in two orthogonal directions, while the floor provides a basis for anchoring the reaction frame to apply axial load to the specimen. The loading frame has three main components: (1) a fixed base placed on the floor of the floor-wall system, and providing fixity to the lower end of the specimen; (2) a loading head similar in shape to the fixed base which is attached to the upper end of the specimen and through which lateral deformations and axial loads are applied; (3) a loading frame to support the axial loading ram and transfer reactions to the floor.

3.1.2 Hydraulic System. The hydraulic system consists of two different components.

The first system is the closed-loop hydraulic system which has three loading rams, three actuators, and a central

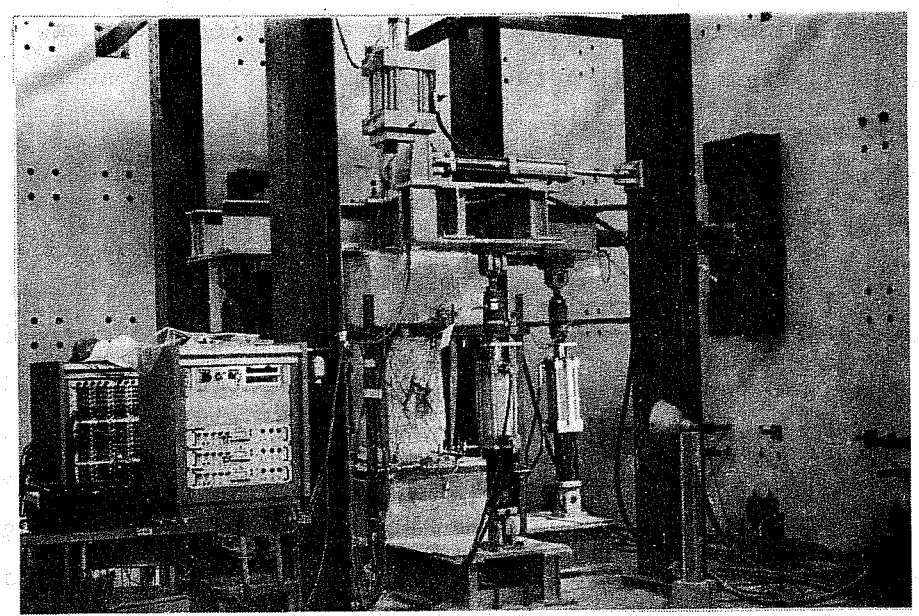

Fig. 3.1 Test set-up

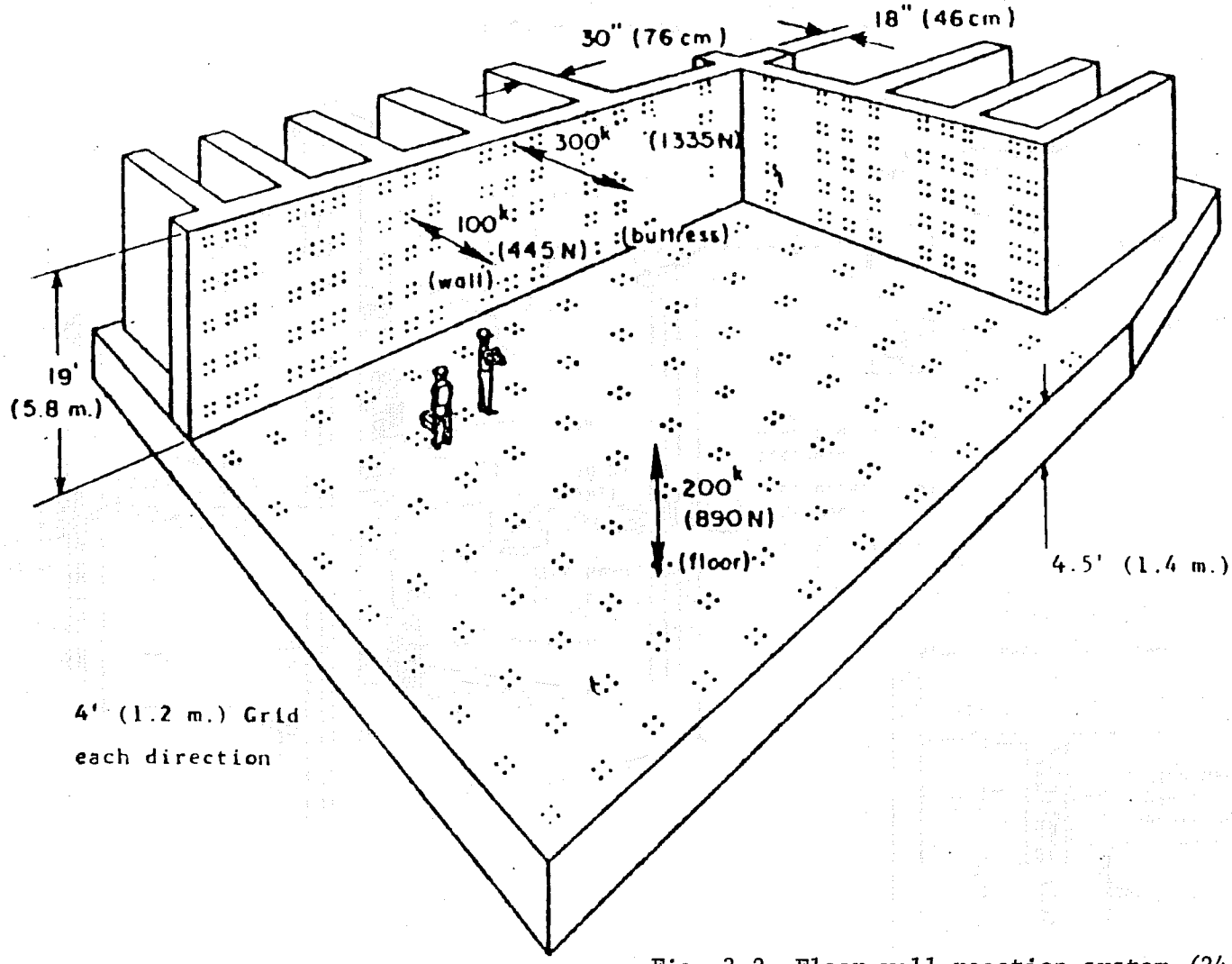

Fig. 3.2 Floor-wall reaction system (24)

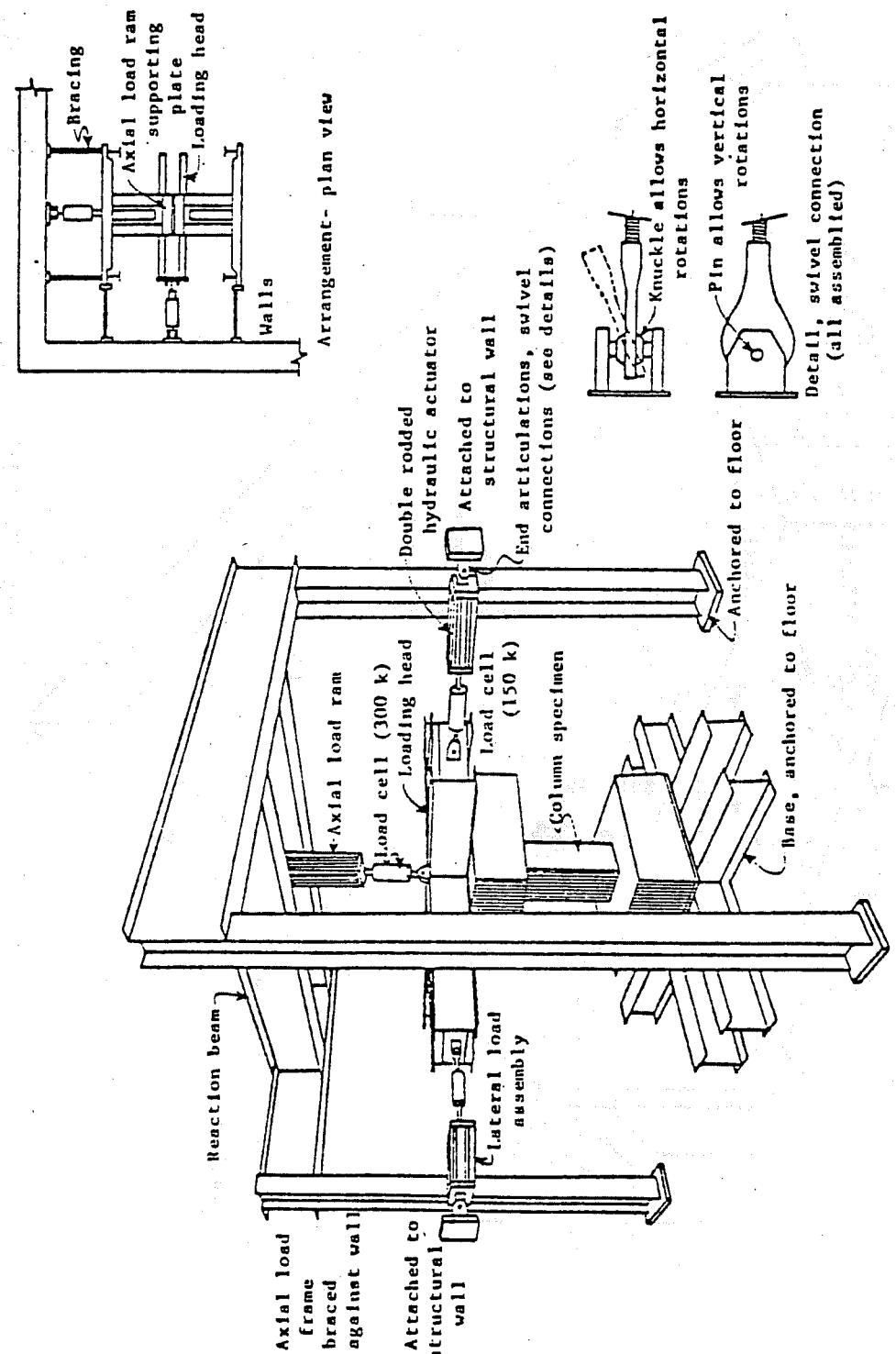

Fig. 3.3 Loading frame (23)

hydraulic pump. As shown in Fig. 3.3, two loading rams are used for the application of lateral displacements and one for vertical load. Servo-controllers were used to obtain predetermined lateral displacements or axial load. The servo-controller can be operated by the computer. However, in the current investigation it was operated manually with the aid of x-y plotters which monitored the load-deflection curves.

The second system is composed of coupled hydraulic positioning rams whose purpose is to prevent the rotation of the specimen ends during testing (Fig. 3.4). There are two pairs of vertical rams to resist the rotation in the vertical plane and one pair of horizontal rams to resist twist in the horizontal plane. In each pair, the bottom chamber of one ram is connected with the top chamber of the other, and vice-versa, as shown in Fig. 3.5. When lateral displacements are imposed on the specimen through the stiff loading head, moments are developed at the ends of the specimen. Those moments are resisted by the oil in the cross-coupled chambers of the rams. Therefore, rotation of the specimen in any direction is restricted; however, translation can be accommodated without restraint.

At both ends of all rams, swivel connections shown in Fig. 3.3 are attached. With swivel connections, a rotation of 180^{o} is permitted in one plane, and about 10^{o} rotation in the other, sufficient for deformation imposed during testing.

3.2 Instrumentation

During testing, loads, deflections, and strains were measured to monitor the behavior of the specimen.

3.2.1 Loads. The lateral loads corresponding to the lateral displacement and the axial load were measured through load cells attached to loading rams. Output from the lateral loading

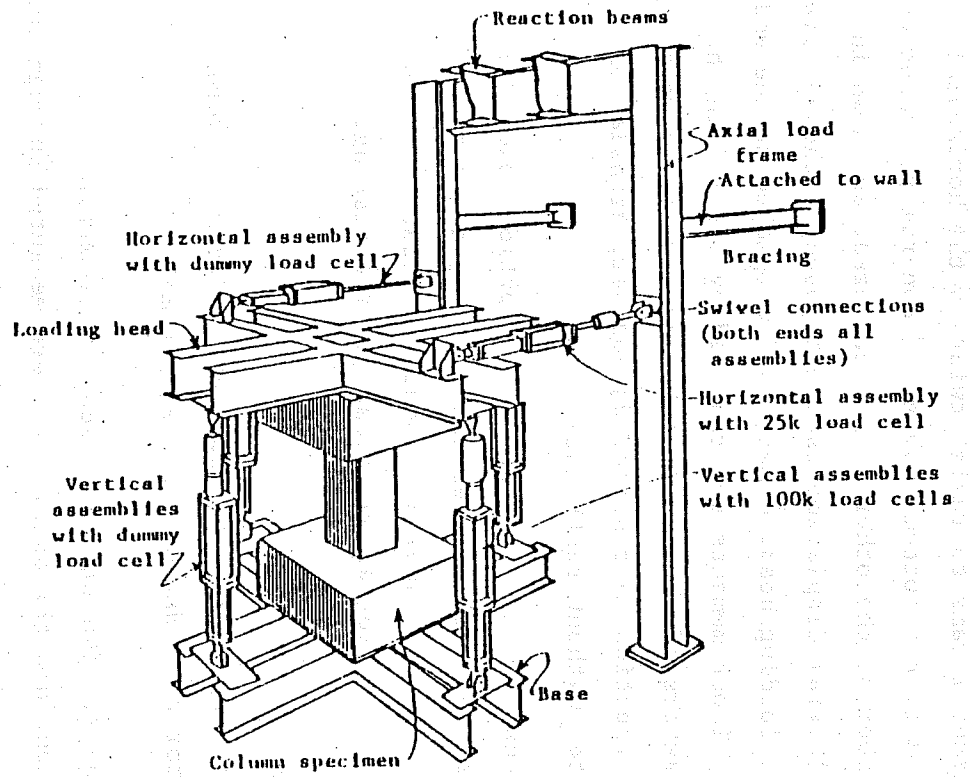

Positioning System - Schematic

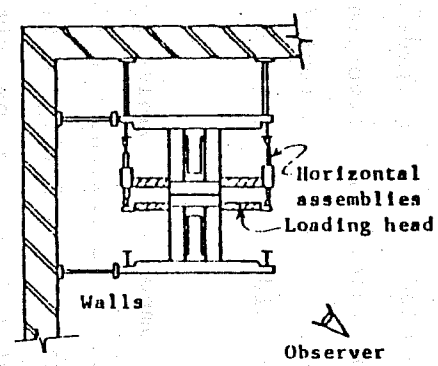

Location - Plan View

Fig. 3.4 Restraining rams (23)

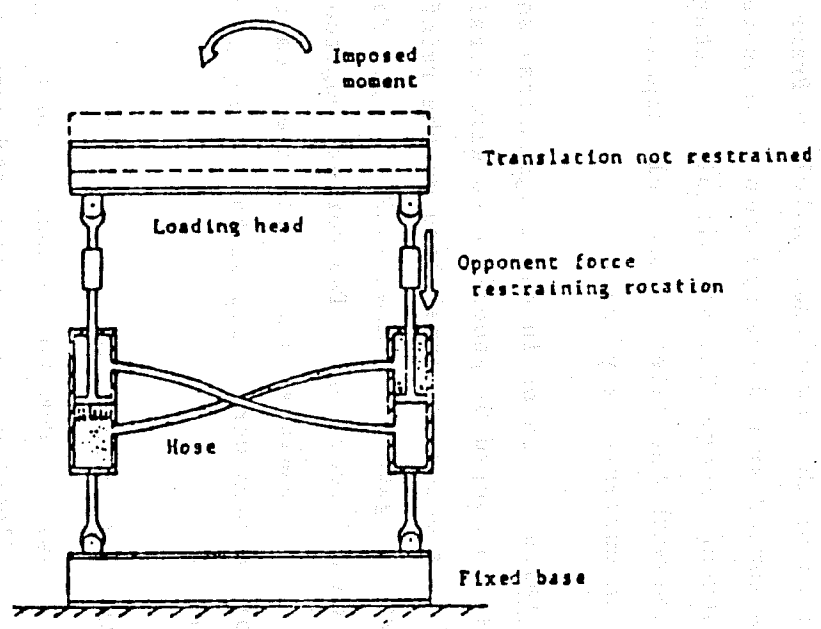

Fig. 3.5 Coupled hydraulic positioning rams (23)

rams were plotted on x-y recorders for control of the loading history. All load-cell output was recorded on magnetic tape for subsequent data reduction.

3.2.2 Deflections. The deflections of the specimen end blocks were measured by twelve linear potentiometers at the locations shown in Fig. 3.6. Eight potentiometers were set to measure rotations and deflections of the upper end and four to measure the rotation of the lower end. A bolted frame shown in Fig. 3.7 was constructed around the specimen to measure deflections relative to the strong floor. The signals of two lateral potentiometers were used with the lateral load cell signals to produce the load-deflection curves on x-y records.

3.2.3 Strains. Strains in the longitudinal and transverse reinforcement were measured by paper-backed wire strain gages to investigate the effect of external load on the reinforcement. The location of strain gages is shown in Fig. 3.8. Four transverse hoops were gaged on all four legs. Two corner longitudinal bars located at opposite diagonals were gaged at nine locations on each bar. Two corner bars were gaged at the intersections of the column and the end blocks.

3.3 Data Recording and Processing

During testing, a VIDAR data scanner read the analog signals for loads, deflections and strains, and converted them to digital voltages. These digital voltages were stored on magnetic tape or on the computer disc unit, and were later processed on the minicomputer to produce data plots, especially load-deflection curves, or tables in the usual engineering units. A block diagram of this process is shown in Fig. 3.9.

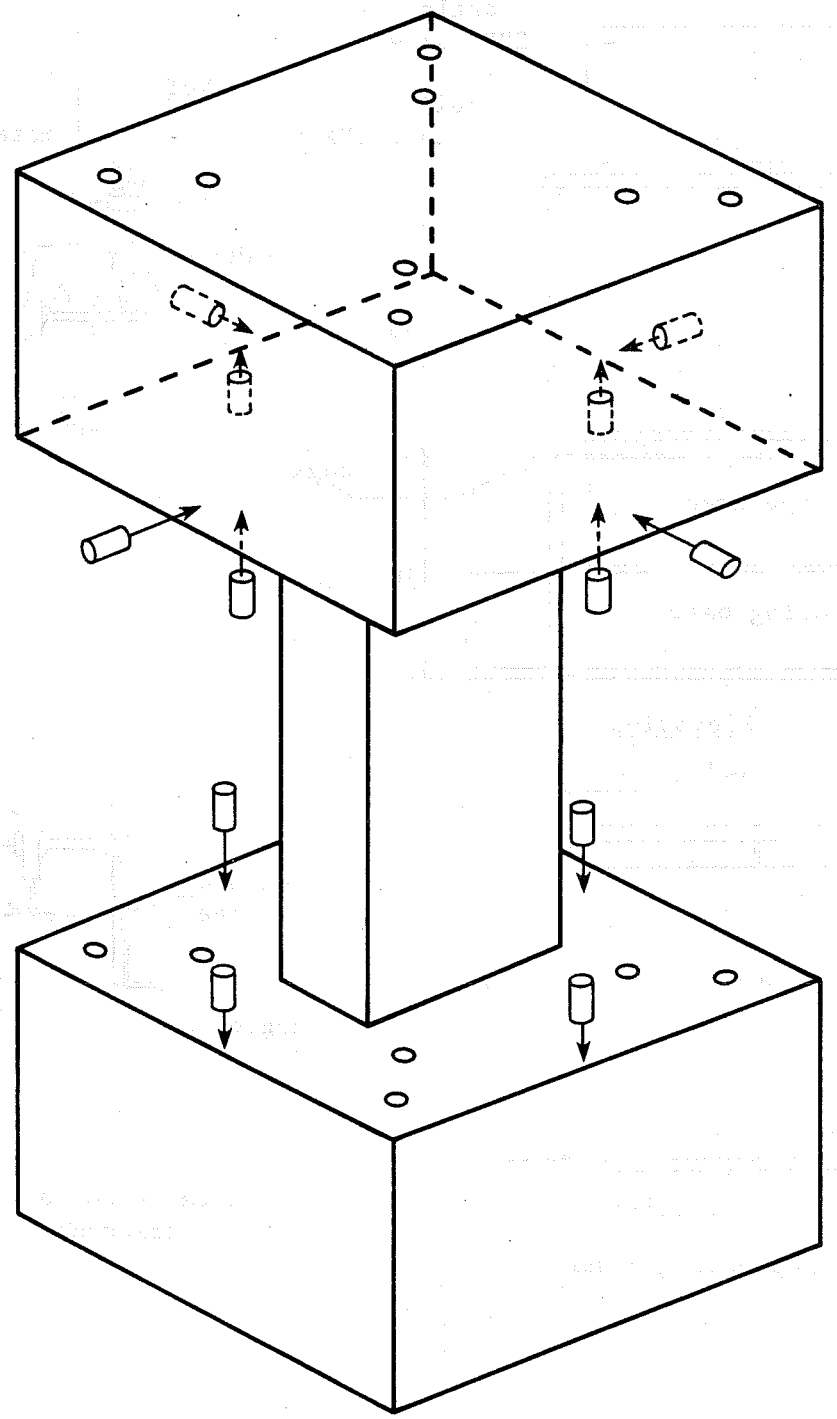

Fig. 3.6 Linear potentiometer locations

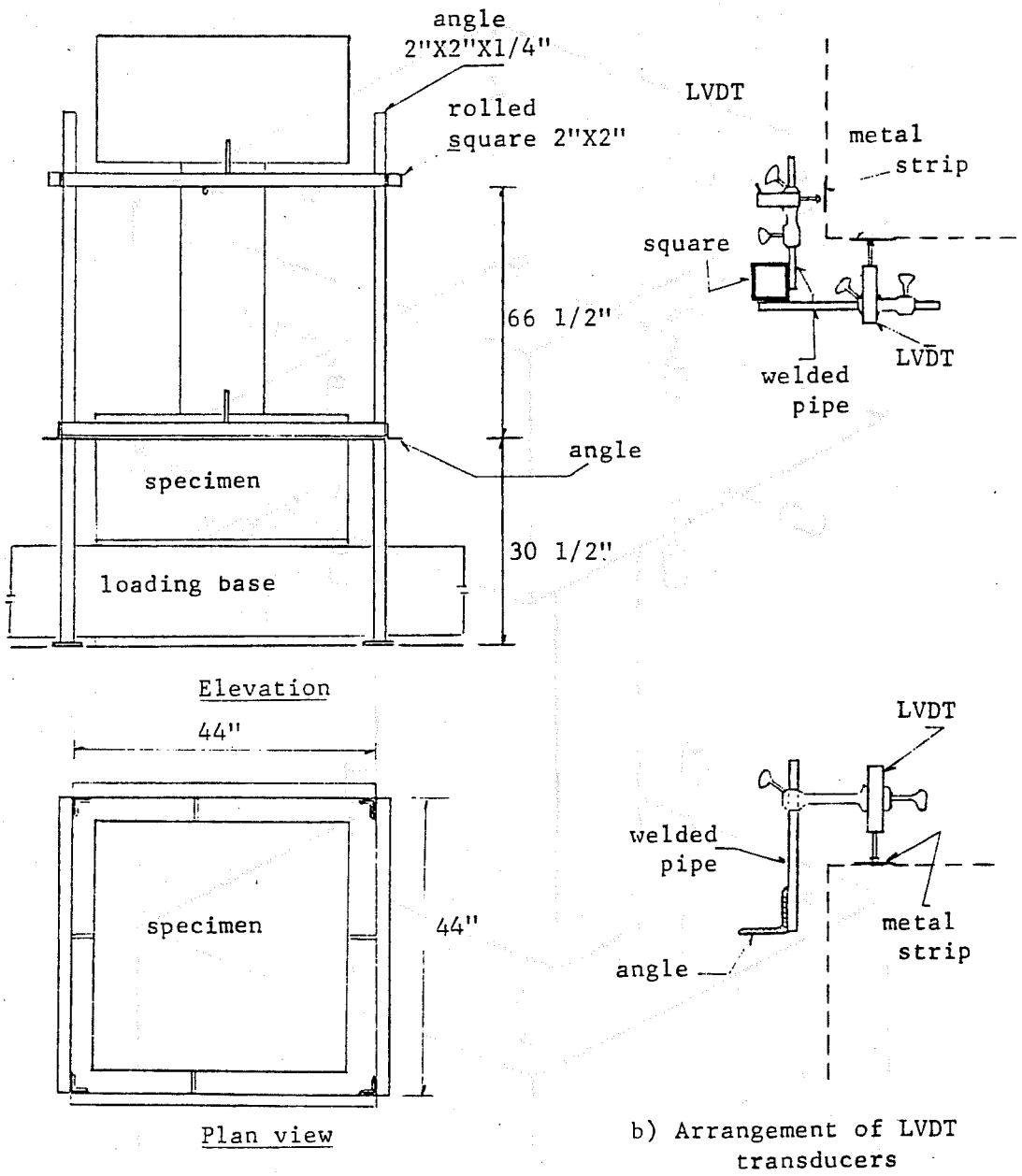

Fig. 3.7 Deformation measurement (23)

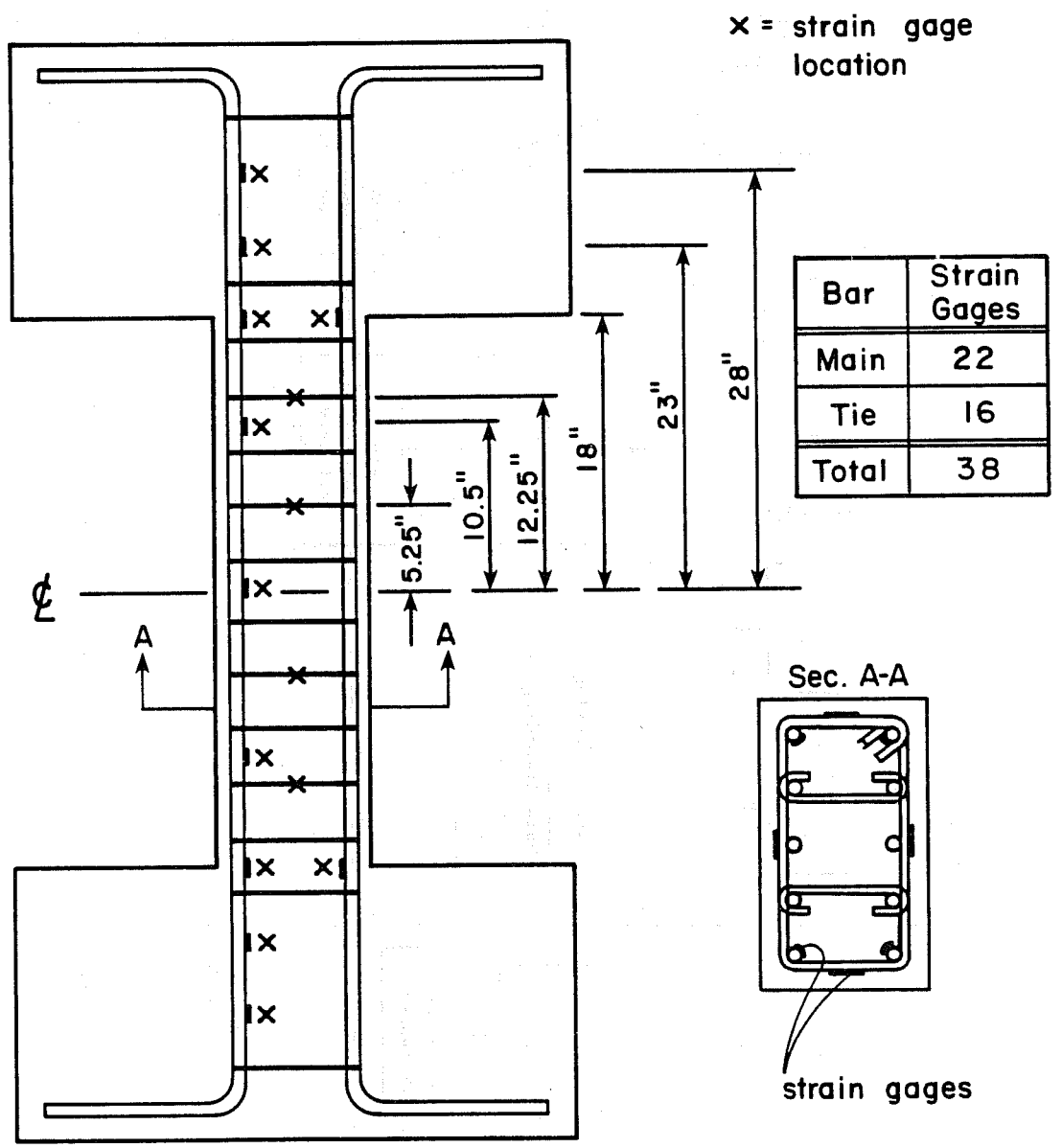

Fig. 3.8 Strain gage locations

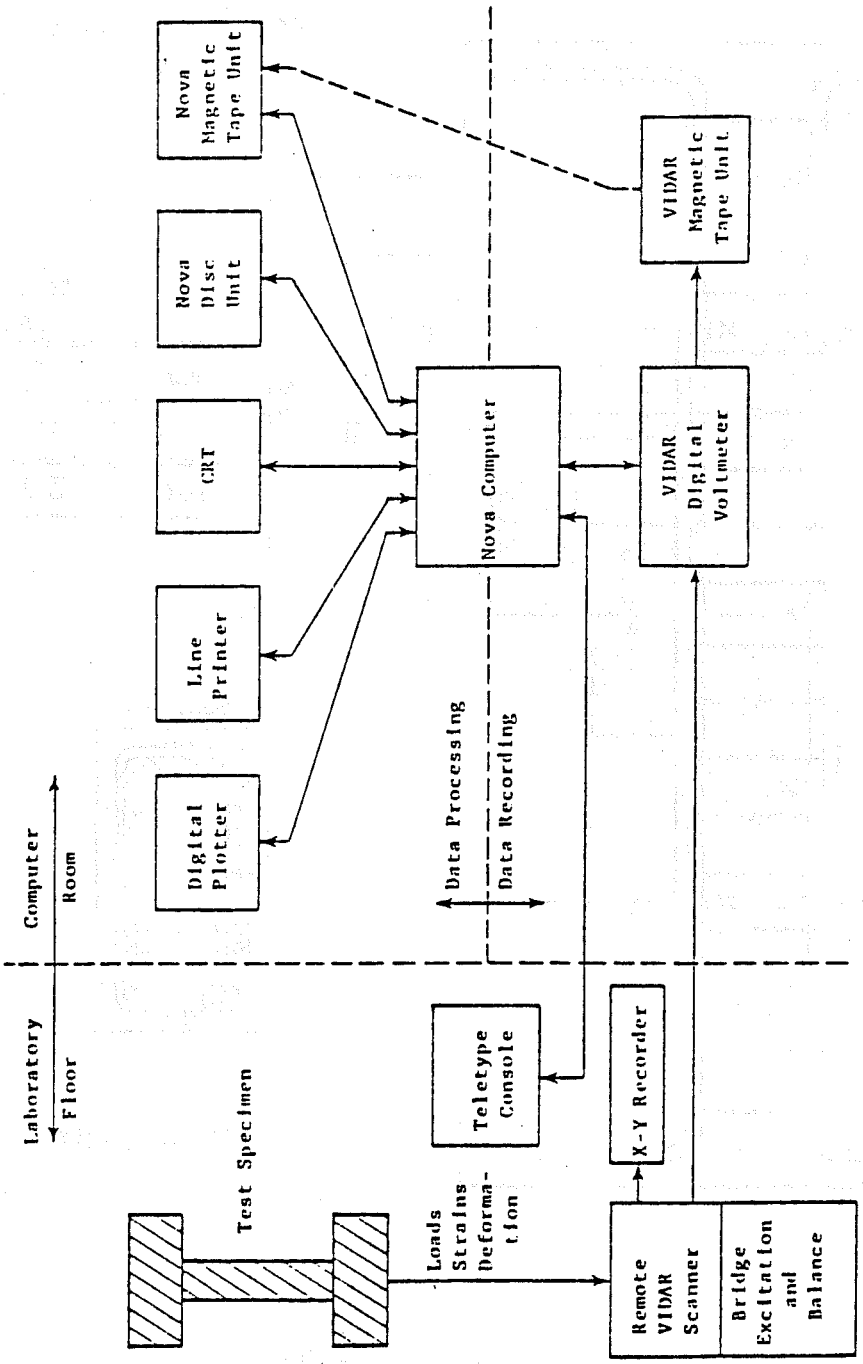

Fig. 3.9 Data recording and processing (22)

CHAPTER 4

BEHAVIOR OF SPECIMENS

4.1 General

The behavior of each test specimen is described in terms of load-deflection curves and crack patterns. Comparisons between test results and explanations of the observed behavior of the specimens are discussed in Chapter 5.

The ten specimens tested are classified into two types according to loading direction, principal or diagonal, as shown in Fig. 4.1. In this study, the term "principal direction" means loading or deflection in North-South or East-West directions. For seven specimens the deflection was applied in the principal directions and the measurements of lateral load and deflection were taken along these principal directions. For three specimens, the deflection was applied in the diagonal directions, but the measurements were taken along principal directions, as shown in Fig. 4.1. The measured loads and deflections were transformed to equivalent values on diagonal axes using vector addition as shown in Fig. 4.2. In describing the three specimens, resultant load-deflection curves are presented.

As mentioned in Sec. 2.3, for each deflection limit ($n\Delta$:n=1,2,. . .), the specimen was cycled three times. Cracks were marked on the surface and pictures were taken at the peaks of the first and third cycle at each deflection limit. The letters are noted on the load-deflection curve for each specimen at points in the load history at which pictures of crack pattern were taken.

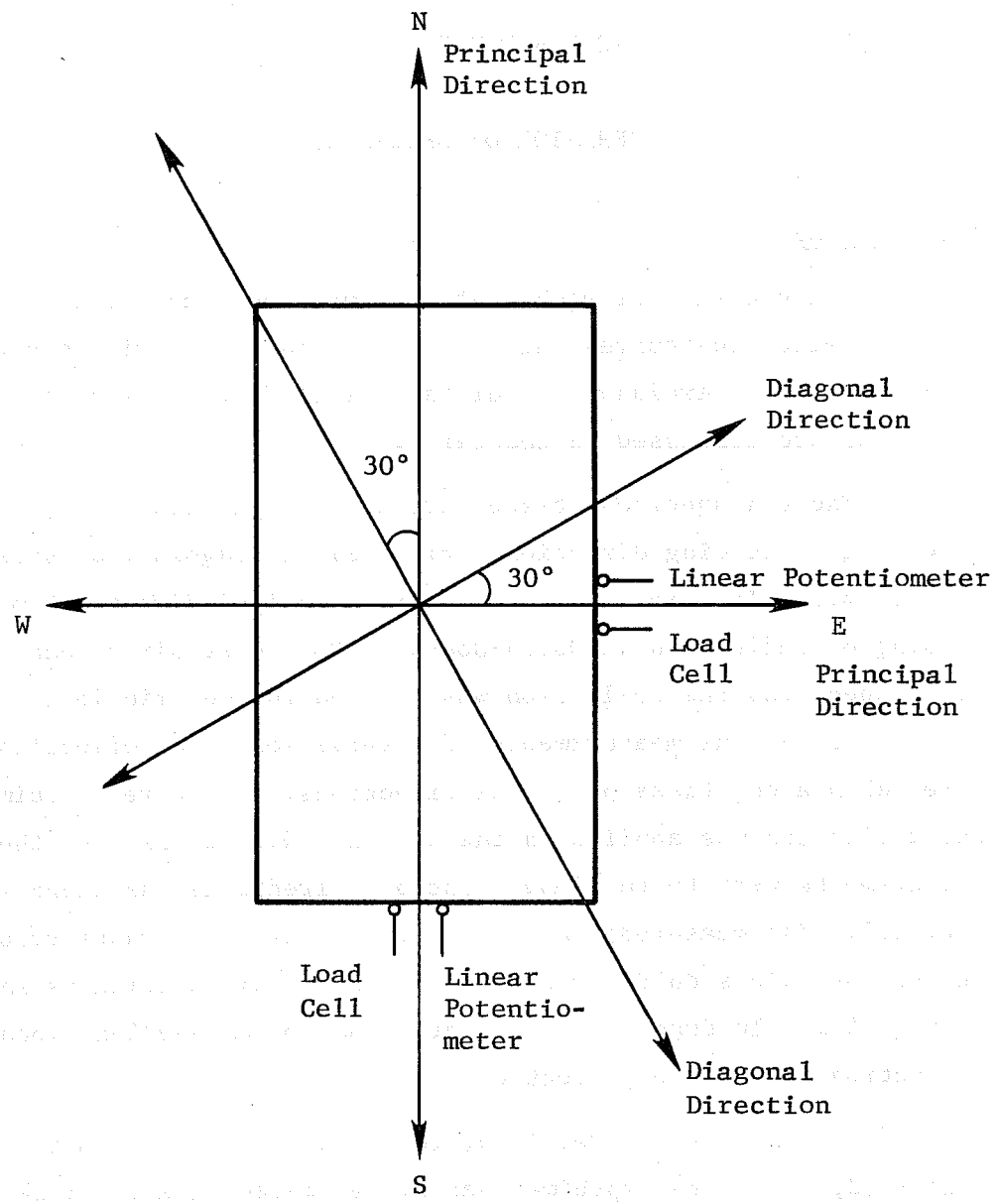

Fig. 4.1 Principal and diagonal direction

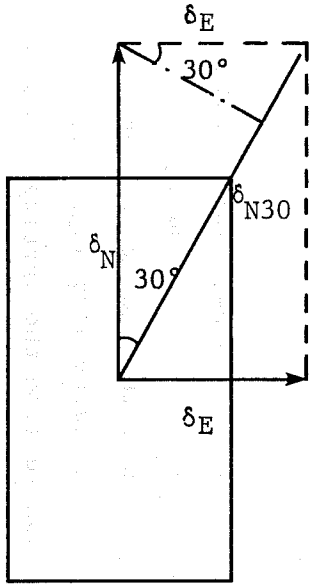

$$\delta_{N30} = \delta_N \cos 30^\circ + \delta_E \sin 30^\circ$$
$$= \tfrac{1}{2}(\sqrt{3}\ \delta_N + \delta_E)$$

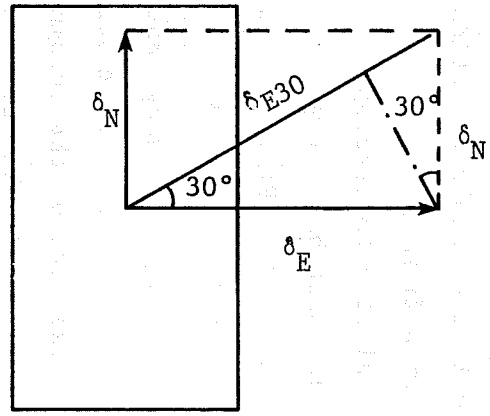

$$\delta_{E30} = \delta_N \sin 30^\circ + \delta_E \cos 30^\circ$$
$$= \tfrac{1}{2}(\delta_N + \sqrt{3}\ \delta_E)$$

Fig. 4.2 Calculation of resultant measurements

4.2 Specimen 0US

The specimen had no axial load and was subjected to unidirectional reversed loading in the strong direction (N-S). The specimen was initially deformed from the south to north. The first deflection limit was selected to develop strains in the longitudinal reinforcement at about half of yield. For the #6 bars used, yield was about 2200×10^{-6} (Fig. 2.3); a 0.2 in. deflection (1Δ) produced a strain of about 1100×10^{-6}.

The load-deflection curves (Fig. 4.3) show that the maximum lateral load occurred at around 3Δ. At 2Δ strain in the longitudinal bars at the intersection of the column and the end block was around 1700×10^{-6} and at 3Δ the strain was around 2000×10^{-6}. At the maximum load (3Δ), longitudinal reinforcement did not yield, because large shear cracks formed in the east and west faces as shown in Fig. 4.4(c). A noticeable drop in lateral load (corresponding to the opening of diagonal cracks) occurred between the first and second cycles at 3Δ. Between the second and third cycles the load did not change significantly. After 3Δ, the shape of the hysteretic loops became increasingly "pinched" toward the origin and the strength and stiffness of the specimen deteriorated rapidly.

Figures 4.4(a) through (c) show crack patterns on the west side at the end of cycling at levels 1Δ, 2Δ, and 3Δ. Figure 4.4(d) shows the crack pattern at the end of testing. At 1Δ (Fig. 4.4(a)), several inclined cracks with angles of inclination of around 45^{o}, as measured from the vertical face of the column, occurred in the east and west faces of the column. At 2Δ (Fig. 4.4(b)), the number of cracks increased and inclined cracks extended all along the column. At 3Δ(Fig. 4.4(c)), cracks opened along a diagonal from the top to bottom of the column in both loading directions. The angle of these

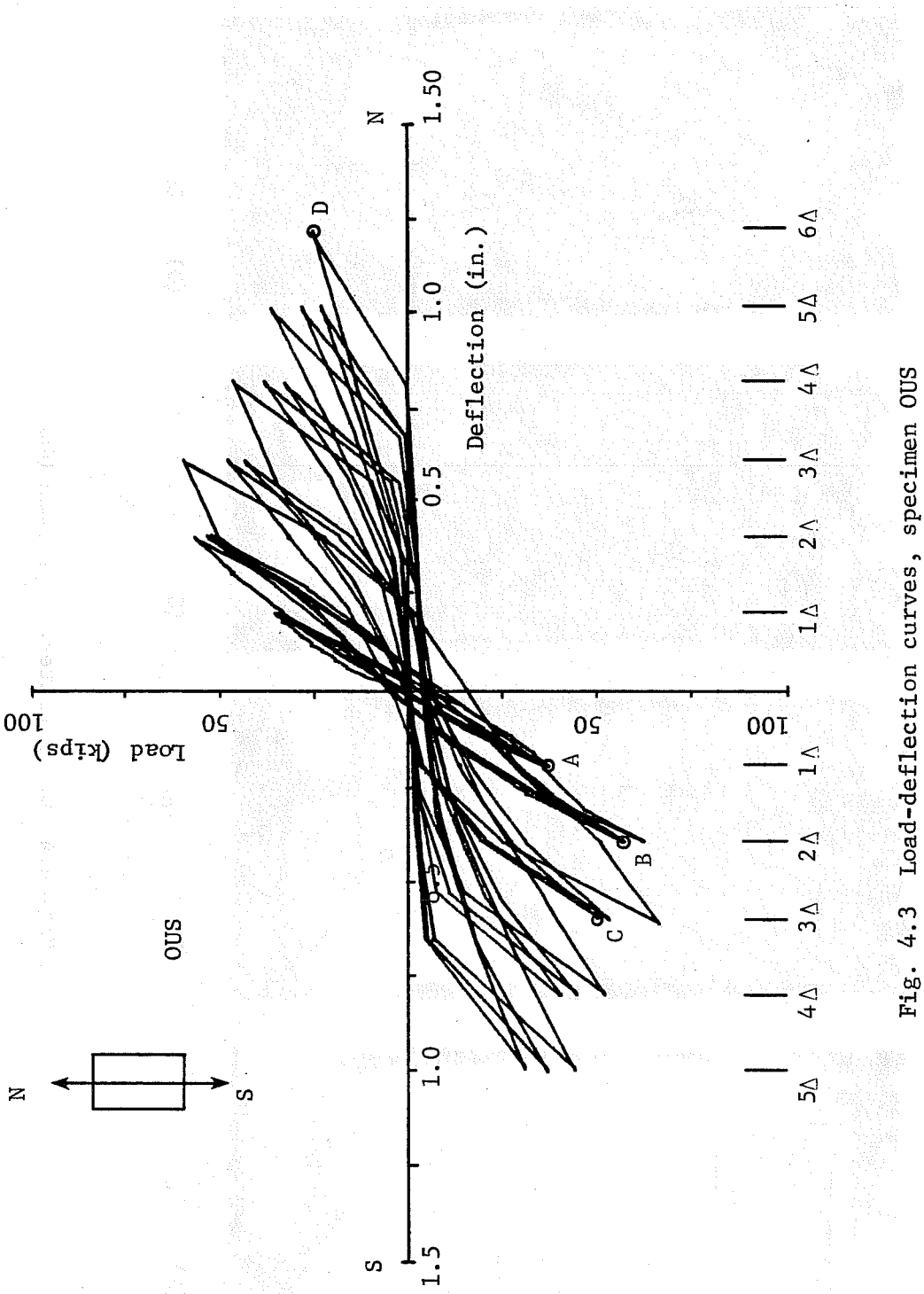

Fig. 4.3 Load-deflection curves, specimen OUS

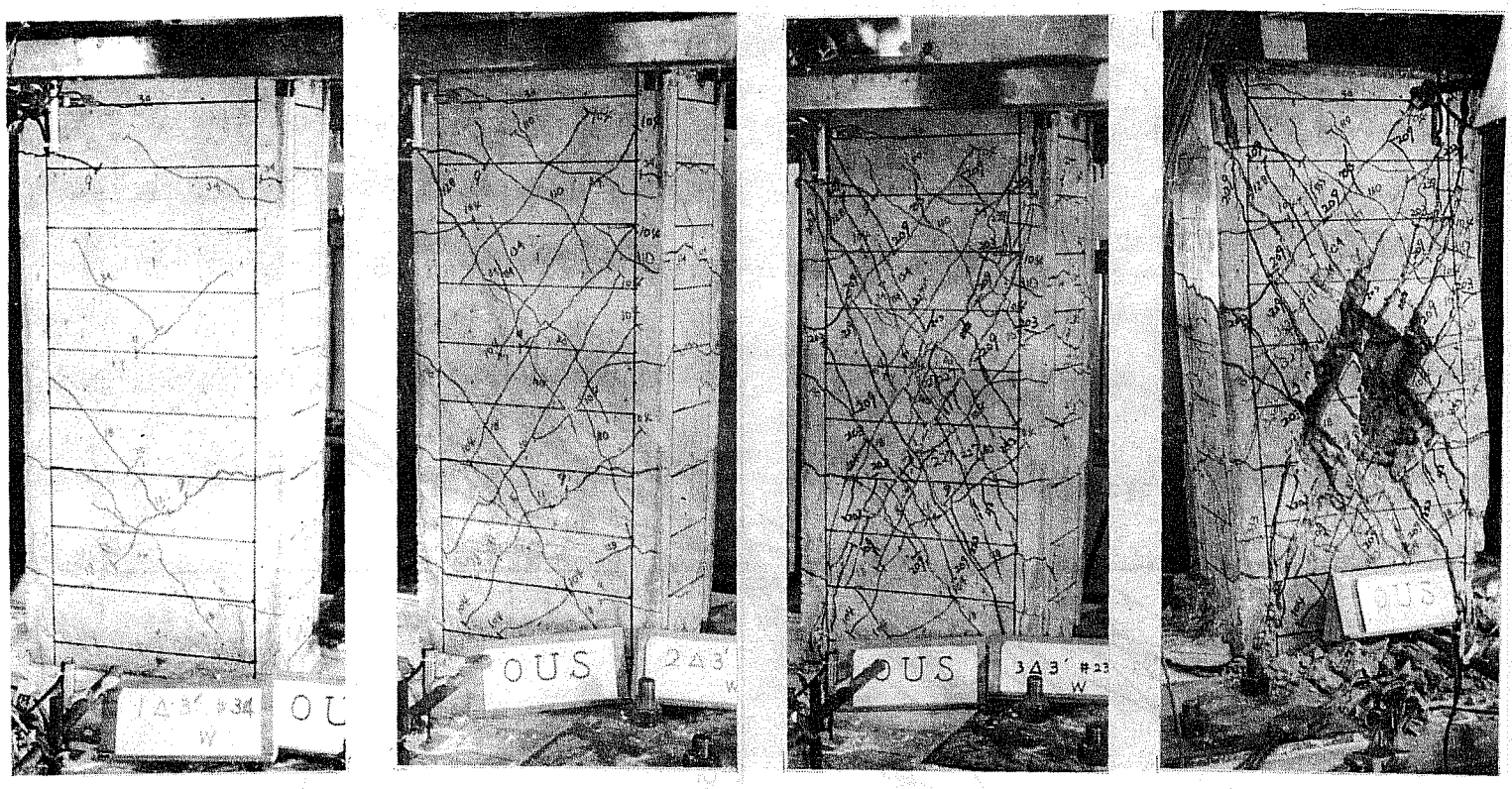

(A) 1Δ (B) 2Δ (C) 3Δ (D) End

Fig. 4.4 Crack pattern, specimen OUS

cracks was steeper than the cracks which formed earlier and was around 35^{o}. After 3Δ, the concrete at the midheight region of the column spalled. Little spalling of the concrete cover near the bottom and top of the column was noted.

4.3 Specimen OUW

This specimen was tested without axial load and subjected to unidirectional loading in the weak direction (E-W). The specimen was initially deformed from the west to east. The first deflection limit was determined as for specimen OUS, with 0.16 in. deflection corresponding to half of yield strain in the longitudinal reinforcement.

The load-deflection curves (Fig. 4.5) show that maximum load was reached at 5Δ, a much larger value than in other tests. Strains in longitudinal bars at the intersection of the column and the end block were 1600×10^{-6}, 2000×10^{-6}, and yield at 2Δ, 3Δ, and 4Δ, respectively. The longitudinal reinforcement yielded before the maximum load was reached. There was not much change in peak lateral load between first and second cycles at each deflection level up to 4Δ. From 3Δ to 6Δ, the strength was almost the same, indicating ductile behavior. After 6Δ, the strength and stiffness deteriorated rapidly.

Figures 4.6(a), (b), and (c) show the crack pattern of the north face at the end of cycling at deflection limits 1Δ, 3Δ, and 5Δ, respectively. The condition of the specimen at the end of the test is shown in Fig. 4.6(d). At 1Δ, there were a few flexural and flexural-shear cracks near the ends of the column. At 3Δ, many inclined cracks occurred all along the column. The angle of these cracks was around 45^{o}. There was not much difference between the crack patterns at 3Δ and 5Δ, but at 5Δ the cracks had opened considerably. The angle of the inclined cracks did not change as cycling progressed and remained at around 45^{o}. Figure 4.6(d)

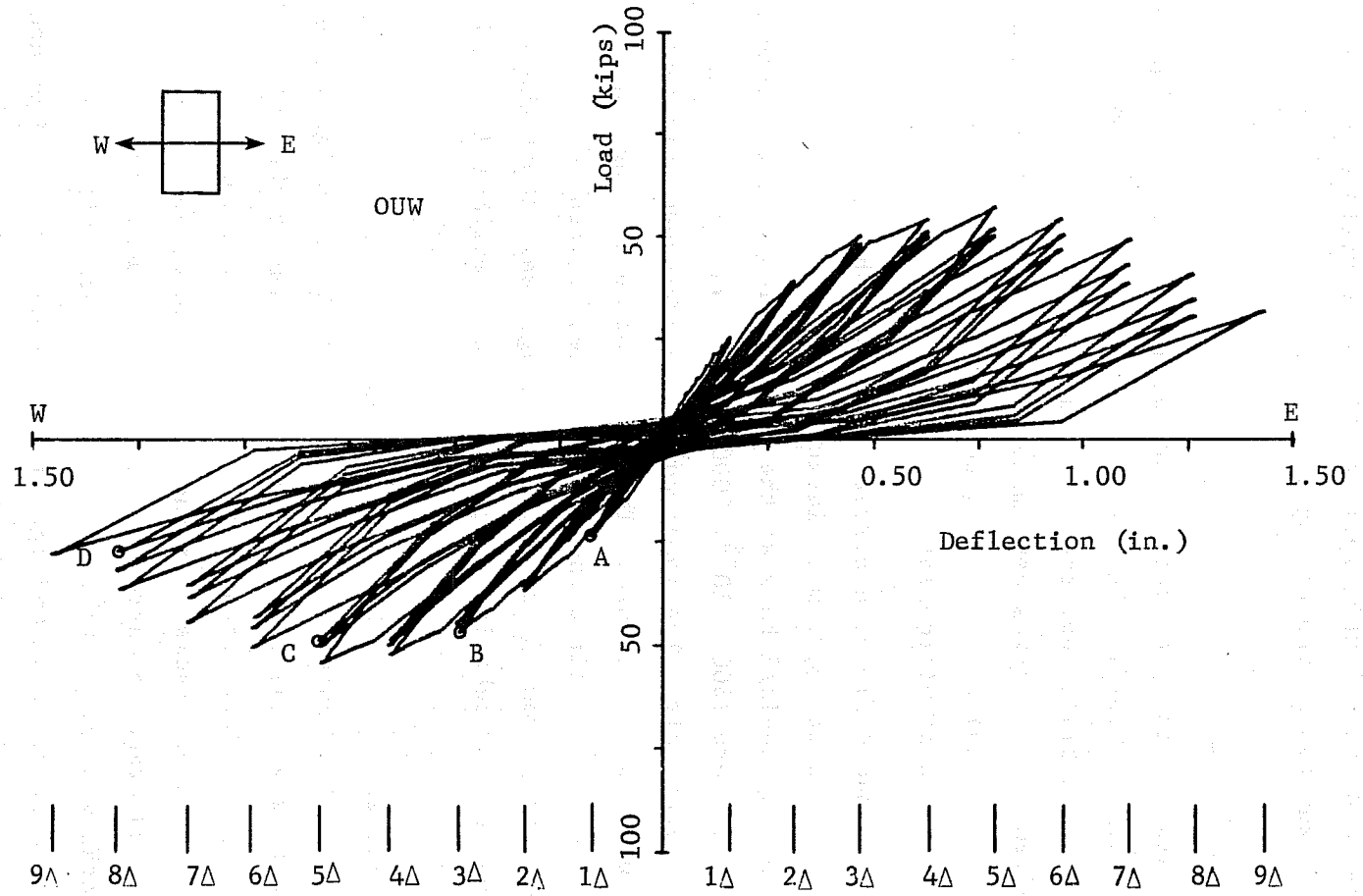

Fig. 4.5 Load-deflection curves, specimen OUW

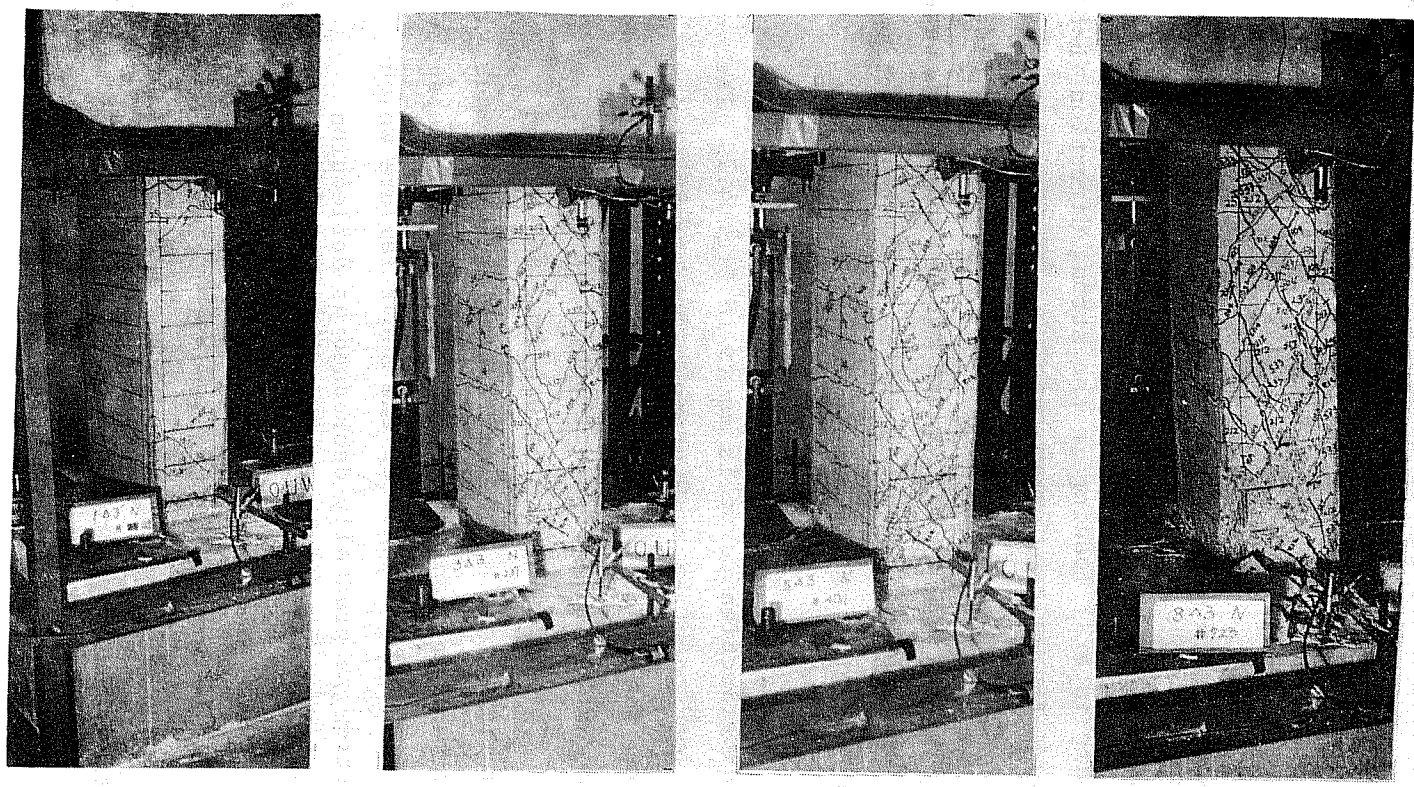

(A) 1Δ (B) 3Δ (C) 5Δ (D) 8Δ

Fig. 4.6 Crack patterns, specimen OUW

shows that the specimen had severe damage and spalling of concrete cover near the bottom of the column. It is interesting to note that there was no spalling of the concrete cover in the midheight region of the concrete.

4.4 Specimen CMS

The specimen was tested with 120 kips axial compressive load and monotonic lateral loading in the strong direction (N-S). The specimen was deformed from the south to north to a deflection of 1.4 in. and then returned to its original position. In order to investigate the behavior of the column after such a high peak deflection, the specimen was deformed in the opposite direction (from the north to south) to the same value of deflection as reached initially.

The load-deflection curve is shown in Fig. 4.7. The maximum lateral load occurred at 0.48 in. The strain of longitudinal bars at the intersection of the column and the end blocks was around 1200×10^{-6} at a deflection of 0.2 in., around 1700×10^{-6} at a deflection of 0.4 in., and around 2000×10^{-6} at maximum load. The longitudinal reinforcement did not yield at maximum load. After reaching maximum capacity, the load suddenly dropped because of the shear failure which occurred. The strength gradually decreased as deflection increased to 1.4 in. When loading was stopped, the capacity was only 40 percent of the maximum load because of the continual deterioration. On loading in the opposite direction, very low loads were maintained as a consequence of the severe damage to the specimen during loading in the first direction.

Figures 4.8(a) through (c) show the crack pattern of the west face of the specimen at deflections of 0.2 in., and 0.48 in. (maximum load), and 1.4 in., respectively. The condition of the

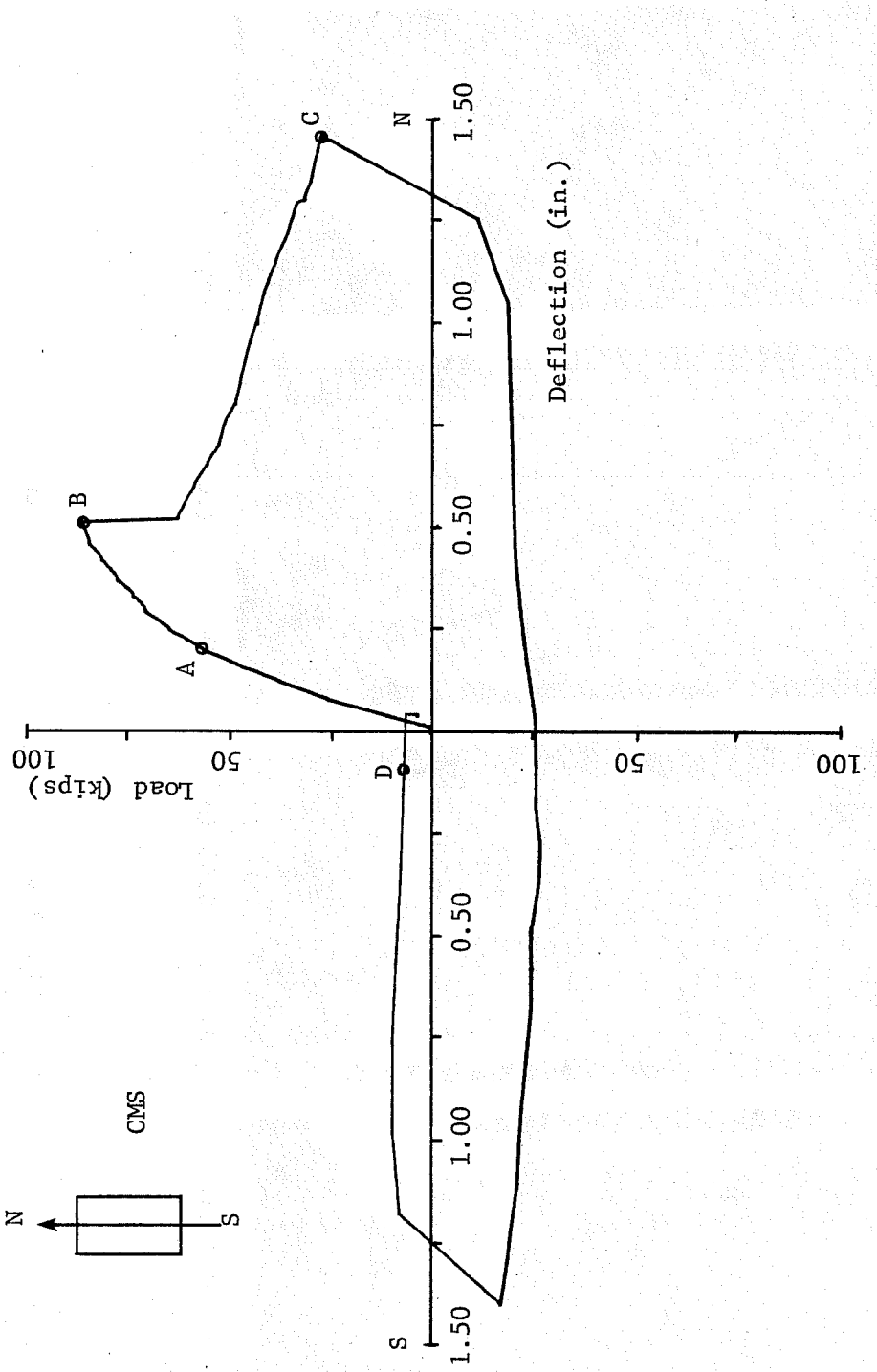

Fig. 4.7 Load-deflection curves, specimen CMS

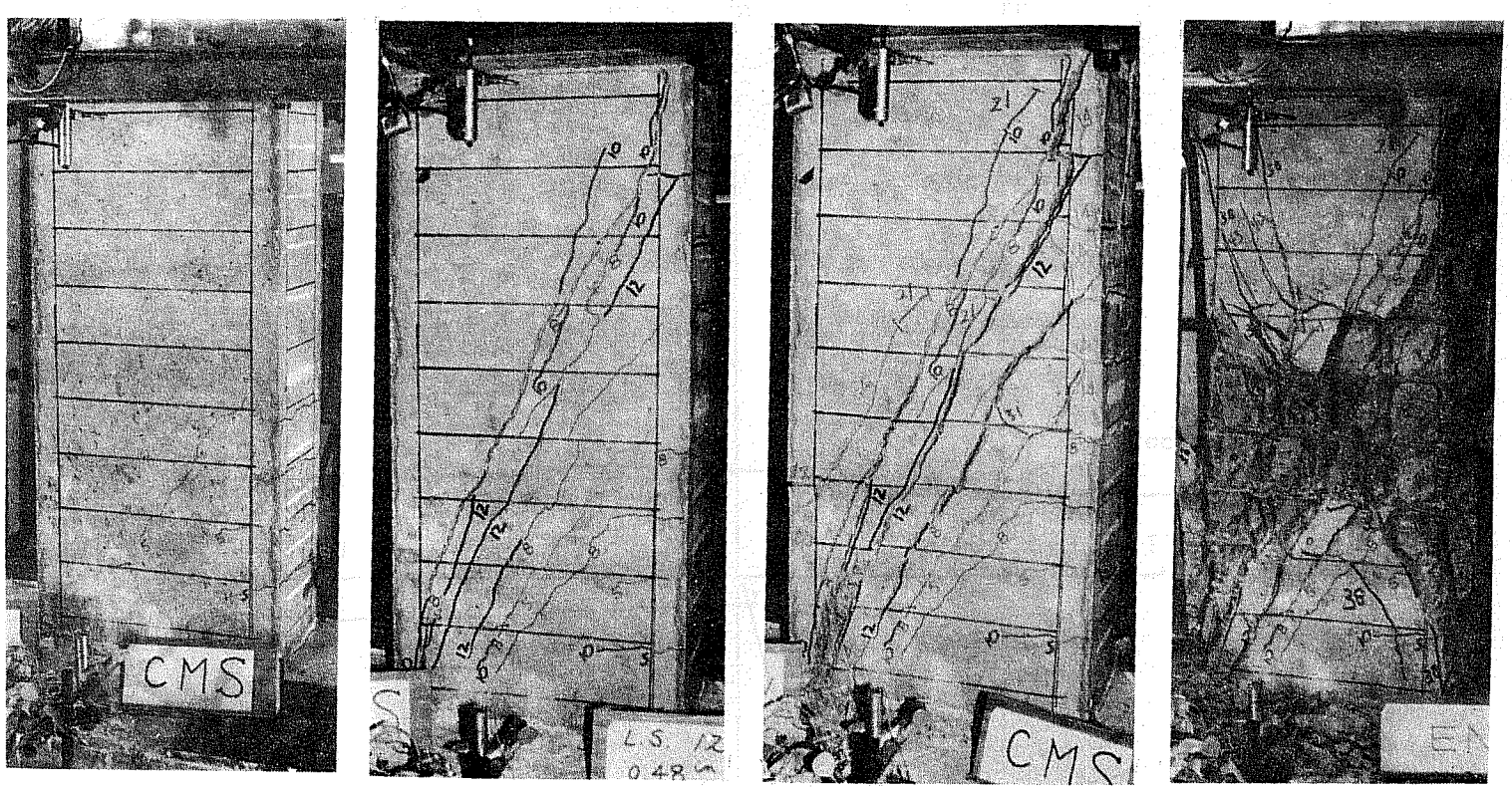

(A) 0.2 in. (B) 0.48 in. (C) 1.4 in. (D) End

Fig. 4.8 Crack patterns, specimen CMS

specimen at the end of the test is shown in Fig. 4.8(d). One inclined crack with an angle of around 45^{o} and a few flexural cracks were noted at a deflection of 0.2 in., but at a deflection of 0.48 in., several diagonal cracks extended from the top to bottom of the column along a diagonal. The angle of these cracks was around 30^{o}, because the axial compressive load caused the angle of the cracks to be steeper. At peak deflection (1.4 in.), the inclined cracks indicated a severe damage to the column. Under loading in the opposite direction, additional diagonal cracks formed and at the end of the test (Fig. 4.8(d)), spalling of the concrete cover occurred in the midheight region of the column.

4.5 Specimen CUS

The specimen was subjected to 120 kips axial compressive load and unidirectional loading in the strong direction (N-S). The first deflection limit was 0.2 in., the same as in the specimen OUS. For CMS strain at the intersection of the column and the end blocks was almost half of yield at the first deflection limit (1Δ) which was 0.2 in.

The load-deflection curve (Fig. 4.9) shows that maximum lateral load was reached at 2Δ in the north direction. At 2Δ, shear cracks opened. Strain in the longitudinal bars was 1200×10^{-6} at 1Δ, and 1700×10^{-6} at 2Δ. At maximum load, the longitudinal reinforcement did not yield. After the specimen reached maximum load in the north direction, it was deformed to the same deflection limit, 2Δ in the south direction. The load was less than that reached previou ly at 1Δ in the south direction. It appeared that once the maximum load in one direction was reached, load in the other direction decreased because of the shear cracks which formed previously. A very large drop in lateral load was observed between the first and second cycles

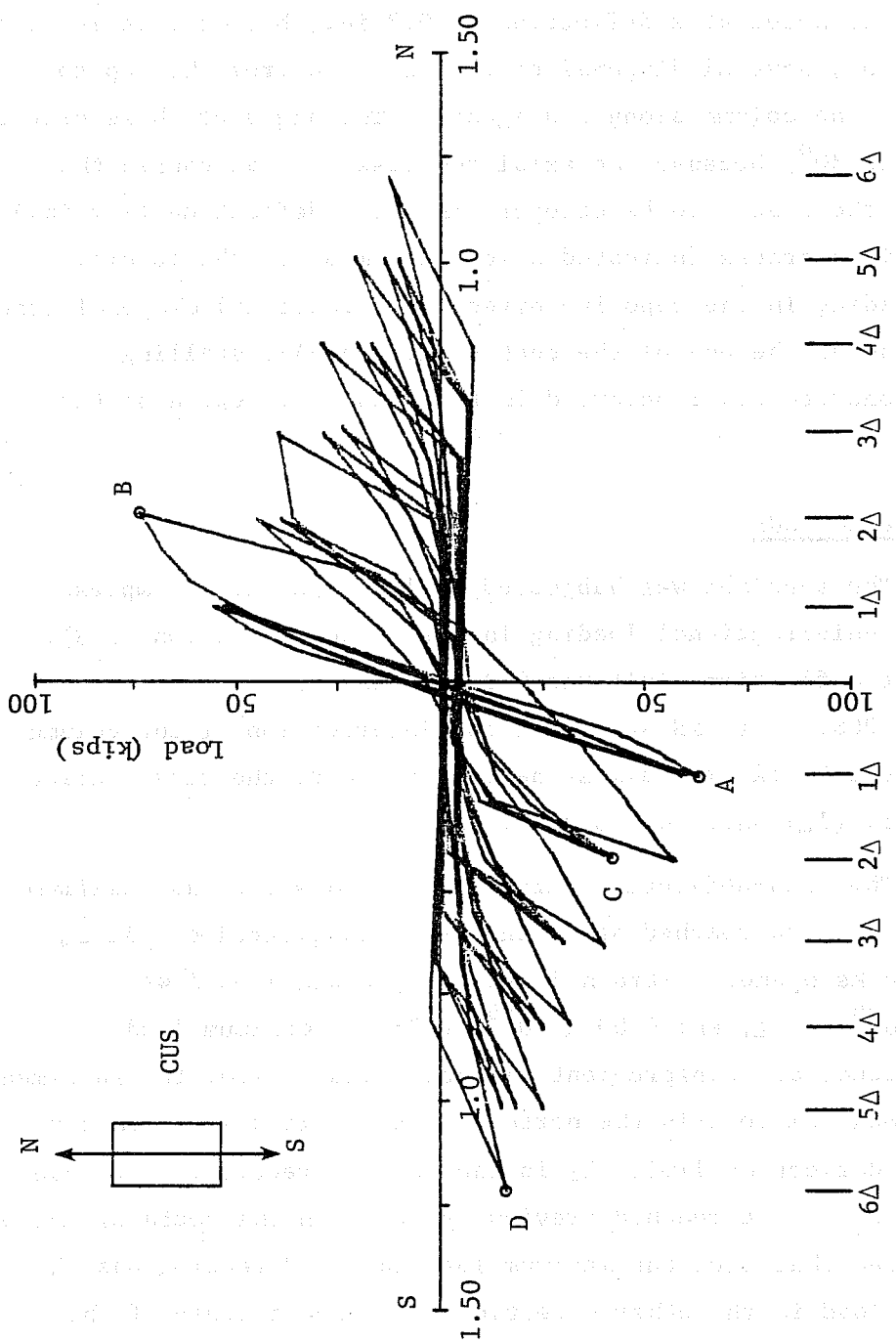

Fig. 4.9 Load-deflection curves, specimen CUS

at 2Δ. This phenomenon confirmed the severity of the damage due to the shear cracks. After reaching maximum load, the strength and stiffness of this specimen deteriorated rapidly.

Figure 4.10(a) shows the crack pattern in the east face at the end of cycling of 1Δ. The angle of initial diagonal cracks is around 45^{o}. Figure 4.10(b) shows the crack pattern in the east face at the maximum load. Some damaging inclined cracks formed from the top to bottom of the column. The angle of these cracks was around 30^{o}, almost the same as noted in specimen CMS. Figure 4.10(c) shows the crack pattern in the east face at the end of cycling at 2Δ. A large number of inclined cracks is visible in both directions causing severe damage. At the end of the test (Fig. 4.11(d)), spalling of the concrete cover was extensive in the midheight region of the column, but there was little damage to the ends of the column. The concrete around the longitudinal bars spalled and left the bars unbonded.

4.6 Specimen CUW

The specimen was loaded with 120 kips axial compression and unidirectional deformation in the weak direction (E-W); east direction first. The first deflection limit (0.16 in.) was the same as that for specimen OUW.

The load-deflection curves are shown in Fig. 4.11. The strain in the longitudinal bars at the intersection of the column and end blocks was around 900×10^{-6}, 1600×10^{-6}, and 1900×10^{-6} at 1Δ, 2Δ, and 3Δ, respectively. Maximum load was reached at 3Δ, with the longitudinal bars not yielding prior to reaching maximum load. The maximum load for OUW was reached at 5Δ. With axial compression, the maximum for CUW was reached at 3Δ, and the specimen deteriorated rapidly. In the first cycle at 4Δ in the

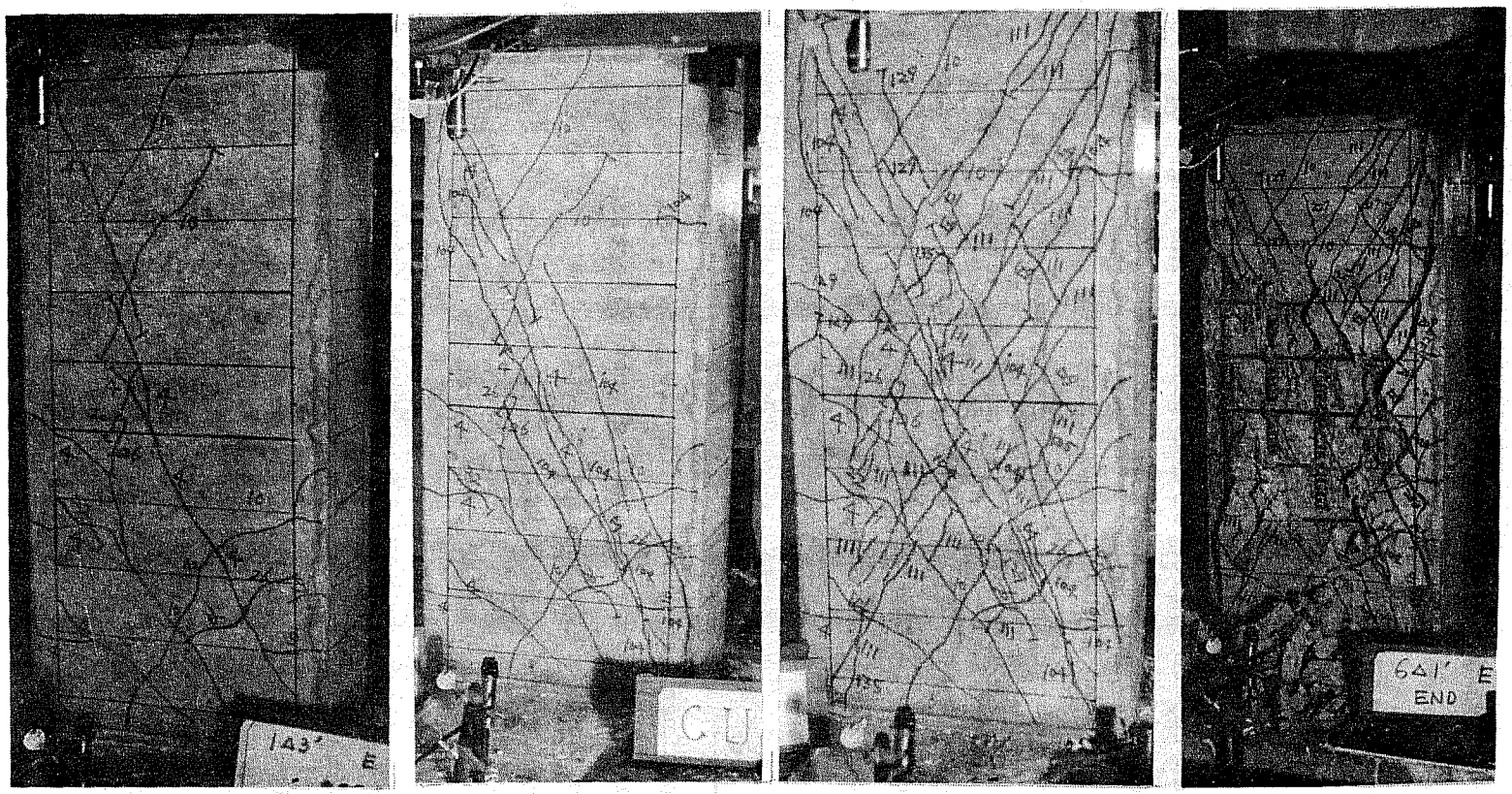

(A) 1Δ (B) 2Δ (S → N) (C) 2Δ (N → S) (D) End

Fig. 4.10 Crack patterns, specimen CUS

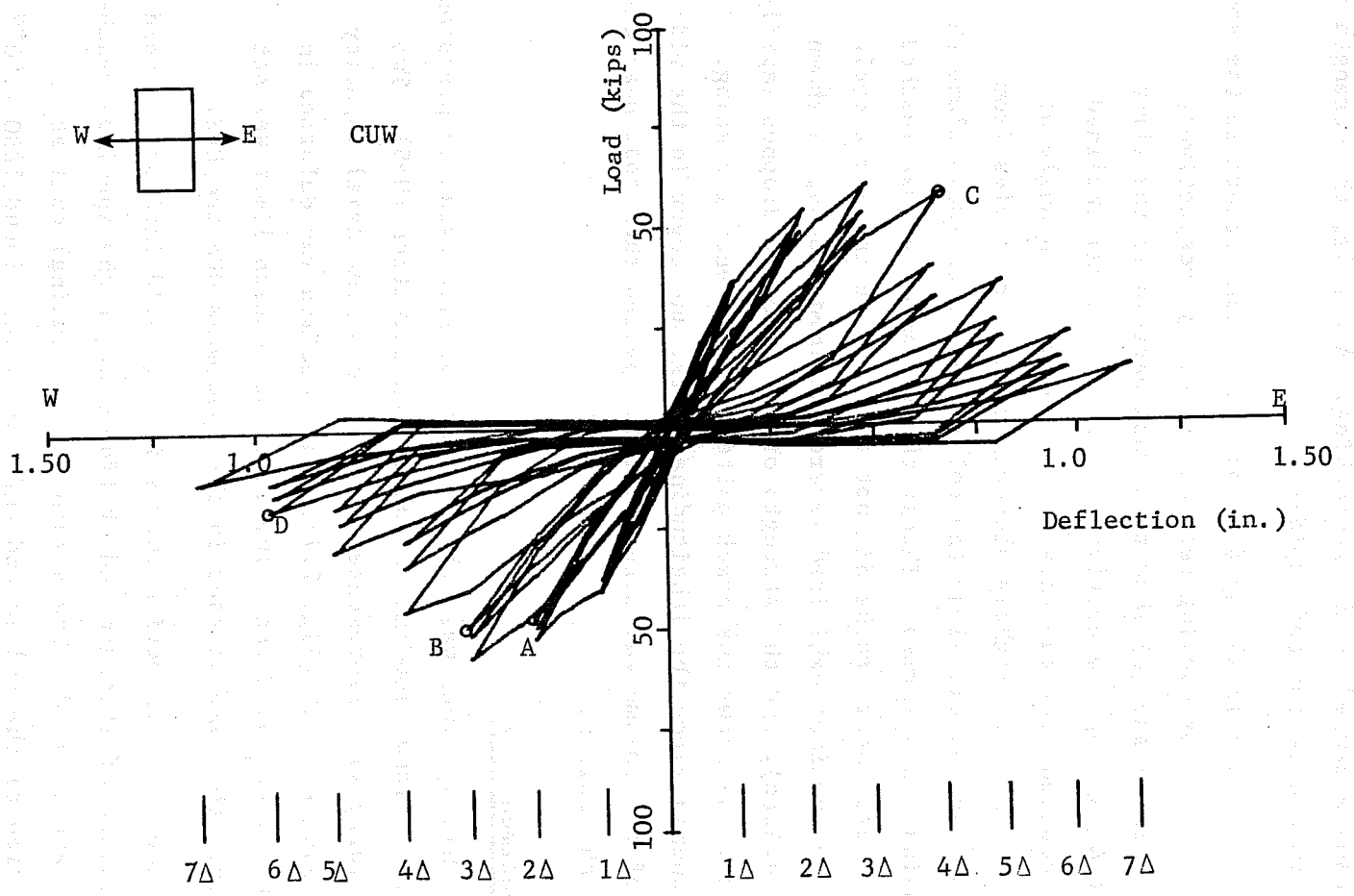

Fig. 4.11 Load-deflection curves, specimen CUW

east direction the load almost reached the previous peak. The load dropped rapidly between this cycle and the next because of the severe damage caused by shear cracking. After 4Δ, the strength of the specimen deteriorated rapidly.

Figures 4.12(a) and (b) show the crack pattern in the south face at the end of cycling between 2Δ and 3Δ, respectively. Figures 4.12(c) and (d) show the crack pattern in the first cycle at 4Δ and 6Δ, respectively. At 2Δ, several inclined cracks occurred near the ends of the column at an angle of about 45°. At 3Δ, slightly steeper cracks with angles from 40° to 45° spread all along the column and some cracks along the longitudinal bars formed. Though the maximum load was reached at 3Δ, severe shear cracks did not appear. In the first cycle at 4Δ, the specimen exhibited severe inclined cracks, as shown in Fig. 4.12(c), and the strength of the specimen dropped rapidly. Figure 4.12(d) shows the crack pattern at the end of testing. Cracks opened along the longitudinal bars, and cover in the mid-height of the column was more severely spalled than that near the ends of the column.

4.7 Specimen 2CUS

This specimen was subjected to 240 kips axial compression and unidirectional loading in the strong direction (N-S). Two hundred forty kips represented 80 percent of the axial capacity at the balance point (Fig. 2.7). The specimen was deformed in the north direction first. The first deflection limit was set as 0.2 in., the same as that in the specimens 0US and CUS.

The load-deflection curves in Fig. 4.13 indicate a rapid deterioration of strength and stiffness after the specimen reached maximum lateral load. The strain in longitudinal bars at the intersection of the column and end blocks was around 1200×10^{-6}

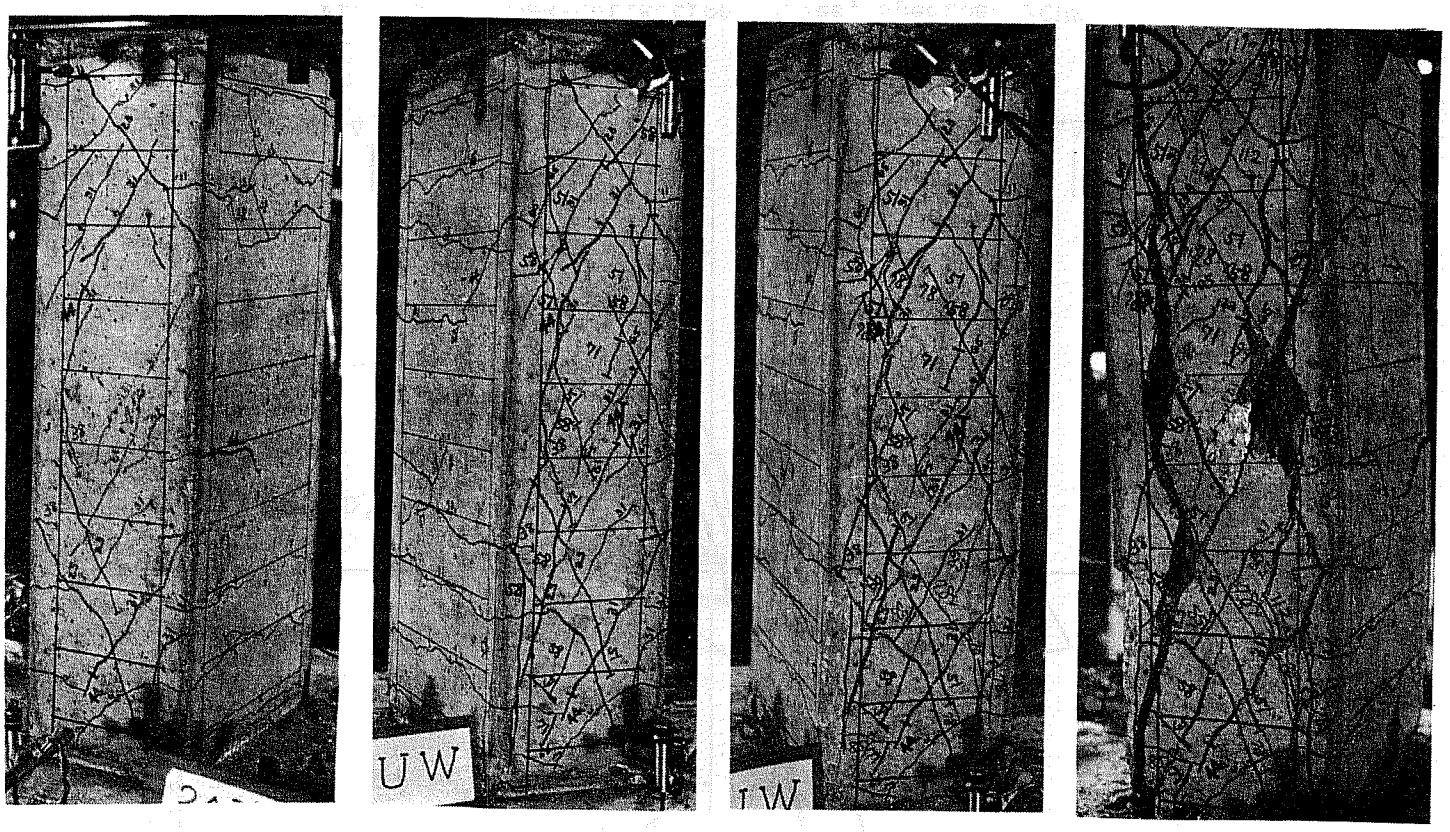

(A) 2Δ (B) 3Δ (C) 4Δ (D) 6Δ

Fig. 4.12 Crack patterns, specimen CUW

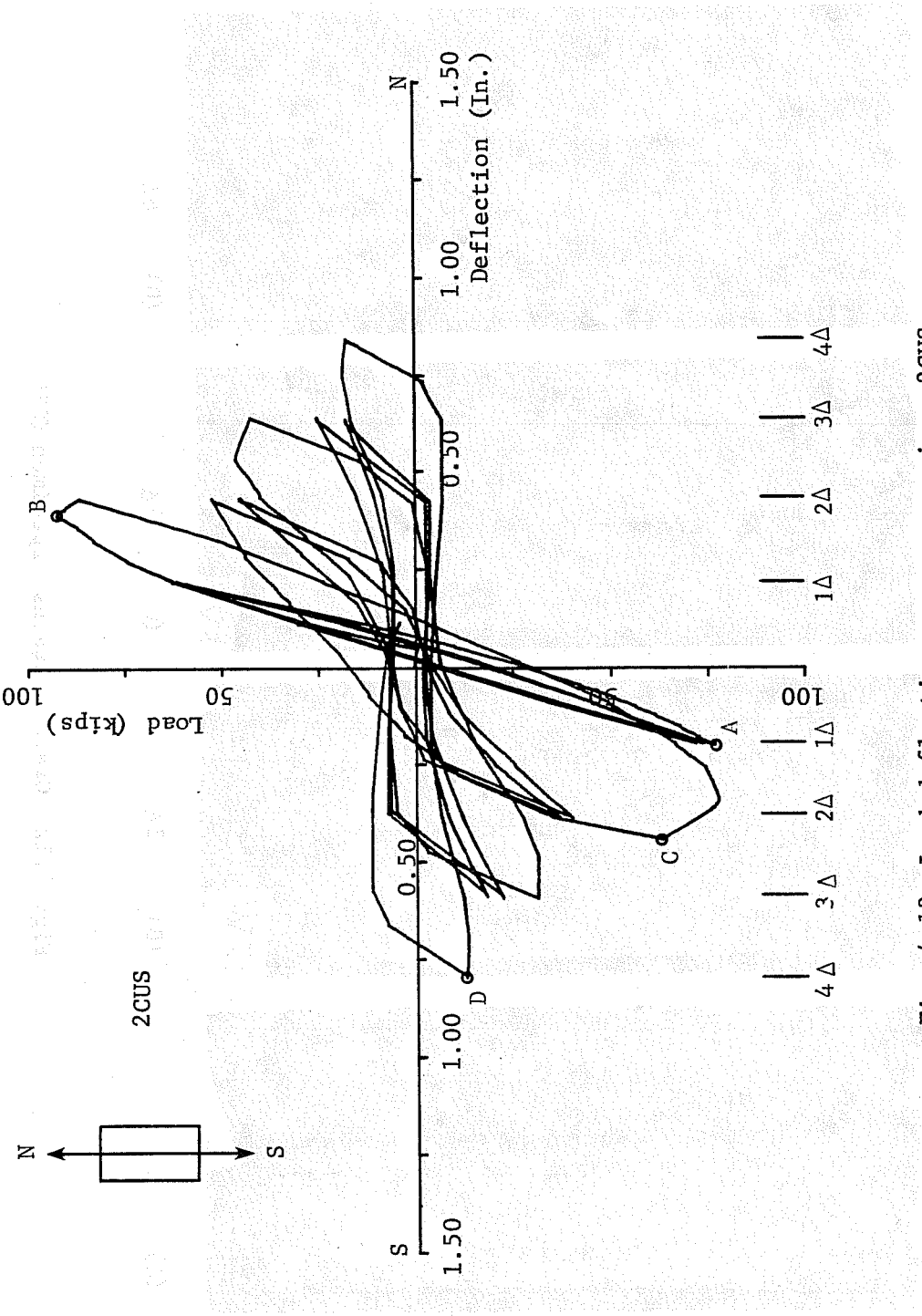

Fig. 4.13 Load-deflection curves, specimen 2CUS

at 1Δ and 1600 x 10^{-6} at 2Δ. The lateral load reached a maximum value at 2Δ without yielding in the longitudinal reinforcement. The remarkable drop in the lateral load between the first and second cycles at 2Δ was the result of severe damage due to shear cracking. The load dropped from a maximum at 2Δ to less than 1/3 of the maximum at 4Δ. High axial load increased degradation of the short column.

Figure 4.14(a) shows the crack pattern in the west face at the end of cycling to 1Δ. A few shear and flexural shear cracks occurred near the end of the column. In the north direction at the first cycle to 2Δ, several long diagonal cracks opened from the top to bottom of the column, as shown in Fig. 4.14(b). The angle of these cracks was around 30^{o}. Figure 4.14(c) shows the crack pattern in the south direction in the first cycle to 2Δ. Extensive diagonal cracks occurred in both directions, and severely damaged the specimen with a large drop in load between the first and second cycles to 2Δ. At the end of the test, Fig. 4.14(d), extensive spalling of the concrete cover was evident in the midheight of the column. Concrete near the ends of the column was relatively intact.

4.8 Specimen CDS30

The specimen was subjected to 120 kips axial compression and skewed unidirectional loading at 30^{o} from the strong axis of the column. The specimen was loaded in the northeast direction first. As mentioned in Sec. 2.3, when the deflection limit in one principal direction and the skew direction of loading are selected, the deflection limit in the other principal direction is also determined. In this case, the deflection limit (1Δ) in the strong axis was set at 0.2 in. and the limit in the direction 30^{o} from the strong direction was 0.2 in./cos 30^{o} = 0.23 in. A

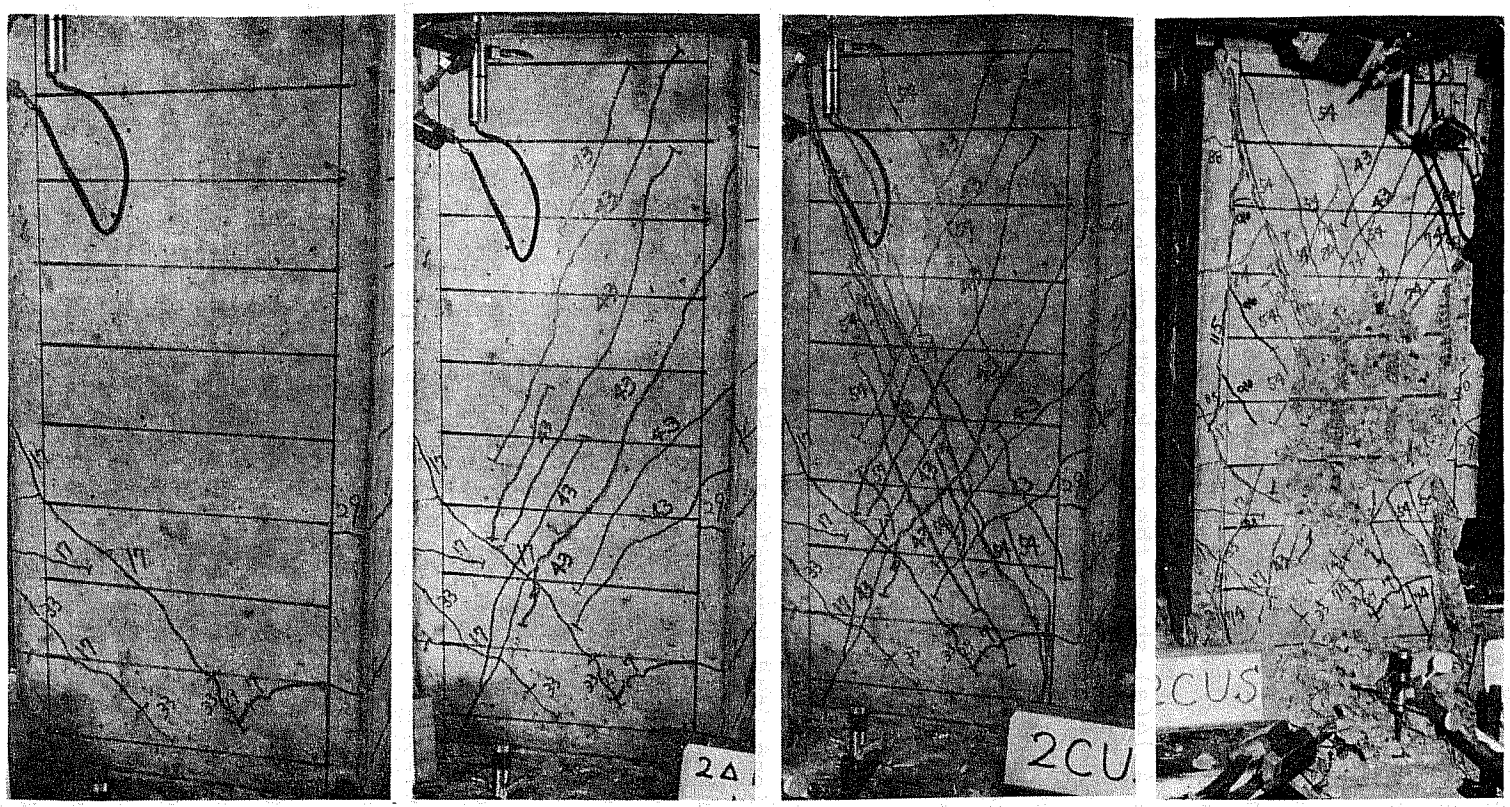

(A) 1Δ (B) 2Δ (S ⟶ N) (C) 2Δ (N ⟶ S) (D) End

Fig. 4.14 Crack patterns, specimen 2CUS

0.2 in. deflection in the strong direction corresponds to the deflection limit used in tests OUS and CUS.

The resultant load-deflection curves (along the diagonal), Fig. 4.15, show that the maximum lateral load was reached at around 2Δ. Strain in the longitudinal bars at the intersection of the column and end blocks was around 1500×10^{-6} at 1Δ and 2000×10^{-6} at 2Δ. No yielding occurred in the longitudinal reinforcement. There was a noticeable drop in the lateral load between the first and second cycles at 2Δ. After the maximum load at 2Δ, the stiffness and strength of the specimen decreased rapidly.

The crack pattern in the north and west faces at the end of cycling at 1Δ is shown in Fig. 4.16(a). There were a few flexural-shear and shear cracks near the end of the column. The angle of the shear cracks was around 45^{o}. Figure 4.16(b) shows the crack pattern when the maximum lateral load was reached. As the loading direction was diagonal, this figure shows that diagonal cracks were present from top to bottom of both faces. The angle of the cracks was around 30^{o} from the vertical indicating that the orientation of the crack pattern had changed. Figure 4.16(c) shows the crack pattern after the first cycle to 3Δ. Wide shear cracks opened and indicated severe damage to the column. At the end of the test, Fig. 4.16(d), the concrete cover spalled in the midheight of the column and the reinforcement was left unbonded.

4.9 Specimen CDW30

The specimen was subjected to 120 kips axial compression and unidirectional loading along a diagonal at 30^{o} from the weak direction. The specimen was loaded first in the northeast direction. The behavior of the specimen loaded at 30^{o} from

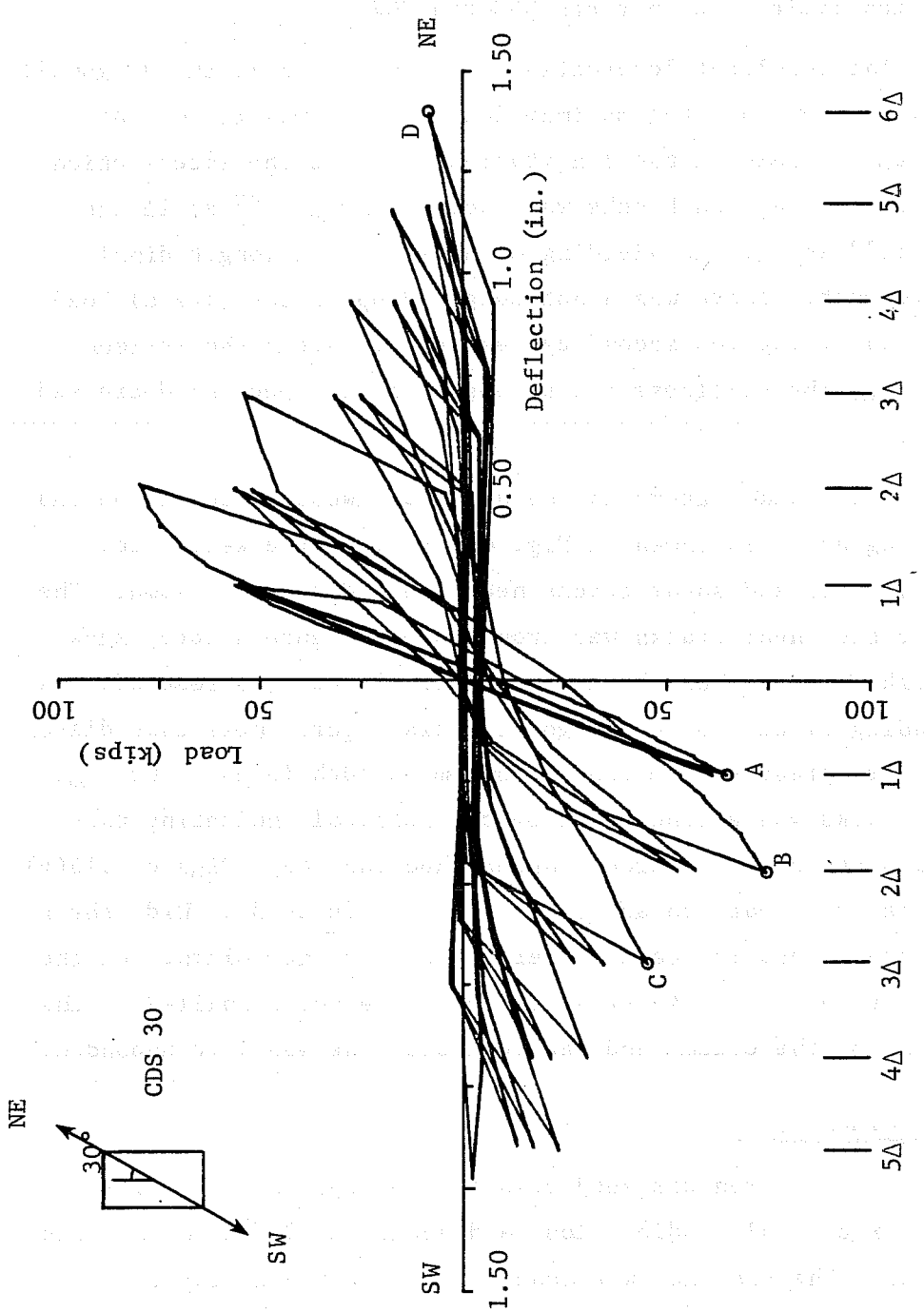

Fig. 4.15 Load-deflection curves, specimen CDS30

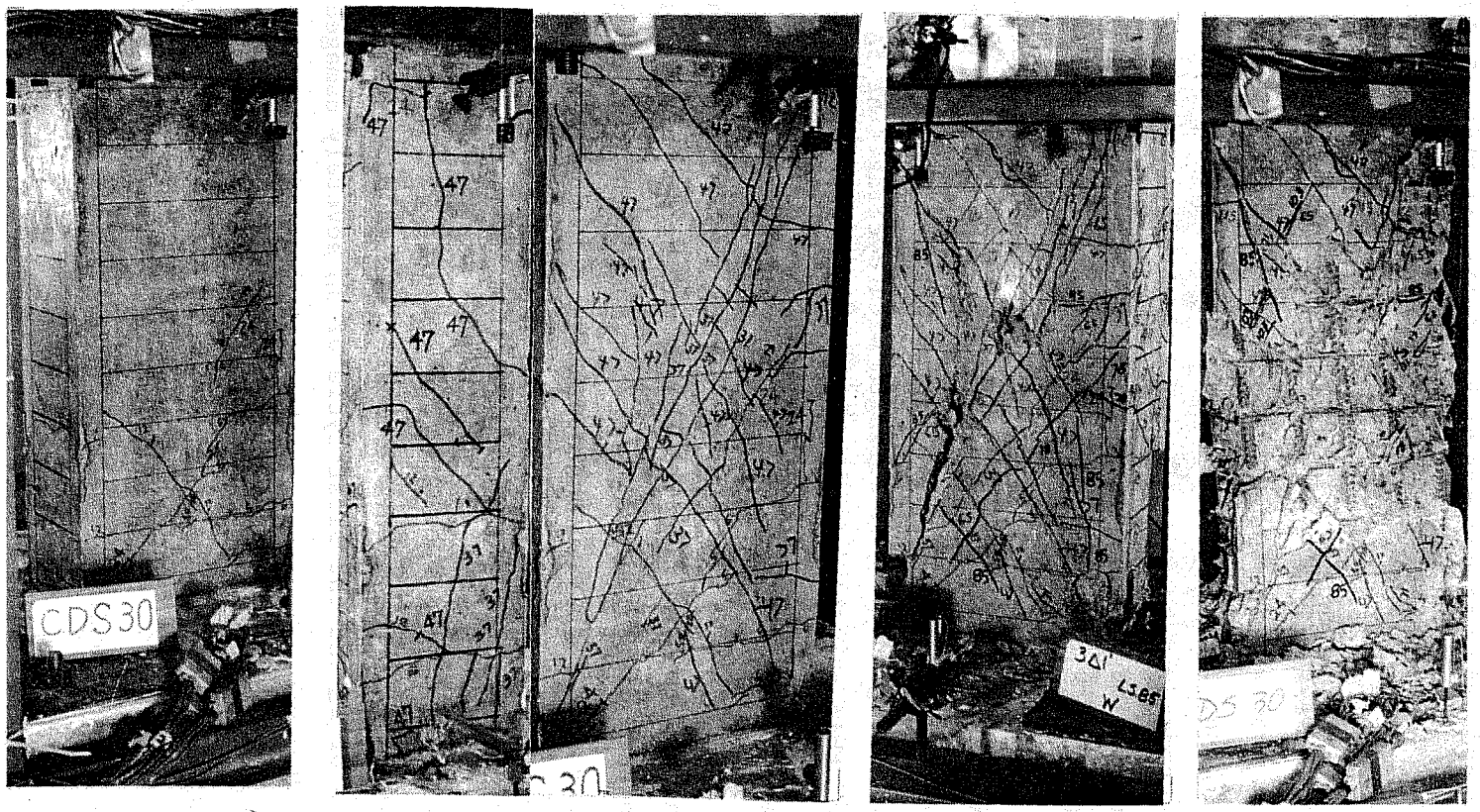

(A) 1Δ (B) 2Δ (C) 3Δ (D) End

N face W face

Fig. 4.16 Crack patterns, specimen CDS30

the weak principal axis was assumed to be similar to that of the specimen loaded in the weak direction. The deflection limit (1Δ) was 0.16 in./cos30° = 0.185 in.

Load-deflection curves are shown in Fig. 4.17. The maximum lateral load was reached at 2Δ. There was a small drop in lateral load between the first and second cycles at 2Δ and almost the same drop between the second and third cycles at 2Δ. Strain in the longitudinal bars at the end of the column was around 1200 x 10^{-6} at 1Δ and 2000 x 10^{-6} at 2Δ was reached. Before maximum load, the load-deflection loop was full indicating flexural behavior and little loss of strength with cycling. After maximum load was reached, the curves became pinched toward the origin and showed degradation of strength with cycling. At 5Δ the strength of this specimen deteriorated almost to zero.

Figures 4.18(a) through (d) show the crack pattern on the south and east faces at the end of cycling to 1Δ, 2Δ, 3Δ, and 5Δ. At 1Δ, there were some flexural cracks on the south and east faces near the ends of the column. At 2Δ, diagonal cracks extended along the entire east face. On the south face, diagonal cracks were located near the ends of the column. The angle of the cracks was around 30° on the east face and around 45° on the south face. The load-deflection curve showed that the strength was less in the first cycle of 3Δ than at 2Δ. The shear cracks observed between the end of 2Δ and the first cycle of 3Δ severely damaged the specimen. However, the shear cracks did not open. At 3Δ a section of the cover near the midheight of the column spalled off and long shear cracks opened. At 5Δ the concrete cover around the longitudinal bars in the midheight of the column spalled and these bars were unbonded.

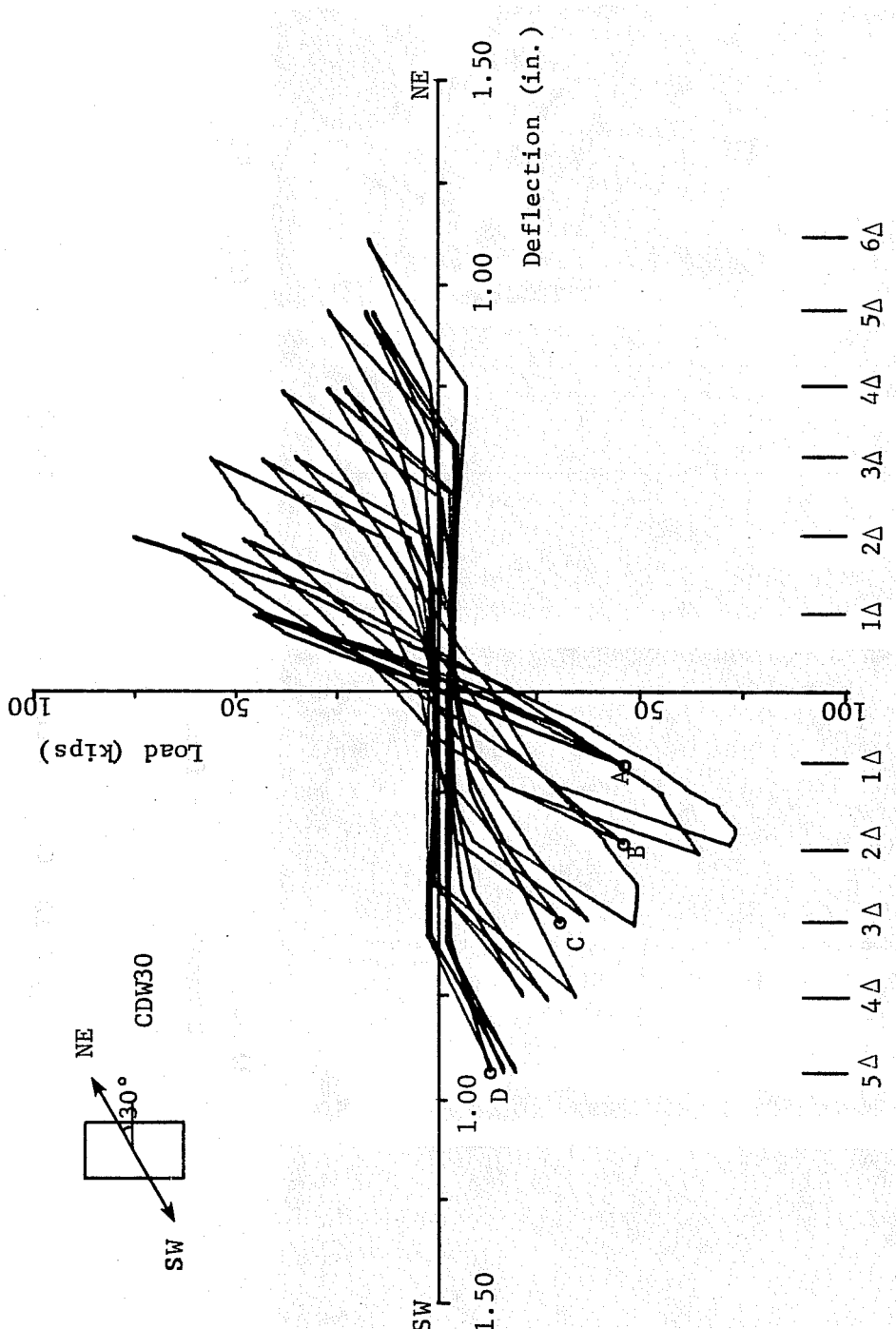

Fig. 4.17 Load-deflection curves, specimen CDW30

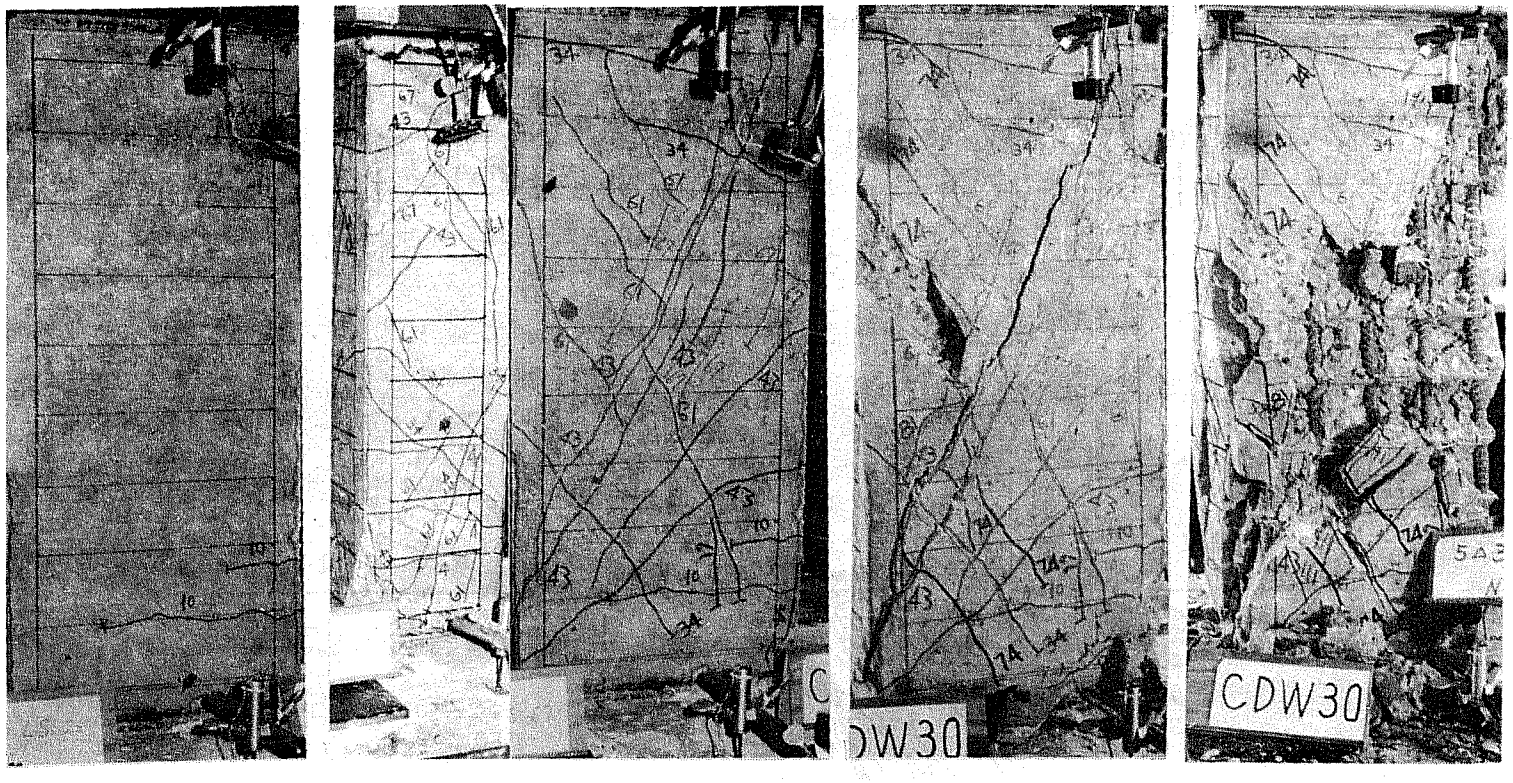

(A) 1Δ (B) 2Δ (C) 3Δ (D) 5Δ

S face E face

Fig. 4.18 Crack patterns, specimen CDW30

4.10 Specimen CBSW

The specimen was subjected to 120 kips axial compression and bidirectional loading alternately in the principal directions at each deflection level. In testing CUS (unidirectional loading in the strong direction) the maximum lateral load occurred at 2Δ, while in the specimen CUW (unidirectional loading in the weak direction) the maximum lateral load occurred at 3Δ. To try to reach maximum load in both directions at about the same deflection level, the specimen was deformed in the weak direction first. The order of loading was always weak (east direction first)-strong (north deflection first) at each deflection level. The deflection limit at 1Δ was 0.16 in. for the weak direction and 0.2 in. for the strong direction. These limits were the same as in CUW and CUS.

The load-deflection curves are shown in Fig. 4.19 (E-W) and in Fig. 4.20 (N-S). The maximum lateral load was reached at 2Δ in both the weak and strong directions. Although specimen CUW reached the maximum load at 3Δ, the maximum load was reached at 2Δ in the strong direction in CBSW and strength in the weak direction was reduced by the presence of shear cracks which formed at 2Δ under loading in the strong direction. Strain in the longitudinal bars at the ends of the column was 900×10^{-6} in the weak direction and 1300×10^{-6} in the strong direction at 1Δ, and 1400×10^{-6} in the weak direction and 1800×10^{-6} in the strong direction at 2Δ. The strain readings showed that the weak direction could have reached higher levels if the specimen had not been damaged by the loading in the strong direction. In the strong direction the drop in the lateral load occurred between the first and second cycles at 2Δ and 3Δ, while in the weak direction there was not a big drop between the first and

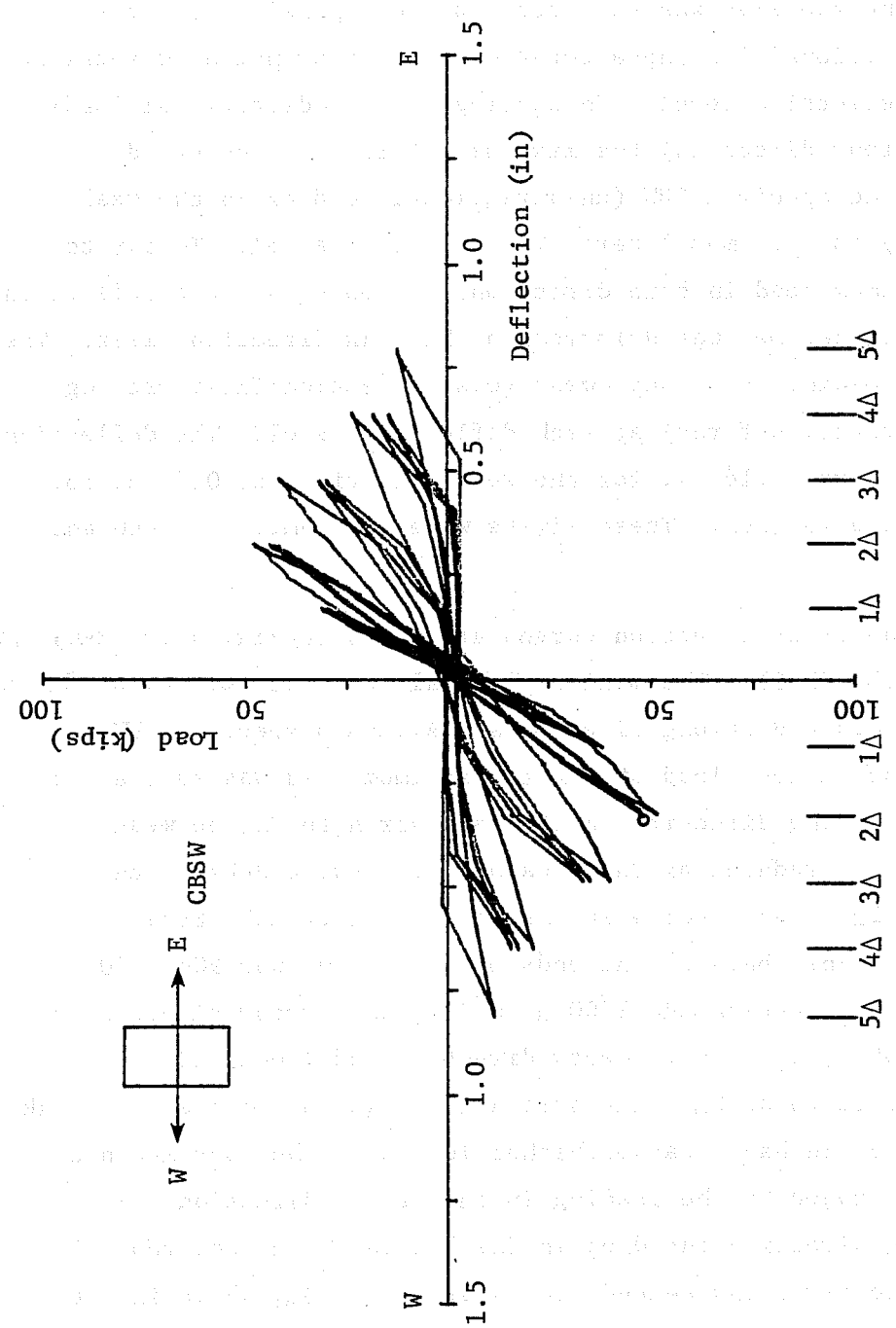

Fig. 4.19 Load-deflection curves, specimen CBSW (E-W)

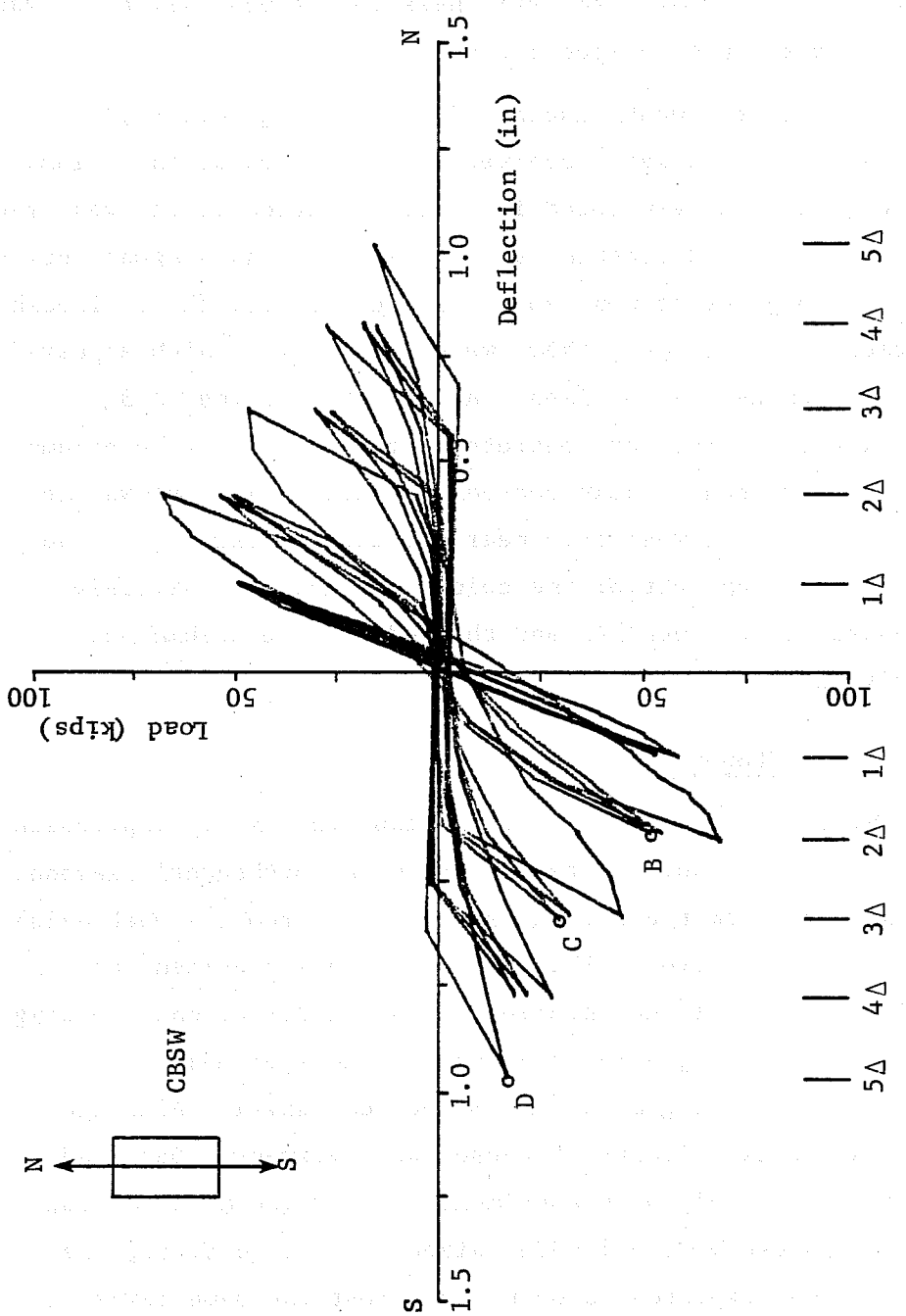

Fig. 4.20 Load-deflection curves, specimen CBSW (N-S)

second cycles at 2Δ and 3Δ. After maximum load was reached, the deterioration of strength and stiffness in the weak direction was rapid in comparison with specimen CUW.

At 2Δ in the weak loading direction (Fig. 4.21(a)), flexural shear cracks were observed near the ends of the column and diagonal cracks were noted from top to bottom of the west face. At 2Δ in the strong direction (Fig. 4.21(b)), many diagonal cracks formed all along the column especially on the west face. Though these cracks did not open, there were many cracks which appeared to severely damage the specimen. At the end loading to 3Δ (Fig. 4.21(c)), a piece of concrete in the middle of the column spalled off and shear cracks opened. Figure 4.21(d) shows the crack pattern on the west face near the end of testing. It was clear that the midheight of the column was the most severely damaged part of the specimen and the ends of the column were relatively intact.

4.11 Specimen CDSW30

The specimen was subjected to 120 kips axial compression and bidirectional loading alternately in the orthogonal diagonal directions (30^{o} from the strong axis and 30^{o} from the weak axis) at each deflection level. The loading of this specimen was compared with that of the specimen CDS30 (unidirectional loading at 30^{o} from the strong axis) and that of the specimen CDW30 (unidirectional loading at 30^{o} from the weak axis). Although the first deflection limits of these two specimens (CDS30 and CDW30) were different, both specimens reached the maximum load at 2Δ. Regardless of the loading direction chosen first, the maximum load was expected to occur at almost the same level in each direction. In specimen CDSW30, after the maximum load in a

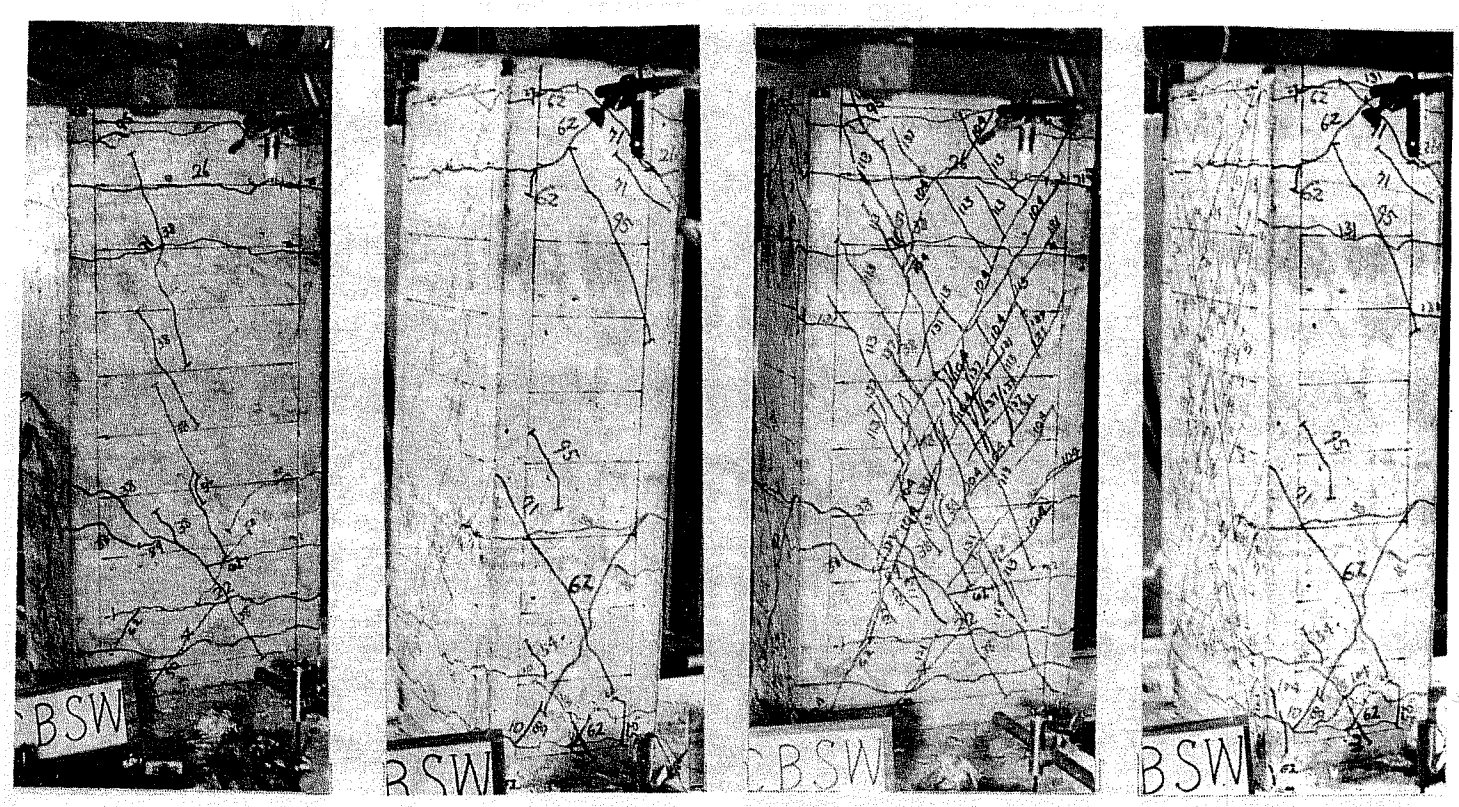

(A) 2Δ (E⟶ W)

W face

N face

(B) 2Δ (N⟶ S)

W face

N face

Fig. 4.21 Crack patterns, specimen CBSW

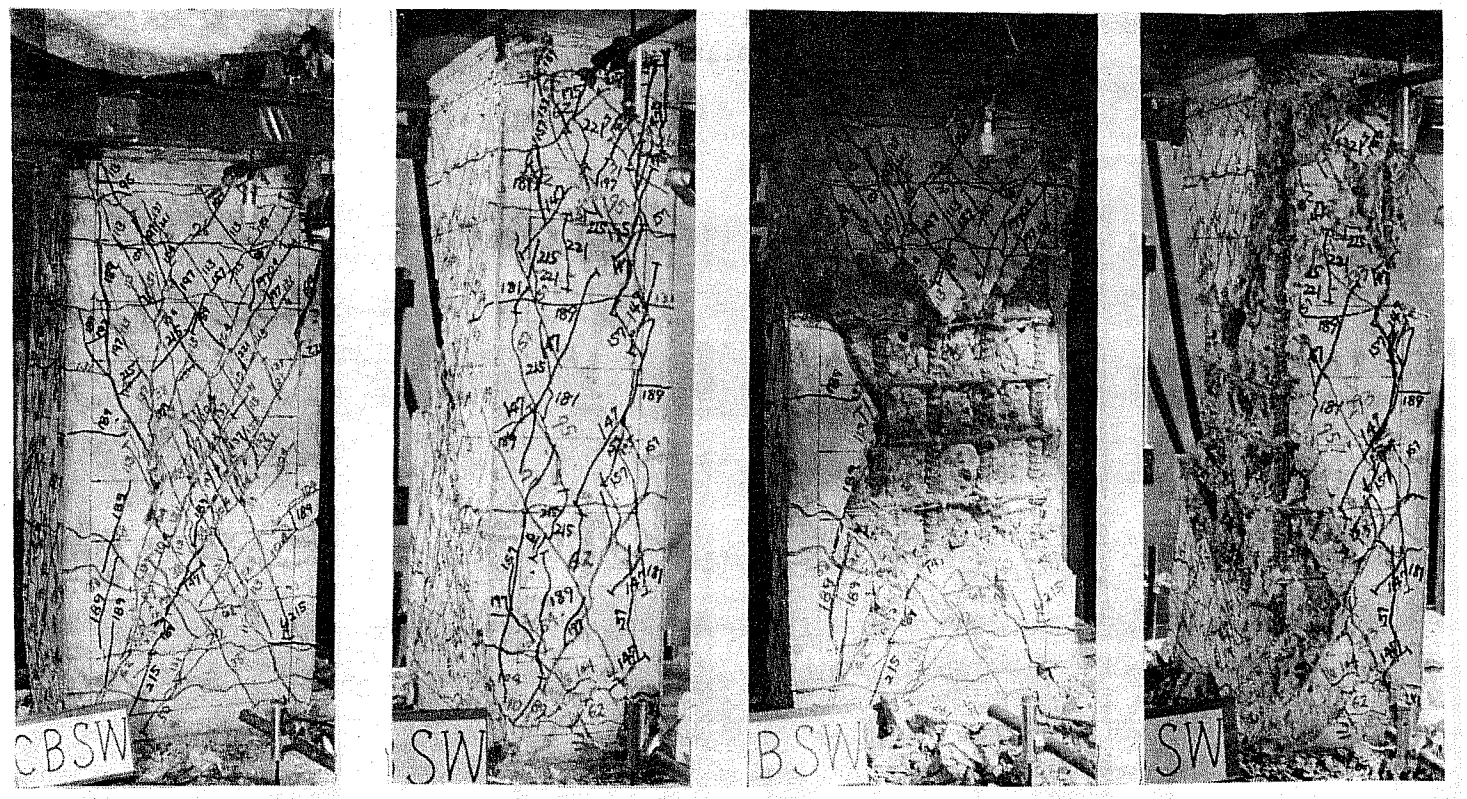

(C) 3Δ (N ⟶ S)

W face

N face

(D) 5Δ (N ⟶ S)

W face

N face

Fig. 4.21 Crack patterns, specimen CBSW (continued)

direction 30° from the weak axis (this direction is nearer the weak axis) was achieved at 2Δ, it was of interest to determine whether the load at 2Δ in a direction 30° from the strong axis (this direction is nearer the strong axis) dropped from the load at 1Δ. Thus, the specimen was deformed in a direction 30° from the weak axis first. In order to compare the behavior with CDS30 and CDW30, the first deflection limit was set as 0.185 in. for 30° from the weak direction and as 0.23 in. for 30° from the strong direction.

The resultant load-deflection curves are shown in Fig. 4.22 (SW-NE; 30° from the weak direction; northeast direction first) and in Fig. 4.23 (SE-NW; 30° from the strong direction; northwest direction first). The maximum load was reached at 2Δ in a direction 30° from the weak axis, while the maximum load was reached at 1Δ in a direction 30° from the strong direction. However, in the latter case, the load at 2Δ was only a little less than that at 1Δ and after 2Δ the load dropped rapidly. Shear cracks formed during loading in one direction reduced capacity in the other direction of loading. Strain in the longitudinal bars at the end of the column was 1200×10^{-6} in the direction 30° from the weak axis and 1600×10^{-6} in the direction 30° from the strong axis at 1Δ, and 1900×10^{-6} in the direction 30° from the weak axis and 1800×10^{-6} in the direction 30° from the strong axis at 2Δ. The strain at 2Δ in the direction 30° from the strong axis also showed only a little increase from the strain at 1Δ in the same direction to confirm the phenomenon in the load-deflection curves. After 2Δ in both loading directions, the strength and stiffness deteriorated more rapidly than under unidirectional loading (CDS30 and CDW30).

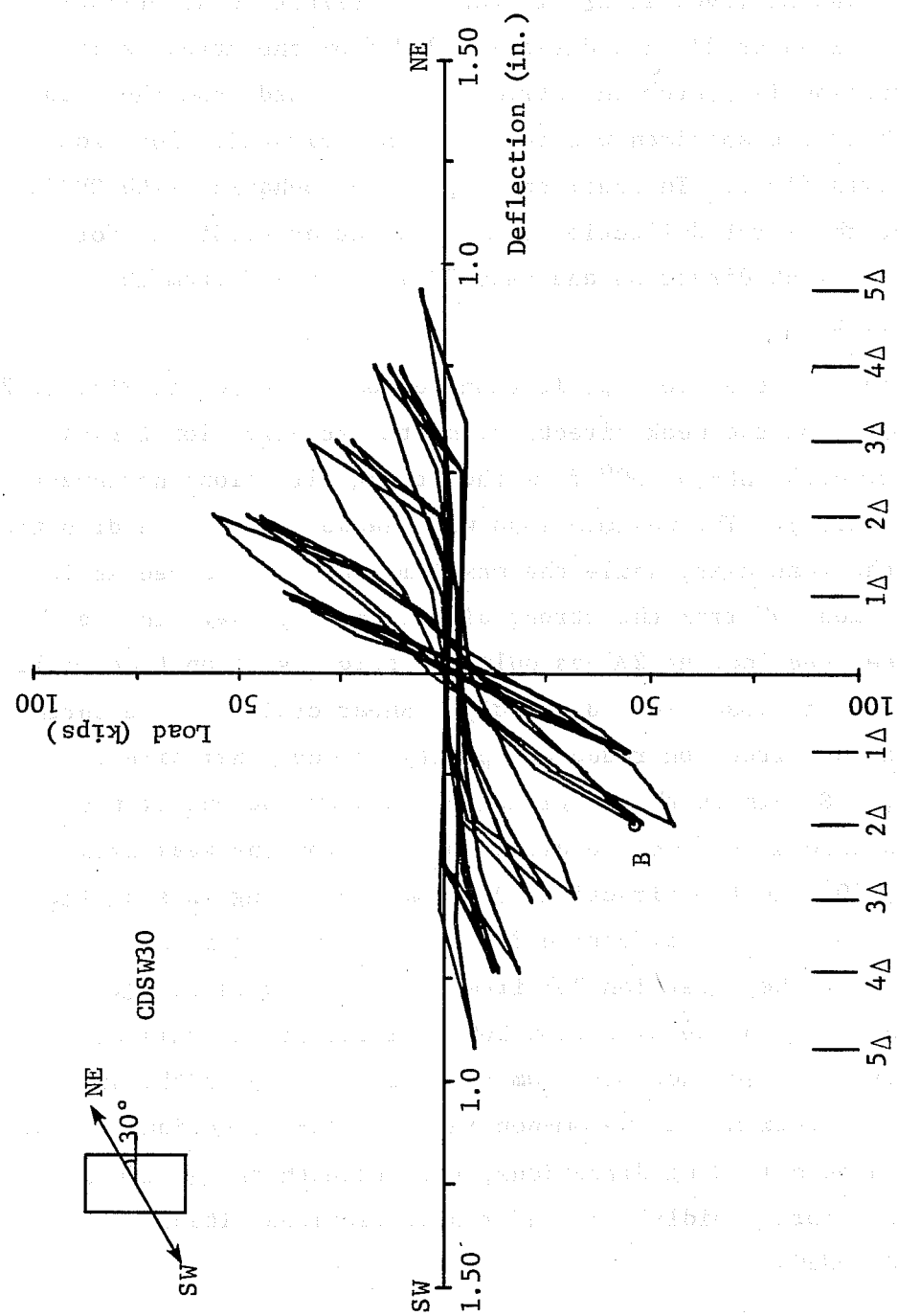

Fig. 4.22 Load-deflection curves, specimen CDSW30 (SW-NE)

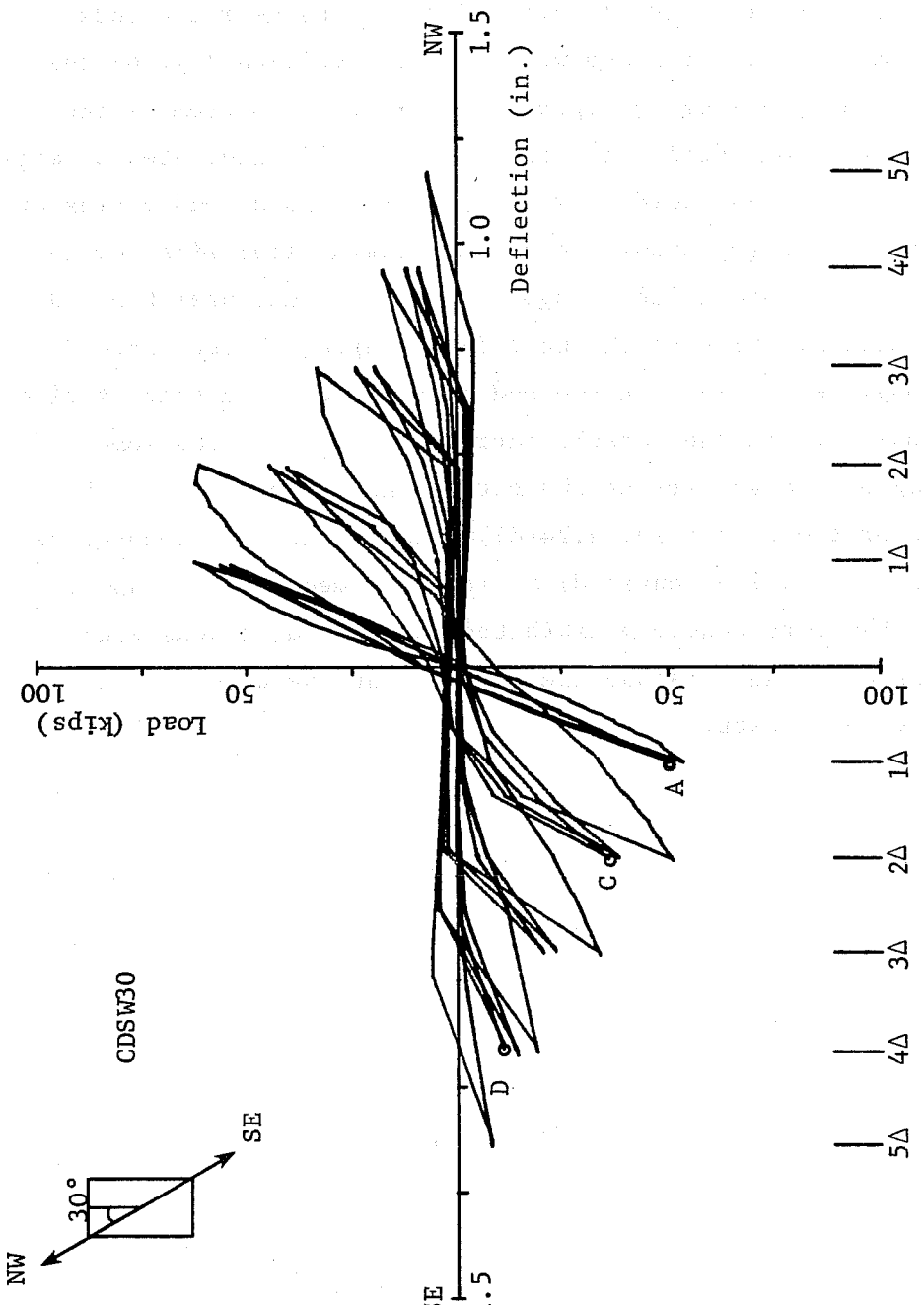

Fig. 4.23 Load-deflection curves, specimen CDSW30 (SE-NW)

Figures 4.24(a) through (d) show crack patterns on the north and west faces. At the end of cycling at 1Δ (Fig. 4.24(a)), there were flexural and flexural-shear cracks near the ends of the column on the north and west faces. Additionally, on the west face diagonal cracks appeared from top to bottom of the column. The load-deflection curve (Fig. 4.23) indicated a large drop in the lateral load between the first and second cycles at 2Δ. Figure 4.24(b) shows the crack pattern after first cycle to 2Δ. On the north face diagonal cracks spread near the ends of the column, while on the west face diagonal cracks spread all along the column. At the end of cycling to 2Δ (Fig. 4.24(c)), the number of diagonal cracks increased and there was some spalling of the corners at the bottom end of the column. By the end of the test (Fig. 4.24(d)), nearly all of the cover had spalled off and the longitudinal reinforcement was unbonded. Some of the core concrete exhibited large shear cracks and crushing or grinding along the cracks, but the core generally seemed to be intact.

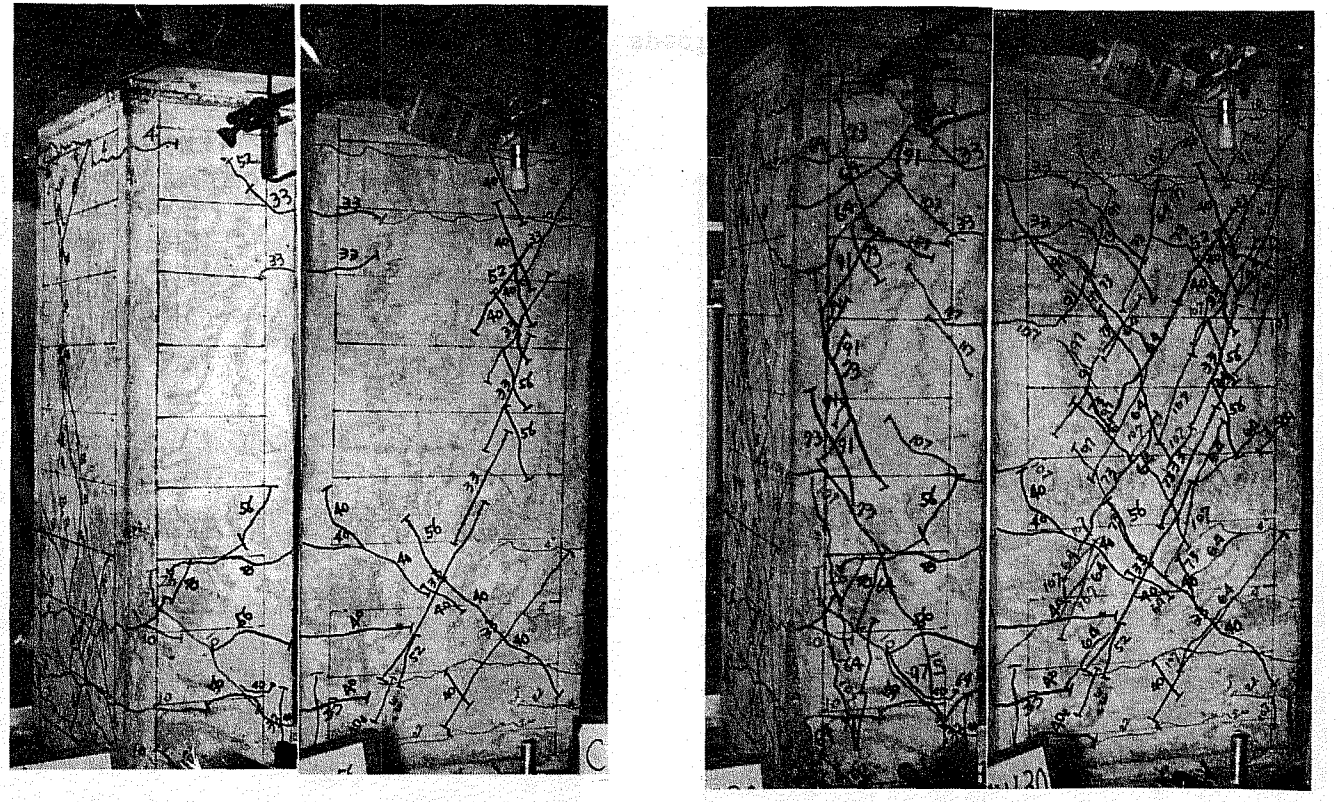

(A) 1Δ (NW ⟶ SW)

N face W face

(B) 2Δ (NE ⟶ SW)

N face W face

Fig. 4.24 Crack patterns, specimen CDSW30

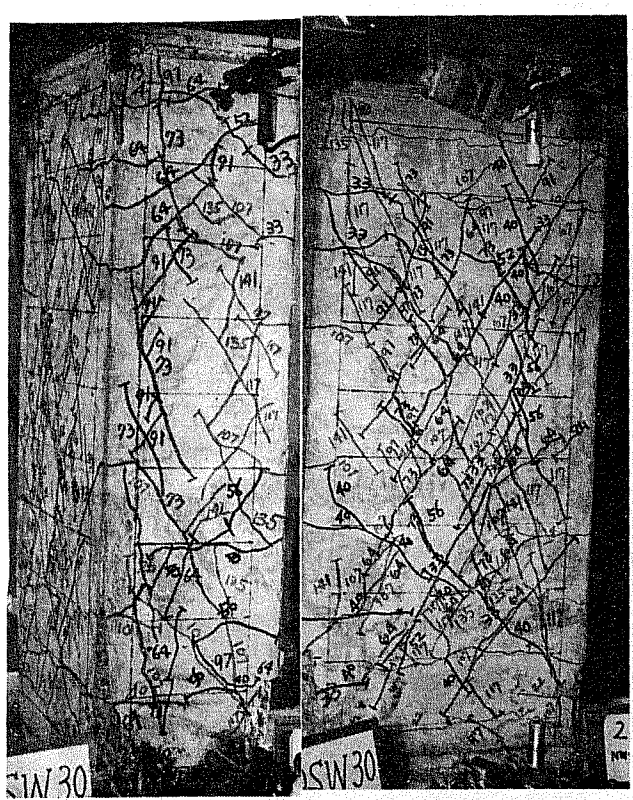

(C) 2Δ (NW ⟶ SE)

N face W face

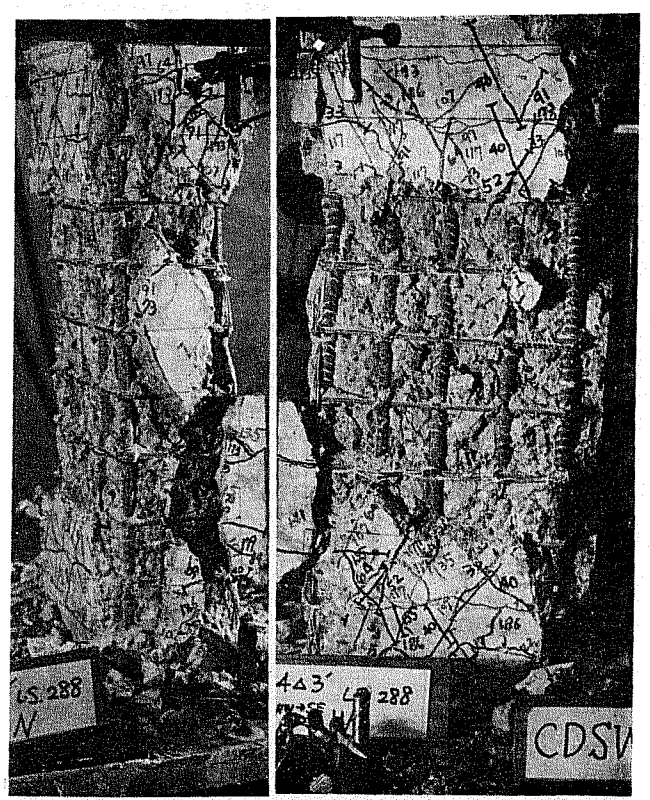

(D) 4Δ (NW ⟶ SE)

N face W face

Fig. 4.24 Crack patterns, specimen CDSW30 (continued)

CHAPTER 5

COMPARISON OF TEST RESULTS

5.1 General

In this chapter the data obtained for each specimen are arranged for comparison with other tests. Comparisons will be made using crack patterns, steel strains, lateral load capacity, and deterioration of strength. In Chapter 6, the comparison of results from rectangular columns will be compared with square columns.[22,23,24]

5.2 Crack Pattern

Typical crack patterns for the ten specimens were discussed in Chapter 4. Four types of idealized crack patterns are classified by loading direction and history. Idealized crack patterns for unidirectional and bidirectional loading in the principal direction are shown in Fig. 5.1. For unidirectional and bidirectional loading in the diagonal direction, idealized crack patterns are shown in Fig. 5.2. The patterns were developed using a crack inclination of 45^{o} with the direction of loading. Six specimens (OUS, OUW, CMS, CUS, CUW, 2CUS) are classified as unidirectional loading in the principal direction, two specimens (CUS30, CUW30) as unidirectional loading in the diagonal direction, and CBSW and CDSW30 as bidirectional loading in the principal and diagonal directions, respectively. A comparison of the observed crack patterns with the idealized patterns provides an indication of the validity of assuming a 45^{o} inclination.

5.2.1 Principal Loading Direction

5.2.1.1 Unidirectional Loading. Two comparisons for unidirectional loading in the principal direction are described

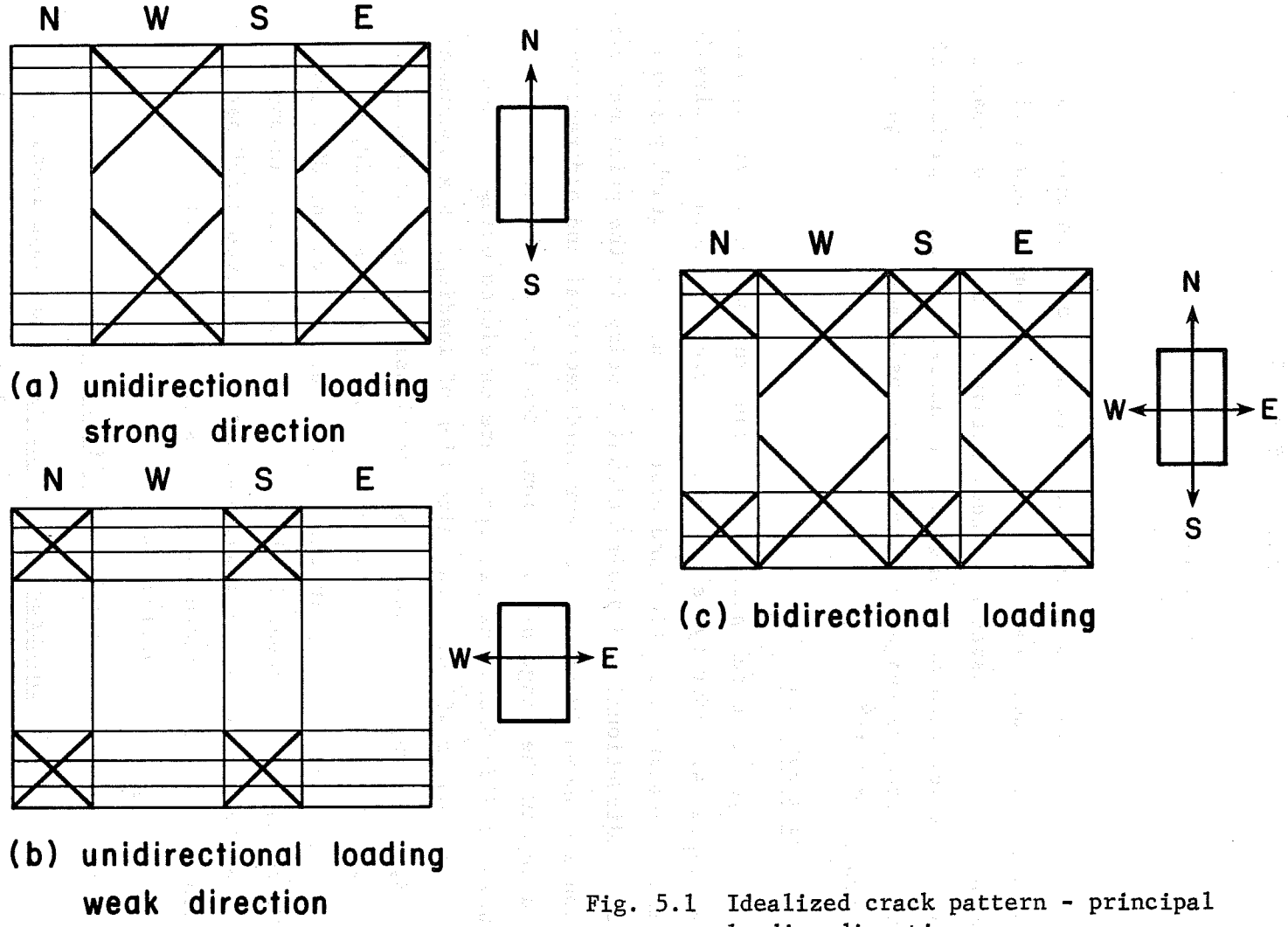

Fig. 5.1 Idealized crack pattern - principal loading direction

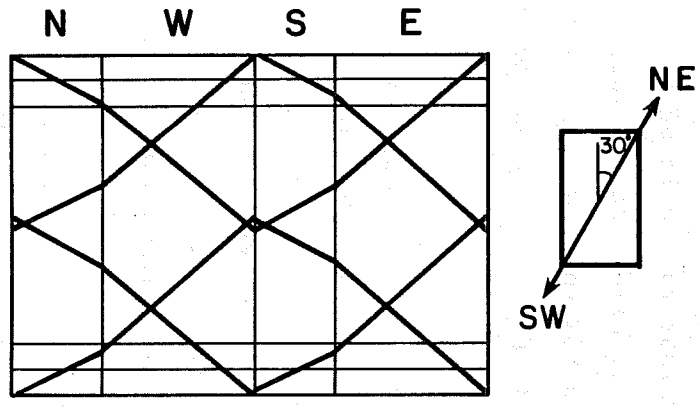

(a) unidirectional loading
30° from strong direction

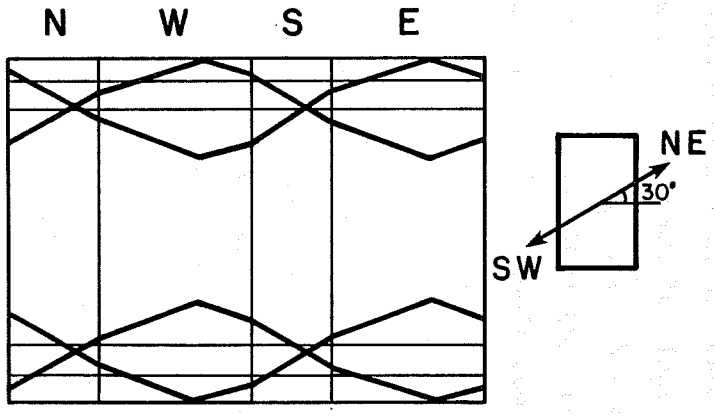

(b) unidirectional loading
30° from weak direction

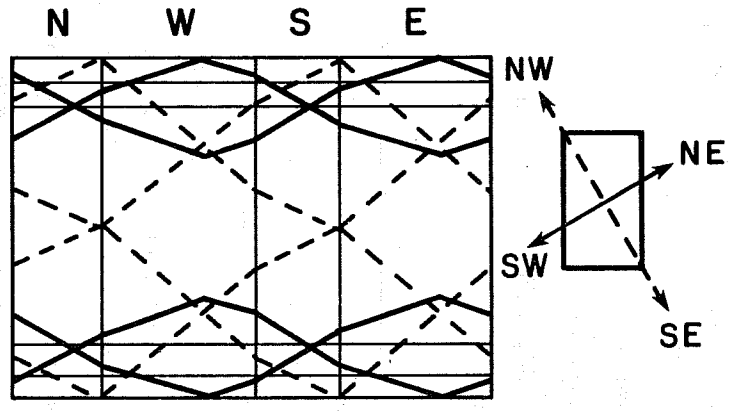

(c) bidirectional loading

Fig. 5.2 Idealized crack pattern - diagonal loading direction

in this section. First crack patterns for the specimens loaded in the strong direction (OUS, CUS) and in the weak direction (OUW, CUW) will be compared. Second, the effect of axial load on the crack patterns of two groups which have different loading directions (strong direction (OUS, CUS, 2CUS), and weak direction (OUW, CUW)) will be discussed.

Strong vs. Weak Loading Direction. Figure 5.3 shows crack patterns near maximum load for specimens OUS, CUS, OUW, and CUW. Figures 5.1(a) and (b) show the idealized crack pattern (45^{o} diagonal shear cracks and flexural cracks) for these specimens. For unidirectional loading in the strong direction (N-S), diagonal cracks were limited to the east and west faces. For unidirectional loading in the weak direction (E-W), diagonal cracks were limited to the north and south faces. Figures 5.3(a) and (b) (OUS and CUS) indicate that the angle of initial cracks was around 45^{o}, but near maximum load, shear cracks opened from top to bottom of the column with an angle of about 30^{o}. It was clear that the angle of initial cracking and cracking leading to failure was different. Figures 5.3(c) and (d) indicate that for specimens OUW and CUW, the crack pattern was almost the same as idealized in Fig. 5.1(b), but not for OUS and CUS.

Effect of Axial Load. Crack patterns at maximum load in specimens OUS, CUS and 2CUS are shown in Fig. 5.4. The angle of the most severe diagonal cracking extended from the top to bottom at the maximum load was 30^{o} to 35^{o} for each specimen. The angle appeared to be a little steeper as axial load increased. With higher axial load, shear cracks opened wider under similar levels of lateral deflections, and the concrete cover in the midheight region of the column spalled off at lower deflection levels. Figure 5.5 shows a comparison of the crack patterns for specimens OUW and CUW. In CUW, slightly steeper cracks with angles from 40^{o} to

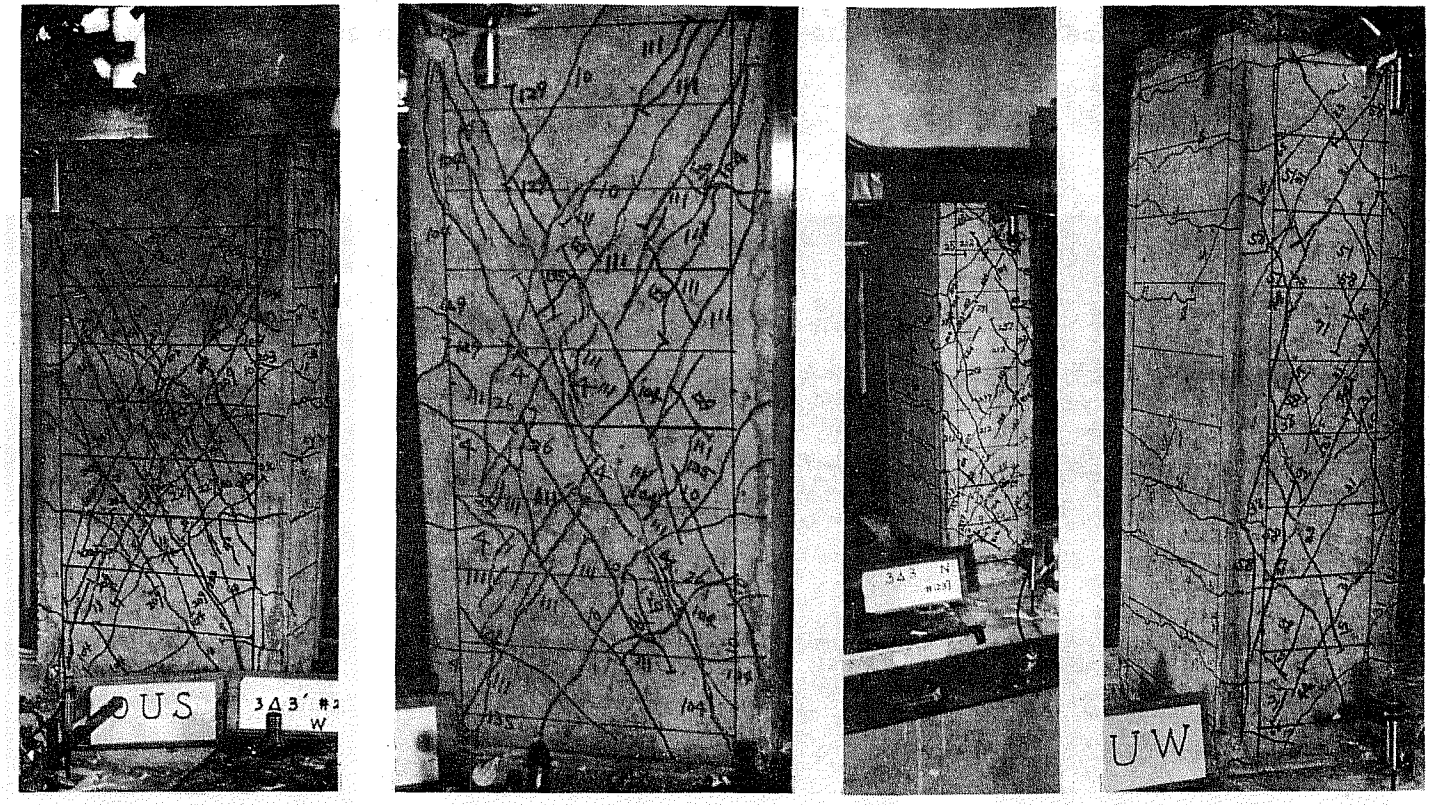

(a) OUS (3Δ) (b) CUS (2Δ) (c) OUW (5Δ) (d) CUW (3Δ)

Fig. 5.3 Crack patterns - strong vs. weak loading direction

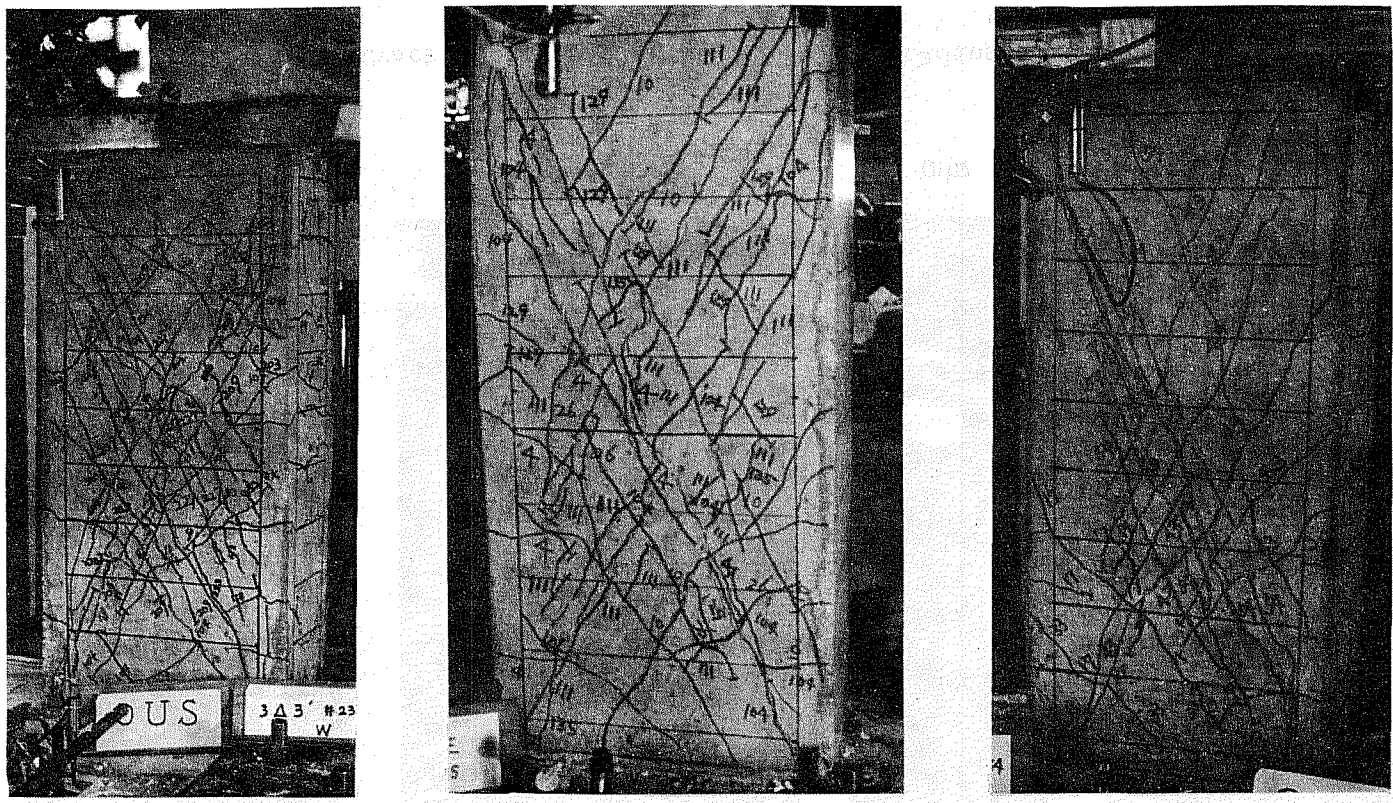

(a) OUS (3Δ) (b) CUS (2Δ) (c) 2CUS (2Δ)

Fig. 5.4 Effect of axial load on crack patterns (strong direction)

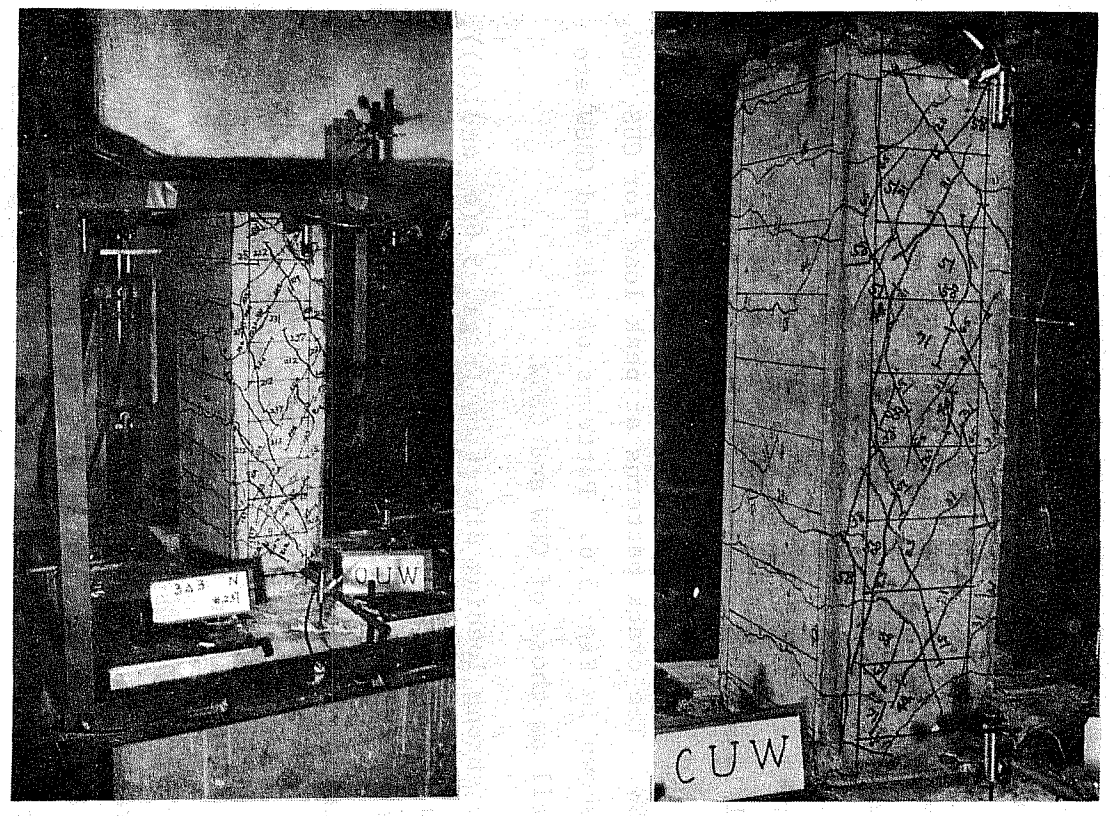

(a) OUW (5Δ) (b) CUW (3Δ)

Fig. 5.5 Effect of axial load on crack patterns (weak direction)

45^{o} opened around midheight of the column, and more cracks along the longitudinal reinforcement occurred with increasing axial compression. Once again with higher axial load, shear cracks opened wider and concrete cover spalled at lower deflection levels.

5.2.1.2 Unidirectional vs. Bidirectional Loading. In this section the influence of loading history (unidirectional or bidirectional loading in the principal direction) on the crack patterns is described. In Fig. 5.1, the idealized crack pattern of the specimen with bidirectional loading is a combination of cracking under unidirectional loading in the strong and weak directions. Therefore, the crack patterns of the specimens with unidirectional loading in the strong direction (specimen CUS) and in the weak direction (specimen CUW) are combined with the results of CBSW. The crack patterns at peak load for CUS, CUW, and CBSW are shown in Fig. 5.6. Patterns of CUS and CBSW are compared as well as those of CUW and CBSW.

In the strong loading direction (Figs. 5.6(a) and (b)), it can be seen that there are no differences in the crack angle leading to failure between CUS and CBSW, and almost the same amount of cracking occurred in both specimens.

In the weak loading direction (Figs. 5.6(c) and (d)), the angle of diagonal cracks in CBSW was similar to that in CUW, but more cracks occurred in CUW. However, after 3Δ (in CBSW the maximum load was already passed), more cracks formed along the longitudinal reinforcement in the north and south faces of CBSW, and the corner concrete spalled at earlier load stages than in CUW.

It was observed that the specimen with bidirectional loading deteriorated more rapidly than the specimen with unidirectional loading after maximum load was reached. The crack patterns

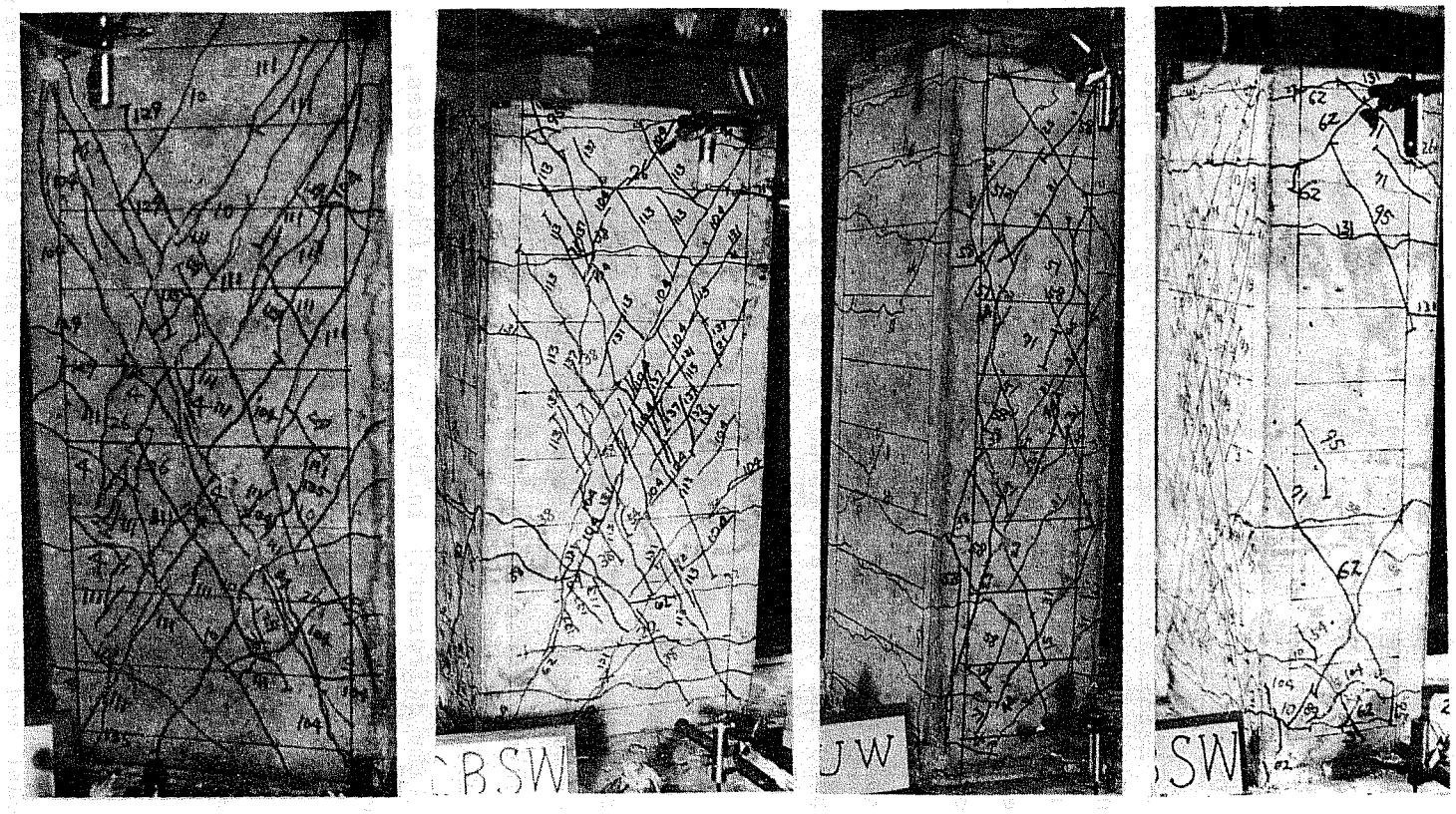

(a) CUS (2Δ) (b) CBSW (strong) (2Δ) (c) CUW (3Δ) (d) CBSW (weak) (2Δ)

Fig. 5.6 Crack patterns - unidirectional vs. bidirectional loading (principal direction)

were similar to the idealized patterns except the angle of inclination in the strong direction was steeper (30° vs. 45°) and cracks along longitudinal reinforcement in the weak direction occurred.

5.2.2 Diagonal Loading Direction

5.2.2.1 Unidirectional Loading. Two specimens were tested under unidirectional loading in the diagonal direction. In one, the loading direction was 30° from the strong axis (CDS30) and in the other the loading direction was 30° from the weak axis (CDW30). Figures 5.2(a) and (b) show the idealized crack patterns for CDS30, and CDW30. It was assumed that the angle of cracks was inclined 45° with the resultant loading direction. Crack patterns for CDS30 and CDW30 are shown in Fig. 5.7.

In the case of CDS30, some diagonal cracks formed in adjacent faces (S-E, N-W) as shown in the idealized crack pattern (Fig. 5.2(a)). However, in the east and west faces, diagonal cracks opened from the top to bottom of the column. These crack patterns were similar to those in specimen CUS (unidirectional loading in the strong direction). The angle of the cracks was around 30°. Therefore, the idealized crack pattern and those observed were quite different. In the north and south faces, there were some diagonal cracks which extended to the adjacent faces and some cracks along the longitudinal reinforcement. The crack patterns in these faces were similar to the idealized ones except for some additional vertical cracks along the bars.

In the case of CDW30, diagonal cracks were spread over all faces. As shown in the idealized crack pattern (Fig. 5.2(b)), the idealized cracks started from the ends of the column near the center of the east and west faces. In the observed crack patterns, a similar phenomenon was observed, but in the east and west faces

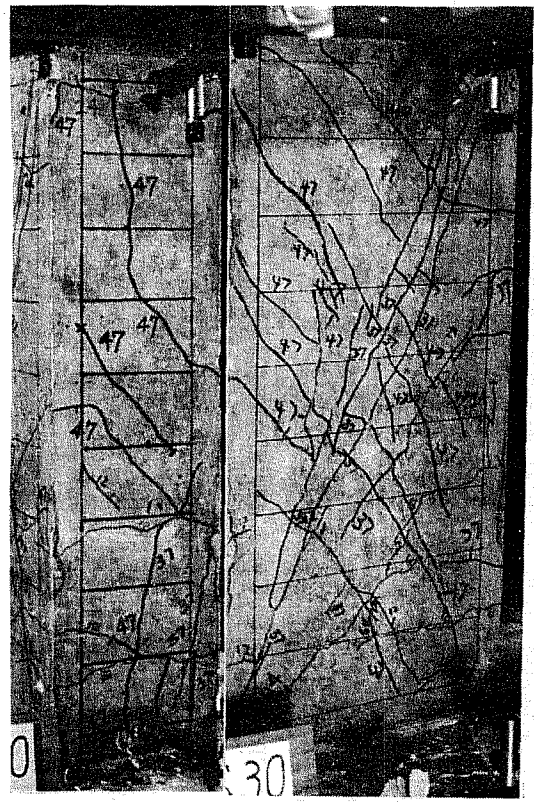

(a) CDS30 (2Δ)

N face W face

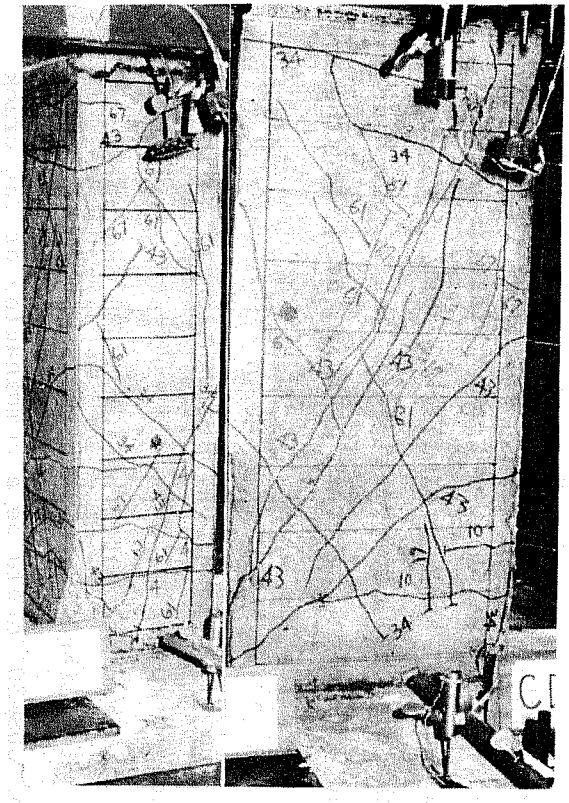

(b) CDW30 (2Δ)

S face E face

Fig. 5.7 Crack patterns - unidirectional diagonal loading

diagonal cracks were steeper and the angle was around 30°. In the north and south faces, there were many diagonal cracks with angles around 40° to 45°.

The crack pattern in CDS30 was similar to that of CUS, while the crack pattern for CDW30 was a combination of that observed in CUS and CUW, and was similar to that of CBSW. Under loading along the diagonal, deformations in the strong direction had a pronounced effect on the crack pattern, even when the loading was skewed only 30° from the weak axis of the column.

5.2.2.2 Unidirectional vs. Bidirectional Loading. The crack pattern in specimen CDSW30 skewed bidirectional loading was compared with the crack patterns for CDS30 and CDW30. According to the idealized crack pattern shown in Fig. 5.2(c), the crack pattern of CDSW30 should be a combination of the crack patterns of CDS30 and CDW30.

At low deflection levels, there were only a few diagonal cracks observed in specimens CDS30 and CDW30. However, in CDSW30, many diagonal cracks formed, especially in the east and west faces. The angle of the cracks ranged from 30° to 45° because of the different combinations of loading direction. At maximum load (Fig. 5.8), more diagonal cracks formed in CDSW30 over all faces and the specimen seemed to be damaged severely. In general, the crack pattern of CDSW30 appeared to be a combination of CDS30 and CDW30.

5.2.3 Review of Crack Patterns. The comparison of crack patterns led to two primary observations. First, initial diagonal cracks produced by deformations in the strong loading direction formed with an angle of around 45°, but cracking leading to failure formed from top to bottom of the column with an angle of around 30°, much steeper than assumed in Figs. 5.1 and 5.2. Diagonal

N face W face S face E face

CDSW30 (2Δ)

Fig. 5.8 Crack patterns - bidirectional diagonal loading

cracks produced by deformations imposed in the weak loading direction formed near the ends of the column and the angle of inclination was around 45° for both initial cracking and cracking leading to failure. Compressive axial load caused these cracks to be slightly steeper. It is likely that the small column height-to-depth ratio in the strong direction had much to do with the inclination of the cracks at failure.

Second, the crack pattern under diagonal loading was affected primarily by deformation in the strong direction. The crack pattern of CDS30 (loading 30° from the strong axis) was almost the same as that observed in CUS (loading only in the strong direction). For CDW30 (loading 30° from the weak axis), the crack pattern was expected to be similar to that of CUW with loading only in the weak direction. However, the crack patterns observed indicated that cracking and distress in the strong direction were dominant over that in the weak direction.

5.3 Strain Distribution

As shown in Fig. 3.8, strain gages were attached to the longitudinal and transverse reinforcement. There were nine gages along two corner longitudinal bars and two gages along the other two corner bars. The purpose of these gages was to study the influence of the bond and anchorage deterioration on the behavior of the short column. Four transverse ties were gaged to investigate the distribution of shear between concrete and steel. From the measured data, strain in the longitudinal and transverse reinforcement at selected load stages was obtained and strain distributions along the column height were plotted. As mentioned in Chapter 4, the unit deflection (Δ) was changed for the different loading directions (strong axis, weak axis, 30° from strong axis, 30° from weak axis), and in each specimen the maximum load was achieved at different deflection levels;

for example, 3Δ, 4Δ, etc. The strain at the resultant deflection corresponding to maximum load defined as Δ_m appeared to be most significant. Therefore, strains are plotted at the following deflection levels: $\Delta_m/2$, Δ_m, and $3\Delta_m/2$. In each plot of strain distribution, the value of Δ_m is indicated.

The strain distributions along longitudinal and transverse reinforcement in each specimen were classified corresponding to the loading direction (as for crack patterns) and compared.

5.3.1 Longitudinal Reinforcement. Two gages inside the top and bottom end blocks on the longitudinal bars provided data regarding bar anchorage. One gage was placed at each end of the column--top and bottom end-block interfaces--and three were spaced along the column.

5.3.1.1 Loading in Principal Direction. The specimens subjected to loading in the principal directions are divided into groups: strong loading direction (OUS, CUS, 2CUS, and CBSW (strong direction only)) and weak loading direction (OUW, CUS and CBSW (weak direction only)).

Strong Direction. The strain distributions of the longitudinal reinforcements at each level ($\Delta_m/2$, Δ_m, $3\Delta_m/2$) for specimens OUS, CUS, 2CUS, and CBSW are shown in Fig. 5.9. The location of strain gages on northwest and southeast corner bars is shown in the right top corner of Fig. 5.9. The strain at each level was taken as the average strain in the two gaged bars under similar loading. In all cases the values of strain were nearly equal. The strain distribution along longitudinal bars is unsymmetrical about the center of the column. Each bar will be subjected to a moment gradient from top to bottom of the column and in the compression zone, the concrete carries part of the force.

All four specimens failed in shear, as indicated by the fact that the strains did not exceed yield. The effect of axial

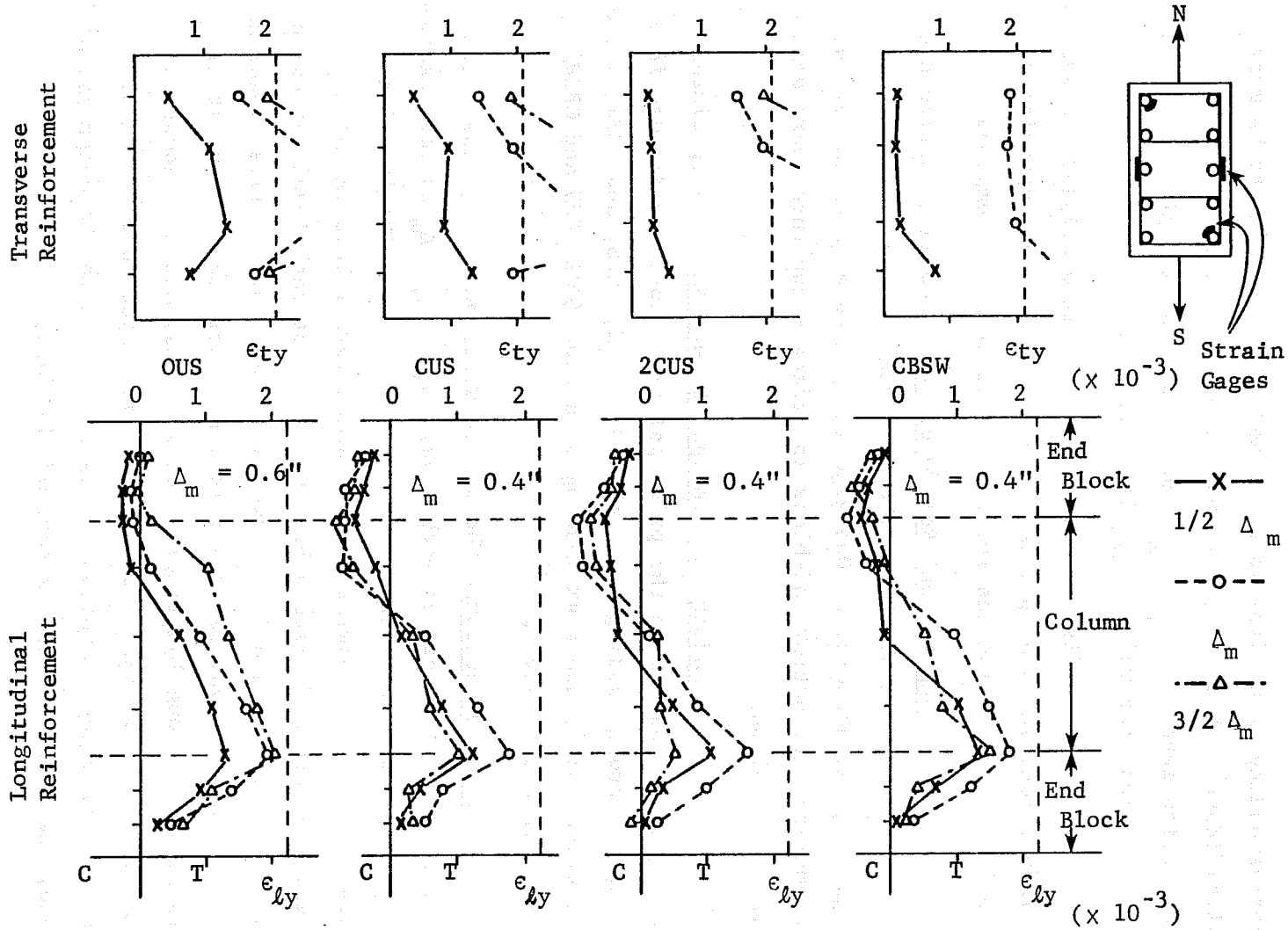

Fig. 5.9 Strain distribution, loading in the strong direction (N-S)

compressive load on the strain distribution can be observed using specimens OUS, CUS, and 2CUS. As compressive load is increased, the strains shift in the direction of compression. The compressive strain in OUS was near zero, while in 2CUS it was about -1000×10^{-6}. Around the midheight of the column, OUS had strain of about 1000×10^{-6} tension, while 2CUS had almost zero strain. Maximum tensile strains were about 1800×10^{-6} in all three specimens. With axial compressive load the strain gradient along the reinforcement from top to bottom was greater than with no axial load. The effect of loading history was investigated in two specimens (CUS, CBSW). There did not appear to be much difference between the strain distributions in these two cases. Large tensile strain (almost yield) occurred at the intersection of the column and end block; however, the strain at a location 10 in. inside the end block was almost zero in all specimens indicating that the hooked anchorage worked well.

Weak Direction. Figure 5.10 shows the strain distribution of the specimens loaded in the weak direction (OUW, CUW, CBSW). The strain at each level was taken as the average strain in the two bars, as before. The distribution for OUW showed that the strains exceeded yield. However, it was observed that shear cracks were predominant. CUW, which was loaded axially, did not reach yield. The strain at Δ_m for CBSW in tension under loading in the weak direction was less than that of CUW. Though CUW reached maximum load at 3Δ (0.48 in.), CBSW reached maximum load at 2Δ (0.32 in.) in the weak loading direction because maximum load in the strong direction had been reached in prior cycles. Therefore, Δ_m was at 3Δ for CUW and 2Δ for CBSW. It is also of interest to note that the strains at Δ_m in CBSW (0.32 in.) were between the strains at $\Delta_m/2$ (0.24 in.) and Δ_m (0.48 in.) of CUW. Therefore, the strain distribution did not appear to be changed by the loading history until the load reached maximum in the strong direction.

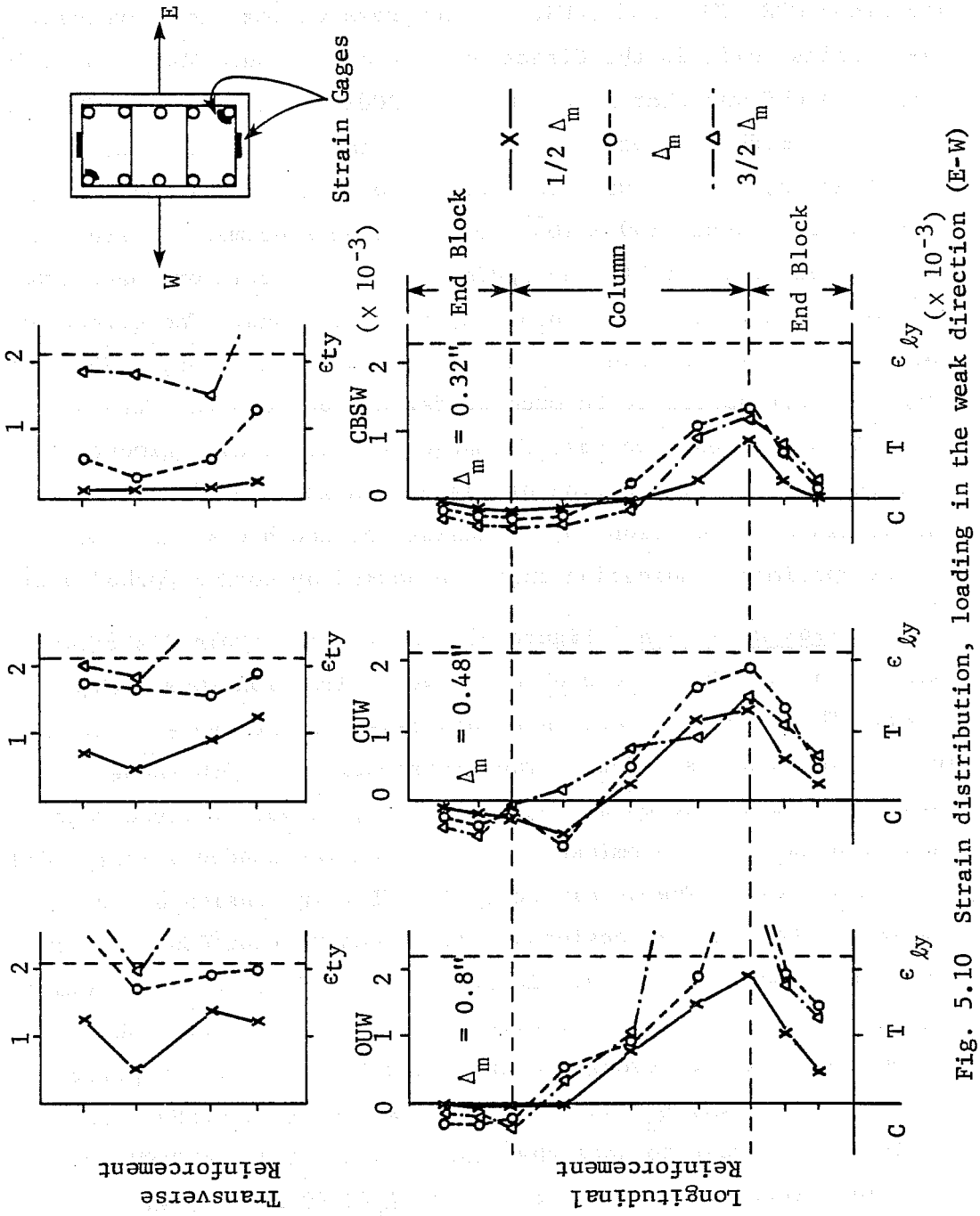

Fig. 5.10 Strain distribution, loading in the weak direction (E-W)

5.3.1.2 Loading in the Diagonal Direction. In this section the strain distributions along the longitudinal reinforcement in the specimens subjected to diagonal loading (CDS30, CDW30, and CDSW30) are discussed. Figure 5.11 shows the strain distribution for loading 30° from the strong axis (CDS30, CDSW30), and Fig. 5.12 for loading 30° from the weak axis (CDW30, CDSW30). Strain gages were attached to the southeast and southwest corner bars. Under diagonal bidirectional loading, one of the bars always reflected maximum strains. Under loading 30° from the strong axis (SE-NW) in Fig. 5.11, the southeast bar reached maximum strains. Under loading 30° from the weak axis (SW-NE) in Fig. 5.12, the southwest bar reached maximum strains. It is interesting to note that differences between the strain distributions under unidirectional or bidirectional diagonal loading (especially at Δ_m) in Fig. 5.11 and Fig. 5.12 were quite small.

5.3.1.3 Review of Longitudinal Strain. The comparison of strain distributions along the longitudinal reinforcement indicate that the hooked bar in the end block anchored the bars well. Along the column height the strain gradient was greater with axial compressive load. The strain distribution was not affected by the loading history until the load reached a maximum value either in the direction considered or in the orthogonal direction.

5.3.2 Transverse Reinforcement. Four transverse hoops were instrumented with gages on all four faces. The location of the gages is shown in Fig. 3.8. The strains in the transverse reinforcement did not increase until a diagonal crack in the concrete crossed the bar. Once the crack crossed the transverse reinforcement, the strain in the bar began to increase rapidly. Therefore, the strain distribution in the transverse reinforcement indicated how and where cracks initiate and propagate in the column.

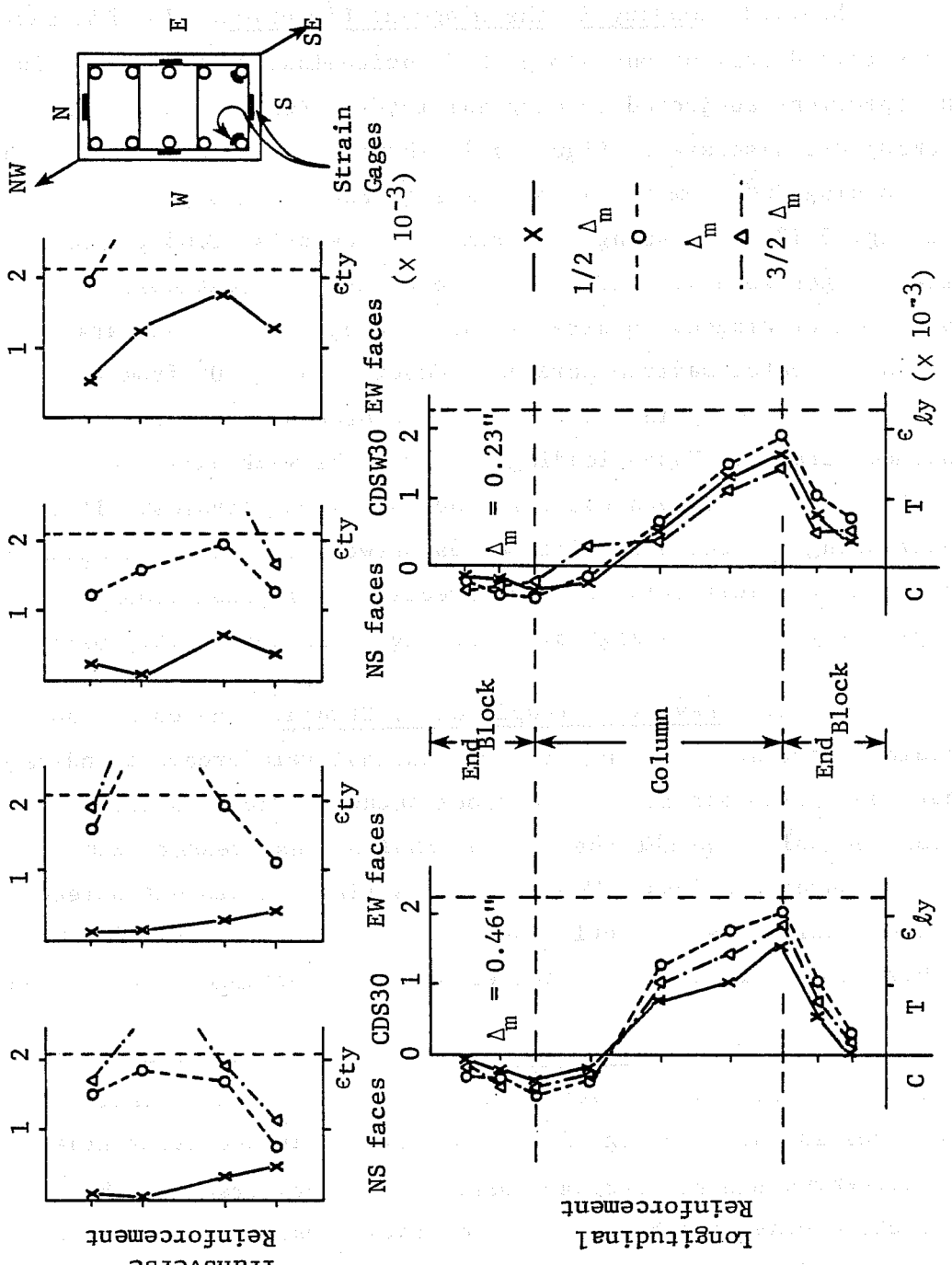

Fig. 5.11 Strain distribution, loading 30° from the strong direction

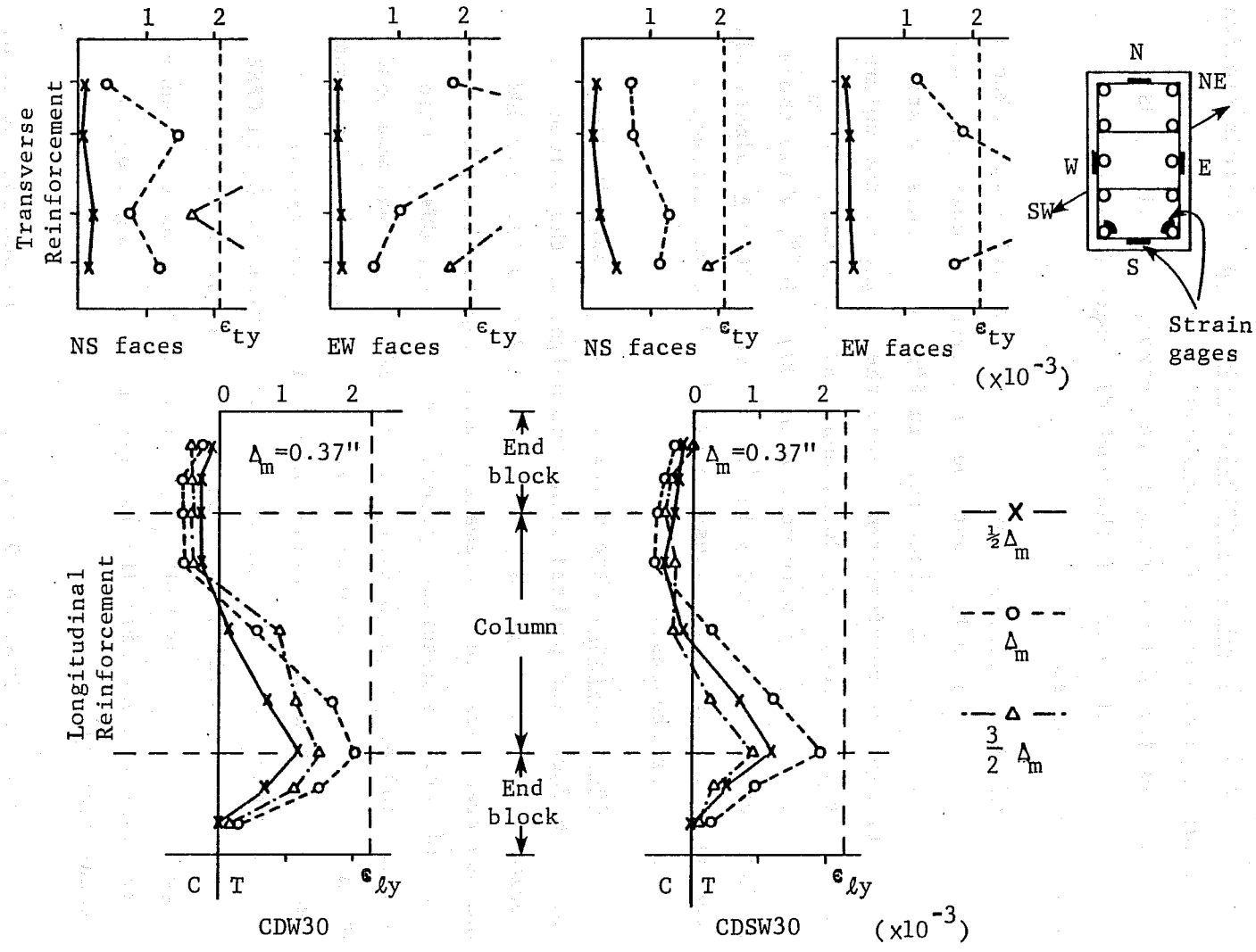

Fig. 5.12 Strain distribution, loading 30° from the weak direction

5.3.2.1 Loading in Principal Direction. In this section the strain distributions for transverse reinforcement in the specimens subjected to loading in the strong direction (0US, CUS, 2CUS, and CBSW) and in the weak direction (0UW, CUW, and CBSW) are discussed.

Strong Direction. The strain at each level was taken as the average strain in the east and west faces because the loading was imposed in the N-S direction. In Fig. 5.9, plots of strain in the transverse reinforcement along the height of the column in the specimens 0US, CUS, 2CUS, and CBSW are shown. At $\Delta_m/2$ the strains of 0US and CUS were more than 1000×10^{-6}, while those of 2CUS were less than 500×10^{-6}. However, after Δ_m almost all strains were near or in excess of yield and it was difficult to see major differences.

Weak Direction. The average strain of bars in the north and south faces was plotted along the height of the column for specimens 0UW, CUW and CBSW, as shown in Fig. 5.10. For 0UW and CUW transverse reinforcement almost reached yield, however, CBSW did not. As described before (Sec. 5.3.1), CUW reached maximum load at 3Δ (0.48 in.), while CBSW reached maximum load at 2Δ (0.32 in.) in the weak loading direction, because maximum load was reached in the strong direction in prior cycles. It is also indicated in the figure that the strains at Δ_m in CBSW (0.32 in.) were similar to those at $\Delta_m/2$ in CUW (0.24 in.). Therefore, it is clear that the strain distribution for transverse reinforcement also did not appear to be changed by the loading history.

5.3.2.2 Diagonal Direction. In this section the strain in the ties in the specimens under diagonal loading (CDS30, CDW30, and CDSW30) is described. Fig. 5.11 shows the strain distribution

for the specimens with loading 30° from the strong axis (CDS30, CDSW30) and Fig. 5.12 30° from the weak axis (CDW30, CDSW30). The crack pattern in the north and south faces was different from that in the east and west faces (Fig. 5.2). Therefore, average strain distributions for the N-S and E-W faces are shown for each specimen (because the strains in each face were nearly the same). In Fig. 5.11 the strain distribution of the specimen with unidirectional diagonal loading (CDS30) and with bidirectional diagonal loading (CDSW30) is compared. Except for the strain distribution in the E-W face at $\Delta_m/2$, there are no major differences. The results in Fig. 5.12 also indicated that the strain distribution for CDSW30 (bidirectional diagonal loading) was almost the same as that for CDW30 (unidirectional diagonal loading).

5.3.2.3 Review of Strains in Transverse Reinforcement. Comparing strains in the transverse reinforcement, it is clear that the strains were not affected by the loading history, and almost all ties reached yield at Δ_m or $3\Delta_m/2$.

5.4 Lateral Load Capacities

The measured maximum lateral load (resultant for diagonal loading), V_m, sustained by each of the columns tested is listed in Table 5.1. Normalized shear strengths, $V_m/A_c\sqrt{f'_c}$, are also listed. A_c is the area (in^2.) of concrete surrounded by transverse reinforcement (core). Shear strength of concrete is considered to be a function of $\sqrt{f'_c}$(25). The core area was used in order to define shear strength under large lateral deflections. When extensive cracking in the faces and spalling of concrete cover occurred, the core was carrying shear. At maximum load, severe shear cracks had opened. Therefore, normalized values were used for comparison of maximum shear capacity and in plotting shear deterioration diagrams. The

TABLE 5.1 MEASURED LATERAL LOAD CAPACITIES

Specimen Name	Loading Direction	f'_c	N	V_m	$\frac{V_m}{A_c\sqrt{f'_c}}$	Δ_m	R
OUS	N↔S	5810	0	66	8.8	0.60	0.017
OUW	E↔W	5820	0	57	7.6	0.80	0.022
CMS	N←S	6090	120	86	11.2	0.48	0.013
CUS	N↔S	5060	120	74	10.6	0.40	0.011
CUW	E↔W	5060	120	60	8.6	0.48	0.013
2CUS	N↔S	6090	240	91	11.9	0.40	0.011
CDS30	NE↔SW	6180	120	80	10.3	0.46	0.013
CDW30	NE↔SW	6120	120	74	9.7	0.37	0.010
CBSW	N↔S	5090	120	69	9.9	0.40	0.011
	E↔W			52	7.4	0.32	0.009
CDSW30	NE↔SW	5090	120	57	8.1	0.37	0.010
	NW↔SE			62	8.8	0.23	0.007

f'_c - concrete compressive strength, psi

N - compressive axial load, kips

V_m - measured maximum lateral load, kips (resultant for diagonal loading)

A_c - core area, $in.^2$

Δ_m - peak deflection, in. (defined in Sec. 5.3)

R - drift ratio, Δ_m/L

L - column height, in.

deflection corresponding to maximum load, Δ_m, and drift ratio, R, which is the ratio of Δ_m to the column height (in this test, 36 in.) are also shown in Table 5.1. For loading exclusively in the weak direction, V_m/A_c reached values of 7.6 to $8.6\sqrt{f'_c}$, and for loads in the strong direction V_m/A_c reached values from 8.8 to $10.6\sqrt{f'_c}$. For loading along the diagonal, V_m/A_c reached values of 9.7 to $10.3\sqrt{f'_c}$. There was little difference in the value of V_m/A_c in spite of varying loading histories.

5.5 Deterioration

Envelopes of the peak values reached in load-deflection curves in the first, second or third cycles at each deflection level for the ten specimens tested were used to investigate the deterioration of strength after maximum load. Figure 5.13 shows an example of the envelope curves. As shown in this figure, the peak loads at each deflection limit in first and third cycles are connected to make envelope curves. The envelope curve in the first loading direction (in this case from south to north) is shown here and is plotted in most cases. Envelope curves provide an indication of the changes in shear with cycling at a given deflection level and permit comparison of these changes between different tests. Using envelope curves of the relationship between normalized shear $V_m/A_c\sqrt{f'_c}$ and lateral deflection, the effect on shear deterioration of each of the following was examined--the effect of the compressive axial load, and the effect of the loading history.

5.5.1 Effect of Axial Compression. Envelope curves for the specimens loaded in the strong direction (0US, CUS, 2CUS) are shown in Fig. 5.14(a) and in the weak direction (0UW, CUW) in Fig. 5.14(b). The envelopes of the load under first cycle in both strong and weak directions indicate that the normalized

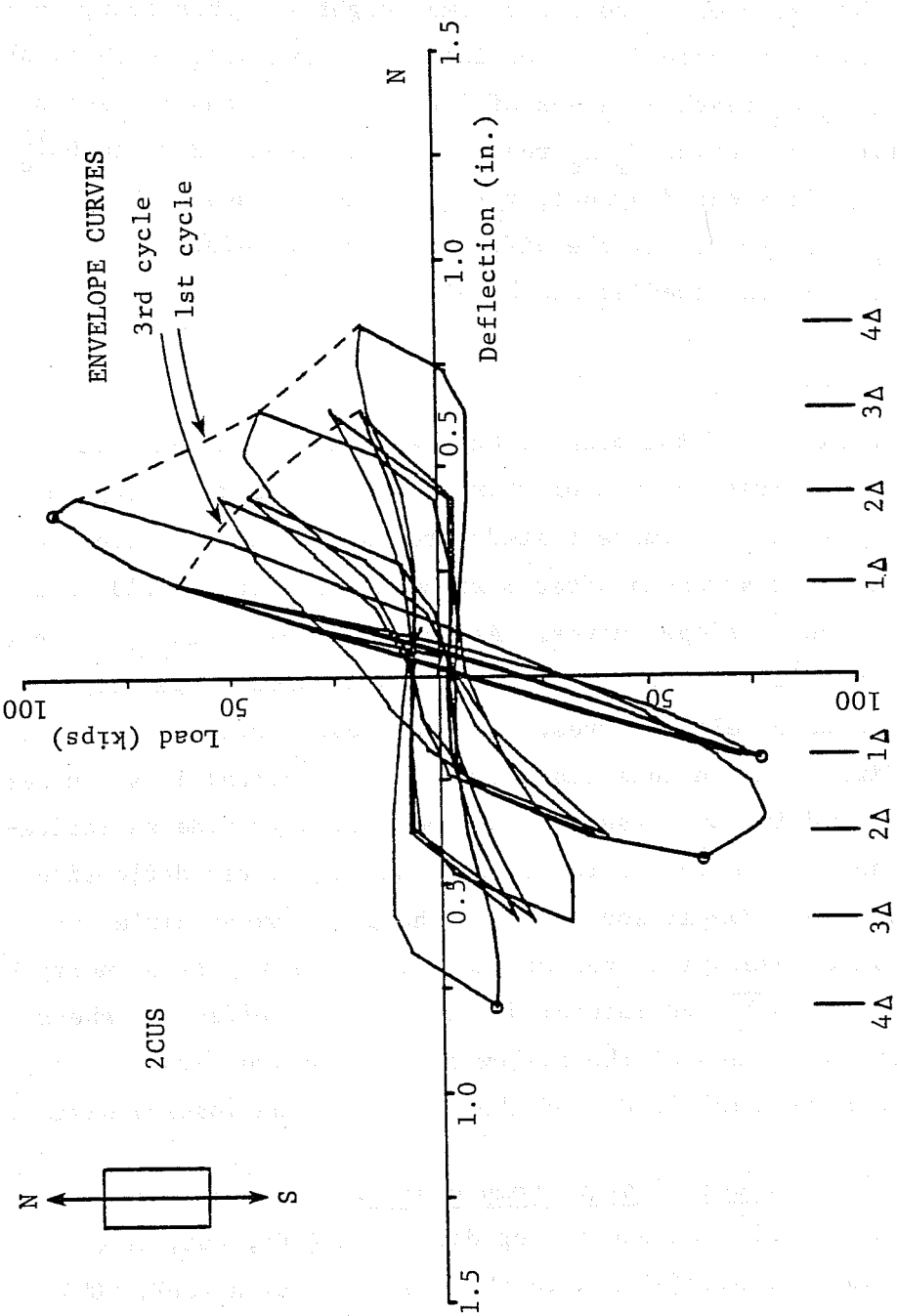

Fig. 5.13 Definition of envelope curve

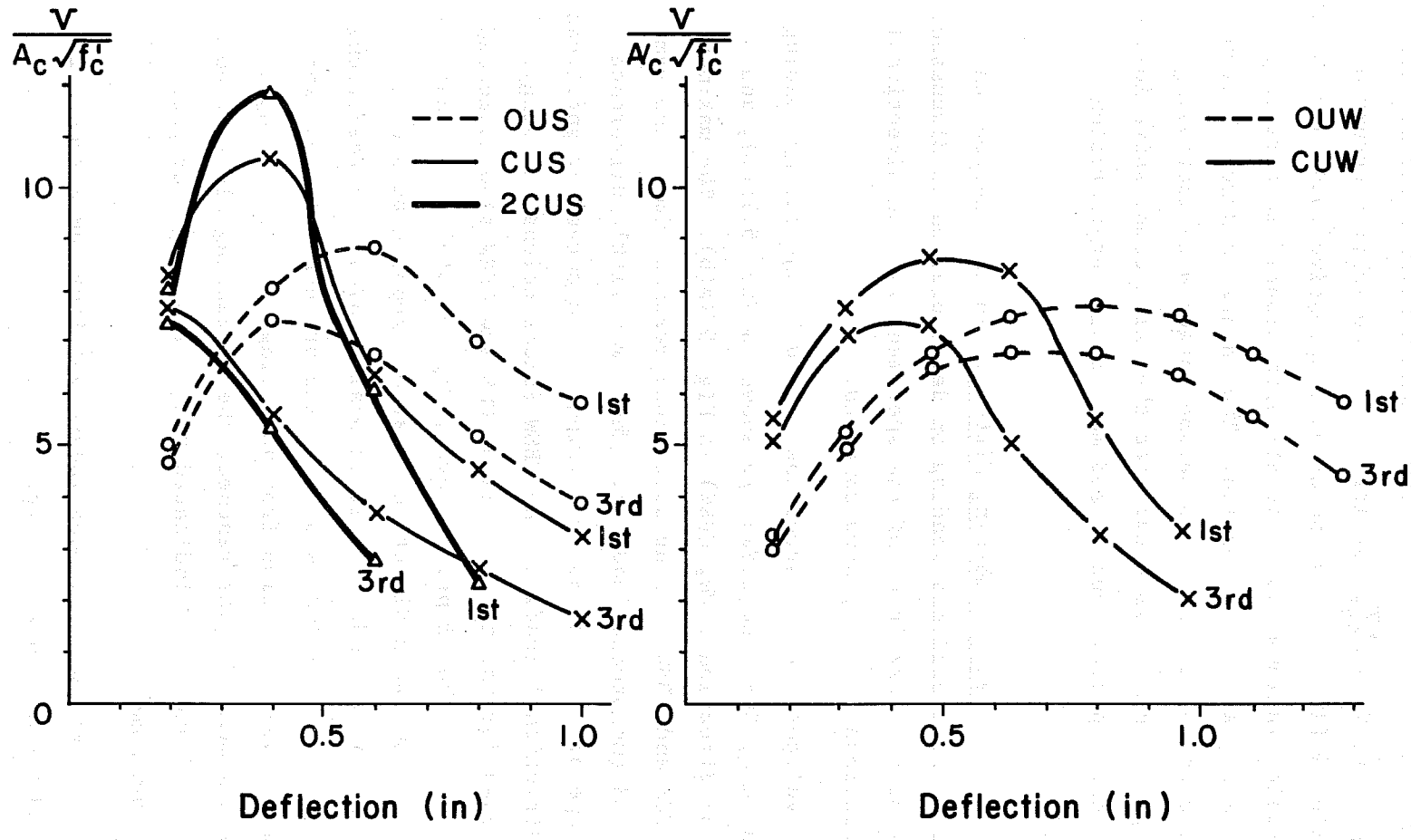

(a) Strong Direction

(b) Weak Direction

Fig. 5.14 Envelope curves--effect of compressive axial load

shear capacity, $V_m/A_c\sqrt{f'_c}$, was larger and the maximum occurred at a smaller deflection as the axial compressive load increased. After reaching maximum load, the strength dropped more rapidly with increasing axial compression. The change in strength from first cycle to third cycle also became larger with increasing axial compression. It is clear that the axial compressive load increased the capacity but caused more rapid deterioration of strength.

5.5.2 Effect of Loading History. In this section the influence of bidirectional loading on deterioration is discussed. Envelopes of the peak loads of the specimens with unidirectional and bidirectional loading were compared.

Envelopes for the specimens loaded in the strong loading direction (CMS, CUS, and CBSW) are shown in Fig. 5.15(a), and in the weak direction (CUW, CBSW) in Fig. 5.15(b). The maximum loads in CUS and CBSW (strong direction) reached almost the same value as CMS (monotonic loading). There was little difference in the slope of the descending portion of the curve for specimens CUS (unidirectional loading) and CBSW (bidirectional loading). The envelopes for the third cycle of CUS and CBSW also indicated no difference in the slope. However, Fig. 5.15(b) shows that the strength of CBSW (weak direction) started dropping before the maximum was reached under unidirectional loading. In the strong direction the maximum load was at 2Δ and produced distress which prevented the weak direction from achieving a higher strength. After the maximum load was reached, the descending slope of both specimens, CUW and CBSW, indicated that the strength dropped at almost the same rate.

Envelopes for specimens loaded 30^o from the strong axis (CDS30, CDSW30) are shown in Fig. 5.16(a) and 30^o from the weak axis (CDW30, CDSW30) in Fig. 5.16(b). First loading on CDSW30

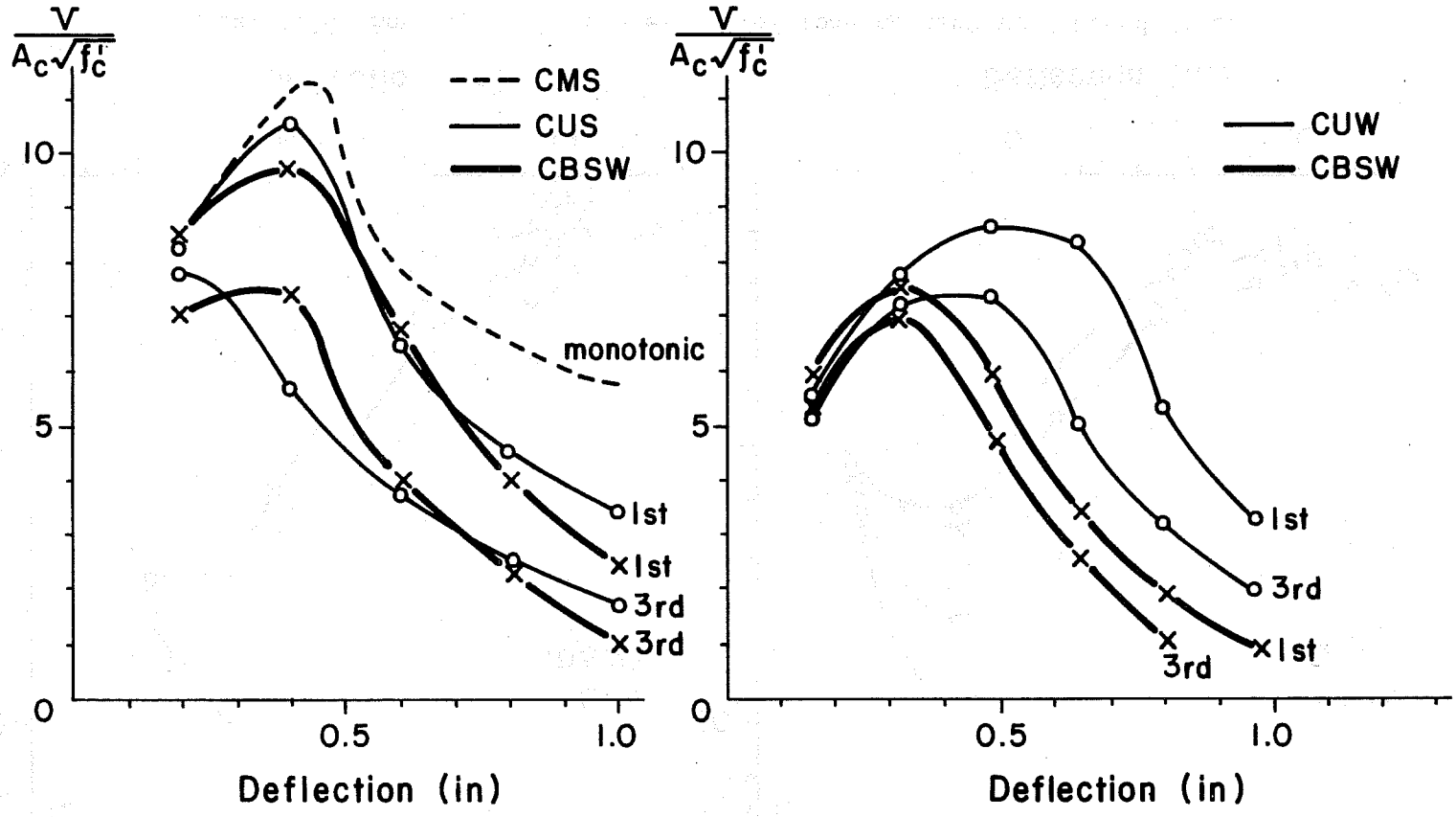

Fig. 5.15 Envelope curves - effect of loading history (principal direction)

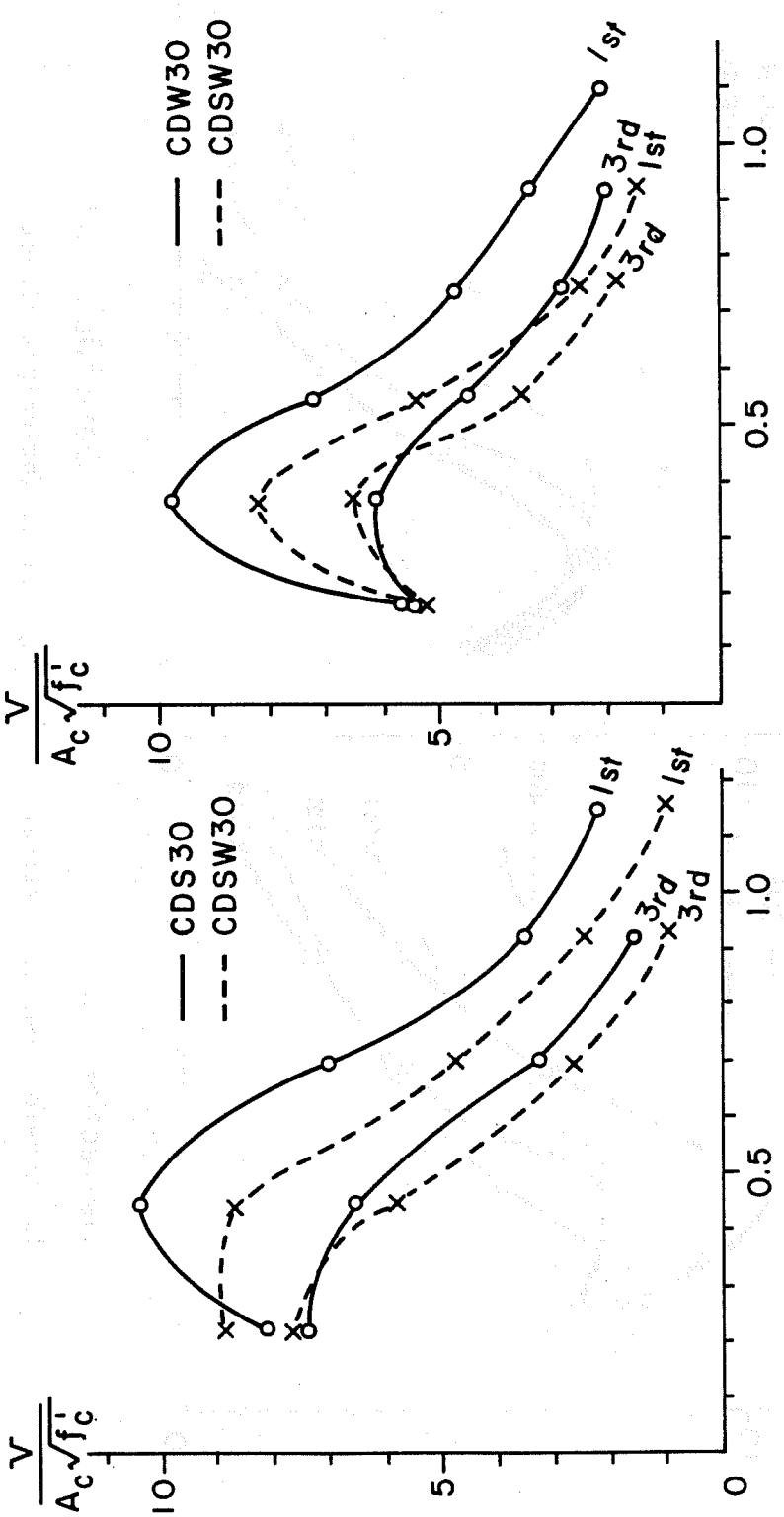

Fig. 5.16 Envelope curves - effect of loading history (skewed direction)

was in the same direction as CDW30 and maximum load was reached at the same deflection level as CDW30(2Δ). The maximum load (CDSW30) was about 85 percent of that sustained by CDW30. At 2Δ with loading in the same direction as CDS30, the load on CDSW30 never exceeded the value at 1Δ. After reaching maximum load, the envelopes of CDS30, CDW30 and CDSW30 indicated that there was little difference in the slope of the descending portion of the curve.

5.5.3 Effect of Loading Direction. The envelopes of the peak loads of the specimens which had different loading directions (CUS, CDS30, CDW30, and CUW) are shown in Fig. 5.17. The shapes of envelopes for CDS30 (loading 30^{o} from the strong axis) and CDW30 (loading 30^{o} from the weak axis) appeared to be similar to that in CUS (loading in the strong axis). Although the loading direction of CDW30 is near that of CUW (loading in the weak axis), the shape of CDW30 is not similar to that of CUW. This phenomenon was observed in the comparison of the crack patterns of these specimens that the crack pattern under diagonal loading was affected primarily by the deflection in the strong direction. The envelope curves confirm this observation.

5.5.4 Review of Deterioration. Based on comparisons of the strength envelopes, it was observed that axial compressive load produced an increase in the capacities, but more rapid deterioration of strength. The maximum load in the column under bidirectional loading reached almost the same value as under unidirectional loading. However, after the deflection at the maximum load under unidirectional loading was reached in columns under bidirectional loading, the strength began to drop in both directions. The slope of the descending part of the curves indicated that there were no significant differences between the columns with

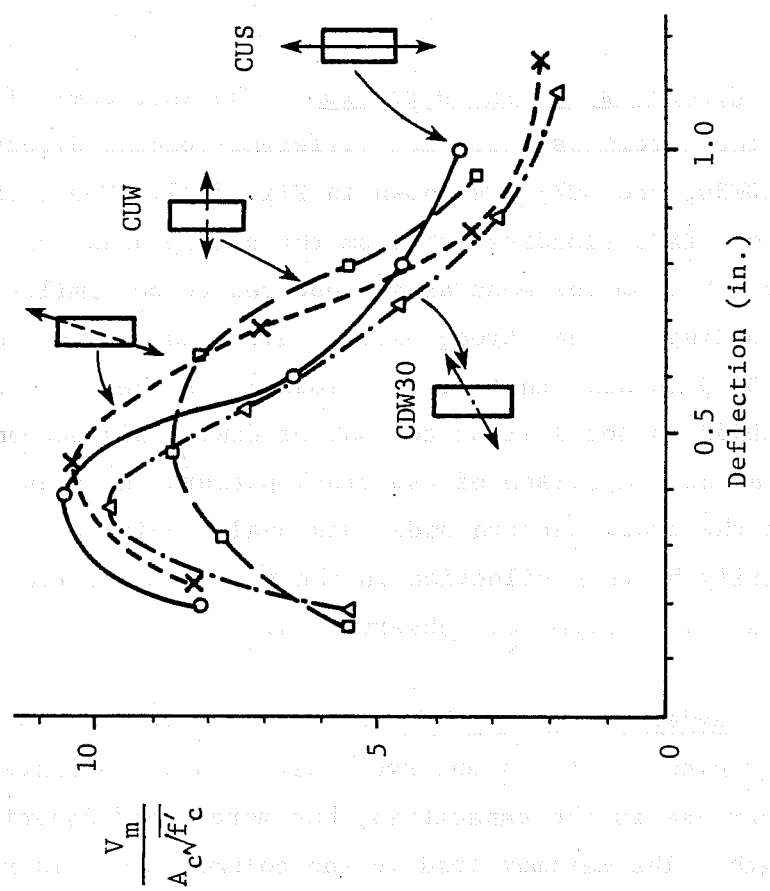

Fig. 5.17 Envelope curves--effect of loading direction

unidirectional and bidirectional loading. In the load-deflection relationship, it was observed that the shape of the strength envelope under diagonal loading was affected primarily by the deflection in the strong direction. This phenomenon was also observed in the comparison of crack patterns.

CHAPTER 6

COMPARISON OF TEST RESULTS—SQUARE AND RECTANGULAR COLUMNS

6.1 General

In this chapter, the results from tests of rectangular columns are compared with those of square columns tested in previous investigations (Maruyama,[22] Ramirez,[23] and Woodward[24]). First, the test results of the square columns are reviewed and followed by comparisons of crack pattern, lateral load capacity and deterioration for square and rectangular sections.

6.2 Review of Results—Square Columns

The test results of square columns shown in Fig. 2.2 are reviewed in this section. These columns were tested in the previous three investigations. In the first investigation,[22] the effect of deformation paths was studied. Deformation paths included in the study ranged from unidirectional deformations along only one axis to bidirectional complex paths as shown in Fig. 1.2. No axial load was applied to the specimens. In the second investigation,[23] the effect of axial load, especially tensile load, on the hysteretic behavior of the column was studied. The applied axial loads ranged from constant tension or compression to reversals of axial load as shown in Fig. 1.4. In the third investigation,[24] the amount of longitudinal and transverse reinforcement was varied as shown in Fig. 1.8 to determine the influence of these variables on the behavior of short columns. A total of about 30 square columns was tested. In this chapter only the results which can be compared directly

with rectangular columns are described. Selected specimens were renamed for this report. The square specimens were classified into two groups; loading in a principal direction and loading in a diagonal direction.

6.2.1 Notation. A three group code was established to simplify comparisons between square columns tested previously with the rectangular columns of this investigation. The general form of the notation is:

A-LH-S

A = level of axial load
- 0 = no axial load
- C = 120 kips axial compression

L = loading direction
- P = principal direction
- D = diagonal direction

H = loading history
- M = monotonic loading
- U = unidirectional loading
- B = bidirectional loading

S = number of ties within the 36 in. column
- 32--1.13 in. spacing
- 21--1.75 in. spacing
- blank--2.57 in. spacing--standard specimen
- 9--4.0 in. spacing
- 3--12.0 in. spacing

The specimens listed in Table 6.1 are identified using this notation. Notations from Refs. 22, 23, and 24 are also listed in this table.

TABLE 6.1 DESCRIPTION OF SQUARE COLUMNS

Specimen New Name	Specimen Old Name	Axial Load (kips)	Loading Direction	Loading History	Tie Spacing (in.)	
0-PU	00-V-0-1	0	P	U	2.57	
C-PU	120C-U	120	P	U	2.57	
0-PB	00-V-V-A	0	P	B	2.57	
C-PB	120C-B	120	P	B	2.57	
0-DM	0-86-14-DM	0	D	M	2.57	
C-DM	C-86-14-DM	120	D	M	2.57	
0-DU	00-V-V-S	0	D	U	2.57	
0-DB	00-V-V-SA	0	D	B	2.57	
C-DB	C-86-14-D	120	D	B	2.57	*
C-DB-32	C-86-32-D	120	D	B	1.13	*
C-DB-21	C-86-21-D	120	D	B	1.75	*
C-DB-9	C-86-09-D	120	D	B	4.00	*
C-DB-3	C-86-03-D	120	D	B	12.00	*

P - principal direction

D - diagonal direction

M - monotonic loading

U - unidirectional loading

B - bidirectional loading

* - tests with variable tie spacing

6.2.2 Loading in the Principal Direction. The specimens loaded in the principal direction were classified into two groups: unidirectional loading and bidirectional loading. The specimens with unidirectional loading are 0-PU (no axial load) and C-PU (120 kips axial compressive load). The loading histories are shown in Fig. 6.1(a). Specimens with bidirectional loading are 0-PB (no axial load) and C-PB (120 kips axial compressive load). The loading histories are shown in Fig. 6.1(b). 0-PU and 0-PB were included in the square column specimens tested by Maruyama.[22] Specimens C-PU and C-PB were in the series of square columns tested by Ramirez.[23]

6.2.3 Loading in the Diagonal Direction. The specimens loaded along the diagonal direction were tested to study the effect of loading history and of tie spacing.

Figures 6.2(a), (b), and (c) indicate the loading histories for specimens with monotonic, unidirectional, and bidirectional loading. The specimens with monotonic loading are 0-DM (no axial load) and C-DM (120 kips axial compression). The specimen with unidirectional loading is 0-DU (no axial load). The specimens with bidirectional loading are 0-DB (no axial load) and C-DB (120 kips axial compression). 0-DU and 0-DB were part of the first series of square columns tested by Maruyama.[22] 0-DM, C-DM, and C-DB were part of a series of square columns tested by Woodward.[24] Five specimens with different tie spacings (C-DB-32, C-DB-21, C-DB, D-DB-9, C-DB-3) were also tested under diagonal bidirectional loading by Woodward.[24]

6.3 Crack Pattern

In Chapter 5, crack patterns observed in the tests of rectangular columns were discussed. In this chapter crack patterns observed in the square column tests (symmetric section) and the

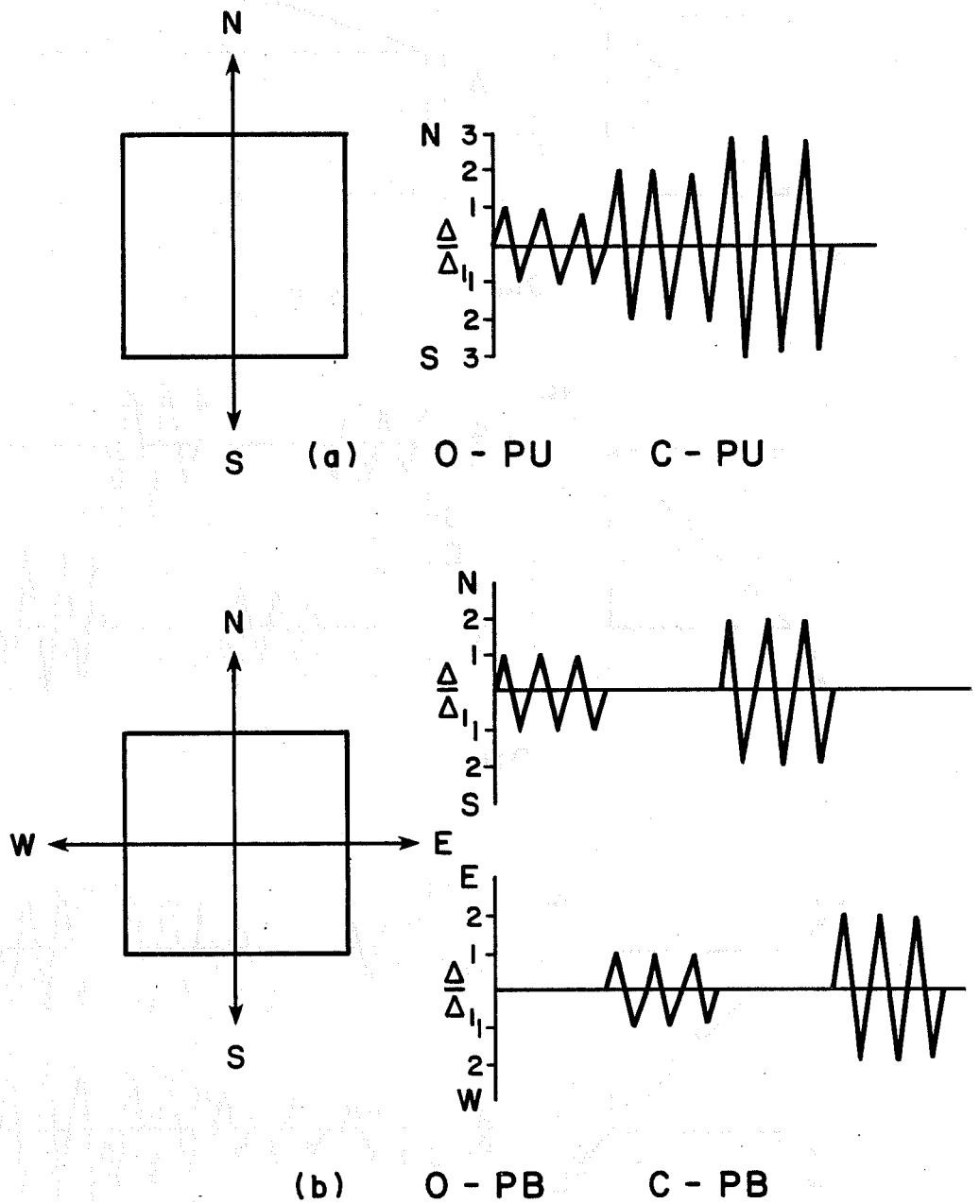

Fig. 6.1 Loading histories on square columns in principal direction

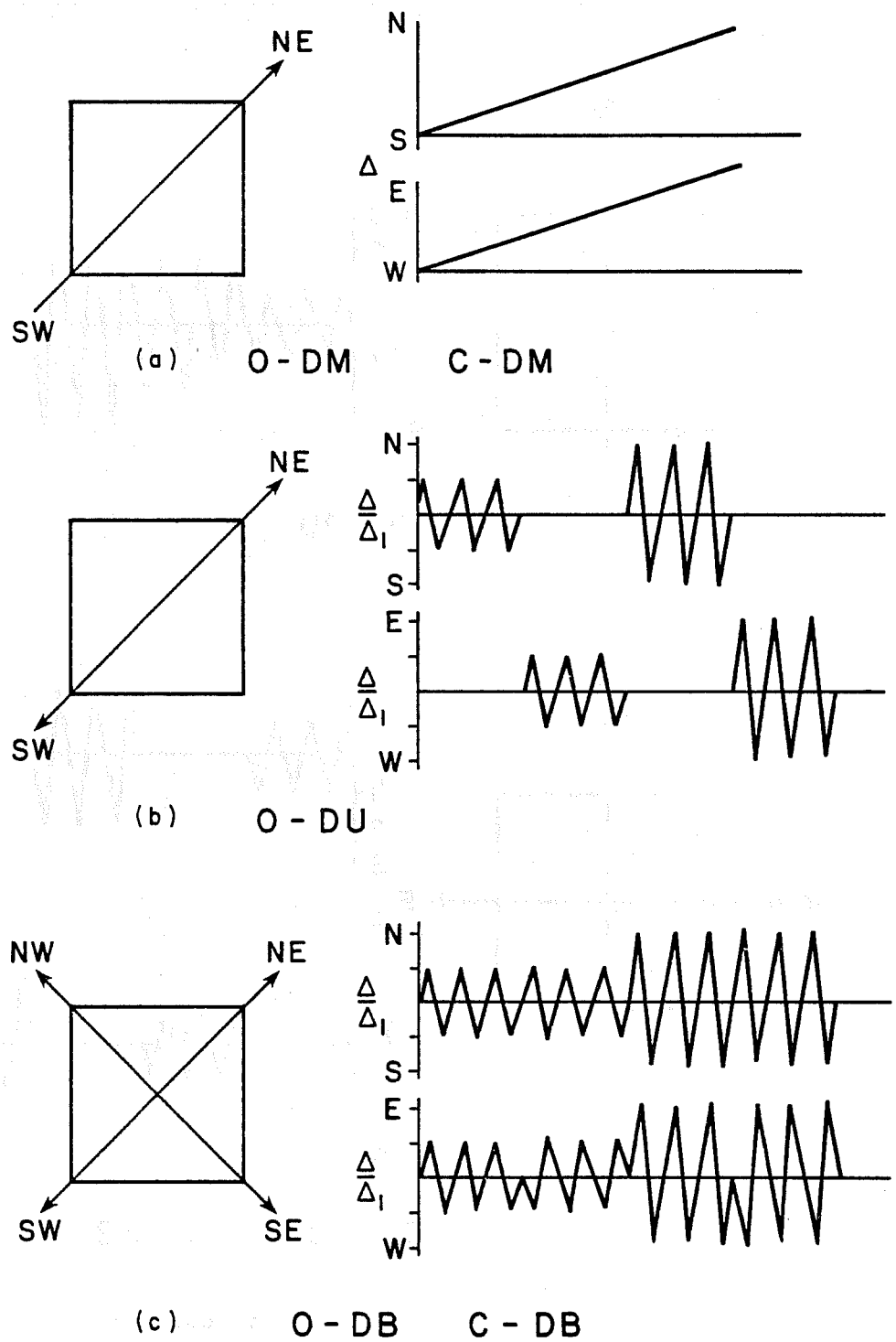

Fig. 6.2 Loading histories on square columns in diagonal direction

rectangular columns (unsymmetric section) are compared. In the rectangular columns it was observed that in specimens loaded in the strong direction (specimens OUS, and CUS), the angle of initial cracks was around 45°, but the inclination of shear cracks leading to failure was around 30°. In specimens loaded in the weak direction (OUW, and CUW), the angle of initial and failure crack patterns remained inclined at around 45°. With compressive axial load, a slight change was noted in the angle of crack inclination in the specimens. The crack pattern of columns under diagonal loading was influenced by deformations in the strong loading direction more than by those in the weak loading direction. The crack pattern of the specimen with bidirectional loading in the strong and weak directions was similar to the crack patterns under unidirectional loading prior to reaching maximum load.

6.3.1 Principal Direction—No Axial Load. Crack patterns at maximum load in the specimens without axial load (OUS, O-PU, and OUW) are shown in Fig. 6.3. The shear span (half of the column height) to effective depth ratios of the specimens OUS, O-PU, and OUW are 1.25, 1.73 and 2.44, respectively. The crack patterns indicate the following results. In OUS diagonal cracks leading to failure occurred from the top to bottom of the column with an angle to the vertical of around 30°. In O-PU, some diagonal cracks opened from near the top to the bottom of the column, but major cracks opened near the ends of the column at an angle of about 45°. Therefore, the angle of cracks ranged from 30° to 45°. In OUW the angle of nearly all cracks was 45°. The angle of cracks leading to failure became smaller as the shear span to effective depth ratio decreased and as the failure mode changed from flexural to shear.

(a) OUS (b) O-PU (c) OUW

Fig. 6.3 Crack patterns - rectangular vs. square (principal direction, no axial load)

6.3.2 Principal Direction—Axial Load. In Fig. 6.4 crack patterns at maximum load for specimens with 120 kips axial compression (CUS, C-PU, and CUW) are shown. In CUS, the diagonal cracks leading to failure opened from the top to bottom of the column and the angle of these cracks from the vertical was almost the same as that in OUS, around 30°. In C-PU, diagonal cracks opened from the top to bottom of the column and more cracks with angles from 30° to 40° were noted than in O-PU. In CUW, the angle of initial cracks which opened near the ends of the column was around 45°, but slightly steeper cracks with angles from 40° to 45° opened around midheight of the column. However, there were no significant differences in the crack patterns of tests OUW and CUW. There were no cracks along longitudinal reinforcement in CUS, but in C-PU and CUW some cracks opened along longitudinal bars and diagonal cracks extended from these cracks. In the specimens with compressive axial load, it was also clear that the angle from the vertical of cracks leading to failure became smaller as the shear span to effective depth ratio decreased.

6.3.3 Diagonal Direction. Crack patterns in the specimen under diagonal loading, CDS30, CDW30, and C-DB, are shown in Fig. 6.5. No square columns with axial compression under diagonal unidirectional loading were tested. Therefore, the crack patterns of C-DB (diagonal bidirectional loading) were compared with CDS30 and CDW30. Specimens O-DU and O-DB tested by Maruyama[22] and the rectangular columns in this study indicated that the crack pattern under bidirectional loading was similar to the crack patterns with deformation in each direction up to the point where maximum load was reached. In CDS30, diagonal cracks opened from the top to bottom of the column, as observed for CUS. In CDW30, diagonal cracks opened from the top to bottom of the column, and also diagonal cracks opened near the ends of the column,

(a) CUS (b) C-PU (c) CUW

Fig. 6.4 Crack patterns - rectangular vs. square
(principal direction, axial load)

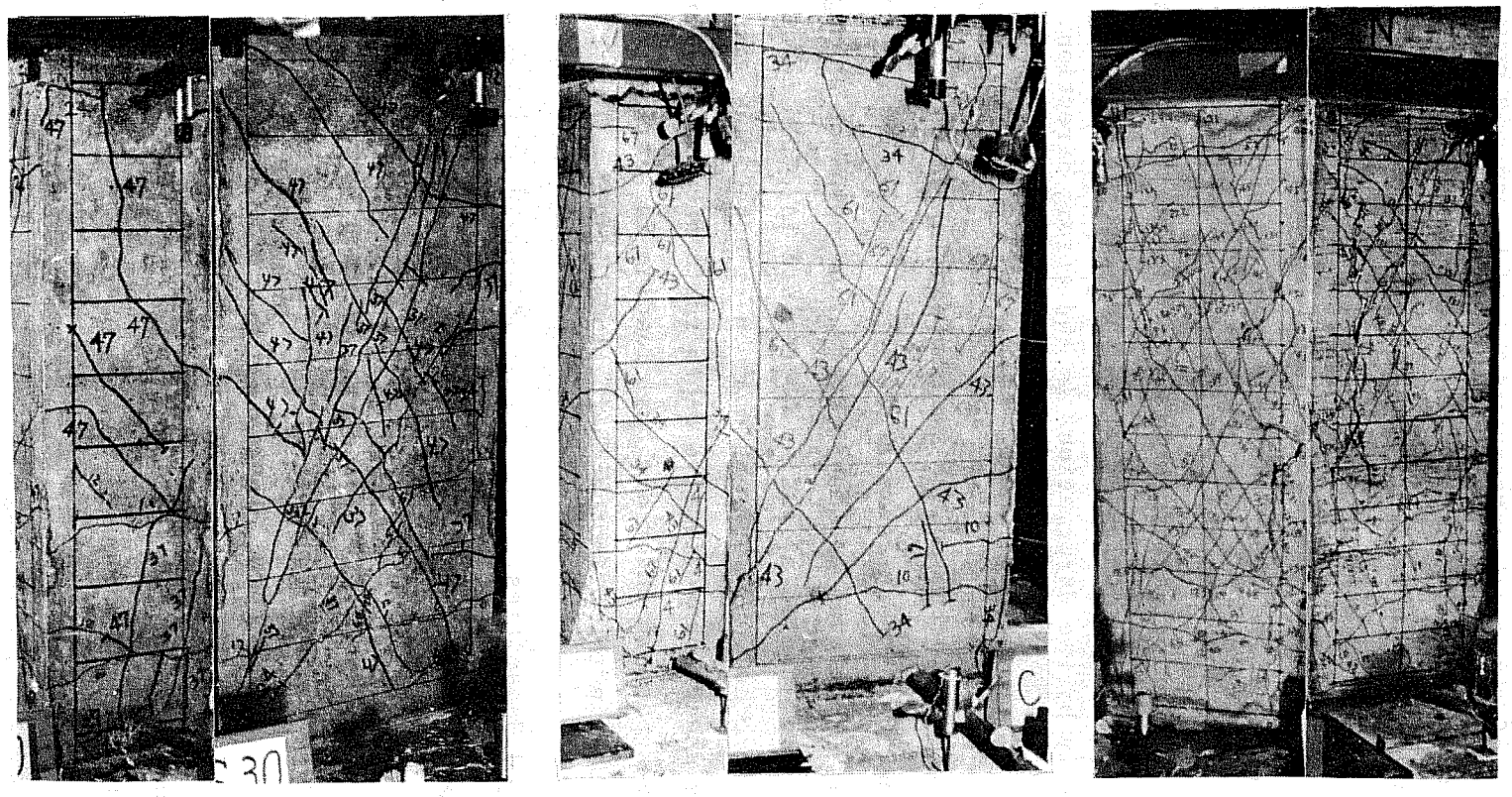

(a) CDS30 (b) CDW30 (c) C-DB

Fig. 6.5 Crack patterns - rectangular vs. square
(diagonal direction, axial load)

as a combination of the crack pattern exhibited by CUS and CUW. In C-DB, diagonal cracks opened from the top to near the bottom of the column as in C-PU. The crack patterns in the square column did not exhibit the phenomenon observed in the rectangular column, because the strength in both directions is identical. However, it is clear that the crack pattern of columns loaded along the diagonal is similar to that of the columns loaded in a principal direction. In rectangular columns, the crack pattern of columns loaded along the diagonal is affected primarily by the deformations in the strong direction.

6.3.4 Review of Observed Crack Patterns. The comparison of the crack patterns in the square and rectangular columns shows that (1) the angle of shear cracks is often assumed to be 45^{o} for design purposes,[25] but even if the initial crack opens at an angle of 45^{o}, the angle of the shear cracks at failure is often less than 45^{o} in a short column. This phenomenon is especially apparent as the shear span-effective depth ratio becomes smaller, and (2) the crack pattern under diagonal loading is similar to that under loading in the principal directions.

6.4 Lateral Load Capacities

In Chapter 5 the lateral load capacities including measured values V_m and normalized values $V_m/A_c\sqrt{f'_c}$ for the rectangular columns were listed. When the maximum shear capacities corresponding to loading in both principal and skewed directions are plotted, interaction diagrams such as shown in Figs 6.6 and 6.7 are obtained. This diagram shows the relationship between shear in the North-South (ordinate) and East-West (abscissa) directions. It is possible to compare the maximum capacities of square and rectangular columns in any loading direction using this diagram. The interaction diagram

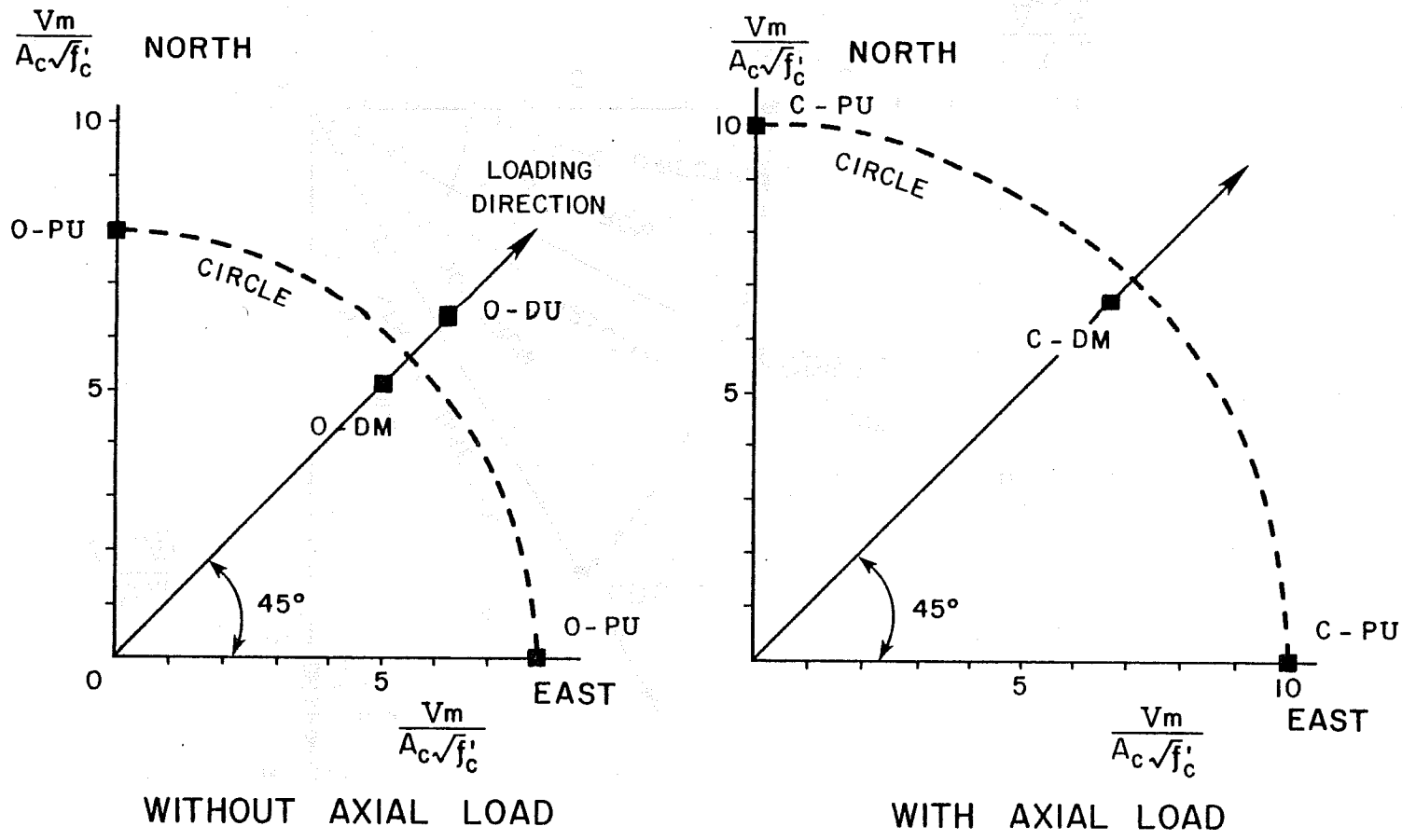

Fig. 6.6 Interaction diagram--square column

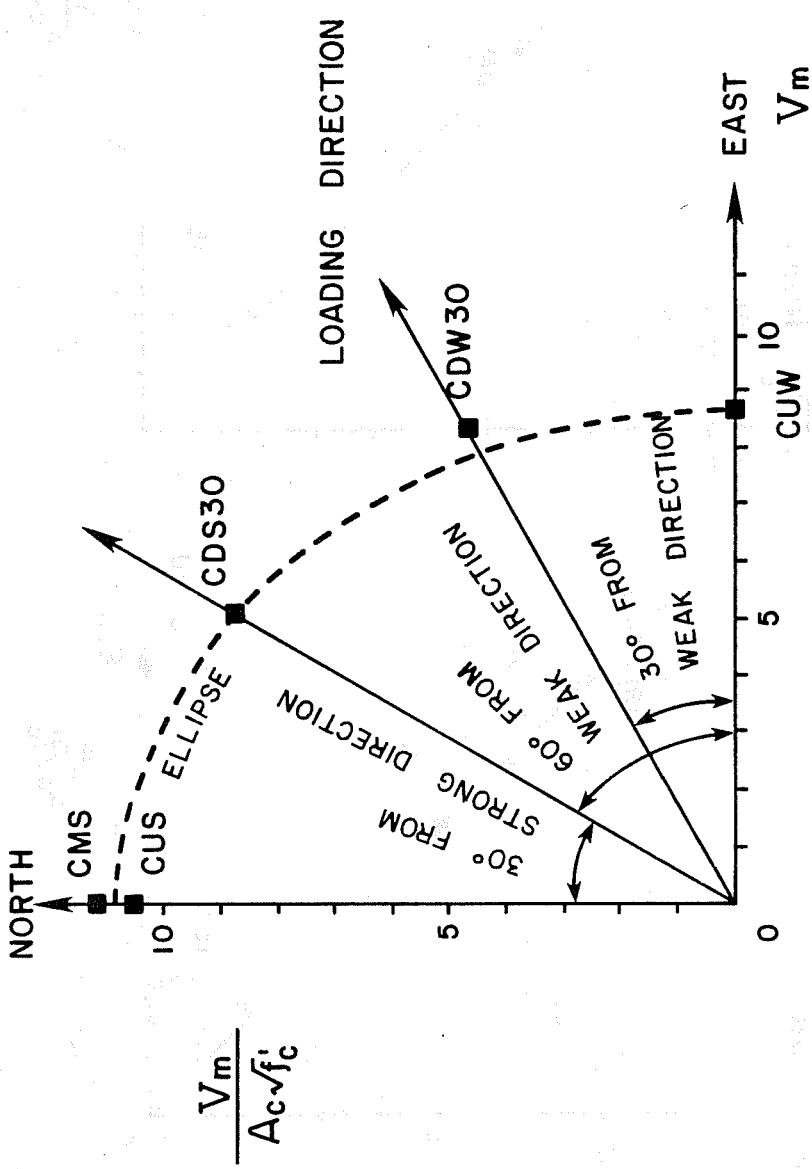

Fig. 6.7 Interaction diagram - rectangular column with axial load

was used for comparing only data of the specimens with monotonic or unidirectional loading. With bidirectional loading, when the deflection corresponding to the maximum load under unidirectional loading was reached, the strength in both directions began to drop. The maximum capacity under bidirectional load reflects deterioration produced by loading in an orthogonal direction. The performance of specimens under bidirectional loading is compared using shear deterioration diagrams on envelopes of peak values in the load-deflection curve.

6.4.1 Interaction Diagram. Interaction diagrams for the square columns are shown in Fig. 6.6. For both interaction diagrams (with and without axial load), the maximum capacity measured unidirectionally in the principal axis was plotted on both principal axes, since the square column has a symmetric section. The strength obtained from O-DM and O-DU for loads on a diagonal are also plotted. The two points for diagonal loading are near the circle drawn through the points on the principal axes (O-PU). The differences between the measured values for O-DM and O-DU are within 15 percent of the value for the circular interaction diagram (Table 6.2). The capacity of C-DM is located very near the circle (see values in Table 6.2). Therefore, based on the maximum capacities of square columns with unidirectional loading directions, it was clear that the maximum capacity of square columns with diagonal loadings can be estimated using strength in the principal loading direction on a circular interaction diagram.

In Fig. 6.7, an interaction diagram for the rectangular column with axial load is shown. No rectangular column without axial load was tested along the diagonal loading direction. As the rectangular column has an unsymmetric section, the maximum capacity in the weak direction (CUW) was plotted on the east-west

TABLE 6.2 RELATIONSHIP OF MAXIMUM CAPACITIES BETWEEN PRINCIPAL AND DIAGONAL LOADING DIRECTION

Square Column

Specimen Name	Loading Direction*	(1) $\frac{V_m}{A_c\sqrt{f'_c}}$	(2) Circle	$\frac{(1)}{(2)}$
0-PU	0°	7.9	7.9	1.00
0-DM	45°	7.1	7.9	0.90
0-DU	45°	9.1	7.9	1.15
C-PU	0°	10.0	10.0	1.00
C-DM	45°	9.4	10.0	0.94

Rectangular Column

Specimen Name	Loading Direction*	(1) $\frac{V_m}{A_c\sqrt{f'_c}}$	(2) Ellipse	$\frac{(1)}{(2)}$
CMS	90°	11.2	Avg. 10.9	1.03
CUS	90°	10.6		0.97
CDS30	60°	10.3	10.2	1.01
CDW30	30°	9.7	9.0	1.08
CUW	0°	8.6	8.6	1.00

* The angle from east-west direction

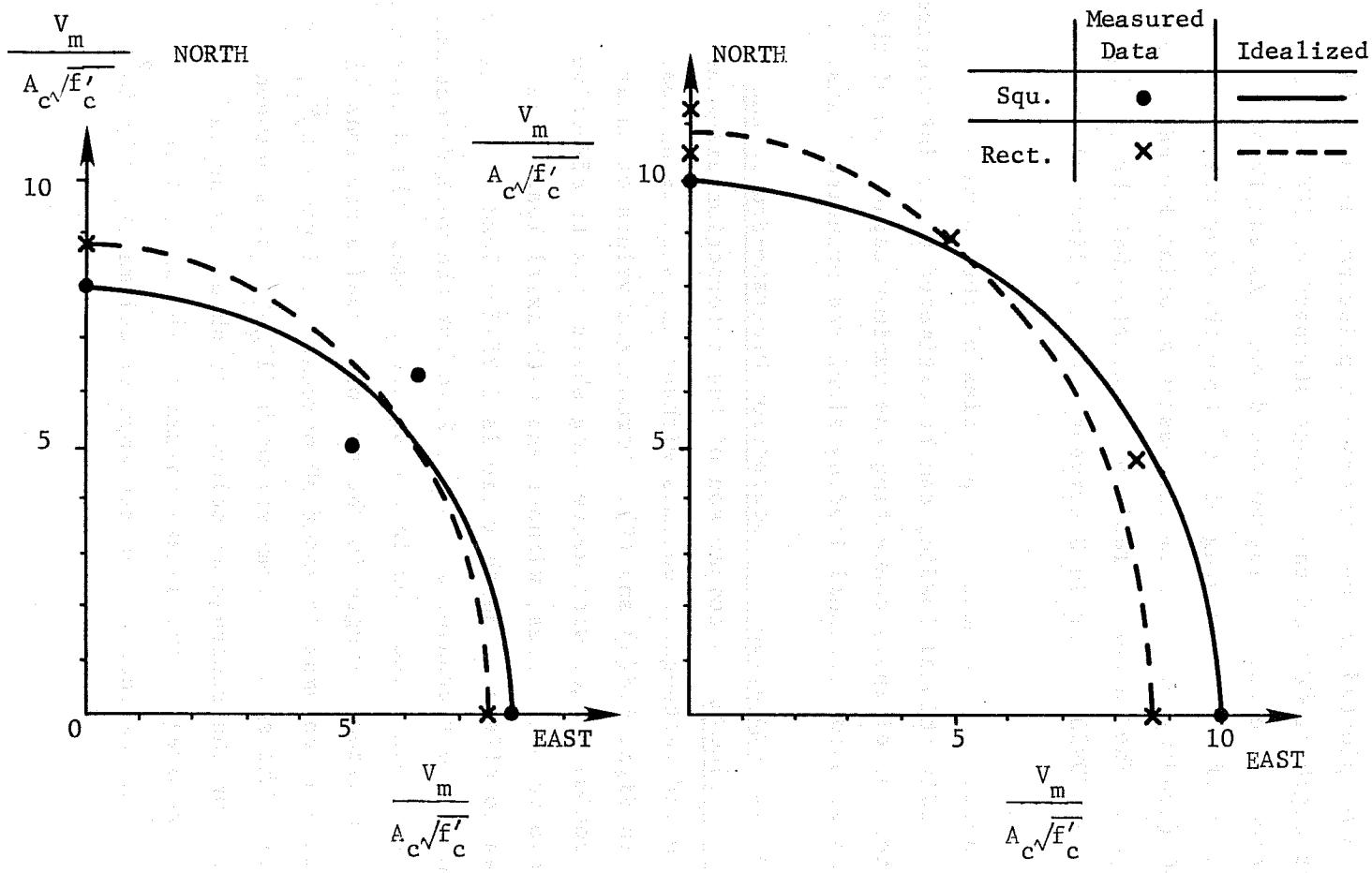

(a) No axial load

(b) With Axial Load

Fig. 6.8 Comparison of interaction diagrams - square and rectangular columns

principal axis and the capacity in the strong direction (CUS and CMS) was plotted on the north-south principal axis. Based on the strength of CUW and the average strength of CUS and CMS, an elliptical interaction diagram was drawn. As can be seen, the capacity of CDS30 (loading of 60^{o} from the east-west axis) and CDW30 (loading of 30^{o} from the east-west axis) lie nearly on the ellipse. The values in Table 6.2 indicate that the strength of CDS30 and CDW30 is within 8 percent of the elliptical interaction line.

Therefore, the maximum capacities of the columns with diagonal unidirectional loading can be estimated by an interaction line (circle or ellipse) connecting the maximum capacities of the columns under unidirectional loading along the principal axis.

6.4.2 Comparison of Interaction Diagram—Square and Rectangular Columns. A comparison of the interaction diagrams for square and rectangular columns without and with axial load is shown in Figs. 6.8(a) and (b). Normalized values of shear $V_m/A_c\sqrt{f'_c}$ become larger with decreasing shear span to effective depth ratio in both cases, without and with axial load. The shear span to effective depth ratio is 1.25 for loading in the strong direction of the rectangular column, 2.44 for the weak direction, and 1.73 for both directions in the square column. The difference between normalized strength in the two principal directions of the rectangular columns is about 30 percent (11.2 vs. $8.6\sqrt{f'_c}$, Table 6.2). The square column strength ($10\sqrt{f'_c}$) falls between the values for the rectangular column. It should be noted that the core area of the square column (A_c = 100 $in.^2$) is almost the same as that of the rectangular column (A_c = 98 $in.^2$).

6.5 Deterioration of Shear Capacity—Deformation Envelopes

In this section the effect of loading history (unidirectional vs. bidirectional), shear span to depth ratio, and axial compression on the deterioration of shear capacity are discussed using envelopes of the relationship between normalized shear and lateral deflection. Also, the effect of tie spacing on deterioration is reviewed using the results of square columns.

6.5.1 Loading History. The effect of loading history on the shear capacity of the rectangular columns was discussed in Sec. 5.5. On the rectangular columns with bidirectional loading in the principal direction (CBSW) and diagonal direction (CDSW30), the maximum load in the column under bidirectional loading reached almost the same value as under unidirectional loading. However, when deflection reached the value corresponding to the maximum load under unidirectional loading, the strength under bidirectional loading began to drop in both directions.

Figures 6.9(a) and (b) provide an indication of shear deterioration in square columns loaded in the principal direction. In Fig. 6.9(a), the comparison of 0-PU (unidirectional) and 0-PB (bidirectional) is shown. The sequence of loading is indicated by (1) loading direction applied first, and (2) loading direction applied second. Direction (1) reached maximum load at 3Δ, the same deflection level where 0-PU reached maximum load. The maximum load in 0-PB is around 85 percent of that of 0-PU. At 3Δ, the load in direction (2) began to drop slightly. In Fig. 6.9(b), C-PU (unidirectional) and C-PB (bidirectional) are compared. Both directions (1) and (2) reached almost the same maximum load as in C-PU. In Figs. 6.10(a) and (b) the envelopes of peak loads in square columns loaded along the diagonal are shown. In Fig. 6.10(a),

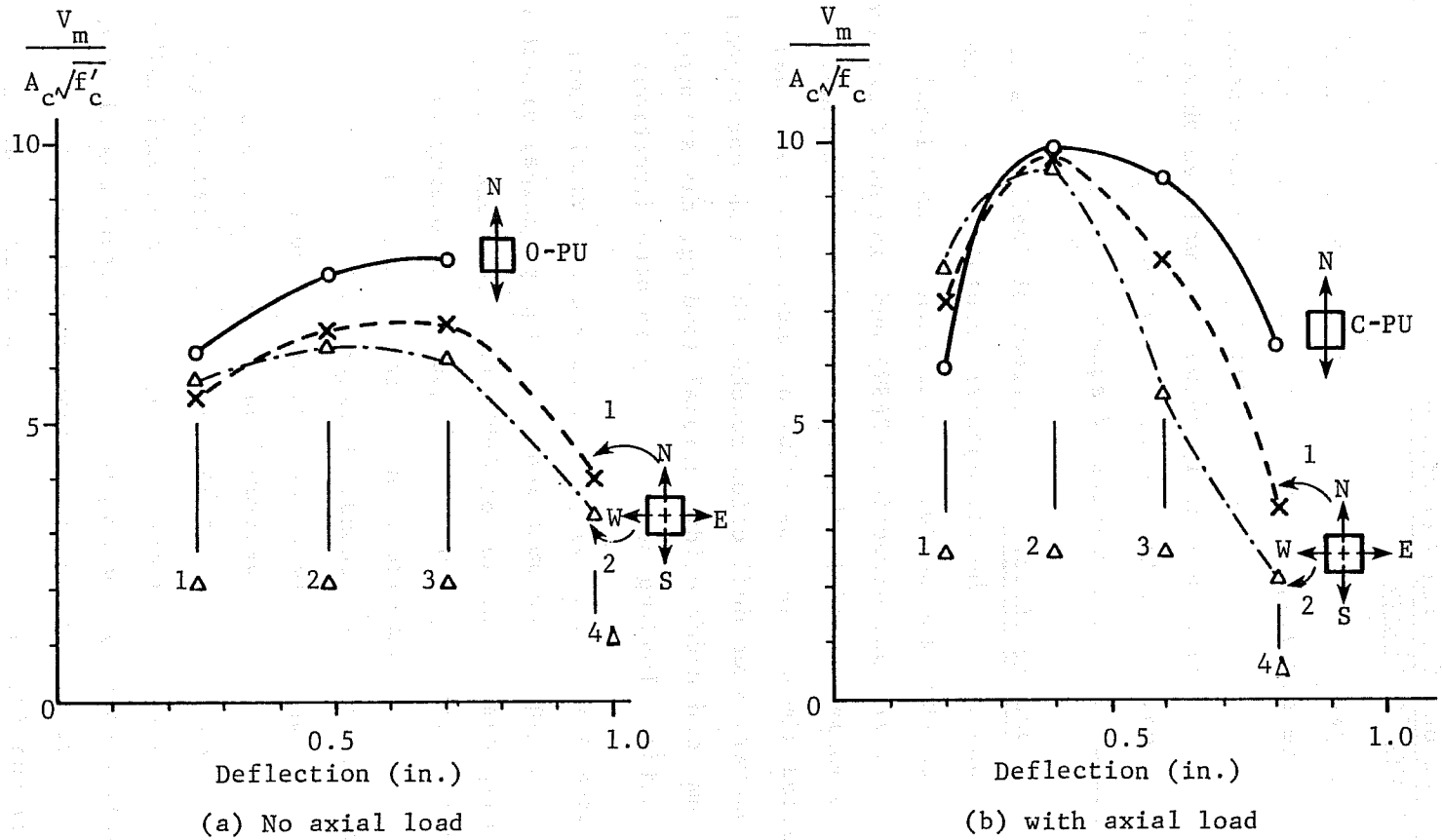

Fig. 6.9 Influence of loading history--square column, loading in principal direction

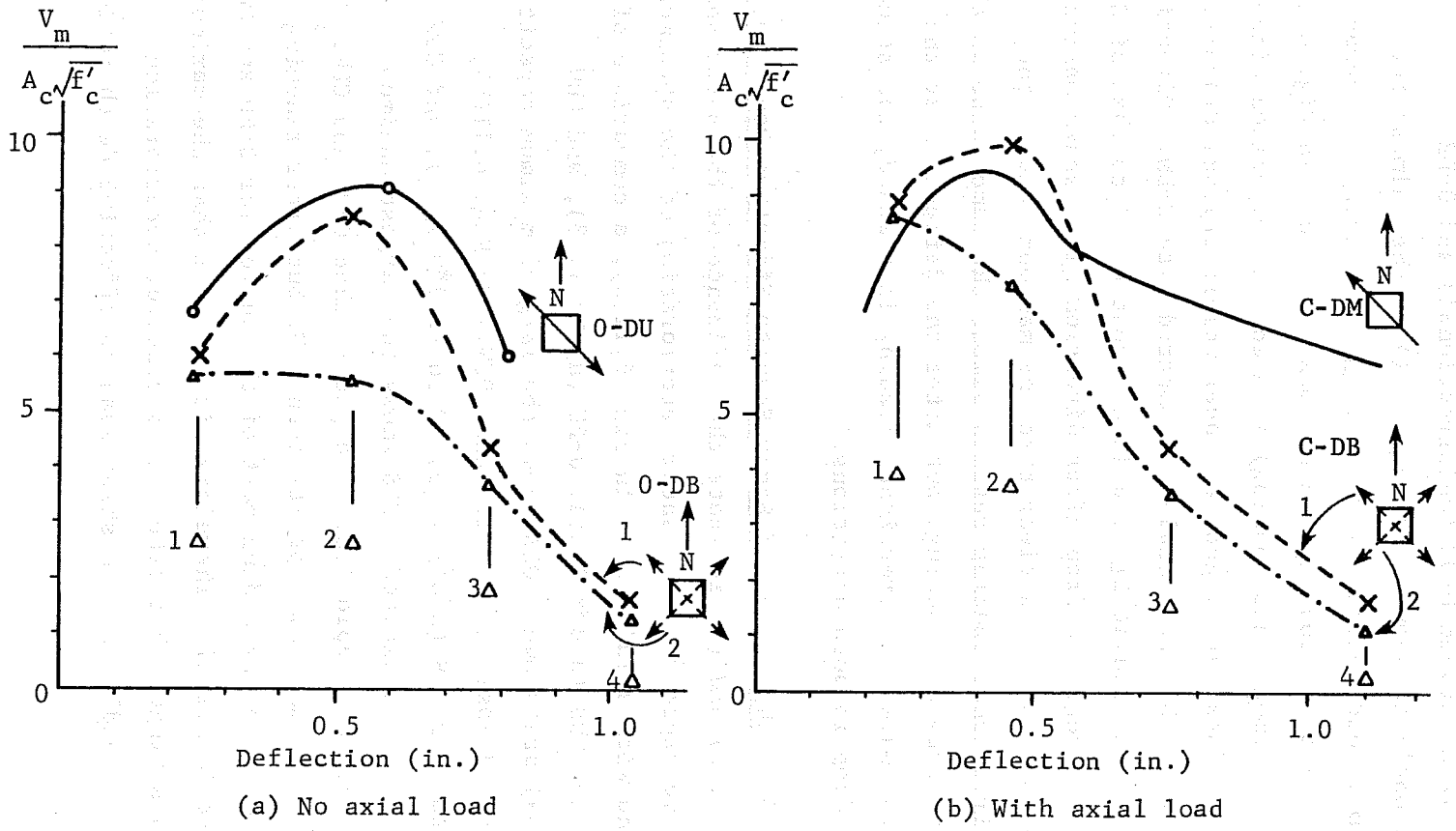

Fig. 6.10 Influence of loading history--square column, loading in diagonal direction

the comparison between O-DU (unidirectional) and O-DB (bidirectional) is shown. Direction (1) reached almost the same maximum load reached by O-DU at 2Δ. Direction (2) began to drop after direction (1) reached maximum load. In Fig. 6.10(b), specimen C-DM (monotonic loading) is used for comparison since there are no data for a specimen under unidirectional diagonal loading. C-DB (bidirectional) is compared with C-DM. Direction (1) reached maximum load at 2Δ at a load almost equal to that of C-DM. Direction (2) began to drop after direction (1) reached maximum. In square columns, it is clear that the maximum load in the column under bidirectional loading reaches almost the same value as that under unidirectional loading, but after the deflection at the maximum load under unidirectional loading is reached, the strength begins to drop in both directions.

6.5.2 The Effect of Shear Span to Effective Depth Ratio. Figures 6.11(a) and (b) indicate the influence of the shear span to effective depth ratio on shear deterioration of the specimen without and with axial load. In Fig. 6.11(a), a comparison of envelopes for OUS ($a/d^*= 1.25$), O-PU ($a/d^*= 1.73$), and OUW ($a/d^*= 2.44$) are shown. OUS shows the largest maximum capacity, but more rapid loss of capacity than OUW. In Fig. 6.11(b), the diagrams for CUS ($a/d^*= 1.25$), C-PU ($a/d^*= 1.73$), and CUW ($a/d^*= 2.44$) are indicated. CUS shows the largest maximum capacity, but more rapid loss of capacity than C-PU and CUW. C-PU had larger maximum capacity than CUW, but after reaching maximum load, the descending part of the curves for C-PU and CUW were almost identical. Therefore, it is clear that the maximum load becomes bigger, but after it is reached, deterioration occurs more rapidly, as the shear span to effective depth ratio decreases.

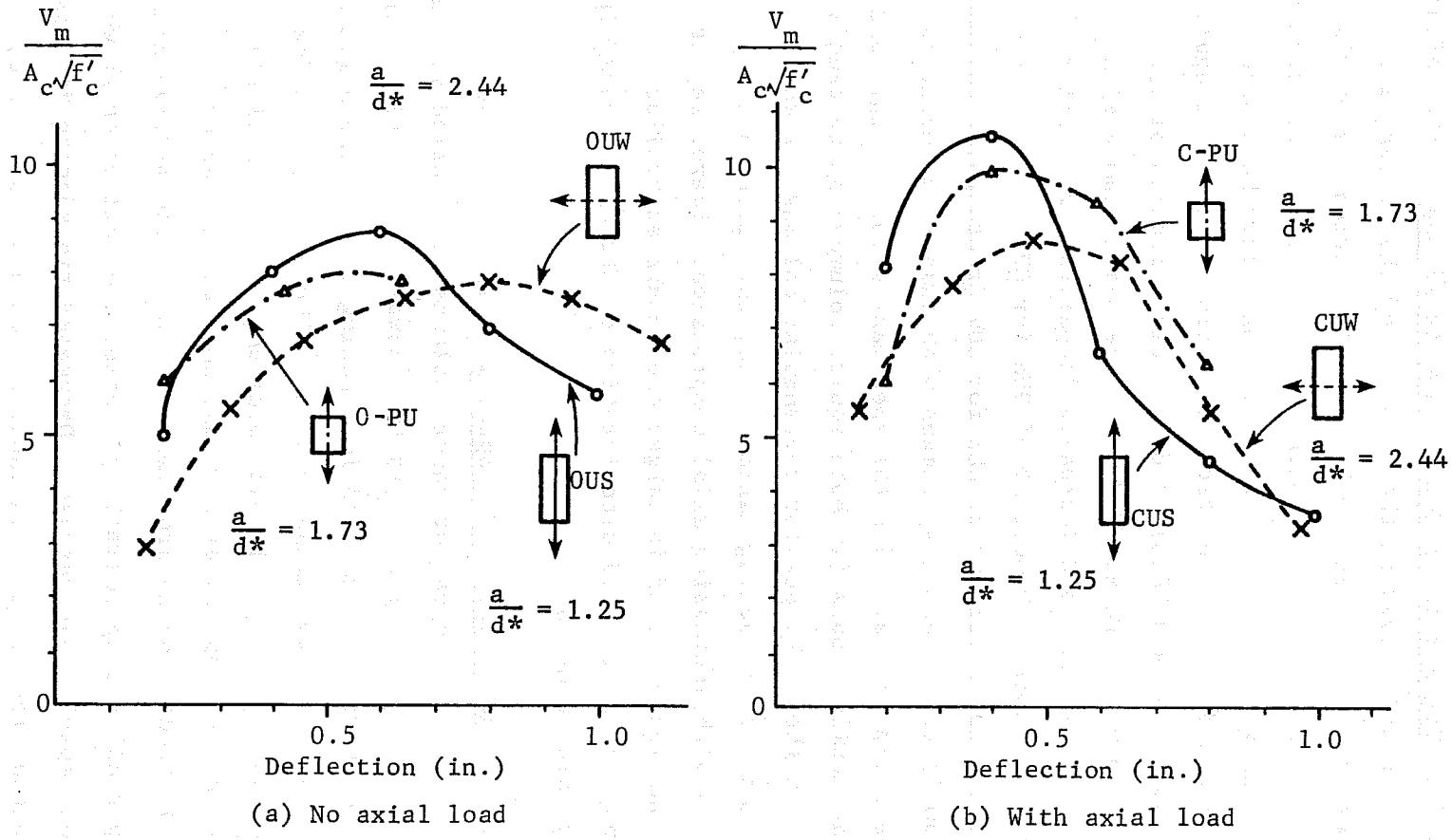

Fig. 6.11 Effect of shear span to effective depth ratio

6.5.3 The Effect of Compressive Axial Load. The influence of compressive axial load on the behavior of the rectangular columns was described in Sec. 5.5. In this section the results of square columns are compared with those of rectangular columns. Figure 6.12 shows envelopes of the peak loads for the square columns (0-PU and C-PU), the strong direction of the rectangular columns (0US, CUS, and 2CUS), and the weak direction of the rectangular columns (0UW and CUW). As the axial compression increases, the maximum load increases 25 percent of 0-PU for C-PU (square columns), 20 percent of 0US for CUS, 35 percent of 0US for 2CUS, and 13 percent of 0UW for CUW (rectangular columns). The maximum lateral load in specimens with axial load occurred at 2/3 of the deflection at which the specimens without axial load reached the maximum loads (in both square columns and rectangular columns). In the envelopes for rectangular columns, it was observed that after reaching maximum load, the strength dropped more rapidly with increasing axial compression. Therefore, it is clear that maximum load is larger and occurs at smaller deflections, but more rapid deterioration of strength occurs with increasing axial compression.

6.5.4 The Effect of Tie Spacing. Figure 6.13 shows the shear-deflection envelopes for square columns with varied spacings of transverse reinforcement tested by Woodward.[24] In this figure, the specimen (C-DB-32) with 1.13 in. spacing reached the highest capacity of all five specimens, but after the maximum load the strength dropped rapidly. In all specimens, there was little difference in the slope after the maximum load is reached. However, the transverse reinforcement increased the maximum capacity about 20 percent and approximately doubled the deflection at which the maximum capacity was reached. Decreased tie spacing increased the deformation levels at which capacity could be maintained, but

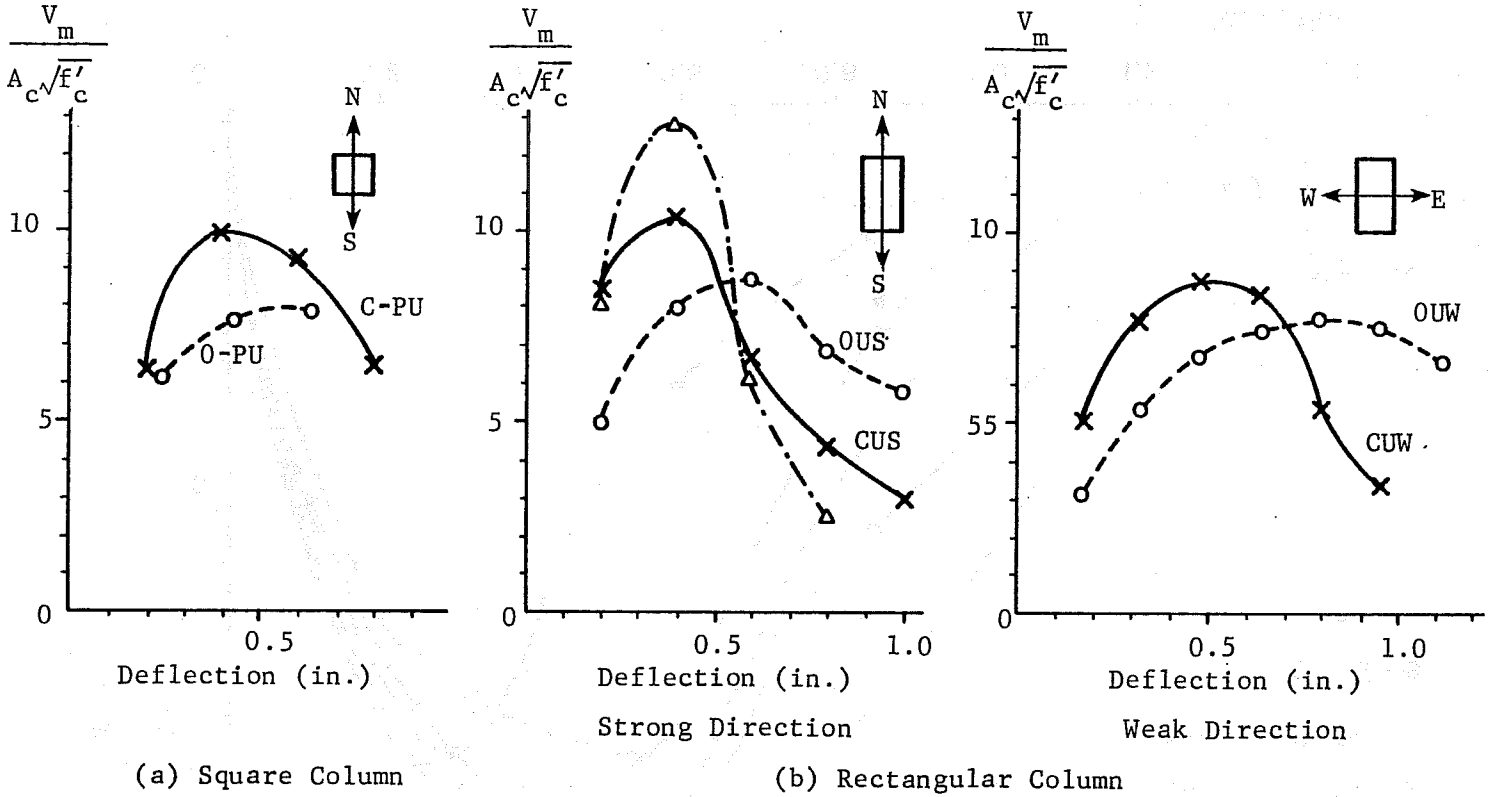

Fig. 6.12 Effect of compressive axial load—square and rectangular columns

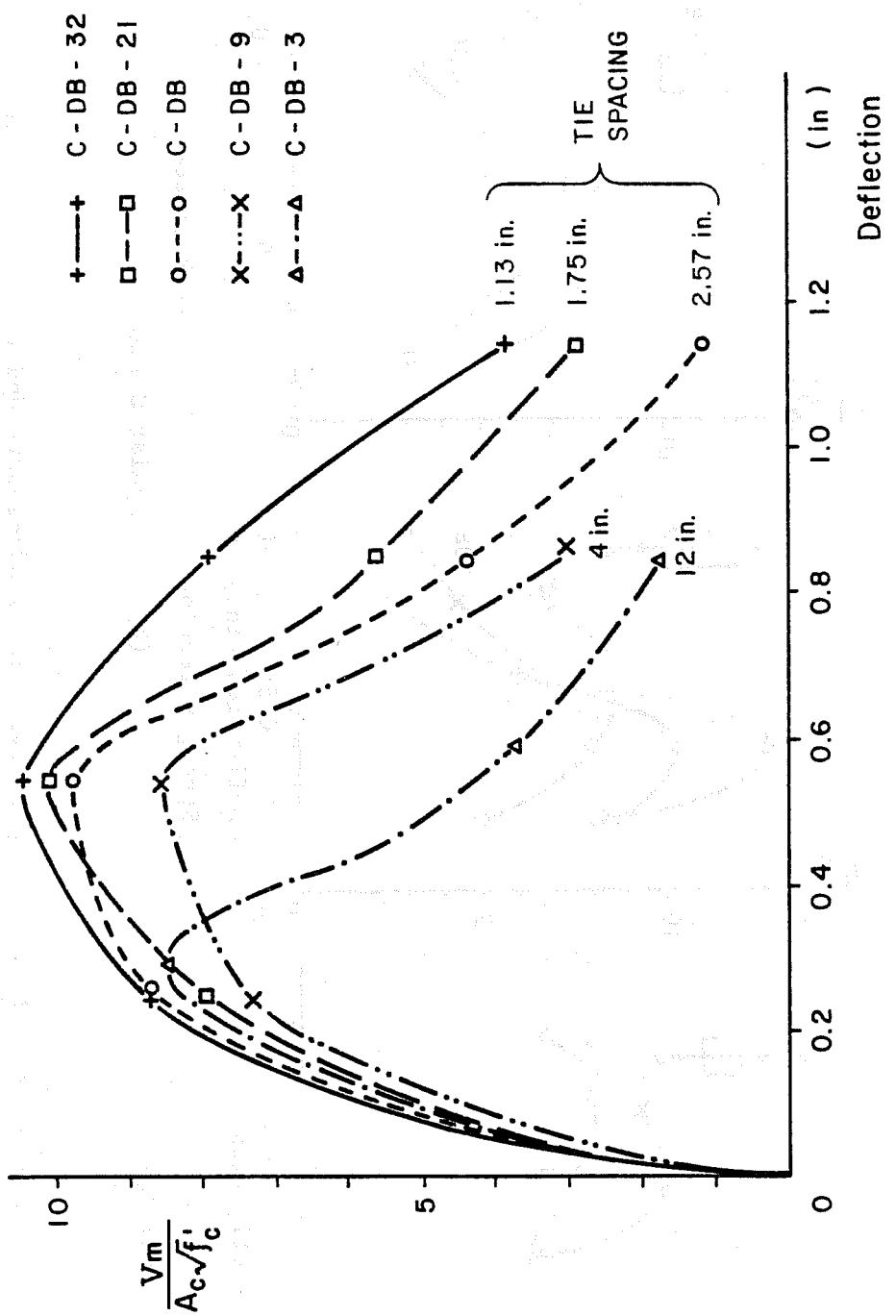

Fig. 6.13 Effect of tie spacing on deterioration

did not significantly improve the rate of deterioration once the capacity began to decrease.

6.5.5 Review of Deterioration. In Sec. 6.5, the deterioration of strength as influenced by the loading history, shear span to effective depth ratio, axial compression, and tie spacing was discussed. Based on comparisons of the strength envelopes, it was observed that the maximum load in the column under bidirectional loading reached almost the same value as that under unidirectional loading, but after the deflection corresponding to the maximum load under unidirectional loading was reached, the strength began to drop in both directions. As the shear span to effective depth ratio decreased, the maximum load in the column increased, but after it was reached, deterioration of the strength occurred more rapidly. As axial compression increased, the maximum load became larger and occurred at smaller deflection levels, but more rapid deterioration of strength occurred. As amounts of transverse reinforcement increased, the maximum capacity increased somewhat and the ability of the specimen to maintain capacity was improved, but after the maximum load was reached deterioration of strength still occurred rapidly.

CHAPTER 7

PREDICTION OF LATERAL CAPACITY

7.1 General

From the discussions and comparisons of experimental results in Chapters 5 and 6, it is clear that two important factors must be considered in evaluating the behavior of short columns: (1) the shear capacity of short columns, and (2) the deterioration of the strength after reaching maximum load. It was observed during testing that in many cases the strength of the short column dropped rapidly after reaching maximum load, even though the maximum load was equal to or greater than the calculated flexural capacity which is described in this chapter. Therefore, to ensure that the short columns will have adequate energy dissipating characteristics, not only must the shear capacity equal or exceed the flexural capacity, but deterioration of strength must be controlled or eliminated. In this chapter several methods of calculating lateral load capacity of reinforced concrete members are presented and in the next chapter the procedure to evaluate the behavior of short columns taken into account shear strength and deterioration of strength is described.

The shear capacity of columns will be evaluated using (1) equations contained in ACI 318-77,[25] (2) formulations based on plasticity theory which have been proposed by Thürlimann[27,28,29] and Nielsen[30,31,32] using a refined truss model, and (3) an equation proposed by Zsutty[33,34] which is based on a statistical analysis of existing experimental data. In addition, an equation based on a statistical analysis of data from various studies of

beams failing in shear is introduced. For each approach, the computed shear capacity is compared with the measured capacity of square and rectangular short columns. The shear capacity is also compared with computed lateral flexural capacity.

7.2 Computed Lateral Flexural Capacity

The lateral load capacity of the short column based on flexure was derived from consideration of a hinging mechanism forming at the ends of the column as shown in Fig. 7.1. The lateral load capacity governed by flexure is

$$V_f = \frac{2M_n}{L} \tag{7.1}$$

where V_f = lateral load capacity based on M_n

M_n = nominal moment strength

L = length of the column

The ultimate moment capacity for each column was calculated using a computer program developed to obtain the relation between moment and curvature of a reinforced concrete section for loading in any direction (bending about any axis).

The program divides the section into a number of elements as shown in Fig. 7.2, and assumes that the strain at the centroid of each element is uniform over that element. In the case of diagonal loading, the calculation of moment is slightly more complicated, but basically is not different from loading in a principal direction. If there are n elements, numbered from the top, each element has depth h/n (h is the overall depth of the section (Fig. 7.2)). The depth from the top to the centroid of element i is (i - 0.5)h/n. If the strain in the top fiber and the neutral axis depth from the top fiber are

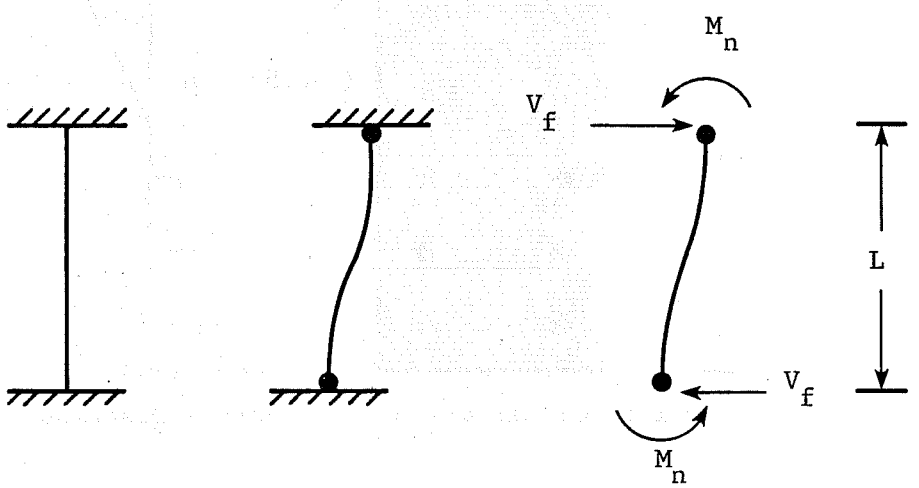

$$V_f = \frac{2M_n}{L}$$

Fig. 7.1 Column hinging mechanism

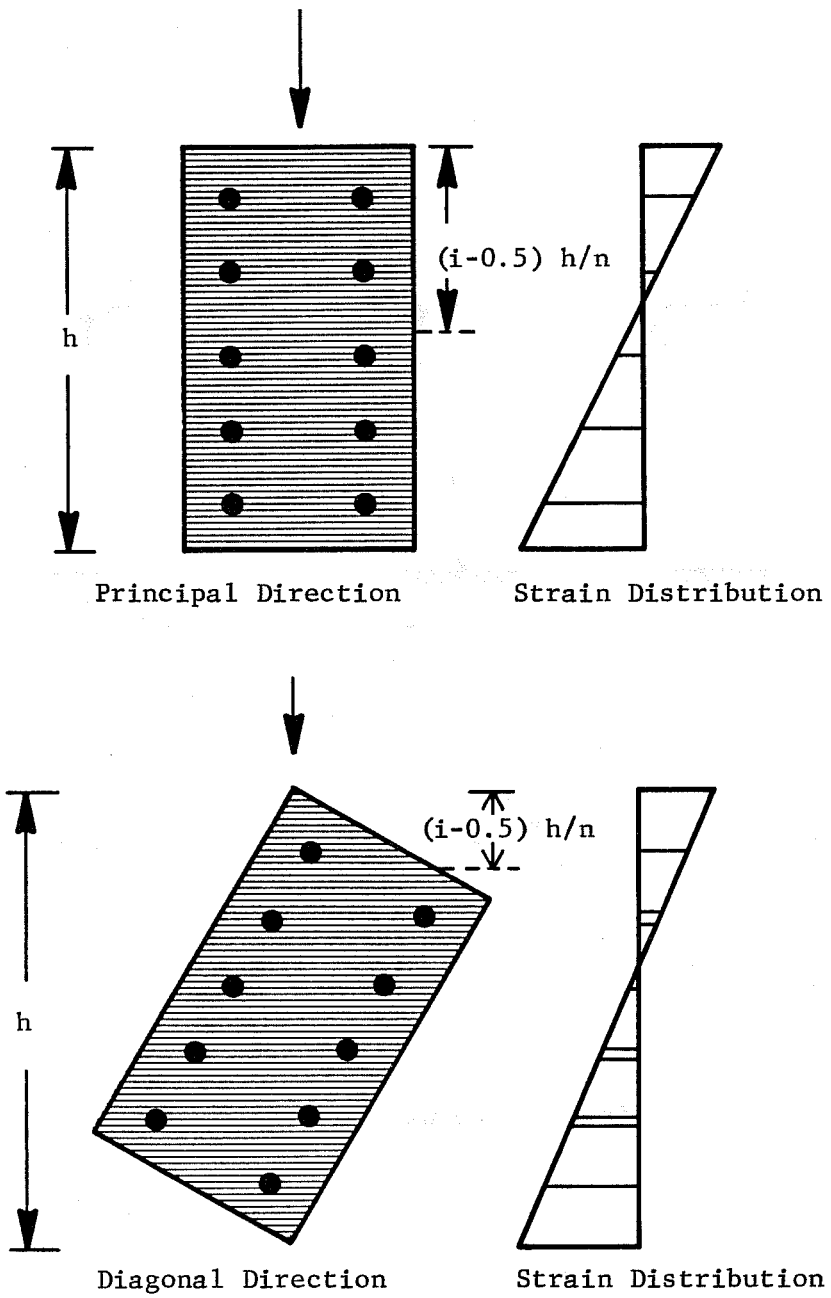

Fig. 7.2 Discrete elements

assumed, the strain at the centroid of the element is calculated. The stress on the element is determined on the basis of assumed stress-strain curves for both concrete and steel. From the stress and the area of the concrete and steel in each element, the force in each element is calculated and summed to compute the axial load. The iterative technique is used to make the computed axial load equal to the given axial load. Each element force times the corresponding moment arm is summed to calculate the moment. Figure 7.3 shows the flow chart used to obtain moment-curvature relationships for the column sections.

The stress-strain curves for the concrete and steel used in the program are shown in Fig. 7.4 and Fig. 7.5, respectively. The stress-strain curve for confined concrete by Kent and Park[26] as shown in Fig. 7.4 was used for the compression zone of the concrete. For the tension zone (first loading cycle only), the same quadratic curve as for the compression zone was used and the descending portion consisted of a line from the concrete tensile strength (f_t) to 85 percent of f_t. The stress-strain curve shown in Fig. 7.5 was used for the steel. The compressive yield strength was assumed the same as the tensile yield strength and before strain hardening, a bilinear stress-strain curve was used. After strain hardening, a quadratic expression defined the curve until ultimate strength was reached.

Measured material strengths were used to compute the moment capacity of the square and rectangular columns. In Table 7.1 the flexural capacities of the columns (V_f) are compared with the measured maximum loads (V_m). For four specimens, primarily square columns, the ratio of V_m to V_f was more than 1.0. On the basis of the computed capacity, those specimens were likely controlled by flexure. However, for the other specimens in which $V_m/V_f < 1.0$, the measured capacity will be compared with computed shear as described in the next section.

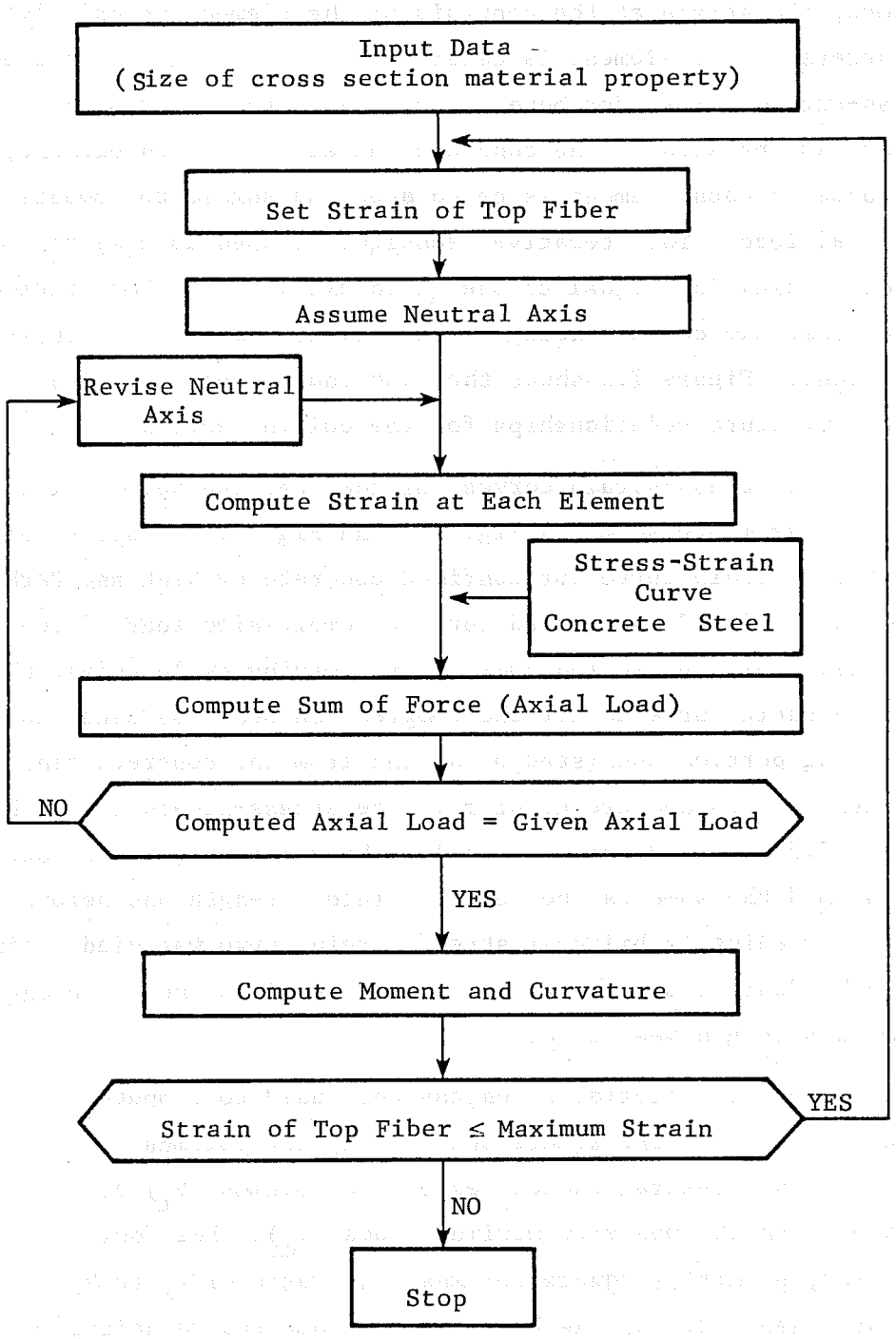

Fig. 7.3 Flow chart of the program

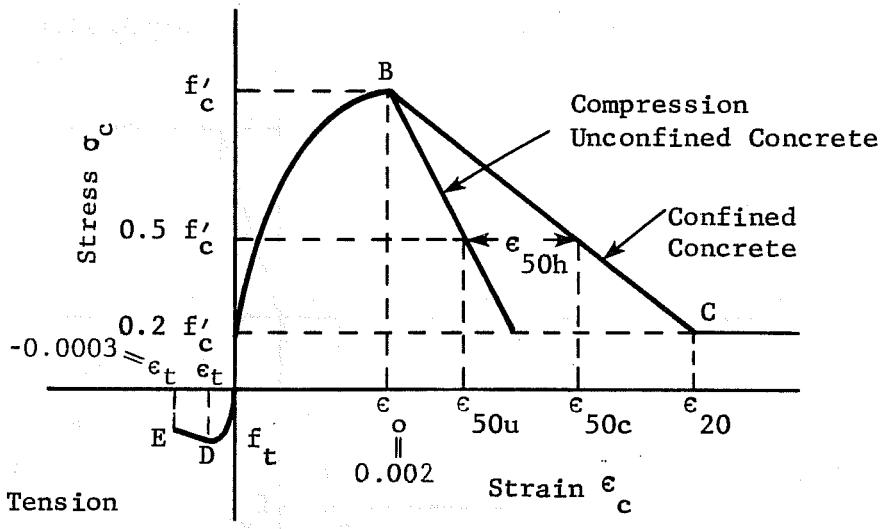

Region D-A-B $\quad \sigma_c = f'_c \left[\frac{2\epsilon_c}{0.002} - \left(\frac{\epsilon_c}{0.002}\right)^2\right]$

$f_t = -7.5\sqrt{f'_c} \qquad \epsilon_t = 0.002\, f_t/f'_c$

Region B-C $\quad \sigma_c = f'_c\, [\, 1 - Z\, (\epsilon_c - 0.002)\,]$

$$Z = \frac{0.5}{\epsilon_{50u} + \epsilon_{50h} - 0.002} \qquad \epsilon_{50u} = \frac{3 + 0.002\, f'_c}{f'_c - 1000}$$

$$\epsilon_{50h} = 0.75\, \rho_s \sqrt{\frac{b''}{s_h}}$$

Region D-E $\quad \sigma_c = f_t \left[\, 1 - 0.15\, \frac{\epsilon_t - \epsilon_c}{\epsilon_t + 0.0003}\, \right]$

σ_c - concrete stress, psi

ϵ_c - concrete strain, in/in

f'_c - concrete compressive strength, psi

f_t - concrete tensile strength, psi

ρ_s - ratio of volume of transverse reinforcement to volume of confined core

b'' - width of confined core

s_h - spacing of hoops

Fig. 7.4 Concrete stress-strain relation

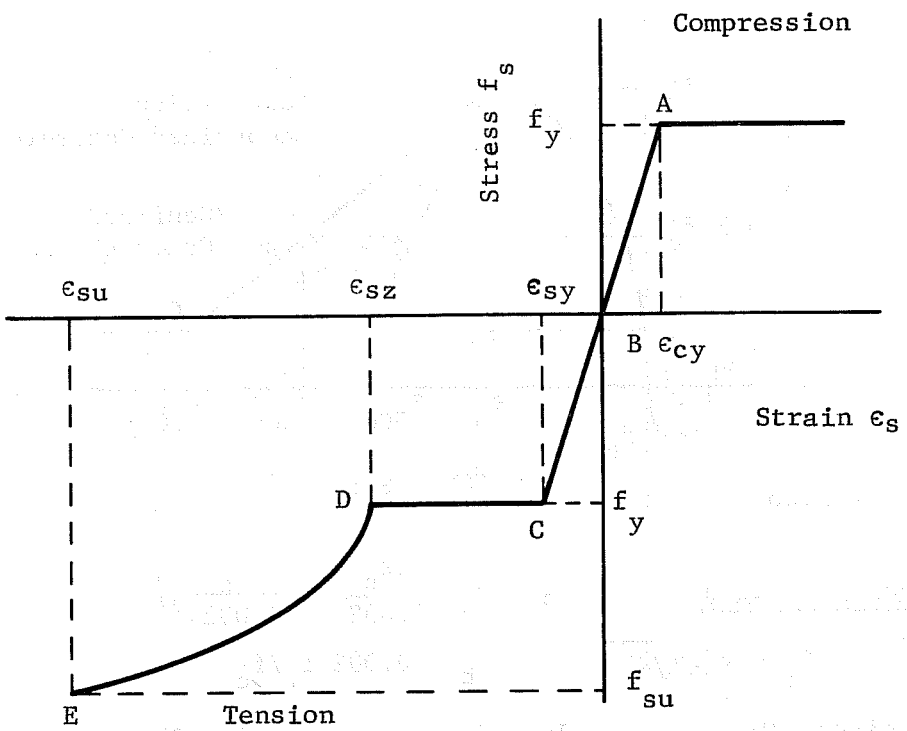

Region A-B-C $\quad f_s = E_s \epsilon_s$

Region C-D $\quad f_s = f_y$

Region D-E $\quad f_s = f_{su} - (f_{su} - f_y)\left[\dfrac{\epsilon_{su} - \epsilon_s}{\epsilon_{su} - \epsilon_{sz}}\right]^2$

f_s - steel stress, psi $\qquad$ ϵ_s - steel strain in/in

f_y - steel yield strength, psi

f_{su} - steel ultimate strength, psi

E_s - steel Young's modulus, psi

Fig. 7.5 Steel stress-strain relation

TABLE 7.1 COMPUTED FLEXURAL AND OBSERVED CAPACITIES

	Specimen Name	f'_c psi	N kips	V_m kips	$\frac{V_m}{A_c\sqrt{f'_c}}$	V_f kips	$\frac{V_f}{A_c\sqrt{f'_c}}$	V_m / V_f
SQUARE COLUMN	O-PU	5000	0	56	7.9	49	6.9	1.14*
	C-PU	4450	120	67	10.0	80	12.0	0.84
	O-PB	6000	0	52	6.7	53	6.8	0.98
	C-PB	5950	120	77	10.0	78	10.1	0.99
	O-DM	5950	0	55	7.1	65	8.4	0.85
	C-DM	5250	120	68	9.4	76	10.5	0.89
	O-DU	4950	0	64	9.1	59	8.3	1.08*
	O-DB	5050	0	61	8.6	59	8.3	1.03*
	C-DB	4650	120	68	10.0	73	10.7	0.93
	C-DB32	5400	120	78	10.6	80	10.9	0.98
	C-DB21	5750	120	76	10.0	84	11.1	0.90
	C-DB9	5750	120	64	8.4	84	11.1	0.76
	C-DB3	6100	120	66	8.5	80	10.2	0.83
RECTANGULAR COLUMN	OUS	5810	0	66	8.8	95	12.7	0.69
	OUW	5820	0	57	7.6	51	6.8	1.12*
	CMS	6090	120	86	11.2	120	15.7	0.72
	CUS	5060	120	74	10.6	113	16.2	0.65
	CUW	5060	120	60	8.6	68	9.8	0.88
	2CUS	6090	240	91	11.9	134	17.5	0.68
	CDS30	6180	120	80	10.3	105	13.6	0.76
	CDW30	6120	120	74	9.7	78	10.2	0.95
	(s) CBSW	5090	120	69	9.9	114	16.3	0.61
	(w)			52	7.4	69	9.9	0.75
	(s) CDSW30	5090	120	62	8.8	98	14.0	0.63
	(w)			57	8.1	73	10.4	0.78

(s) - strong direction

(w) - weak direction

* - reached computed flexural capacity

7.3 Computed Lateral Shear Capacity

Several methods to calculate the shear capacities of short columns are described and compared with the experimental results. From the tests of short columns, it was concluded (Sec. 6.4) that if the maximum capacities in the principal directions are calculated, the capacity in a diagonal loading direction can be calculated easily using a circle for the square columns and an ellipse for the rectangular columns to define the interaction curve. It was also concluded that with bidirectional loading, the capacity in at least one loading direction would reach almost the same capacity as a similar column under unidirectional loading in the same direction.

The shear capacity of a diagonally loaded member is not specifically defined in all methods described in this chapter. However, from the empirical results of this study, it is not necessary to calculate that capacity because an interaction relationship can be defined. For example, the shear capacity of the square column under loading 45^{o} from the principal direction is equal to that in a principal direction, because the interaction is a circular curve. In a rectangular column, the shear capacity under loading 30^{o} from the strong axis can be calculated from the shear capacities using the strength in the strong and weak directions and constructing an elliptical interaction curve.

The shear capacity equations in all methods to be described in this report are based on beams loaded monotonically. The short columns were loaded cyclically. However, previous investigations of the square columns[22,23,24] showed that the maximum shear capacity was not significantly affected by the loading history--monotonic, unidirectional or bidirectional. The results of the current investigation indicate that the

specimens with monotonic, unidirectional and bidirectional loading (CMS, CUS and CBSW) had almost the same maximum shear capacities (Fig. 5.8). Therefore, all methods based on monotonic tests are assumed to be appropriate for determining the capacity of cyclically loaded columns, provided that the proper effective shear area is considered in each case. For bidirectional loading only the shear capacity in the direction reaching the deflection corresponding to the maximum shear strength of columns under unidirectional loading was compared with the calculated shear capacity.

7.3.1 Shear Capacity--ACI 318-77. The shear strength of a member according to the 1977 ACI Building Code[25] is taken as the summation of the contribution of the concrete (V_c) and the contribution of the transverse reinforcement (V_s). The V_c term represents the capacity of the concrete at the onset of shear cracking. There are two equations for V_c. The first one is given by Eq. (11.3) in the ACI Code:

$$V_c = 2b_w d \sqrt{f'_c} \tag{7.2}$$

where V_c = nominal shear strength provided by concrete, lbs.

b_w = web width, in.

d = distance from extreme compression fiber to centroid of longitudinal tension reinforcement, in.

For members subjected to axial compression, Eq. (11.4) in the ACI Code is used.

$$V_c = 2\left(1 + \frac{N}{2000A_g}\right)b_w d \sqrt{f'_c} \tag{7.3}$$

where N = applied axial compression

A_g = gross area of cross section

N/A_g is expressed by psi unit.

The second one is given by Eq. (11.6) in the ACI Code:

$$V_c = b_w d \left(1.9\sqrt{f'_c} + 2500\rho_w \frac{V_u}{M_u} d\right) \tag{7.4}$$

where ρ_w = ratio of longitudinal reinforcement, $A_s/b_w d$

A_s = area of longitudinal tension reinforcement, in^2

V_u = factored shear force at section, lbs.

M_u = factored moment at section, lbs. in.

M_u is occurring simultaneously with V_u at section considered.

The calculated value of V_c by this equation should be less than $3.5b_w d\sqrt{f'_c}$. For members subjected to axial compression, M_m shall be substituted for M_u (Eq. (11.7) in the ACI Code).

$$M_m = M_u - N\frac{(4h - d)}{8} \tag{7.5}$$

where h = overall depth of section, in.

However, V_c shall not be taken greater than (Eq. (11.8) in the ACI Code)

$$V_c = 3.5b_w d\sqrt{f'_c}\sqrt{1 + 0.002N/A_g} \tag{7.6}$$

For transverse reinforcement perpendicular to the axis of member, the equation for V_s (Eq. (11.17) in the ACI Code) is

$$V_s = \frac{A_v f_{ys} d}{s_h} \tag{7.7}$$

where V_s = nominal shear strength provided by transverse reinforcement

A_v = area of transverse reinforcement within a distance s_h, $in.^2$

f_{ys} = yield strength of transverse reinforcement, psi

s_h = spacing of transverse reinforcement, center-to-center, in.

The total shear capacity is $V_n = V_c + V_s$.

The ACI Code also contains special provisions for deep beams. Deep beams are defined by the ACI Code as having a length-to-effective depth (d) ratio of less than 5 and loaded on the compression face. The deep beam provisions are based on simple beam tests with one or two loading points on the compression face as shown in Fig. 7.6(a). The applied load is transferred to the reaction through a compression strut. In the deep beam, two compressive struts occur from the applied load to the supports. As shown in Fig. 7.6(b), the short column can be considered to have only one compressive strut from top to bottom in the column. Unlike the simple beam of Fig. 7.6(a) which has moment of the same sign over its entire length, moment in the short column changes sign at the midheight of the column. The mechanism of the short column is similar to that of continuous beams. Therefore, deep beam provisions were not considered in calculations for the shear capacity of the short columns.

In the ACI Code the effective depth (d) is defined as the distance from extreme compression fiber to centroid of longitudinal tension reinforcement. Therefore, the values of effective depth as shown in Fig. 7.7 were used. In comparison with calculated shear using this effective depth, the effective depth (d^*) defined as the distance from extreme compression fiber

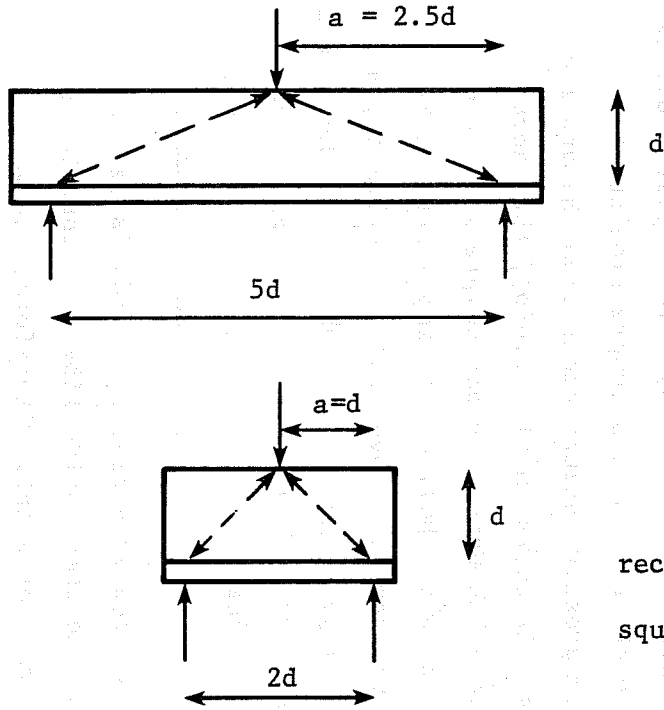

(a) Deep Beams

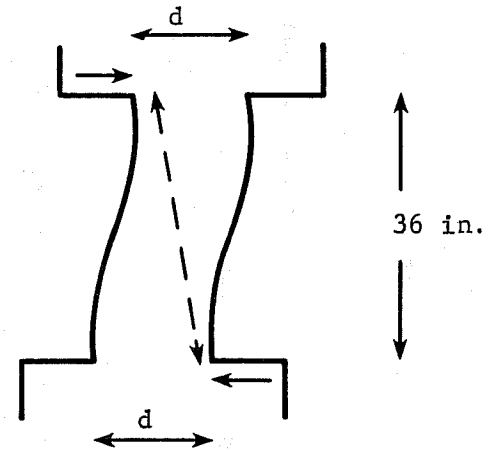

rectangular { d = 11.20 in. strong direction
d = 7.39 in. weak direction

square d = 8.63 in.

(b) Short Column

Fig. 7.6 Comparison of deep beam and short column

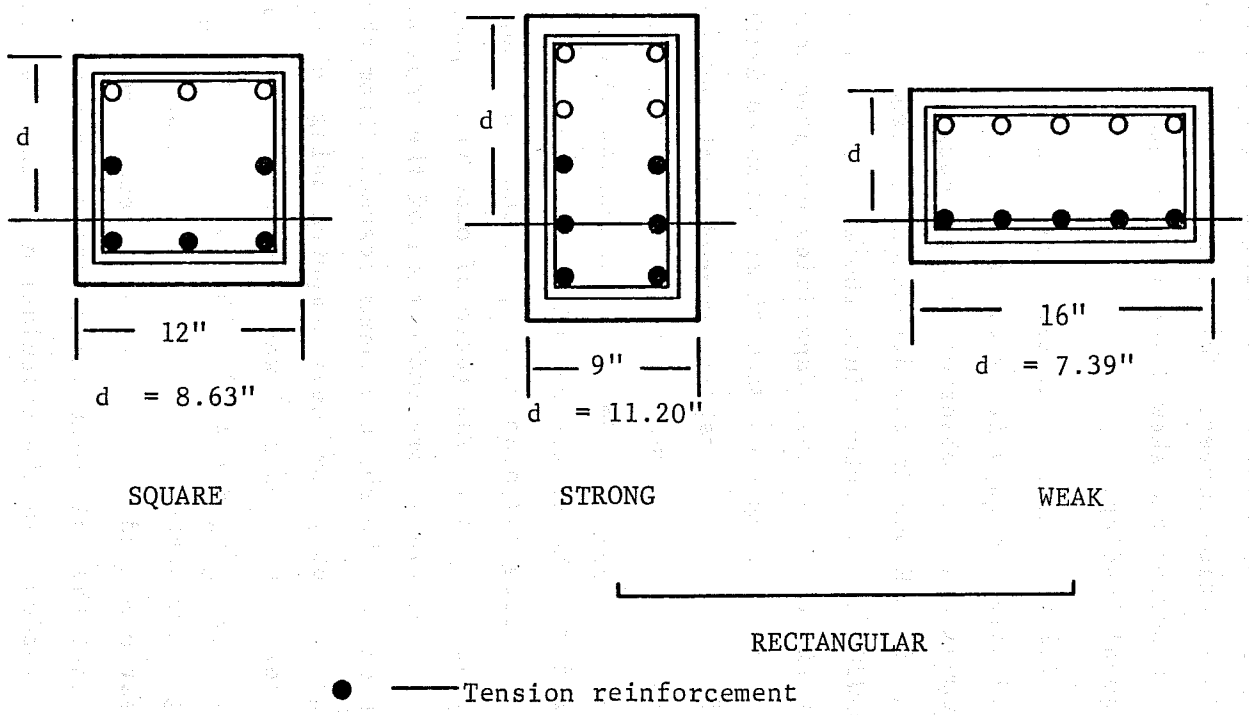

Fig. 7.7 Definition of effective depth by ACI method

to extreme tension reinforcement is also used. The shear capacity of the column under diagonal loading was computed from the shear capacities in the principal loading directions using circular and elliptical interaction curves. Therefore, there was no need to attempt to define the skewed sectional area carrying shear under diagonal loading.

In Table 7.2 the shear capacities computed using the ACI equations and observed capacities are compared. For the rectangular columns, only the observed shear capacities in the strong direction of CBSW and in the direction 30^{o} from the weak axis of CDSW30 were selected since those directions reached maximum capacity first. The shear capacities computed using Eqs. (7.2) and (7.3) are compared with those computed using Eqs. (7.4), (7.5), and (7.6) first (d is used as the effective depth in both cases). The calculated values using the former equations are slightly greater than those using the latter equations. Therefore, the former equations are used to compare with observed capacities and also to compute the shear capacities using the effective depth d^*. The ratio of observed capacity to the capacity by ACI provides some indication of the applicability of the ACI equations to the short columns tested. From the values of V_m/V_n (average is 1.66), the shear computed using the ACI equations is conservative. When d^* was selected as the effective depth, the average of V_m/V_n was 1.38. The values of V_m/V_n calculated using d^* are nearer 1.0 than those calculated using d. However, the shear computed using d^* is still conservative. It should be noted that the specimens which reached computed flexural capacity are not included in the calculation of the average and standard deviation of V_m/V_n. The results of some short columns tested in Japan[20,21] (Fig. 7.8) show that shear deterioration occurred after maximum capacity was reached. In this case V_n(ACI)

TABLE 7.2 ACI METHOD AND OBSERVED CAPACITIES

	Specimen Name	V_m kips	$\frac{V_m}{A_c\sqrt{f'_c}}$	(1) V_c kips	V_s kips	(1) V_n	(2) V_c	(2) V_n	(1) $\frac{V_n}{A_c\sqrt{f'_c}}$	(3) V_c	(3) V_s	(3) V_n	(3) $\frac{V_n}{A_c\sqrt{f'_c}}$	V_m / V_n (1)	V_m / V_n (3)
SQUARE COLUMN	O-PU	56	7.9	15	21	36	16	37	5.1	18	24	42	5.9	1.56	1.33*
	C-PU	67	10.0	20	21	41	18	39	6.1	24	24	48	7.2	1.63	1.40
	O-PB	52	6.7	16	21	37	17	38	4.8	19	24	43	5.5	1.41	1.21
	C-PB	77	10.0	23	21	44	19	40	5.7	27	24	51	6.6	1.75	1.51
	O-DM	55	7.1	16	22	38	18	40	4.9	19	26	45	5.8	1.45	1.22
	C-DM	68	9.4	21	22	43	19	41	5.9	26	26	52	7.2	1.58	1.31
	O-DU	64	9.1	15	21	36	16	37	5.1	17	24	41	5.8	1.78	1.56*
	O-DB	61	8.6	15	21	36	16	37	5.1	18	24	42	5.9	1.69	1.45*
	C-DB	68	10.0	20	22	42	18	40	6.1	24	26	50	7.3	1.62	1.36
	C-DB32	78	10.6	22	50	72	19	69	9.8	26	59	85	11.6	1.08	0.92
	C-DB21	76	10.0	22	33	55	19	52	7.3	27	39	66	8.7	1.38	1.15
	C-DB9	64	8.4	22	14	36	19	33	4.7	27	17	44	5.8	1.78	1.45
	C-DB3	66	8.5	23	5	28	20	25	3.6	27	6	33	4.1	2.36	2.00
RECTANGULAR COLUMN	OUS	66	8.8	15	19	34	19	38	4.6	20	24	44	5.9	1.94	1.50
	OUW	57	7.6	18	25	43	19	44	5.8	18	25	43	5.8	1.33	1.32*
	CMS	86	11.2	22	19	41	21	40	5.4	29	24	53	6.9	2.10	1.62
	CUS	74	10.6	20	19	39	20	39	5.6	26	24	50	7.2	1.90	1.48
	CUW	60	8.6	24	25	49	19	44	7.0	24	25	49	7.0	1.22	1.22
	2CUS	91	11.9	29	19	48	27	46	6.3	37	24	61	8.0	1.90	1.49
	CDS30	80	10.3	--	--	43	--	41	5.6	--	--	53	6.9	1.86	1.51
	CDW30	74	9.7	--	--	48	--	44	6.3	--	--	52	6.8	1.54	1.42
	(s) CBSW	69	9.9	20	19	39	20	39	5.6	26	24	50	7.1	1.80	1.38
	(w) CDSW30	57	8.1	--	--	46	--	43	6.6	--	--	50	7.1	1.24	1.14
													Average	1.66	1.38
													Standard Deviation	0.31	0.22

(s) - strong direction

(w) - weak direction

* - specimens reached computed flexural capacities neglected in average and standard deviation

(1) - ACI Eqs. 11.3 and 11.4 } using d

(2) - ACI Eqs. 11.6, 11.7 and 11.8 }

(3) - ACI Eqs. 11.3 and 11.4 using d*

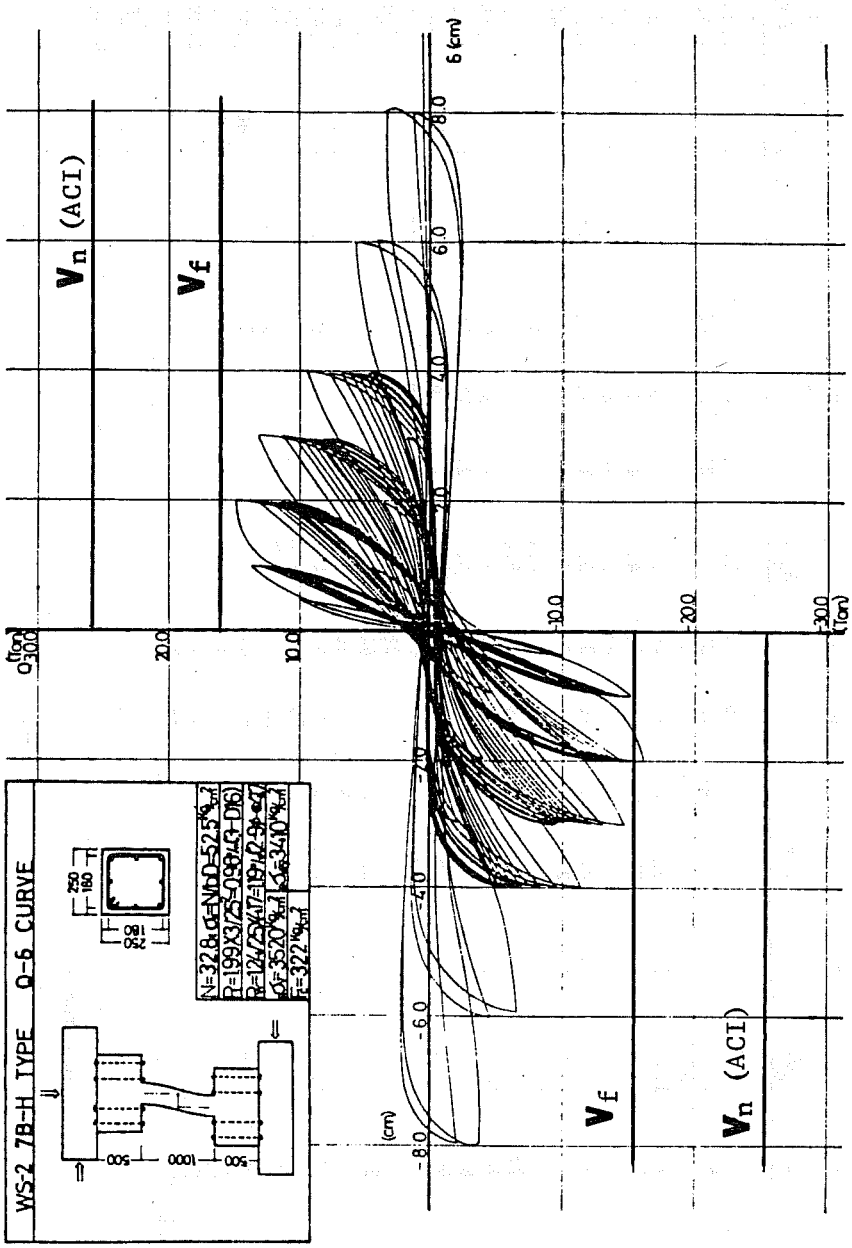

Fig. 7.8 Shear deterioration of short columns with V_n (ACI) ≥ V_f

was much larger than V_f because a large amount of transverse reinforcement was used. For $V_n > V_f$, the behavior of a short column should be governed by flexure. Therefore, in some short columns designed using ACI equations the deterioration of shear capacity may occur leading to a severe reduction of energy dissipating capacity. The tests in which shear deterioration occurred (Refs. 20 and 21) will be discussed in detail in Sec. 7.3.4.4 and in Chapter 8.

7.3.2 Shear Capacity-Plasticity Theory. Over the past ten years research groups at the Swiss Federal Institute of Technology at Zurich and at the Technical University of Denmark have been developing approaches to design for shear and torsion in reinforced concrete and prestressed concrete members using plasticity theorems. The plasticity theorems are applied to a refined truss model. A similar approach has been proposed by researchers in Canada (Collins and Mitchell[54]), but was not available at the time this evaluation was made.

7.3.2.1 Thürlimann. Thürlimann's approach[27,28,29] is based on the plasticity theory applied to the truss model shown in Fig. 7.9. The truss model consists of longitudinal reinforcement, concrete in the compression zone acting as a chord, vertical stirrups, and concrete diagonals as inclined compression struts. In the ACI method, the inclination α of the concrete compression strut is assumed to be at 45^o. In the Thürlimann approach, α is a variable. Since the section is analyzed using plasticity theorems, the inclination α corresponds to ultimate and not to first inclined cracking. This approach is intended to provide the maximum strength of the reinforced concrete member. The development is based on six assumptions:

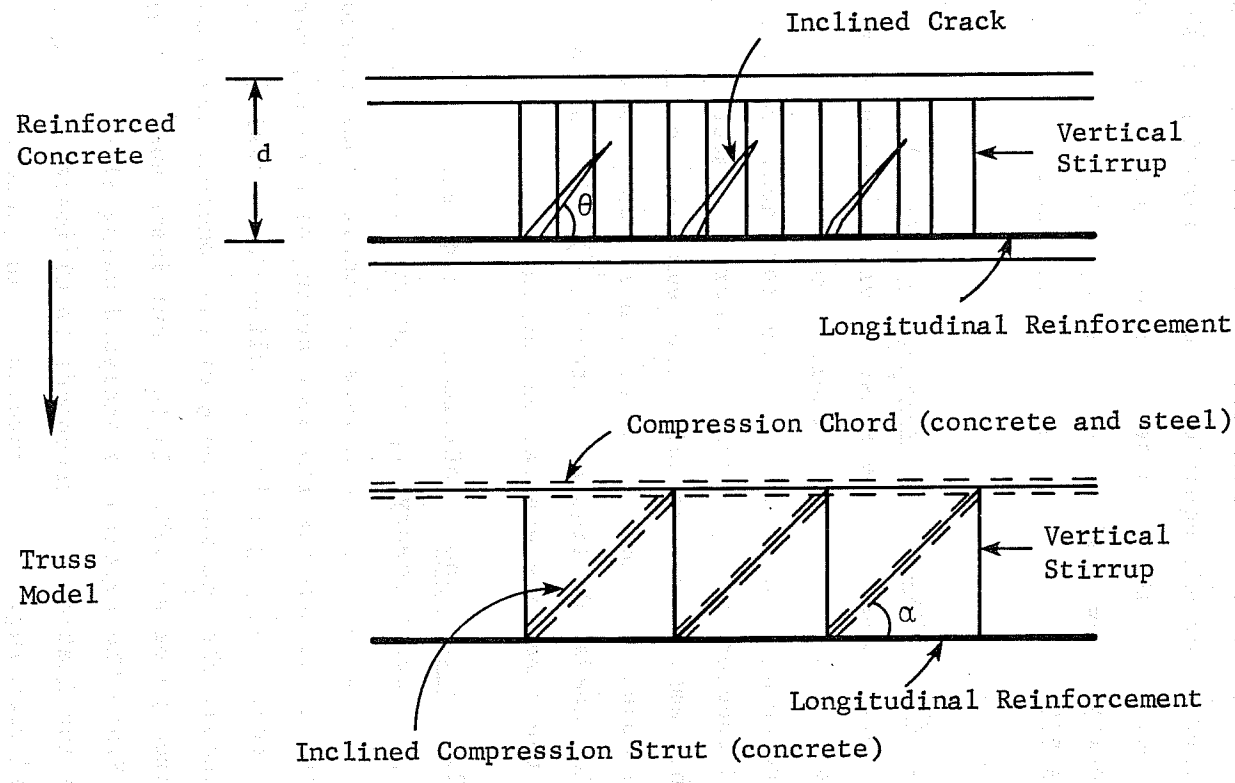

Fig. 7.9 Truss model

(1) At ultimate load the concrete resists only compression.

(2) The reinforcement causes only uniaxial forces (no dowel forces).

(3) Failure occurs due to yielding of the longitudinal reinforcement prior to crushing of the concrete (underreinforced section).

(4) The reinforcement must be properly detailed to prevent local failure.

(5) At ultimate load, after all elastic and inelastic deformations and redistribution of internal forces have taken place, the following holds true: uniaxial yielding of the steel reinforcement and the opening of the final cracks in the concrete is normal to the crack direction.

(6) To prevent crushing of the concrete, there must be an upper limit for the concrete stresses, and also limits on the angle of inclination α of the compression struts.

Figure 7.10 shows the idealized web of a concrete section where shear V, bending M, and axial force N are acting. The truss forces are the upper and lower stringer forces F_u and F_ℓ, the stirrup forces S, and the resultant diagonal force D resisted by the concrete compression struts under the variable inclination α. From an equilibrium analysis, the following relations can be developed. The diagonal force D:

$$D = \frac{V}{\sin\alpha} \tag{7.8}$$

Therefore the compressive stress in the concrete diagonals is σ_c:

$$F_{\ell} = F_{y\ell} \tag{7.18}$$

$$S = S_y \tag{7.19}$$

Neglecting the axial force, the ultimate values of moment M_P, and shear V_P along with Eqs. (7.18) and (7.19) can be substituted into Eqs. (7.11) and (7.13):

$$F_{y\ell} = \frac{M_P}{h'} + \frac{V_P}{2} \cot\alpha \tag{7.20}$$

$$S_y = V_P \times \frac{s_h}{h'} \tan\alpha \tag{7.21}$$

$$\tan\alpha = \frac{S_y h'}{V_P s_h} \tag{7.22}$$

Combining Eqs. (7.20) and (7.22):

$$F_{y\ell} = \frac{M_P}{h'} + \frac{1}{2} \times \frac{V_P^2 s_h}{S_y h'} \tag{7.23}$$

For convenience, the following reference values are used. For $V_P = 0$, the "plastic moment" M_{P0} is derived from Eq. (7.23)

$$M_{P0} = F_{y\ell} h' = A_{\ell} f_{y\ell} h' \tag{7.24}$$

For $M_P = 0$, the "plastic shear force" V_{P0} is derived from Eq. (7.23)

$$V_{P0} = \sqrt{\frac{2F_{y\ell} S_y h'}{s_h}} \tag{7.25}$$

Equations (7.23), (7.24), and (7.25) produce the following equation for the interaction between shear and bending:

$$\frac{M_P}{M_{PO}} + \left(\frac{V_P}{V_{PO}}\right)^2 = 1 \qquad (7.26)$$

Ultimate shear in the beam and the column as shown in Fig. 7.11 can be computed using Eq. (7.26). M_P and V_P are related as follows:

$$\frac{M_P}{V_P} = a \qquad (7.27)$$

where a is the shear span. Combining Eqs. (7.26) and (7.27):

$$V_P^2 + \frac{aV_{PO}^2}{M_{PO}} V_P - V_{PO}^2 = 0 \qquad (7.28)$$

The quadratic equation (7.28) is solved for ultimate shear V_P:

$$V_P = \frac{V_{PO}}{2M_{PO}} \left\{ \sqrt{a^2 V_{PO}^2 + 4M_{PO}^2} - aV_{PO} \right\} \qquad (7.29)$$

From experimental results reviewed by Thürlimann, the crack angle α has the limits:

$$0.5 \leq \tan\alpha \leq 2.0 \qquad (7.30)$$

The bending-shear interaction diagram, based on Eq. (7.26) can be divided into three types of failure mechanisms as shown in Fig. 7.12. These mechanisms are governed by the inclination of the angle α. The limiting values of $\tan\alpha$ are represented as dashed lines in the figure. For values of $\tan\alpha$ less than 0.5, a shear mechanism will occur. It means that the transverse reinforcement yields without yielding of the longitudinal reinforcement. For values

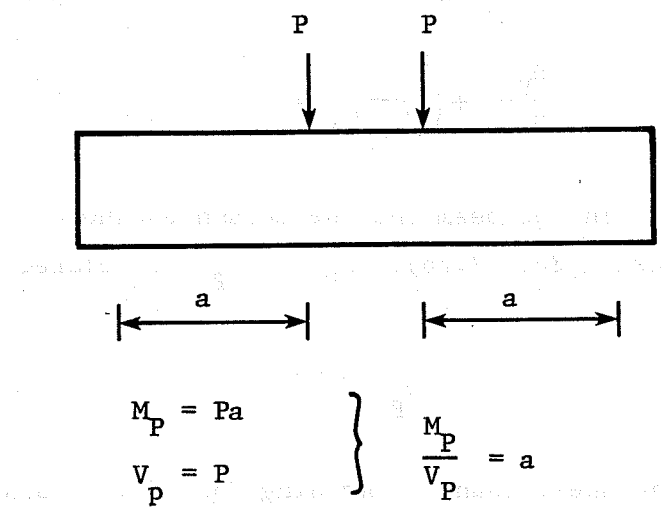

$$M_P = Pa \qquad V_P = P \qquad \left\} \quad \frac{M_P}{V_P} = a \right.$$

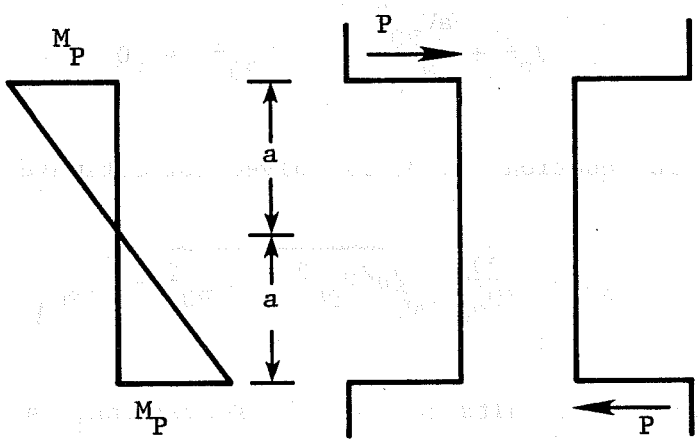

$$M_P = Pa \qquad V_P = P \qquad \left\} \quad \frac{M_P}{V_P} = a \right.$$

Fig. 7.11 Relation between M_P and V_P

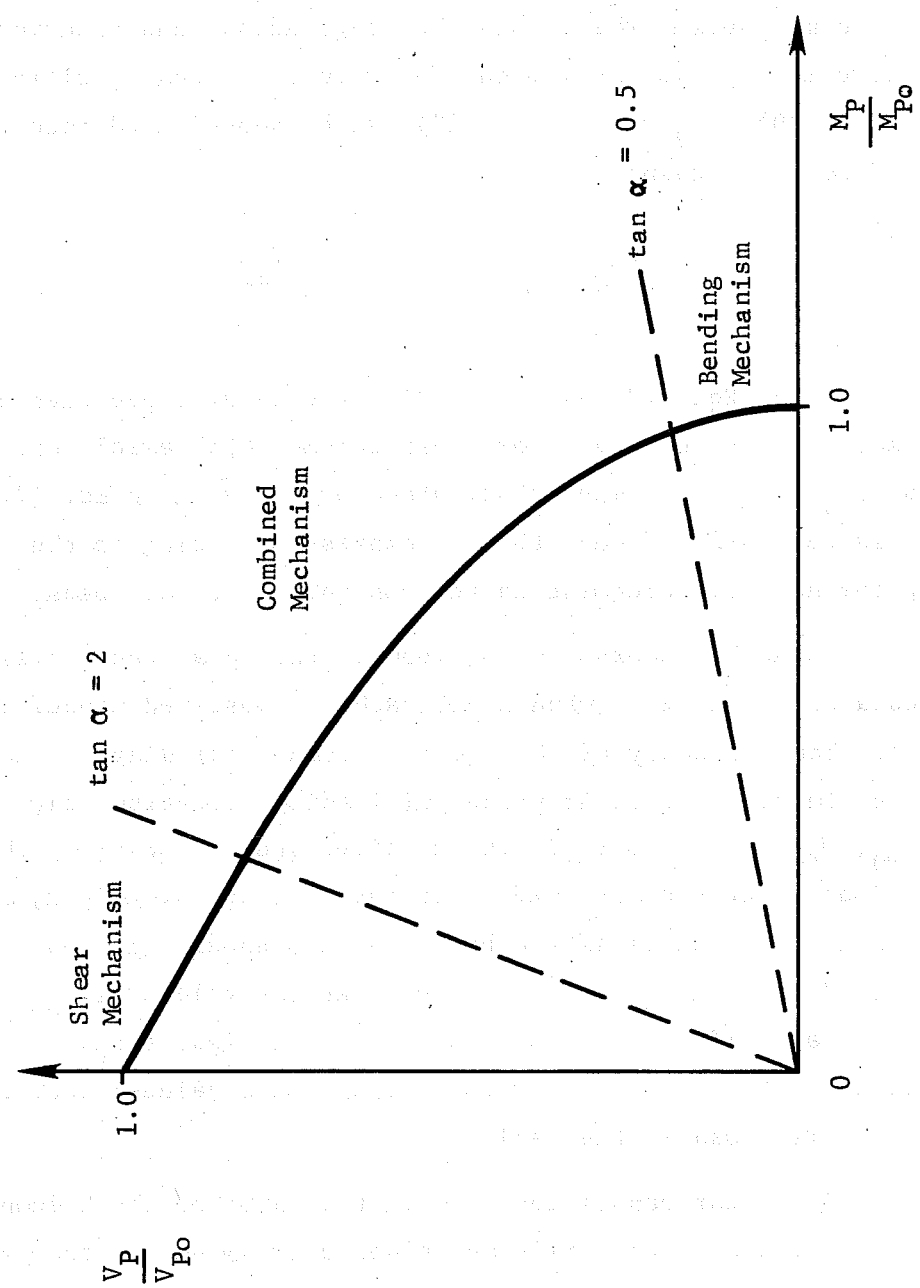

Fig. 7.12 Interaction diagram between bending and shear (from Ref. 27)

of $\tan\alpha$ greater than 2.0, a bending mechanism will occur, which means the longitudinal reinforcement yields without yielding of the transverse reinforcement. Thürlimann suggests that a combined mechanism, where both the longitudinal and transverse reinforcement yield, will occur for values of $\tan\alpha$ specified in Eq. (7.30). V_p from Eq. (7.22) can be substituted into Eq. (7.30) to obtain:

$$0.5 \times \frac{S_y h'}{s_h} \leq V_p \leq 2.0 \times \frac{S_y h'}{s_h} \qquad (7.31)$$

Using Eqs. (7.29) and (7.31), the shear capacities of short columns were calculated. For short columns with axial compression, $F_{\ell y} = F_\ell - N/2$ was substituted for $F_{\ell y} = F_\ell$ in Eq. (7.18). In this case N/2 is equal to the compression acting on the longitudinal reinforcement in tension under lateral loads.

Table 7.3 shows a comparison of the shear capacities calculated using Thürlimann's approach and observed capacities. As the shear capacity of the square column under diagonal loading is the same as that under principal loading direction, the values of V_{P0}, M_{P0}, $\tan\alpha$ and V_p in the specimen under loading in the principal direction are used. For the rectangular column, the value of V_p can be estimated by the values under principal loading directions using an ellipse, but the values of V_{P0}, M_{P0}, and $\tan\alpha$ are different from those under principal loading directions. There is no way to estimate such values; therefore, no entry is shown in the table.

The shear capacities of more than half of the columns were determined by the limiting values of $\tan\alpha$ ($0.5 \leq \tan\alpha \leq 2.0$). The values of α corresponding with $\tan\alpha = 0.5$ is about 27^o. From observations of the crack pattern, the angle of the cracks in all

TABLE 7.3 THÜRLIMANN'S APPROACH AND OBSERVED CAPACITIES

	Specimen Name	V_{po} kips	M_{po} kips in.	tanα	V_p kips	V_m kips	V_m/V_p
SQUARE COLUMN	O-PU	66	905	0.52	36	56	1.56**
	C-PU	76	1203	0.5 (0.42)*	37	67	1.81
	O-PB	66	905	0.52	36	52	1.44
	C-PB	69	986	0.5 (0.49)*	38	77	2.03
	O-DM	78	1196	0.5 (0.44)*	40	55	1.38
	C-DM	79	1211	0.5 (0.44)*	40	68	1.70
	O-DU	73	1110	0.5 (0.45)*	37	64	1.73**
	O-DB	73	1110	0.5 (0.45)*	37	61	1.65**
	C-DB	82	1288	0.5 (0.42)*	40	68	1.70
	C-DB32	120	1273	0.79	56	78	1.39
	C-DB21	97	1273	0.56	51	76	1.49
	C-DB9	64	1273	0.5 (0.30)*	25	64	2.56
	C-DB3	37	1273	0.5 (0.15)*	8	66	8.25
RECTANGULAR COLUMN	OUS	76	1704	0.5 (0.33)*	34	66	1.94
	OUW	79	936	0.57	39	57	1.46**
	CMS	78	1828	0.5 (0.31)*	34	86	2.53
	CUS	79	1838	0.5 (0.31)*	34	74	2.18
	CUW	83	1025	0.53	42	60	1.43
	2CUS	81	1959	0.5 (0.30)*	34	91	2.68
	CDS30	--	--	--	39	80	2.05
	CDW30	--	--	--	44	74	1.68
(s)	CBSW	79	1838	0.5 (0.31)*	34	69	2.03
(w)	CDSW30	--	--	--	40	57	1.43
						Average	2.19
						Standard Deviation	1.48

(s) - strong direction

(w) - weak direction

* - V_p governed by tanα = 0.5,
tanα from calculation in ( )

** - specimens reached computed flexural capacities
neglected in average and standard deviation

specimens was less than 45°. In the rectangular columns loaded in the strong direction (OUS, CUS, CMS, etc.) the angle of the cracks leading to failure is around 30°. However, the average of the ratios of the measured-to-computed capacity (V_m/V_p) is around 2.0 and is very conservative. In the case of the square columns with a large spacing of transverse reinforcement, C-DB9 and C-DB3, the measured shear capacities are almost the same, but the ratios of V_m/V_p are 2.6 and 8.3. From tests and experience Thürlimann divides the state of behavior of the member into a transition zone and a full-truss zone. In the transition zone, a diminishing tensile force is transmitted by such mechanisms as aggregate interlock and Eqs. (7.8) through (7.31) are corrected to satisfy the experimental results. In the full-truss zone, the member exhibits fully plastic behavior and Eqs. (7.8) through (7.31) can be applied. For short columns, the contribution of the concrete is much more important than that of transverse reinforcement and the member may fall into the transition zone where equations must be adjusted to fit the experimental data. A comparison using the approach for a transition zone was omitted, because the adjustments proposed for beams were not appropriate for short columns. Therefore, comparing the ratios of the measured-to-calculated capacities using Eqs. (7.8) through (7.31) for the full-truss zone, it may be concluded that Thürlimann's approach is very conservative and does not provide a good measure of the performance of short columns.

7.3.2.2 Nielsen. Nielsen's approach[30,31,32] is based on the plasticity theory applied to the truss model as in Thürlimann's approach. The same assumptions are used and the procedure is similar to Thürlimann's. The difference between the two approaches is in determining the forces which affect the shear capacity of the truss model shown in Fig. 7.9. In Thürlimann's approach, the equation for shear capacity is derived from the equations of

lower stringer force F_ℓ (Eq. 7.11)), and the force in the stirrup S (Eq. (7.13)). In Nielsen's approach, the equation for shear capacity is derived from the equations of the diagonal force resisted by the concrete compression struts D (Eq. (7.8)) and the force in the stirrup S (Eq. (7.13)).

From Fig. 7.10 which shows the idealized web of a concrete section, the equilibrium equations are developed as described before.

The diagonal force D:

$$D = \frac{V}{\sin\alpha} \tag{7.8}$$

Therefore, the compressive stress in the concrete diagonals is σ_c:

$$\sigma_c = \frac{D}{bh'\cos\alpha} = \frac{V}{bh'} \times \frac{1}{\sin\alpha\cos\alpha} \tag{7.9}$$

and the shear force V:

$$V = \sigma_c bh'\cos\alpha\sin\alpha \tag{7.32}$$

where the positive sign indicates compression in the concrete. The stringer force F_u and F_ℓ:

$$\text{Upper:} \quad F_u = \frac{N}{2} - \frac{M}{h'} + \frac{V}{2}\cot\alpha \tag{7.10}$$

$$\text{Lower:} \quad F_\ell = \frac{N}{2} + \frac{M}{h'} + \frac{V}{2}\cot\alpha \tag{7.11}$$

The force in the stirrup S:

$$S = V \times \frac{s_h}{h'}\tan\alpha \tag{7.13}$$

The following assumptions are added. The yield strength of the lower stringer is $F_\ell = F_{\ell y} = A_\ell f_{y\ell}$. The yield strength of the stirrups is $S = S_y = A_v f_{ys}$. The crushing strength of the web concrete is $\sigma_c = \nu f'_c$ where f'_c is the compression strength of the concrete and ν is a web effectiveness factor. The beam is assumed to be underreinforced in flexure, and the strength of the upper stringer is immaterial. The effectiveness factor is determined empirically. Therefore, it is necessary to find a value of ν which will fit the shear capacity of the short column. However, if ν is constant or depends on some function in the short column, an estimate may be obtained by using this approach.

There are two equations for the shear force.

From Eq. (7.32) $$V = \sigma_c b h' \cos\alpha \sin\alpha \tag{7.33}$$

From Eq. (7.13) $$V = \frac{S h'}{s_h} \cot\alpha \tag{7.34}$$

Eliminating α between Eqs. (7.33) and (7.34),

$$\sin\alpha = \sqrt{\frac{S}{\sigma_c b s_h}}$$

$$\cos\alpha = \sqrt{1 - \frac{S}{\sigma_c b s_h}}$$

$$V = b h' \sqrt{\frac{S}{b s_h}\left(\sigma_c - \frac{S}{b s_h}\right)} \tag{7.35}$$

The two criteria to be satisfied are

$$\sigma_c = \nu f'_c \tag{7.36}$$

$$S = A_v f_{ys} \tag{7.37}$$

Assuming the beam has failure due to crushing the concrete, V in Eq. (7.35) is represented by

$$V = bh' \sqrt{\frac{S}{bs_h}\left(\nu f'_c - \frac{S}{bs_h}\right)} \tag{7.38}$$

Eq. (7.38) can be expressed by only one function--S. The maximum shear capacity V_N is calculated using the maximum value of $S = A_s f_y$. If the stirrup reaches yielding $\left(f_{ys} \leq \left(bs_h/2A_v\right)\nu f'_c\right)$:

$$V_n = bh' \sqrt{\frac{A_v}{bs_h} f_{ys}\left(\nu f'_c - \frac{A_v}{bs_h} f_{ys}\right)} \tag{7.39}$$

$$\cot\alpha = \sqrt{\frac{bs_h}{A_v f_{ys}} \nu f'_c - 1} \tag{7.40}$$

If the stirrup does not reach yielding $\left(f_{ys} > \left(bs_h/2A_v\right)\nu f'_c\right)$:

$$V_N = \frac{1}{2} bh' \nu f'_c \tag{7.41}$$

$$\cot\alpha = 1.0 \qquad (\alpha = 45^o) \tag{7.42}$$

In this case the lower stringer is assumed to have sufficient capacity so that the beam can achieve the maximum shear capacity given by the web crushing criterion. To ensure this,

$$F_{y\ell} \geq \frac{N}{2} + \frac{M}{h'} + \frac{V}{2} \cot\alpha \tag{7.43}$$

where $F_{y\ell}$ is the yield force of lower stringer.

For the short columns with axial compression, $f'_c + \sigma_N$ was substituted for f'_c in Eqs. (7.39) to (7.43). In this case σ_N is equal to the concrete stress under axial compression. As before,

the shear capacity of the column under diagonal loading was computed from the shear capacities under principal loading directions using circular and elliptical interaction relationships.

As mentioned before, the value of ν is determined empirically. Nielsen applied the equation to the results of one hundred ninety-eight shear tests on simply supported T-beams with vertical stirrups in order to calculate the web effectiveness factor ν and the best fit was obtained with $\nu = 0.74$, standard deviation $\sigma = 0.03$. He concluded that for reasonably designed beams, the effectiveness factor appeared to be fairly constant. However, this result was not valid in the case of $a/d \leq 2.4$. Therefore, in the case of short columns, the value of ν must be calculated using the empirical results to determine if a constant value for ν can be derived.

Table 7.4 indicates a comparison of the shear capacities calculated using Nielsen's approach and observed capacities. The value of ν for each specimen was calculated using measured capacities. In the square columns ν ranged from 0.3 to 0.6, except for a specimen with large spacing of transverse reinforcement ($\nu = 1.0$ for C-DB3). In the rectangular columns loaded in the strong direction, ν ranged from 0.5 to 0.7 and in the weak direction, ν ranged from 0.25 to 0.3. Shear span-effective depth ratio (a/d) is 2.09 for the square column, 1.61 for the rectangular column loaded in the strong direction, and 2.44 for the rectangular loaded in the weak direction. The effectiveness factor appears to increase as the shear span-effective depth ratio becomes smaller. Using this observation, ν was assumed to be equal to d/a, and the shear capacity of each specimen V_N was calculated and compared with observed capacity. For these calculations, the stirrups reached yielding in calculations of all specimens. The average of the ratios of the measured-to-computed capacity (V_m/V_N) is around 1.0 and the standard

TABLE 7.4 NIELSEN'S APPROACH AND OBSERVED CAPACITIES

	Specimen Name	V_m kips	ν	tanα	$\nu = d/a$	V_N kips	V_m/V_N
SQUARE COLUMN	0-PU	56	0.40	0.33		62	0.90*
	C-PU	67	0.54	0.28		63	1.06
	0-PB	52	0.30	0.35		68	0.76
	C-PB	77	0.54	0.24		72	1.07
	0-DM	55	0.31	0.36		70	0.79
	C-DM	68	0.45	0.30		71	0.96
	0-DU	64	0.52	0.29	0.48	62	1.03*
	0-DB	61	0.47	0.30		62	0.98*
	C-DB	68	0.50	0.30		67	1.01
	C-DB32	78	0.32	0.56		101	0.77
	C-DB21	76	0.37	0.39		87	0.87
	C-DB9	64	0.56	0.20		59	1.08
	C-DB3	66	1.00	0.08		36	1.83
RECTANGULAR COLUMN	0US	66	0.52	0.26	0.62	72	0.92
	0UW	57	0.27	0.39	0.41	72	0.79*
	CMS	86	0.73	0.20	0.62	79	1.09
	CUS	74	0.64	0.23	0.62	72	1.02
	CUW	60	0.29	0.38	0.41	71	0.85
	2CUS	91	0.74	0.19	0.62	83	1.10
	CDS30	80	--	--	--	78	1.03
	CDW30	74	--	--	--	76	0.97
(s)	CBSW	69	0.57	0.24	0.62	72	0.96
(w)	CDSW30	57	--	--	--	71	0.80
					Average		1.00
					Standard Deviation		0.23

(s) - strong direction

(w) - weak direction

* - specimens reached computed flexural capacities neglected in average and standard deviation

deviation is 0.23. Although the average is around 1.0, the value of ν must be known for all cases of columns and beams in order to calculate design shear capacity. For this reason Nielsen's approach involves too many uncertainties to apply to design.

It should be noted that the specimens with large spacing of transverse reinforcement had almost the same capacity as those with small spacing. The longitudinal reinforcements in the rectangular columns loaded in the strong direction did not yield. Therefore, in the short columns the strength of the concrete compression strut appears to control the shear capacity. Nielsen's approach, in which it is assumed that maximum shear capacity occurs when the concrete compression reaches crushing, seems to be more appropriate than Thürlimann's approach (in the full-truss zone) in which it is assumed that crushing of the concrete compression struts does not occur. However, for practical calculations of shear capacity, Thürlimann's approach is much easier to apply than Nielsen's.

7.3.3 Shear Capacity--Zsutty. Zsutty developed an equation to calculate shear capacity of beams using statistical analysis. Experimental data indicated that beams with shear span-effective depth ratio a/d less than about 2.5 increased in strength after first shear cracks occurred. Therefore, beams were divided into two categories based on the a/d ratio as follows:

(1) Beam action, meaning combined bending and shear stress, $a/d > 2.5$. The load at first shear cracking is equivalent to ultimate strength.

(2) Arch action, meaning some type of compression stress or direct load transfer to supports, $a/d < 2.5$. The load at first shear cracking is less than the ultimate strength.

Zsutty proposed the following equation to predict the ultimate shear strength (concrete contribution) of beams with $a/d < 2.5$ and no vertical stirrups.

$$V_{zc} = 60bd \left(f'_c \rho_w \frac{d}{a}\right)^{\frac{1}{3}} \tag{7.44}$$

For beams with $a/d > 2.5$ and vertical stirrups, a V_s term as in the ACI method was added to obtain the shear capacity.

$$V_z = 60bd \left(f'_c \rho_w \frac{d}{a}\right)^{\frac{1}{3}} + \frac{A_v f_{ys} d}{s_h} \tag{7.45}$$

For beams with $a/d' < 2.5$ and no vertical stirrups, Eq. (7.44) is modified as follows.

$$V_{zc} = 150bd \left(f'_c \rho_w\right)^{\frac{1}{3}} \left(\frac{d}{a}\right)^{\frac{4}{3}} \tag{7.46}$$

For the beams with $a/d < 2.5$ and vertical stirrups,

$$V_z = 150bd \left(f'_c \rho_w\right)^{\frac{1}{3}} \left(\frac{d}{a}\right)^{\frac{4}{3}} + \frac{A_v f_{ys} d}{s_h} \tag{7.47}$$

However, Eqs. (7.46) and (7.47) are intended for simple beams with direct load and cannot be directly applied for calculating the shear capacities of the short test columns, because the mechanism of the short column is similar to that of continuous beams. Therefore, Eq. (7.45) was used to calculate shear strength. Since this equation does not include the effect of axial load, specimens with axial load were not considered. The shear capacity of the column with diagonal loading was calculated using the circular or elliptical interaction lines.

Table 7.5 shows a comparison of the shear capacities calculated using Zsutty's equation (Eq. (7.45)) and measured values for the short columns without axial load. The ratio of the measured-to-calculated shear capacity ranges from 1.2 to 1.5. These ratios indicate the Zsutty equation is conservative, but it does not include the effect of axial load on the shear capacity of short columns.

7.3.4 Development of Equation for Shear Capacity. The measured shear capacity of short columns was compared with values obtained using ACI 318-77, plasticity approaches developed by Thürlimann and Nielsen, and statistical equations proposed by Zsutty. There appears to be several reasons why these methods did not accurately estimate shear capacity of the short columns. In most cases, short column shear strength increases after first shear cracking. Some type of arch or strut action in the concrete governs shear behavior and emphasizes the contribution of the concrete as opposed to that of the transverse reinforcement. In some cases the computed shear capacity may be greater than the flexural capacity, however, the member exhibits rapid deterioration of shear capacity and energy dissipating characteristics. In addition, the loading and deflection of the short columns is not the same as that of simple beams (shown in Fig. 7.6) from which most shear data have been obtained. Therefore, a new equation for the shear capacity of short columns was developed. The equation was derived from empirical data using statistical methods (regression analysis). Only empirical data from beams with a/d^* ratios less than 2.5 were considered. The effective depth (d^*) is defined as the distance from extreme compression fiber to extreme tension reinforcement. These data were separated into two groups. One group consisted of the data from simple beams as shown in Fig. 7.13(a), and the other from continuous beams as shown in Fig. 7.13(b). The intent

TABLE 7.5 ZSUTTY'S EQUATION AND OBSERVED CAPACITIES

	Specimen Name	f'_c psi	a/d	V_{ZC} kips	V_Z kips	V_m kips	V_m/V_Z
A	0-PU	5000	2.09	23	44	56	1.27*
	0-PB	6000	2.09	24	45	52	1.16
	0-DM	5950	2.09	24	46	55	1.20
	0-DU	4950	2.09	23	44	64	1.45*
	0-DB	5050	2.09	23	44	61	1.39*
B	0US	5810	1.61	27	46	66	1.43
	0UW	5820	2.44	25	50	57	1.14*
						Average	1.26
						Standard Deviation	0.04

A - square column

B - rectangular column

* - specimens reached computed flexural capacities neglected in average and standard deviation

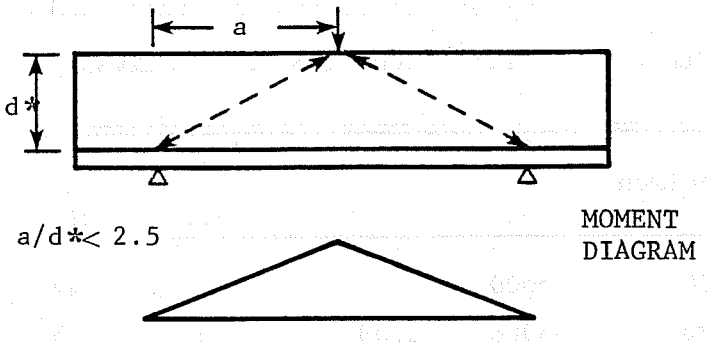

(a) Simply supported Beam

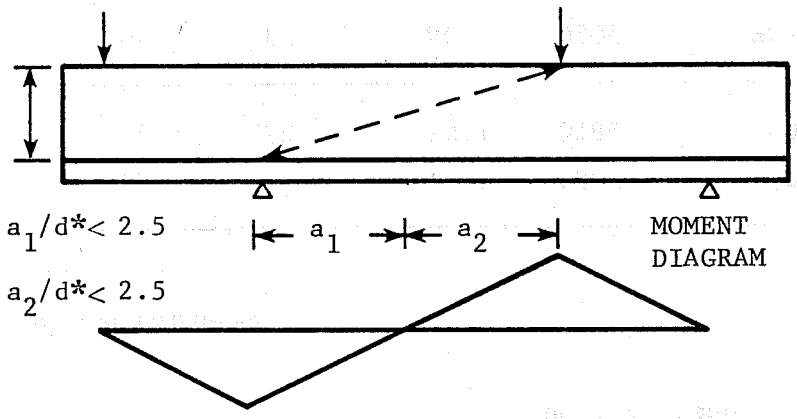

(b) Continuous beam

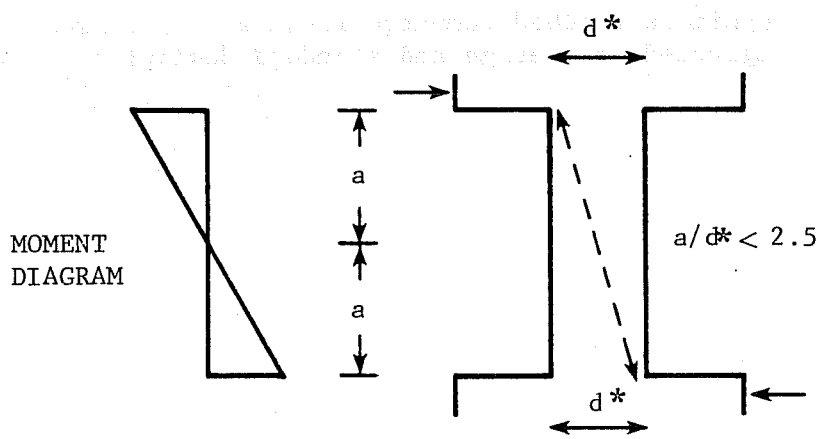

(c) Short column

Fig. 7.13 Schematic diagrams of compression struts

was to examine which beams (simple or continuous) behaved in a manner similar to that of the short column shown in Fig. 7.13(c). The equation could not be derived directly from the short columns tested, because the data base was insufficient, even when data on short columns reported in Japan[20,21] were included.

The following procedure was used to derive the equation for shear capacity. First, the contribution of the concrete was derived using data from beams without web reinforcement. To include the capacity provided by the compressive struts after the concrete first cracks, the ultimate capacity of beams without web reinforcement was used. For the statistical analysis, a computer program for stepwise multiple regression[35] was used. Second, the contribution of web reinforcement was derived using data from beams with web reinforcement. The equation for the contribution of web reinforcement was derived by subtracting computed concrete capacity from the total measured capacity. Third, the equation was modified for influence of axial compressive load.

7.3.4.1 Beams without Web Reinforcement. To derive the equation, only tests in which (1) shear failure occurred, and (2) the maximum load was less than the calculated flexural capacity were used. From the test results of short columns, it was found that the shear capacity increases with increasing axial compression and decreasing shear span to effective depth ratio a/d^*. In the regression analysis, the effective shear area, the concrete strength, the ratio of longitudinal tension reinforcement, and shear span to effective depth ratio were chosen for parameters. It should be noted that almost the same parameters are included in the equation proposed by Zsutty. The Zsutty approach seemed to provide the closest correlation with measured results. A review of short column results indicates the importance of the selected parameters also.

Simply Supported Beams. The results of seventy-one simply supported beams with $1 \leq a/d^* \leq 2.5$ and without web reinforcement (Refs. 36 to 47) were used to derive an equation for the contribution of concrete (Table 7.6). Using regression analysis, the following equation was derived:

$$\frac{V_{rc}}{bd^*\sqrt{f'_c}} = 10.6 - 5.0\,\frac{a}{d^*} + 3.7\sqrt{\rho^*} \qquad (7.48)$$

where d^* was defined as the distance from the extreme compression fiber to the extreme longitudinal tension reinforcement. Figure 7.14 shows the distribution of the ratio of test to calculated values. The average ratio was 1.0 and the standard deviation was 0.12.

Continuous Beams. The results of fifty-eight continuous beams with $1 \leq a/d^* \leq 2.5$ (the definition of a is shown in Fig. 7.13) without web reinforcement[36,40,41,48] were used to derive a second equation representing the contribution of concrete. The data are shown in Table 7.7. Using a regression analysis, the following equation was derived:

$$\frac{V_{rc}}{bd^*\sqrt{f'_c}} = 7.3 - 2.6\,\frac{a}{d^*} + 1.7\sqrt{\rho^*} \qquad (7.49)$$

Figure 7.15 shows the distribution of the ratio of test to calculated values. The average of the ratio was 1.0 and the standard deviation was 0.11.

Both equations, Eqs. (7.48) and (7.49), provide a good estimation of the shear capacity contributed by concrete because the standard deviation is around 0.1.

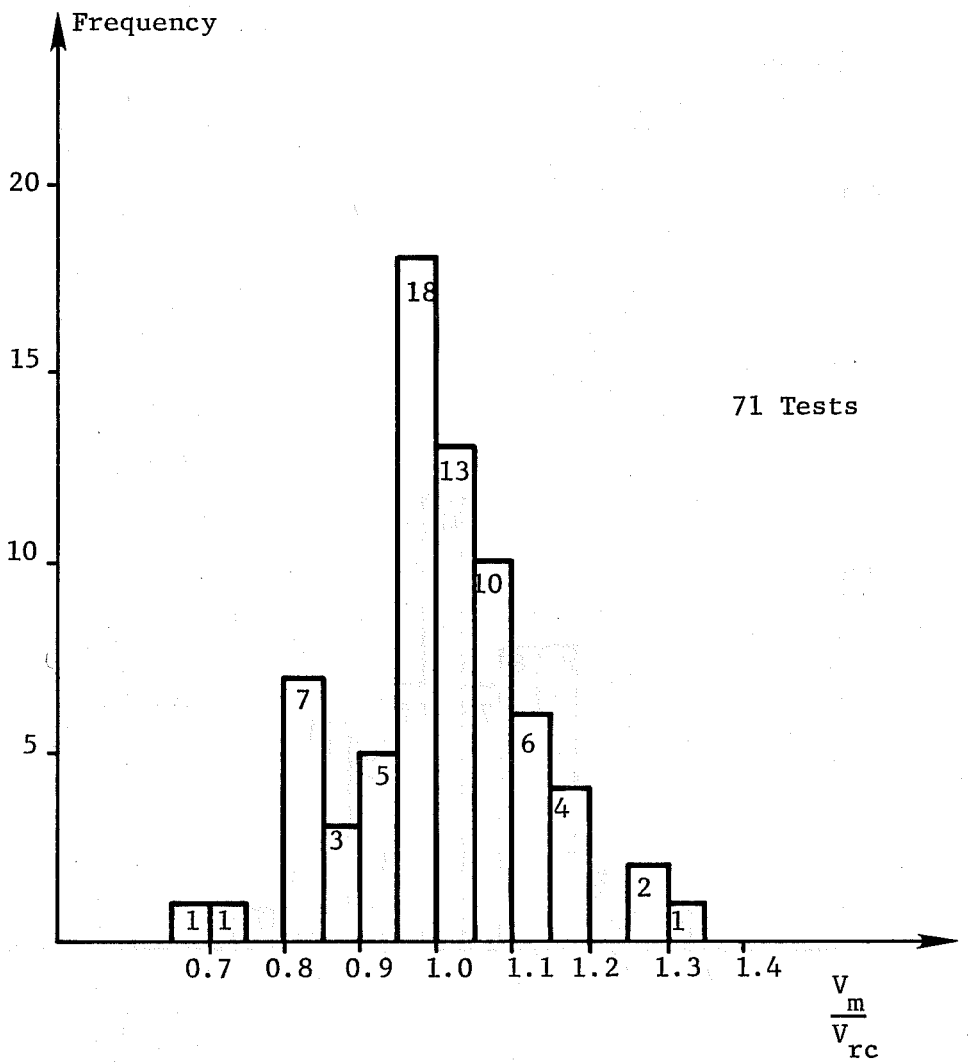

Average = 1.0

Standard deviation = 0.12

Fig. 7.14 Histogram of the ratio of test to calculated shear strength - simply supported beams without web reinforcement

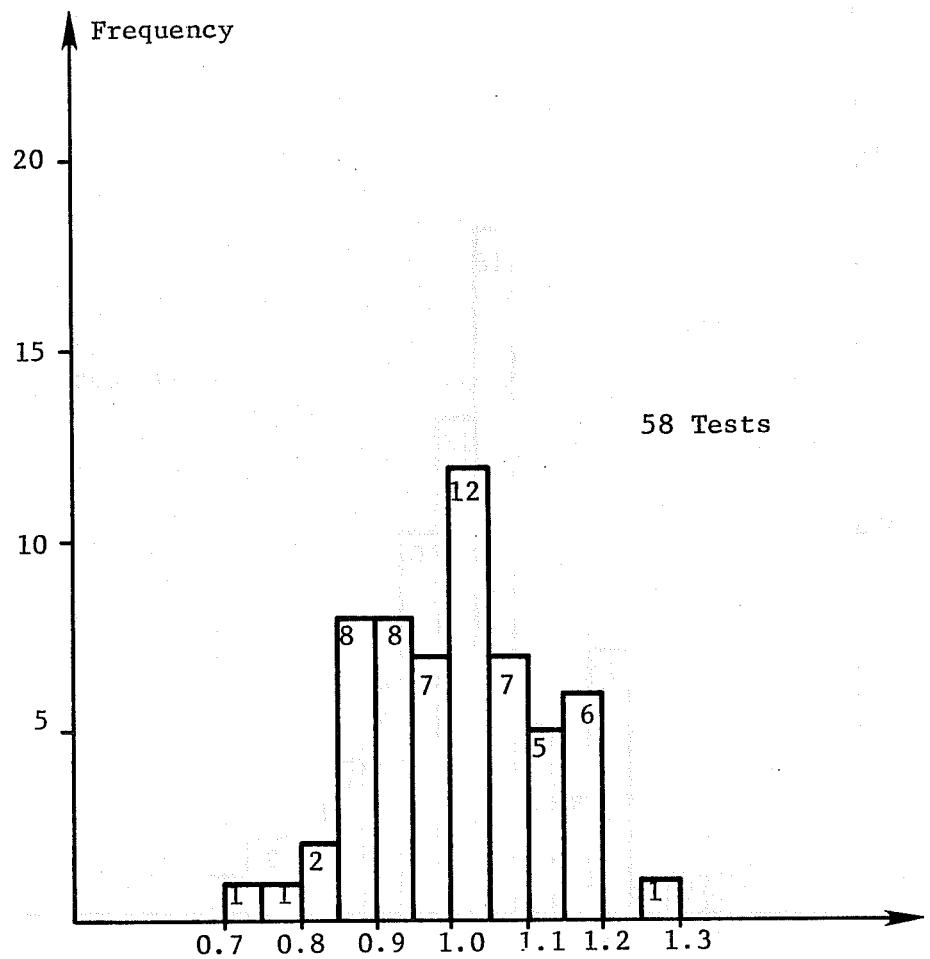

Fig. 7.15 Histogram of the ratio of test to calculated shear strength - continuous beams without web reinforcement

TABLE 7.6 COMPARISON OF MEASURED AND CALCULATED CAPACITY-- SIMPLY SUPPORTED BEAMS WITHOUT WEB REINFORCEMENT

Beam	a/d^*	ρ^*%	$\frac{V_m}{bd^*\sqrt{f'_c}}$	$\frac{V_{rc}}{bd^*\sqrt{f'_c}}$	$\frac{V_m}{V_{rc}}$
Source: Moody, Elstner, Viest, Hognestad (36)					
III 24a	1.52	2.72	8.91	9.16	0.97
24b	1.52	2.72	8.46	9.16	0.92
25a	1.52	3.46	8.12	9.94	0.82
25b	1.52	3.46	8.85	9.94	0.89
26a	1.52	4.25	11.47	10.70	1.07
26b	1.52	4.25	11.07	10.70	1.03
27a	1.52	2.72	9.53	9.16	1.04
27b	1.52	2.72	9.44	9.16	1.03
28a	1.52	3.46	7.96	9.94	0.80
28b	1.52	3.46	9.13	9.94	0.92
29a	1.52	4.25	10.61	10.70	0.99
29b	1.52	4.25	11.08	10.70	1.03
Source: Bower, Viest (40)					
IA-1a	2.50	1.59	3.21	2.82	1.13
1b	2.50	1.59	3.64	2.82	1.29
Source: Morrow, Viest (37)					
B14-B2	1.00	1.85	10.30	10.82	0.95
E2	1.00	0.57	8.23	8.67	0.95
A4	1.00	2.50	11.76	11.60	1.01
B4	1.00	1.85	10.46	10.82	0.97
E4	1.00	1.24	10.21	9.91	1.03
A6	1.00	3.83	14.84	12.90	1.15
B6	1.00	1.85	12.21	10.83	1.12
B21-B2	1.45	1.86	6.89	8.44	0.82
A4	1.45	2.46	10.27	9.21	1.11
B4	1.45	1.85	8.16	8.43	0.97
A6	1.50	3.83	9.55	10.40	0.92
B2	1.96	1.88	5.70	5.93	0.96
E2	1.91	0.57	3.66	3.87	0.95
A4	1.93	2.46	6.60	6.81	0.97
B4	1.93	1.85	4.83	6.03	0.80
E4	1.93	1.24	4.98	5.11	0.97
A6	2.01	3.83	5.39	7.86	0.69
B6	1.93	1.85	5.14	6.03	0.85
Source: Baldwin, Viest (38)					
OB28	1.93	1.86	5.08	6.05	0.84
OF28	1.93	1.83	5.05	6.00	0.84
Source: Cossio, Siess (39)					
L-1	2.01	3.36	7.92	7.40	1.07
A-1	2.00	1.00	4.31	4.34	0.99
A-11	2.00	3.33	6.05	7.42	0.82

Beam	a/d^*	ρ^*%	$\frac{V_m}{bd^*\sqrt{f'_c}}$	$\frac{V_{rc}}{bd^*\sqrt{f'_c}}$	$\frac{V_m}{V_{rc}}$
Source: Watstein, Mathey (42) (46)					
A-15	2.06	1.53	6.49	4.93	1.31
B18-1	1.51	3.05	9.07	9.57	0.95
B18-2	1.51	3.05	9.47	9.57	0.99
C18-1	1.51	1.85	8.39	8.13	1.02
C18-2	1.51	1.88	8.89	8.17	1.09
D18-1	1.51	1.17	7.73	7.09	1.09
D18-2	1.51	1.16	7.54	7.07	1.07
E18-1	1.51	0.75	6.85	6.29	1.09
E18-2	1.51	0.75	6.32	6.29	1.00
II-3	1.51	1.88	8.24	8.17	1.01
III-6	1.51	1.85	8.45	8.13	1.04
IV-7	1.51	1.86	8.71	8.14	1.07
IV-8	1.51	1.86	8.96	8.14	1.10
V-9	1.51	1.16	6.86	7.07	0.97
VI-11	1.51	1.17	6.54	7.09	0.92
Source: Chang, Kesler (43)					
I-B1	2.42	1.86	3.54	3.60	0.98
II-C1	2.42	2.89	5.80	4.86	1.19
III-A2	1.86	2.37	7.43	7.05	1.05
III-C1	2.42	2.89	6.35	4.86	1.29
Source: Taub, Neville (44)					
1.2	2.09	4.47	8.51	8.05	1.06
Source: Kresfeld, Thurston (45)					
II-4A3	1.42	1.55	3.02	4.21	0.72
5A3	1.42	1.55	4.74	5.42	0.87
Source: Acharya, Kemp (47)					
ER1b	2.53	2.06	3.96	3.32	1.19
AR4b	2.14	2.60	5.72	5.93	0.96
DR1b	2.44	4.15	7.21	6.01	1.19
2b	1.63	4.15	10.23	10.06	1.02
4b	1.63	4.15	11.23	10.06	1.12
AR3a	2.22	7.57	10.16	9.77	1.04
Source: Rodriguez (41)					
E6N1	1.36	2.64	10.95	9.87	1.11
2	1.36	2.64	9.62	9.87	0.98
3	1.36	2.64	9.79	9.87	0.99
C6N1	1.36	2.64	10.80	9.87	0.94
2	1.36	2.64	9.32	9.87	0.94
3	1.36	2.64	10.03	9.87	1.02

$$\frac{V_{rc}}{bd^*\sqrt{f'_c}} = 10.6 - 5.0\,a/d^* + 3.7\sqrt{\rho^*}$$

$$1.0 \le a/d^* \le 2.5$$

71 tests

TABLE 7.7 COMPARISON OF MEASURED AND CALCULATED CAPACITY--CONTINUOUS BEAMS WITHOUT WEB REINFORCEMENT

Beam	a/d^*	ρ^*%	$\frac{V_m}{bd^*\sqrt{f'_c}}$	$\frac{V_{rc}}{bd^*\sqrt{f'_c}}$	$\frac{V_m}{V_{rc}}$
Source: Bower, Viest (40)					
IA-2a	2.45	1.59	3.72	3.18	1.17
3b	2.50	1.59	3.17	3.05	1.04
4a	2.50	1.59	2.93	3.05	0.96
5b	2.50	1.59	2.79	3.05	0.91
6b	2.50	1.59	3.55	3.05	1.16
7b	2.50	1.59	3.10	3.05	1.02
8a	2.45	1.59	2.72	3.18	0.86
8b	2.50	1.59	3.33	3.05	1.09
IIB 2	2.00	1.59	3.67	4.34	0.85
3	2.00	1.59	3.21	4.34	0.74
IIA 1b	1.50	1.59	4.63	5.63	0.82
2	2.00	1.59	3.67	4.34	0.85
3	2.50	1.59	2.80	3.05	0.92
Source: Rodriguez, Bianchini, Viest, Kesler (41)					
E3 N1	2.04	2.64	5.33	4.86	1.09
2	2.04	2.64	5.30	4.86	1.09
C3 N2	2.04	2.64	5.49	4.86	1.13
Source: Guralnick (48)					
IA-IM	1.43	2.37	5.73	6.28	0.91
IC-IM	1.44	4.29	5.74	7.16	0.80
Source: Moody, Elstner, Hognestad, Viest (36)					
I-h	1.36	1.47	6.05	5.90	1.02
i	1.36	2.10	6.92	6.31	1.09
1a	1.36	2.86	6.25	6.72	0.93
b	1.36	2.86	6.74	6.72	1.00
2a	1.36	3.76	6.26	7.15	0.88
b	1.36	3.76	7.38	7.15	1.03
c	1.36	3.76	6.26	7.15	0.88
3a	1.36	4.76	7.54	7.56	1.00
3b	1.36	4.76	7.51	7.56	0.99
j	1.36	1.47	6.11	5.90	1.03
k	1.36	2.10	7.16	6.31	1.13
4a	1.36	2.86	6.17	6.72	0.92
b	1.36	2.86	5.74	6.72	0.85
5a	1.36	3.76	7.62	7.15	1.06
b	1.36	3.76	7.02	7.15	0.98
6a	1.36	4.76	6.92	7.56	0.92
b	1.36	4.76	8.14	7.56	1.08
1	1.36	1.47	6.01	5.90	1.02
m	1.36	2.10	6.42	6.31	1.02
7a	1.36	2.86	6.73	6.72	1.00
b	1.36	2.86	5.73	6.72	0.85
8a	1.36	3.76	8.50	7.15	1.18
b	1.36	3.76	6.51	7.15	0.91
9a	1.36	4.76	7.25	7.56	0.96
b	1.36	4.76	7.73	7.56	1.02
n	1.36	1.47	6.60	5.90	1.12
o	1.36	2.10	7.28	6.31	1.15
p	1.36	2.86	6.98	6.72	1.04
q	1.36	3.76	8.08	7.15	1.13
r	1.36	4.76	7.37	7.56	0.97
IV h	2.04	1.47	3.97	4.15	0.96
i	2.04	2.10	3.97	4.56	0.87
j	2.04	2.86	4.84	4.97	0.97
k	2.04	3.76	5.05	5.39	0.94
l	2.04	4.76	4.53	5.81	0.78
IV d	1.82	2.86	6.41	5.54	1.16
e	1.82	3.76	6.71	5.96	1.13
g	1.82	2.86	6.38	5.54	1.15
h	1.82	3.76	7.75	5.96	1.29
i	1.82	4.76	6.87	6.38	1.08

Source: Moody, Elstner, Hognestad, Viest (continued)

$$\frac{V_{rc}}{bd^*\sqrt{f'_c}} = 7.3 - 2.6\, a/d^* + 1.7\sqrt{\rho^*}$$

$$1.0 \leq a/d^* \leq 2.5$$

58 tests

7.3.4.2 Web Reinforcement. Using the measured shear capacity of the beams with web reinforcement in which the load in shear failure is less than the calculated flexural capacity, the contribution of the web reinforcement to the shear capacity was derived. Two assumptions were made. It was assumed that the total shear capacity was the sum of the contribution of concrete and web reinforcement. Therefore, the contribution of the web reinforcement was computed by subtracting computed concrete capacity from total measured shear capacity. It was assumed that the contribution of web reinforcement could be expressed by an equation similar to that in ACI 318-77, Eq. (7.7). The following equation was assumed for the contribution of web reinforcement:

$$V_{rs}\ (\text{simple}) = \beta_1 \frac{A_v f_{ys} d^*}{s_h} \qquad (7.50)$$

or

$$V_{rs}\ (\text{continuous}) = \beta_2 \frac{A_v f_{ys} d^*}{s_h} \qquad (7.51)$$

where β_1 and β_2 represent reduction factors to reflect the reduced efficiency of transverse reinforcement in short members. The values of β_1 and β_2 were selected so that the sum of the computed contribution of concrete and web reinforcement is equal to the total measured shear capacity.

From thirty-six simply supported beams with web reinforcement,[49,50,51] a value of $\beta_1 = 0.42$ was computed by averaging the reduction factors shown in Table 7.8. For simply supported beams with web reinforcement (no axial load), the shear capacity is:

TABLE 7.8 EFFICIENCY OF TRANSVERSE REINFORCEMENT--β_1 FOR SIMPLY SUPPORTED BEAMS

Beam	$\frac{V_m}{bd^*\sqrt{f'_c}}$	$\frac{V_{rc}}{bd^*\sqrt{f'_c}}$	$\frac{V_{rs}}{bd^*\sqrt{f'_c}}$	$\frac{A_v f_{ys}}{bs_h\sqrt{f'_c}}$	β_1
Source: Moretto (49)					
1V 1/4	9.87	9.32	0.55	2.62	0.21
2V 1/4	9.71	9.32	0.39	2.22	0.18
1I 1/4	9.78	9.32	0.46	3.26	0.14
2I 1/4	9.59	9.32	0.27	2.94	0.09
1D 1/4	10.02	9.32	0.70	3.68	0.19
2D 1/4	11.91	9.32	2.49	3.70	0.67
1V 3/8	13.11	9.32	3.79	5.28	0.72
2V 3/8	11.15	9.32	1.83	4.56	0.40
1I 3/8	12.96	9.32	3.64	6.44	0.57
2I 3/8	12.76	9.32	3.44	5.96	0.58
2D 3/8	11.79	9.32	2.47	6.86	0.36
Source: Clark (50)					
A1-1	6.82	5.43	1.39	3.10	0.45
2	6.55	5.43	1.12	3.16	0.36
3	7.00	5.43	1.57	3.18	0.50
4	7.49	5.43	2.06	3.12	0.66
B1-1	8.78	7.38	1.40	3.04	0.46
2	7.75	7.38	0.37	2.92	0.13
3	8.91	7.38	1.53	3.04	0.50
4	8.45	7.38	1.07	3.06	0.35
5	7.41	7.38	0.03	2.96	0.01
C3-1	9.08	8.12	0.96	3.68	0.26
2	8.21	8.12	0.09	3.70	0.02
C4-1	9.52	9.32	0.20	2.80	0.07
D1-6	8.37	7.80	0.57	3.50	0.16
7	8.53	7.80	0.73	3.48	0.21
8	8.88	7.80	1.08	3.48	0.31
D2-6	7.81	5.36	2.45	4.54	0.54
7	7.35	5.36	1.99	4.60	0.43
8	8.30	5.36	2.94	4.82	0.61
D4-1	8.11	5.36	2.75	3.76	0.73
2	7.82	5.36	2.46	3.88	0.63
D5-1	6.99	5.36	1.63	2.80	0.58
2	7.36	5.36	2.00	2.76	0.73
3	7.61	5.36	2.25	2.84	0.79
Source: Siess, De Paiva (51)					
G33 S12	14.36	10.42	3.96	6.50	0.61
32	17.61	11.60	6.01	6.48	0.93
				Average	0.42

$$\frac{V_m}{bd^*\sqrt{f'_c}} - (10.6 - 5.0\,{}^{a}/_{d^*} + 3.7\sqrt{\rho^*}) = \beta_1 \frac{A_v f_{ys}}{bs_h\sqrt{f'_c}}$$

$$1.0 \le {}^{a}/_{d^*} \le 2.5$$

36 tests

$$V_{rt} = (10.6 - 5.0\frac{a}{d}^{*} + 3.7\sqrt{\rho^{*}})\, bd^{*}\sqrt[3]{f'_c} + 0.42\,\frac{A_v f_{ys} d^{*}}{s_h} \qquad (7.52)$$

From thirty-four continuous beams with web reinforcement,[36,41,48] a value of $\beta_2 = 0.61$ was calculated by averaging the reduction factors shown in Table 7.9. For continuous beams with web reinforcement (no axial load), the shear capacity is:

$$V_{rt} = (7.3 - 2.6\frac{a}{d}^{*} + 1.7\sqrt{\rho^{*}})\, bd^{*}\sqrt[3]{f'_c} + 0.61\,\frac{A_v f_{ys} d^{*}}{s_h} \qquad (7.53)$$

Tables 7.10 and 7.11 give the ratio of calculated capacity V_{rt} to measured capacity V_m using Eq. (7.52) for simply supported beams and Eq. (7.53) for continuous beams. Figures 7.16 and 7.17 indicate the distribution of the ratio of test to calculated values in simply supported and continuous beams. Both equations seem to provide a good estimate of the shear capacity of specimens with web reinforcement with values of standard deviation less than 0.1.

7.3.4.3 Axial Compression. The effect of axial compression on the shear capacity of beams was estimated by using a concept shown in Fig. 7.18 proposed in the Swedish and Nordic codes. It is assumed that the axial load restricts the deformation of the member and the occurrence of the shear crack is delayed until the deformation due to the axial load is overcome by lateral displacement or by moment. Therefore, V_a, the contribution of axial compression to the shear capacity, was derived by calculating the applied lateral load necessary to

TABLE 7.9 EFFICIENCY OF TRANSVERSE REINFORCEMENT-- β_2 FOR CONTINUOUS BEAMS

Beam	$\frac{V_m}{bd^*\sqrt{f'_c}}$	$\frac{V_{rc}}{bd^*\sqrt{f'_c}}$	$\frac{V_{rs}}{bd^*\sqrt{f'_c}}$	$\frac{A_v f_{ys}}{bs_h\sqrt{f'_c}}$	β_2
Source: Rodriguez, Bianchini, Viest, Kesler (41)					
C3 A2	8.30	4.85	3.45	4.36	0.79
E2 A1	6.34	4.36	1.98	3.10	0.63
2	6.72	4.36	2.36	3.58	0.66
3	6.98	4.36	2.62	3.50	0.75
C2 A1	5.18	4.36	0.82	3.32	0.25
2	6.34	4.35	1.99	3.32	0.60
E3 H1	8.58	4.86	3.72	6.26	0.59
C3 H1	9.72	4.86	4.86	8.58	0.57
2	8.90	4.86	4.04	6.84	0.59
E2 H1	8.01	4.36	3.65	7.24	0.50
2	7.34	4.36	2.98	4.64	0.64
C2 H1	7.98	4.36	3.62	7.34	0.49
2	6.47	4.36	2.11	4.12	0.51
B2 A1	4.96	3.95	1.01	2.32	0.43
H1	7.25	3.95	3.30	4.90	0.67
H2	6.38	3.95	2.43	3.00	0.81
Source: Elstner, Moody, Viest, Hognestad (36)					
I 10a	11.67	7.64	4.03	4.52	0.89
b	10.32	7.64	2.68	4.72	0.57
11a	12.63	7.64	4.99	7.12	0.70
b	12.24	7.64	4.60	7.92	0.58
12a	11.93	7.64	4.29	9.50	0.45
b	11.13	7.64	3.49	10.52	0.33
I s	14.82	7.64	7.18	15.92	0.45
t	15.67	7.64	8.03	16.70	0.48
I 13a	12.48	7.64	4.84	5.98	0.81
b	12.60	7.64	4.96	6.58	0.75
14b	15.80	7.64	8.16	10.0	0.82
15a	15.91	7.64	8.27	14.94	0.55
I u	10.38	6.80	3.58	4.70	0.76
v	11.27	6.80	4.47	6.32	0.70
w	11.00	6.80	4.20	6.82	0.61
Source: Guralnick (48)					
I A2	8.80	6.61	2.64	3.76	0.70
B2	7.24	5.53	1.71	3.80	0.45
C2	9.70	7.16	2.54	2.82	0.80
				Average	0.61

$$\frac{V_m}{bd^*\sqrt{f'_c}} = (7.3 - 2.6\ {}^{a}/_{d^*} + 1.7\sqrt{\rho^*}) = \beta_2 \frac{A_v f_{ys}}{bs_h\sqrt{f'_c}}$$

$$1 \le {}^{a}/_{d^*} \le 2.5$$

34 tests

TABLE 7.10 RATIO OF TEST TO CALCULATED STRENGTH--SIMPLY SUPPORTED BEAMS WITH WEB REINFORCEMENT

Beam	$0.42 \frac{A_v f_{ys}}{b s_h \sqrt{f'_c}}$	$\frac{V_m}{bd^* \sqrt{f'_c}}$	$\frac{V_{rt}}{bd^* \sqrt{f'_c}}$	$\frac{V_m}{V_{rt}}$
Source: Moretto (49)				
1V 1/4	1.10	9.87	10.42	0.95
2V 1/4	0.93	9.71	10.25	0.95
1I 1/4	1.37	9.78	10.69	0.92
2I 1/4	1.23	9.59	10.55	0.91
1D 1/4	1.55	10.02	10.87	0.92
2D 1/4	1.55	11.91	10.87	1.09
1V 3/8	2.22	13.11	11.54	1.13
2V 3/8	1.92	11.15	11.24	0.99
1I 3/8	2.70	12.96	12.02	1.08
2I 3/8	2.50	12.76	11.82	1.08
2D 3/8	2.88	11.79	12.20	0.97
Source: Clark (50)				
A1-1	1.30	6.82	6.73	1.01
2	1.33	6.55	6.76	0.97
3	1.34	7.00	6.77	1.03
4	1.31	7.49	6.74	1.11
B1-1	1.28	8.78	8.66	1.01
2	1.23	7.75	8.61	0.90
3	1.28	8.91	8.66	1.03
4	1.29	8.45	8.67	0.97
5	1.24	7.41	8.62	0.86
C3-1	1.55	9.08	9.67	0.94
2	1.55	8.21	9.67	0.85
C4-1	1.18	9.52	10.50	0.91
D1-6	1.47	8.37	9.27	0.90
7	1.46	8.53	9.26	0.92
8	1.46	8.88	9.26	0.96
D2-6	1.91	7.81	7.27	1.07
7	1.93	7.35	7.29	1.01
8	2.02	8.30	7.38	1.12
D4-1	1.58	8.11	6.94	1.17
2	1.63	7.82	6.99	1.12
D5-1	1.18	6.99	6.54	1.07
2	1.16	7.36	6.52	1.13
3	1.19	7.61	6.55	1.16
Source: Siess, De Paiva (51)				
G33S12	2.73	14.36	13.15	1.09
32	2.72	17.61	14.32	1.23

$$\frac{V_{rt}}{bd^* \sqrt{f'_c}} = 10.6 - 5.0 \, {}^{a}/_{d^*} + 3.7 \sqrt{\rho^*} + 0.42 \frac{A_v f_y}{b s_h \sqrt{f'_c}}$$

$$1.0 \leq {}^{a}/_{d^*} \leq 2.5$$

36 tests

TABLE 7.11 RATIO OF TEST TO CALCULATED STRENGTH--
CONTINUOUS BEAMS WITH WEB REINFORCEMENT

Beam	$0.61\frac{A_v f_{ys}}{bs_h\sqrt{f'_c}}$	$\frac{V_m}{bd^*\sqrt{f'_c}}$	$\frac{V_{rt}}{bd^*\sqrt{f'_c}}$	$\frac{V_m}{V_{rt}}$
Source:	Rodriguez, Bianchini, Viest, Kesler (41)			
C3 A2	2.66	8.30	7.51	1.10
E2 A1	1.89	6.34	6.35	1.00
2	2.18	6.72	6.54	1.03
3	2.14	6.98	6.50	1.07
C2 A1	2.03	5.18	6.39	0.81
2	2.03	6.34	6.38	0.99
E3 H2	3.82	8.58	8.68	0.99
C3 H1	5.23	9.72	10.09	0.96
2	4.17	8.90	9.03	0.99
E2 H1	4.42	8.01	8.78	0.91
2	2.83	7.34	7.29	1.01
C2 H1	4.48	7.98	8.84	0.90
2	2.51	6.47	6.87	0.94
B2 A1	1.42	4.96	5.47	0.91
H1	2.99	7.25	6.94	1.04
H2	1.83	6.38	5.78	1.10
Source:	Elstner, Moody, Viest, Hognestad (36)			
I10a	2.76	11.67	10.40	1.12
b	2.88	10.32	10.52	0.98
11a	4.34	12.63	12.00	1.05
b	4.83	12.24	12.47	0.98
12a	5.80	11.93	13.44	0.89
b	6.42	11.13	14.06	0.80
Is	9.71	14.82	17.35	0.85
t	10.19	15.67	17.83	0.88
I13a	3.65	12.48	11.29	1.10
b	4.01	12.60	11.65	1.08
14a	6.10	15.80	13.74	1.15
15a	9.11	15.91	16.75	0.95
Iu	2.87	10.38	9.67	1.07
v	3.85	11.27	10.65	1.06
w	4.16	11.00	10.96	1.00
Source:	Guralnick (48)			
IA2	2.29	8.80	8.45	1.04
B2	2.32	7.24	7.85	0.92
C2	1.72	9.70	8.88	1.09

$$\frac{V_{rt}}{bd^*\sqrt{f'_c}} = 7.3 - 2.6\,{}^{a}/_{d^*} + 1.7\sqrt{\rho^*} + 0.61\frac{A_v f_{ys}}{bs_h\sqrt{f'_c}}$$

$$1.0 \le {}^{a}/_{d^*} \le 2.5$$

34 tests

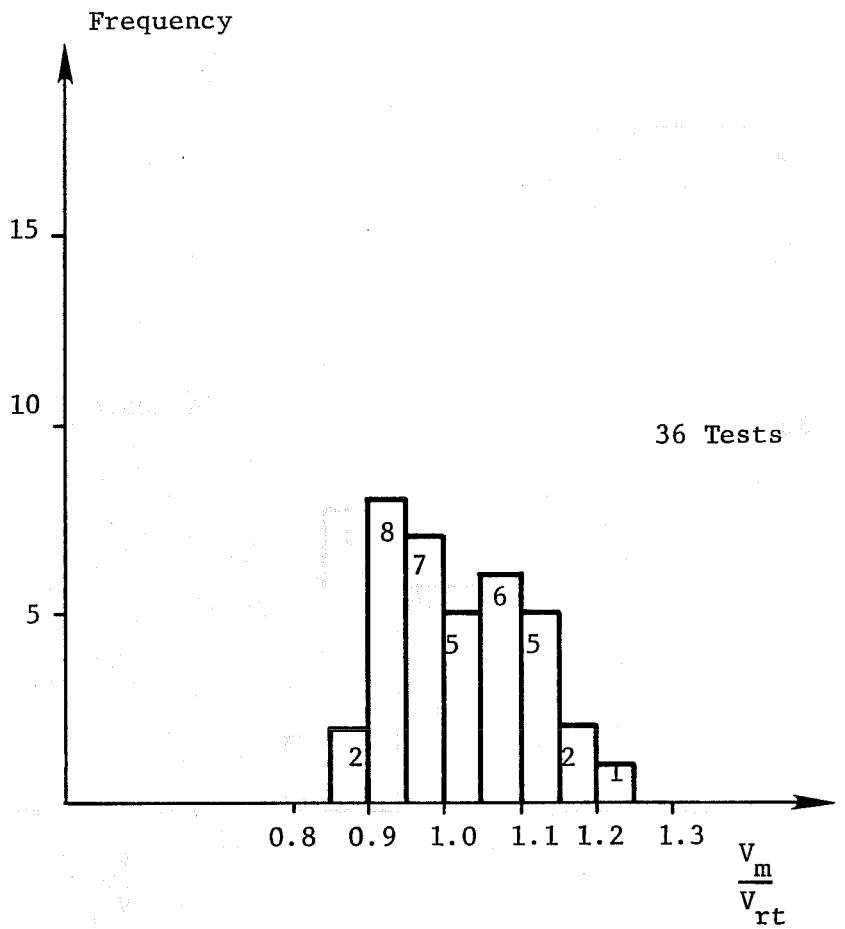

Average = 1.01

Standard deviation = 0.09

Fig. 7.16 Histogram of the ratio of test to calculated shear strength - simply supported beams with web reinforcement

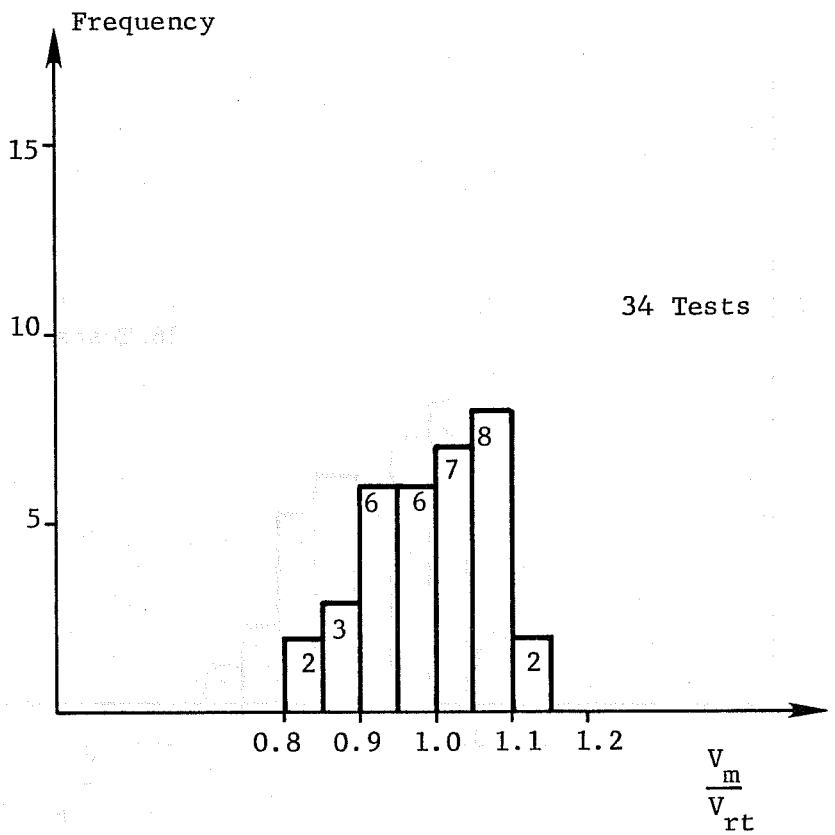

Fig. 7.17 Histogram of the ratio of test to calculated shear strength - continuous beams with web reinforcement

$$V_a = \frac{M}{a} = \frac{2NI}{aA_g h}$$

when $N > 0.4P_b$

$N = 0.4P_b$

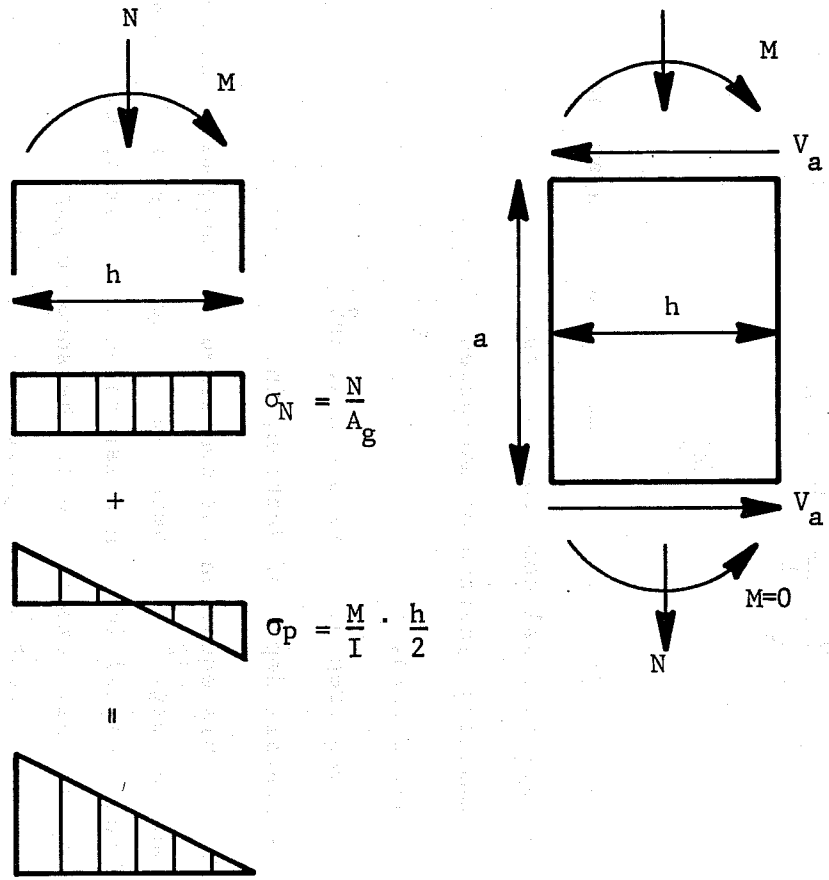

Fig. 7.18 Effect of axial load on shear capacity

produce a stress of zero in the tension face of the concrete with axial compression acting on the section.

$$\frac{N}{A_g} - \frac{aV_a}{I} \times \frac{h}{2} = 0$$

$$V_a = \frac{2NI}{aA_g h} \qquad (7.54)$$

where V_a = contribution of axial compression to shear capacity, lbs.

N = applied axial compression, lbs.

I = moment of inertia of uncracked section, $in.^4$

a = shear span, in.

A_g = gross area of cross section, $in.^2$

h = overall depth of section, in.

The validity of this equation was confirmed in experiments conducted by Hedman and Losberg.[52] To check the applicability of the equation for the effect of axial load on shear to short columns, the contribution of axial compression to the shear capacity for the specimens in the current investigation was studied. In Table 7.12, each pair of specimens listed were identical except for the level of axial compression. The measured contribution of axial compression ΔV_m was obtained by subtracting the measured strength of the specimens without axial compression from the measured strength of the specimen with axial compression. Because the concrete compressive strength was different in some pairs, ΔV_m was adjusted using equations for the contribution of the concrete (Eqs. (7.48) and (7.49)). For simply supported beams, the corrected difference in shear strength is:

$$\Delta V'_m = \Delta V_m + bd^*(10.6 - 5.0\frac{a}{d^*} + 3.7\sqrt{\rho^*})(\sqrt{f'_{c1}} - \sqrt{f'_{c2}}) \qquad (7.55)$$

TABLE 7.12 CONTRIBUTION OF AXIAL COMPRESSION TO SHEAR CAPACITY

Specimen Name	f'_c psi	V_m kips	ΔV_m kips	V_a kips	$\Delta V'_m$ kips		$\Delta V'_m / V_a$	
					Simp.	Cont.	Simp.	Cont.
O-PB	6000	52	25	14	25	25	1.79	1.79
C-PB	5950	77						
O-DM	5950	55	13	14	16	16	1.14	1.14
C-DM	5250	68						
OUS	5810	66	8	17	13	13	0.77	0.77
CUS	5060	74						
OUS	5810	66	20	17	18	19	1.06	1.12
CMS	6090	86						
OUS	5810	66	25	34	23	24	0.68	0.71
2CUS	6090	91						

$\Delta V_m = V_m$ (axial compression) - V_m (no axial compression)

$\Delta V'_m = \Delta V_m$ adjusted using Eqs. 7.55 or 7.56

$V_a = \frac{2NI}{aA_g h}$

For continuous beams, the corrected difference in shear strength is:

$$\Delta V'_m = \Delta V_m + bd^* (7.3 - 2.6\frac{a}{d^*} + 1.7\sqrt{\rho^*})(\sqrt{f'_{c1}} - \sqrt{f'_{c2}}) \qquad (7.56)$$

where $\Delta V'_m$ = adjusted measured contribution of axial compression

f'_{c1} = concrete compressive strength in the specimen without axial compression

f'_{c2} = concrete compressive strength in the specimen with axial compression

It should be noted that virtually the same correction would have been obtained if $\sqrt{f'_{c1}/f'_{c2}}$ had been applied to V_m. The values of $\Delta V'_m$ (simply supported beam, and continuous beam) are compared with the calculated contribution of axial compression (Eq. (7.54)). The ratio of $\Delta V'_m$ to V_a in both equations ((7.55) and (7.56)) shows the equation of calculating the contribution of axial compression is acceptable. However, in the case of 2CUS, $\Delta V'_m$ is less than V_a. Specimen 2CUS is the only specimen with 80 percent of the axial load corresponding to balanced strain condition (P_b). All other specimens were subjected to 40 percent of P_b. Therefore, it seems reasonable to limit the level of V_a because of the lack of data for specimens with high axial compression (more than $0.4P_b$). Based on the available data, the limit was set as the value corresponding to an axial compressive load equal to $0.4P_b$, as follows:

$$\text{for } N > 0.4P_b, \quad \text{use } N = 0.4P_b$$

to compute V_a.

The contribution of axial compression was added to the Eqs. (7.52) and (7.53). The total shear capacity for beams with web reinforcement and axial compression is:

$$V_r \text{ (simply supported)} = \left(10.6 - 5.0\frac{a}{d^*} + 3.7\sqrt{\rho^*}\right) bd^*\sqrt{f'_c} + 0.42\frac{A_v f_{ys} d^*}{s_h} + \frac{2NI}{aA_g h} \quad (7.57)$$

$$V_r \text{ (continuous)} = \left(7.3 - 2.6\frac{a}{d^*} + 1.7\sqrt{\rho^*}\right) bd^*\sqrt{f'_c} + 0.61\frac{A_v f_{ys} d^*}{s_h} + \frac{2NI}{aA_g h} \quad (7.58)$$

$$1 \leq \frac{a}{d^*} \leq 2.5$$

$$N = 0.4P_b \quad \text{when} \quad N > 0.4P_b$$

7.3.4.4 Short Columns. In this section the application of Eqs. (7.57) and (7.58) for beams to short columns is discussed. As mentioned before, the only studies of the shear behavior of short columns under monotonic or reversal loading are those in several Japanese laboratories and at The University of Texas. The results of the Japanese investigations have been compiled by the Building Research Institute.[20,21]

Japanese Tests. One hundred eleven short columns with $1 \leq a/d^* \leq 2.5$ under reversal loading were reported. However, in almost all of the columns the measured maximum capacities were greater than calculated flexural capacities, because the longitudinal extreme tension reinforcement ratio ρ^*, was relatively small—less than 1.0 percent in more than half of all columns. Equations (7.58) and (7.59) were used to estimate the capacity of the one hundred eleven tests. In one hundred tests, the measured maximum capacities were greater than calculated flexural capacities. Therefore, only eleven tests were appropriate for confirming the

validity of the equations. It is interesting to note that nearly half of the columns showed rapid deterioration of capacity after each peak load in spite of the fact that the flexural capacity was reached. Therefore, the tests provide data for a more detailed study of shear deterioration in the next chapter.

Table 7.13 indicates the comparison of computed (simply supported beam in Eq. (7.57), and continuous beam in Eq. (7.58)) to measured capacity for the 11 Japanese tests. The ratio of measured-to-computed capacity (V_m/V_r) shows that the average for both equations is the same, but the standard deviation for the continuous beam equation (0.03) is much better than the simply supported beam equation (0.14). It should be noted that in some cases, the computed shear capacity was larger than computed flexural capacity, especially when the simple beam equation was used. Therefore, to calculate the shear capacity of the short columns, the equation derived from the data of continuous beams provides a better estimate of strength than that derived from the data of simply supported beams for the Japanese tests of short columns.

Table 7.14 provides an estimate of the effect of transverse reinforcement on shear capacity. The contribution of transverse reinforcement was obtained by subtracting the contribution of concrete (V_{rc}) and axial load (V_a) from measured shear capacity (V_m). The equation derived from the data of continuous beam is used for calculating V_{rc}. From the continuous beam tests, the reduction factor β_2 is 0.61; however, for the Japanese column tests, the average value of β_2 is 0.51. The ratio of the contribution of transverse reinforcement-to-measured capacity ranges from 0.15 to 0.45, and the average of this ratio is 0.29. The average ratio of the steel contribution to the the total strength indicates that more than 70 percent of the strength is contributed by the concrete.

TABLE 7.13 COMPARISON OF COMPUTED AND MEASURED CAPACITY — JAPANESE COLUMN TESTS

Specimen Name		V_m kips	V_f kips	COMPUTED SHEAR CAPACITY						V_m/V_r	
				a/d^*	ρ^* %	$\frac{A_v f_{ys} d^*}{s_h}$ kips	V_a kips	V_r kips Simp.	V_r kips Cont.	Simp.	Cont.
AF	310B	36	37	1.16	1.12	19.3	0.0	45	38	0.80*	0.95*
	320A	18	20	2.33	1.12	11.2	0.0	17	19	1.06	0.95
	32CB	30	31	2.33	1.12	16.5	9.3	28	32	1.07	0.94*
	420B	26	27	2.33	1.58	19.3	0.0	23	26	1.13	1.00
WS2	5BH	39	45	1.16	0.74	13.1	4.0	50	41	0.78*	0.95
	5BT	41	45	1.16	0.74	13.1	4.0	50	41	0.82*	1.00
AR	15B5H	31	35	1.74	1.23	16.5	4.0	38	34	0.92*	0.91
	15B5T	31	35	1.74	1.23	16.5	4.0	38	34	0.82*	0.91
	20A5H	18	20	2.33	0.73	12.0	3.1	17	19	1.06	0.95
AR2	5BH 1/4	32	34	2.33	1.23	22.4	6.0	30	34	1.07	0.94
	5BT 1/4	33	34	2.33	1.23	23.4	6.0	31	35	1.06	0.97*
									Average	0.95	0.95
									Standard Deviation	0.14	0.03

* the computed shear capacity V_r is greater than computed flexural capacity V_f

TABLE 7.14 EFFECT OF TRANSVERSE REINFORCEMENT — JAPANESE COLUMN TESTS

	Specimen Name	V_m kips	V_{rc} kips	V_a kips	$\frac{A_v f_{ys} d^*}{s_h}$ kips	β_2	$\frac{V_m - V_{rc} - V_a}{V_m}$
AF	310B	36	26.0	0.0	19.3	0.52	0.28
	320A	18	12.2	0.0	11.2	0.52	0.32
	32CB	30	12.6	9.3	16.5	0.49	0.27
	420B	26	14.2	0.0	19.3	0.61	0.45
WS2	5BH	39	29.0	4.0	13.1	0.46	0.15
	5BT	41	29.0	4.0	13.1	0.61	0.19
AR	15B5H	31	20.0	4.0	16.5	0.42	0.23
	15B5T	31	20.0	4.0	16.5	0.42	0.23
	20A5H	18	8.6	3.1	12.0	0.53	0.35
AR2	5BH 1/4	32	14.3	6.0	22.4	0.52	0.37
	5BT 1/4	33	14.7	6.0	23.4	0.53	0.37
					Average	0.51	0.29

$$V_m - V_{rc} - V_a = \beta_2 \frac{A_v f_{ys} d^*}{s_h}$$

Current Investigation. Equations (7.57) and (7.58) were used to calculate the shear capacity of the square and rectangular short columns ($1 \leq a/d^* \leq 2.5$) in the current investigation. Table 7.15 shows the comparison of computed and measured results for the short columns. For four specimens, 0-PU, 0-DU, 0-DB, and 0UW, the measured maximum capacities (V_m) were greater than the calculated flexural capacities (V_f). The calculated shear capacity V_r for 0-PU, 0-DB, and 0UW was not greater than V_f, but was nearly equal to V_f. For the other tests, the ratio of measured-to-computed capacity (V_m/V_r) was calculated. The shear capacity of the column under diagonal loading was computed from the shear capacities in the principal loading direction using circular and elliptical interaction curves. Once again, the ratio V_m/V_r indicates that the average and standard deviation for the continuous beam equation (average = 0.97, standard deviation = 0.08) is better than the simply supported beam equation (0.90, 0.12).

Based on the two test series (Japanese tests and current investigation) it is clear that the equation based on continuous beam results is more appropriate for calculating the shear capacity of short columns than that based on the data of simply supported beams. The results confirm the hypothesis that shear behavior of short columns is closer to that of continuous beams than that of simply supported beams. The applicability of these equations for the control of shear deterioration is described in the next chapter.

Table 7.16 indicates the effect of transverse reinforcement on the measured shear capacity. The contribution of transverse reinforcement is obtained by subtracting the contribution of concrete (V_{rc}) calculated using the equation based on the data of continuous beams and the contribution of axial load (V_a). Specimens in which the computed flexural capacity (V_f) was less than measured maximum capacity (V_m) and rectangular

TABLE 7.15 COMPARISON OF COMPUTED AND MEASURED CAPACITY — UNIVERSITY OF TEXAS COLUMN TESTS

	Specimen Name	V_m kips	V_f kips	V_r kips Simp.	V_r kips Cont.	V_m/V_r Simp.	V_m/V_r Cont.
SQUARE COLUMN	0-PU	56	49	61	55	-- **	-- **
	C-PU	67	80	72	67	0.93	1.00
	0-PB	52	53	66	59	0.79*	0.88*
	C-PB	77	78	79	72	0.97*	1.07
	0-DM	55	65	66	60	0.83*	0.92
	C-DM	68	76	77	71	0.88*	0.96
	0-DU	64	59	61	55	-- **	-- **
	0-DB	61	59	61	55	-- **	-- **
	C-DB	68	73	74	68	0.93	1.00
	C-DB32	78	80	92	92	0.85*	0.85*
	C-DB21	76	84	85	81	0.89*	0.94
	C-DB9	64	84	75	67	0.85	0.96
	C-DB3	66	80	72	62	0.92	1.06
RECTANGULAR COLUMN	0US	66	95	83	69	0.80	0.96
	0UW	57	51	42	45	-- **	-- **
	CMS	86	120	103	88	0.83	0.98
	CUS	74	113	96	83	0.77	0.89
	CUW	60	68	50	54	1.20	1.11
	2CUS	91	134	104	88	0.88	1.03
	CDS30	80	105	84	79	0.95	1.01
	CDW30	74	78	66	67	1.12	1.10
(s)	CBSW	60	114	96	82	0.72	0.84
(w)	CDSW30	57	73	55	58	1.04	0.98
					Average	0.90	0.97
					Standard Deviation	0.12	0.08

(s) - strong direction

(w) - weak direction

* - the computed shear capacity V_r is greater than computed flexural capacity V_f

** - the computed flexural capacity V_f is less than measured maximum capacity V_m

TABLE 7.16 EFFECT OF TRANSVERSE REINFORCEMENT — UNIVERSITY OF TEXAS COLUMN TESTS

	Specimen Name	V_m kips	V_{rc} kips	V_a kips	$\frac{A_v f_{ys} d^*}{s_h}$ kips	β_2	$\frac{V_m - V_{rc} - V_a}{V_m}$
SQUARE COLUMN	O-PU	56	40.1	0.0	24.4	-- *	-- *
	C-PU	67	37.8	13.0	24.4	0.66	0.25
	O-PB	52	43.9	0.0	24.4	0.33	0.16
	C-PB	77	43.7	13.0	24.4	0.83	0.26
	O-DM	55	43.7	0.0	26.2	0.43	0.21
	C-DM	68	41.1	13.0	26.2	0.53	0.20
	O-DU	64	39.9	0.0	24.4	-- *	-- *
	O-DB	61	40.3	0.0	24.4	-- *	-- *
	C-DB	68	38.7	13.0	26.2	0.61	0.24
	C-DB32	78	41.7	13.0	59.4	0.39	0.30
	C-DB21	76	43.0	13.0	39.2	0.51	0.26
	C-DB9	64	43.0	13.0	17.1	0.47	0.13
	C-DB3	66	44.3	13.0	6.1	1.43	0.13
RECTANGULAR COLUMN	OUS	66	53.8	0.0	24.1	0.51	0.18
	OUW	57	29.6	0.0	25.2	-- *	-- *
	CMS	86	55.1	17.0	24.1	0.58	0.16
	CUS	74	50.2	17.0	24.1	0.28	0.09
	CUW	60	27.6	10.0	25.2	0.89	0.37
	2CUS	91	55.1	17.0	24.1	0.78	0.21
	CDS30	80	--**	--**	--**	--**	--**
	CDW30	74	--**	--**	--**	--**	--**
(s)	CBSW	69	50.3	17.0	24.1	0.07	0.02
(w)	CDSW30	57	--**	--**	--**	--**	--**
					Average	0.58	0.20

$$V_m - V_{rc} - V_a = \beta_2 \frac{A_v f_{ys} d^*}{s_h}$$

(s) - strong direction

(w) - weak direction

* - the computed flexural capacity V_f is less than measured maximum capacity V_m

** - the rectangular column with diagonal loading direction; there is no way to calculate V_{rc}, V_a, $\frac{A_v f_{ys} d^*}{s_h}$, and β_2

columns loaded in the diagonal direction were not included in this comparison. Note that although the average of β_2 is 0.58 (with a range of 0.07 to 1.43), the ratio of the contribution of transverse reinforcement-to-measured capacity ranges from 0.02 to 0.37 with an average of only 0.2. In spite of the large amounts of transverse reinforcement in specimens C-DB32 and C-DB21, only 30 percent of the measured capacity was attributed to the transverse reinforcement. The contribution of the transverse reinforcement to the measured capacity in specimens, CUS and CBSW, was nearly zero. It is clear that the concrete contribution to the total shear capacity is of primary importance and that the concrete contributes at least 70 to 80 percent of the total shear capacity of a short column.

7.4 Summary

In this chapter the shear capacity of short columns was calculated using the ACI 318-77 approach, formulations based on plasticity theory and equations proposed by Zsutty. The equations reviewed have been developed from simple beams with moderate a/d^* ratios. The shear strength contributed by the concrete is based on first cracking. Short columns have extra strength after first cracking, because lateral forces may be transferred by compression (through arch or strut action) in the concrete. In addition, the shear behavior of short columns between stiff floors is similar to that of continuous beams. Based on data from continuous beams with $1 \leq a/d^* \leq 2.5$ which failed in shear, an equation for shear strength was proposed. This equation was used to calculate the shear capacities of short columns tested in Japan and at The University of Texas in order to evaluate the applicability of the equation to short columns. The comparison of measured and calculated shear strength indicates that the equation is acceptable.

CHAPTER 8

PROCEDURE TO CONTROL THE PERFORMANCE OF SHORT COLUMNS

8.1 General

In Chapter 7, an empirical equation for calculating the shear capacity of short columns was derived from data of continuous beams failing in shear. However, this equation considers only the shear capacity and does not address the problem of deterioration of strength and the control of energy dissipating characteristics of the columns.

In this chapter a procedure to control the performance of short columns is introduced. First, an equation for calculating shear strength is proposed. This equation is a simplification of the empirical equation introduced in Chapter 7. Second, this proposed equation is examined relative to the results of Japanese tests of short columns in which almost half of one hundred eleven columns exhibited rapid deterioration after reaching maximum load even though the calculated flexural capacity was achieved or exceeded. Third, the procedure to control the performance is described and characteristics of this approach are compared with those in Appendix A of ACI 318-77.

8.2 Shear Strength

As described in Chapter 7, empirical equations for calculating the shear capacity of short columns were derived from the data of simply supported and continuous beams with $1 \leq a/d^* \leq 2.5$ which failed in shear. From the application of these equations to short columns, it was clear that the equation based on data of

continuous beams was more appropriate to short columns than that based on data of simply supported beams. The empirical equation introduced in Chapter 7 was

$$V_r = (7.3 - 2.6\frac{a}{d^*} + 1.7\sqrt{\rho^*}\,(bd^*\sqrt{f'_c} + \frac{2NI}{aA_g h} + 0.61\frac{A_v f_{ys} d^*}{s_h} \quad (8.1)$$

$$1 \leq \frac{a}{d^*} \leq 2.5$$

$$N = 0.4P_b \quad \text{when} \quad N > 0.4P_b$$

As mentioned in Chapter 5, at maximum load, spalling of concrete at the corner of the column and extensive cracking of the faces occurred. Therefore, the core area of concrete (measured out-to-out of transverse reinforcement, A_c) was substituted for bd^* in calculating the contribution of concrete using Eq. (8.1). Since the equation provided a good estimate of the shear capacity of Japanese column tests and those of the current investigation, the value of the contribution of concrete V_{rc} was kept the same by adjusting the constants in the equation. Since bd^* is about equal to $1.2A_c$, Eq. (8.1) takes the following form:

$$V_r = (9 - 3\frac{a}{d^*} + 2\sqrt{\rho^*})\,A_c\sqrt{f'_c} + \frac{2NI}{aA_g h} + 0.61\frac{A_v f_{ys} d^*}{s_h} \quad (8.2)$$

$$1 \leq \frac{a}{d^*} \leq 2.5$$

$$N = 0.4P_b \quad \text{when} \quad N > 0.4P_b$$

The equation will be simplified further by examining each term in the equation and eliminating any terms which do not significantly change the strength for typical column geometries.

8.2.1 Transverse Reinforcement. As mentioned in Sec. 7.3.4.4, the contribution of transverse reinforcement is not likely to exceed 30 percent of the total shear capacity of short columns even when large amounts of transverse reinforcement are used. Figure 8.1 indicates the relationship between the measured maximum capacities and the spacing of transverse reinforcement in square columns specimens, C-DB32, C-DB21, C-DB, C-DB9, and C-DB3. This figure indicates that there was a 20 percent increase in measured shear capacity when the tie spacing was reduced from 12 in. to 1.13 in. It appears that the contribution of transverse reinforcement to the shear capacity can be ignored without significant loss of accuracy, but with considerable improvement as far as simplicity is concerned.

$$V_r = (9 - 3\frac{a}{d^*} + 2\sqrt{\rho^*})\, A_c\sqrt{f'_c} + \frac{2NI}{aA_g h} \qquad (8.3)$$

In addition, the equation becomes more conservative with regard to shear failure of short columns than Eq. (8.1).

8.2.2 Ratio of Longitudinal Extreme Tension Reinforcement ρ^* (Percent). In Appendix A (Seismic Design) of ACI 318-77, the total longitudinal reinforcement ratio ρ_g in columns ranges from 0.01 to 0.06. Therefore, ρ^*, the reinforcement in the extreme tension layer ranges from a minimum of 0.5 percent to a maximum of 3.0 percent. Figure 8.2 shows the range of V_r (axial load = 0.0, Eq. (8.3)) for varying values of ρ^* at $a/d^* = 1.0$ and $a/d^* = 2.5$. Because the flexural capacity will be limited to permit development of desirable hysteretic behavior, the ratio of longitudinal extreme tension reinforcement will probably fall in a range from 0.5 percent to 1.5 percent for typical designs. This range will be examined further in Sec. 8.5.3. Note that the difference of V_r for values of ρ^* between 0.5 percent and 1.5 percent is about

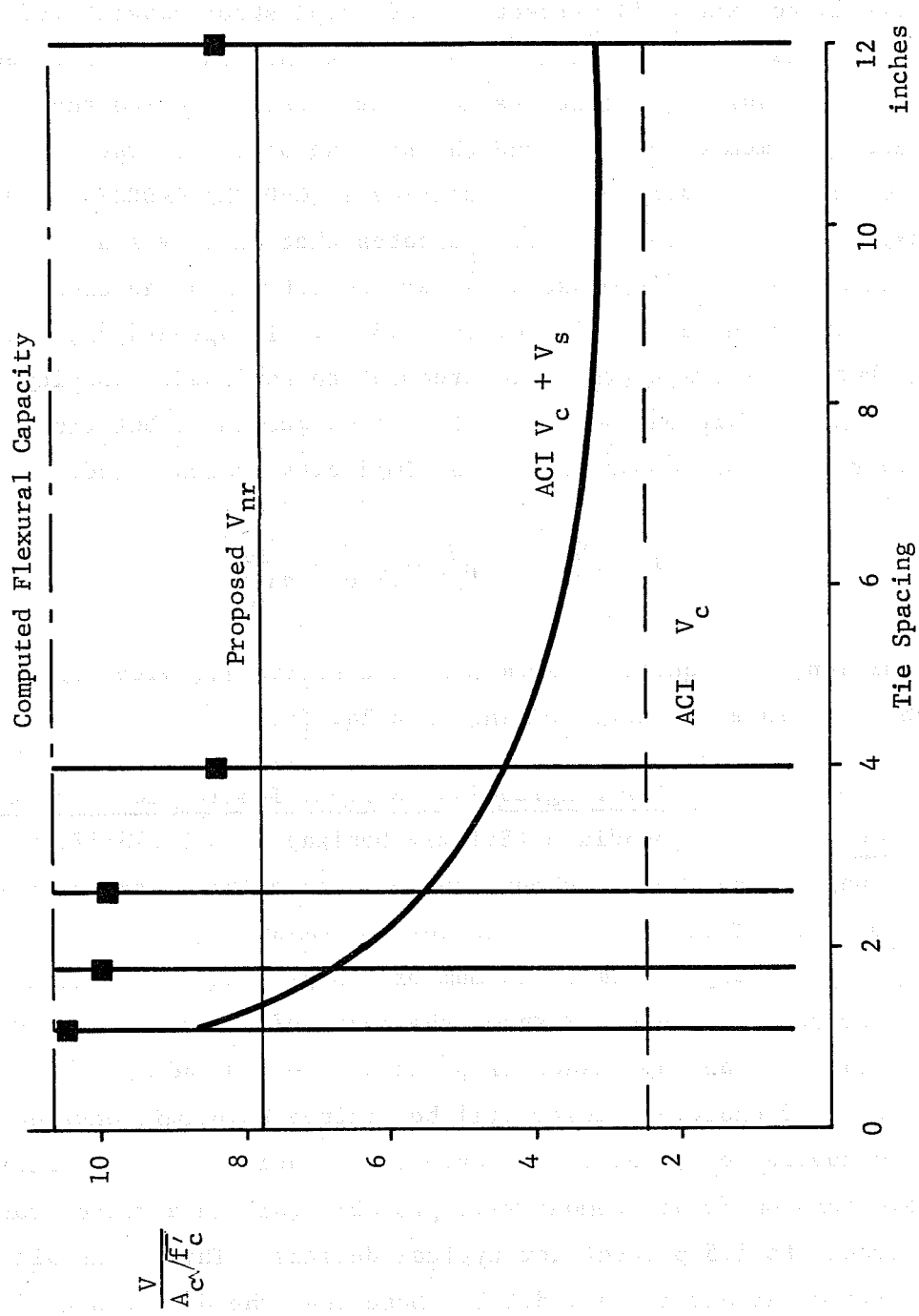

Fig. 8.1 Effect of tie spacing to shear capacity

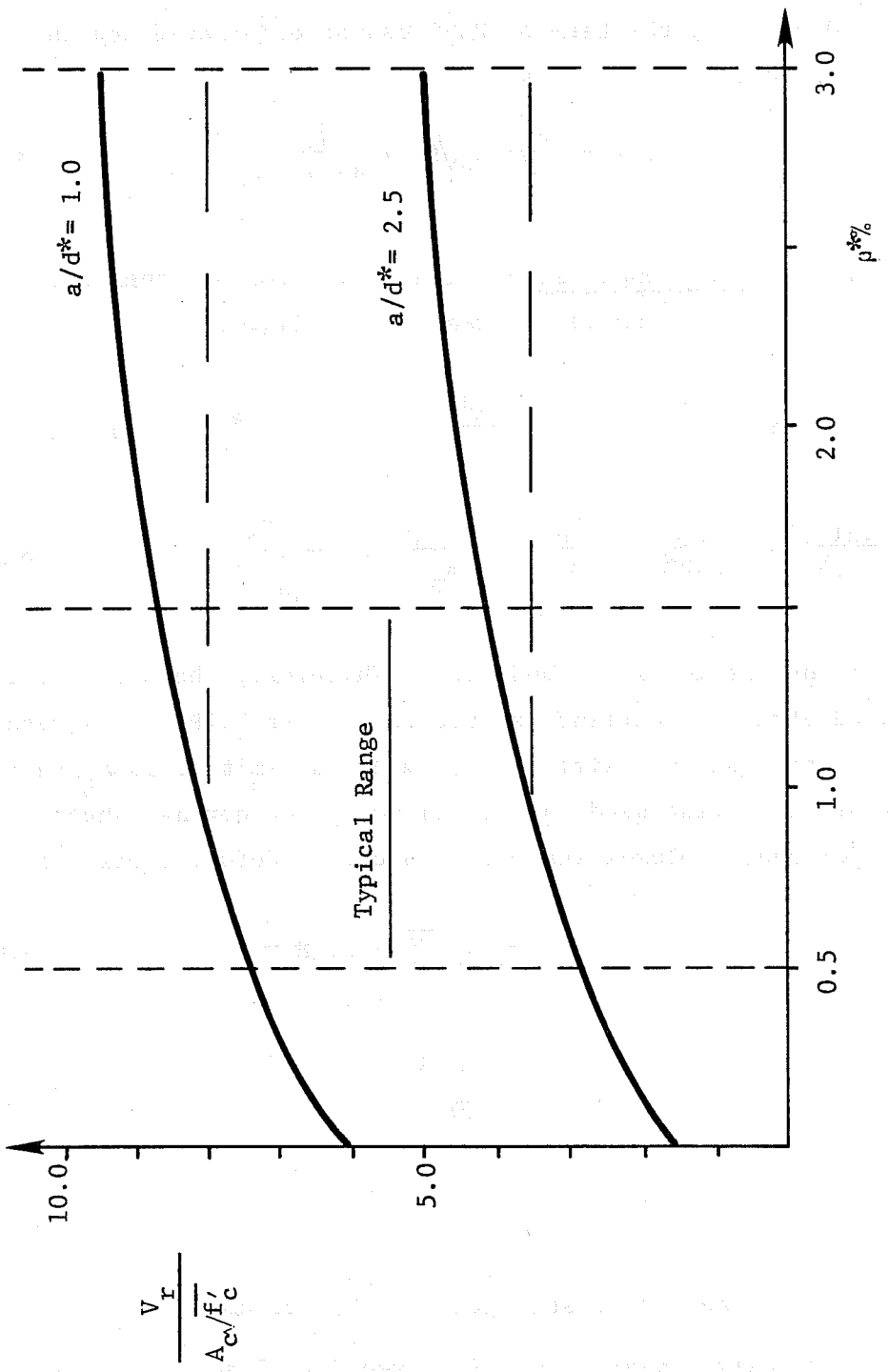

Fig. 8.2 Effect of ρ^* on shear capacity

$1.0A_c\sqrt{f'_c}$ (Fig. 8.2). If it is assumed that the contribution of ρ^* to the concrete portion of the equation is constant at a value of $\rho^* = 1.0$ percent, the term of $2\sqrt{\rho^*}$ can be eliminated and the constant (9) increased to 11 as follows:

$$V_r = (11 - 3\frac{a}{d^*}) A_c\sqrt{f'_c} + \frac{2NI}{aA_g h} \qquad (8.4)$$

8.2.3 Axial Compression. The term involving the contribution of axial compression is rearranged as follows:

$$A_g = bh \qquad I = \frac{bh^3}{12} \qquad d^* \approx 0.85h$$

$$\frac{2NI}{aA_g h} = \frac{Nbh^3}{6abh^2} = \frac{Nh}{6a} = \frac{0.2N}{\frac{a}{d^*}} \leq \frac{0.08P_b}{\frac{a}{d^*}} \qquad (8.5)$$

P_b for all the specimens was 300 kips. Therefore, the axial stress at balanced stress conditions is 2000 psi and at $0.4P_b$ the stress is 800 psi, so that the axial load term has a limit of $160A_g/(a/d^*)$. In terms of the format used in the ACI Code, the nominal shear strength for short columns subjected to cyclic deformations is:

$$V_{nr} = (11 - 3\frac{a}{d^*}) A_c\sqrt{f'_c} + 0.2N\frac{d^*}{a} \qquad (8.6)$$

$$\frac{0.2N}{\frac{a}{d^*}} \leq \frac{160A_g}{\frac{a}{d^*}}$$

$$1 \leq \frac{a}{d^*} \leq 2.5$$

where V_{nr} = nominal shear strength of short columns = V_u/φ

V_u = design shear force, factored dead load plus live load shear

Table 8.1 shows the comparison of the shear forces of the specimens in the current investigation calculated using the empirical equation (8.1) for V_r and the proposed equation V_{nr} (8.6). Shear capacities of all specimens calculated using the proposed equation were less than the flexural capacity. The average ratio of V_m to V_{nr} is 1.27 and the standard deviation is 0.17. The average ratio of V_m to V_r is 0.97 with a standard deviation of 0.08. The difference can be attributed to the removal of the term for the contribution of transverse reinforcement in the proposed equation. It should be noted that computed capacities using V_{nr} are obviously more conservative.

8.3 Effect of Deterioration

The proposed equation is examined vis-a-vis the Japanese data on short columns. Almost half of the one hundred eleven column tests reported deteriorated rapidly after reaching maximum load. Table 8.2 shows a comparison of measured maximum and calculated shear capacities and the flexural capacity for the Japanese tests. The behavior was classified as flexural or degrading in shear. Examples of each type of behavior are shown in Figs. 8.3 and 8.4. The commentary of the SEAOC code[53] indicates that the flexural behavior is satisfactory if the displacement ductility factor, μ (defined as the ratio of deflection at ultimate strength, Δ_u, to that at yield strength, Δ_y), is at least 3.0. Figure 8.3 illustrates this concept of flexural ductility. The observed specimen behavior is indicated in column 5 of Table 8.2. The calculated flexural capacity V_f (col. 3) and the capacity calculated using the proposed equation V_{nr} (col. 1) were compared to determine whether flexure or shear degrading behavior would be expected. It is interesting to note that whenever V_{nr} is greater than V_f, the flexural behavior requirement stated in the SEAOC code was met (cols. 5 and 8).

TABLE 8.1 COMPARISON OF EMPIRICAL EQUATION V_r AND PROPOSED NOMINAL STRENGTH V_{nr}

	Specimen Name	V_m kips	V_f kips	V_r kips	V_{nr} kips	V_m / V_r	V_m / V_{nr}
SQUARE COLUMN	O-PU	56	49	55	41	-- *	-- *
	C-PU	67	80	67	53	1.00	1.26
	O-PB	52	53	59	45	0.88**	1.15
	C-PB	77	78	72	59	1.07	1.30
	O-DM	55	65	60	45	0.92	1.22
	C-DM	68	76	71	56	0.96	1.21
	O-DU	64	59	55	41	-- *	-- *
	O-DB	61	59	55	42	-- *	-- *
	C-DB	68	73	68	53	1.00	1.28
	C-DB32	78	80	92	57	0.85**	1.37
	C-DB21	76	84	81	58	0.94	1.31
	C-DB9	64	84	67	58	0.96	1.10
	C-DB3	66	80	62	59	1.06	1.12
RECTANGULAR COLUMN	OUS	66	95	69	54	0.96	1.22
	OUW	57	51	45	28	-- *	-- *
	CMS	86	120	88	75	0.98	1.15
	CUS	74	113	83	69	0.89	1.07
	CUW	60	68	54	36	1.11	1.66
	2CUS	91	134	105	75	1.03	1.21
	CDS30	80	105	79	58	1.01	1.38
	CDW30	74	78	67	43	1.10	1.72
	(s) CBSW	69	114	82	69	0.84	1.00
	(w) CDSW30	57	73	58	40	0.98	1.43
					Average	0.97	1.27
					Standard Deviation	0.08	0.17

(s) - strong direction

(w) - weak direction

* - the computed flexural capacity V_f is less than measured maximum capacity V_m

** - the computed shear capacity V_r is greater than computed flexural capacity V_f

TABLE 8.2 CLASSIFICATION OF THE BEHAVIOR OF JAPANESE TEST COLUMNS

Specimens		(1) V_{nr} kips	(2) V_n kips	(3) V_f kips	(4) V_m kips	(5) Behavior	(6) $V_m \geq V_f$	(7) $V_n \geq V_f$	(8) $V_{nr} \geq V_f$	(9) Accepting ACI Code
AF	210A	24	19	25	25	D	0	X	X	X
	22CB	22	33	23	23	D	0	0	X	X
	310A	24	43	38	38	D	0	0	X	0
	310B	24	31	37	36	D	X	X	X	X
	320A	14	29	20	18	D	X	0	X	0
	32CA	22	43	29	29	D	0	0	X	X
	32CB	22	40	31	30	D	X	0	X	X
	410A	31	43	49	49	D	0	X	X	X
	420A	14	43	27	28	D	0	0	X	0
	420B	14	31	27	26	D	X	0	X	0
	42CB	22	43	36	36	D	0	0	X	0
WS2	1BH	40	51	41	41	D	0	0	X	0
	1BT	40	51	41	42	D	0	0	X	0
	2BH	24	25	21	22	F	0	0	0	0
	2BT	24	25	21	22	F	0	0	0	0
	5BH	37	51	45	39	D	X	0	X	0
	5BT	37	51	45	41	D	X	0	X	X
	6BH	21	23	24	24	D	0	X	X	X
	6BT	21	23	24	24	D	0	X	X	X
	7BH	24	56	36	36	D	0	0	X	0
	7BT	24	56	36	36	D	0	0	X	0
LS	1AA	29	44	29	29	F	0	0	0	0
	1AB	29	44	29	29	F	0	0	0	0
	1BA	24	44	25	26	D	0	0	X	0
	1BB	24	29	25	26	D	0	0	X	0
	2AA	28	44	29	29	D	0	0	X	0
	2AB	28	36	29	30	D	0	0	X	0
	2BA	24	22	18	19	F	0	0	0	0
	2BB	24	15	18	19	F	0	X	0	X
	0BB	28	44	31	32	D	0	0	X	0
LE	2BAL	21	27	20	22	F	0	0	0	0
	6ACL	18	22	20	20	F	0	0	X	X
	7BCL	21	46	31	31	F	0	0	X	0
	8ACL	20	46	27	27	F	0	0	X	0
	8BAL	20	39	27	27	D	0	0	X	0
AR	15B5H	25	46	35	31	D	X	0	X	0
	15B5T	25	46	35	31	D	X	0	X	0
	20A2H	17	29	18	18	D	0	0	X	0
	20A2T	17	29	18	18	D	0	0	X	X
	20A5H	17	29	20	18	D	X	0	X	0
	20B2H	17	46	22	22	D	0	0	X	0
	20B2T	17	46	22	22	D	0	0	X	X
	20B5H	17	46	20	20	D	0	0	X	0
	20B5T	17	46	23	24	D	0	0	X	X

(1) - V_{nr} nominal shear strength of short columns

(2) - V_n nominal shear strength in ACI Code

(3) - V_f calculated flexural capacity

(4) - V_m measured maximum lateral load

(5) - Behavior observed specimen behavior
F = flexure
D = shear deterioration

(6) - $V_m \geq V_f$
(7) - $V_n \geq V_f$
(8) - $V_{nr} \geq V_f$
0 = Yes
X = No

(9) Accepting ACI Code checking $V_n \geq V_f$ and details (tie spacing, tie diameter)

TABLE 8.2 CLASSIFICATION OF THE BEHAVIOR OF JAPANESE TEST COLUMNS (Cont.)

Specimens		(1) V_{nr} kips	(2) V_n kips	(3) V_f kips	(4) V_m kips	(5) Behavior	(6) $V_m \geq V_f$	(7) $V_n \geq V_f$	(8) $V_{nr} \geq V_f$	(9) Accepting ACI Code
AR2	2BH 1/8	20	48	25	29	F	0	0	X	0
	2BH 1/4	23	48	32	33	D	0	0	X	0
	2BT 1/8	20	48	25	27	F	0	0	X	X
	2BT 1/4	23	48	32	33	D	0	0	X	X
	5BH 1/8	20	48	29	32	D	0	0	X	0
	5BH 1/4	23	48	34	33	D	X	0	X	0
	5BT 1/8	20	48	29	32	D	0	0	X	X
	5BT 1/4	23	48	34	33	D	X	0	X	X
	2AH 1/8	20	43	20	22	F	0	0	0	0
	2AH 1/4	23	43	25	27	D	0	0	X	0
	2AT 1/8	20	42	20	22	F	0	0	0	0
	2AT 1/4	23	42	25	27	D	0	0	X	0
	5AH 1/8	20	43	19	24	F	0	0	0	0
	5AH 1/4	23	43	25	28	D	0	0	X	0
	5AT 1/8	20	42	19	25	F	0	0	0	0
	5AT 1/4	23	42	25	28	D	0	0	X	0
LE2	3ACL	26	38	28	29	D	0	0	X	0
	3BCL	26	29	28	29	D	0	0	X	X
AF2	1	22	45	24	25	D	0	0	X	0
CHT	1	98	136	89	95	F	0	0	0	0
	2	74	114	77	80	D	0	0	X	0
	3	74	129	87	87	F	0	0	X	0
	4	74	127	95	95	D	0	0	X	0
LM2	1B	38	49	39	39	D	0	0	X	0
	2A	22	38	20	21	F	0	0	0	0
	2B	22	25	20	20	F	0	0	0	0
	3A	35	46	30	31	F	0	0	0	0
	3B	35	28	30	31	F	0	X	0	X
	4A	19	18	15	15	F	0	0	0	0
	4B	19	14	15	15	F	0	X	0	X
	5A	35	49	40	44	D	0	0	X	0
	5B	35	49	40	44	D	0	0	X	0
	6A	19	31	19	22	F	0	0	0	0
	6B	19	22	19	22	F	0	0	0	X
	7A	22	49	31	31	D	0	0	X	0
	7B	22	49	31	31	D	0	0	X	0
	8A	19	49	26	26	F	0	0	X	0
	8B	19	35	26	26	D	0	0	X	0
FC	1B	50	51	51	53	D	0	0	X	X
	3A	45	23	38	40	F	0	X	0	X
	3B	45	17	38	39	F	0	X	0	X
	4A	23	16	19	20	F	0	X	0	X
	5A	45	59	47	47	F	0	0	X	0
	5B	45	38	47	47	D	0	X	X	X
	6A	23	27	21	24	F	0	0	0	0
	6B	23	18	21	24	F	0	X	0	X
	7A	28	66	33	36	F	0	0	X	0
	7B	28	45	33	36	F	0	0	X	0
	8A	23	37	27	28	F	0	0	X	0
	8B	23	25	27	28	F	0	X	X	X
	2A	28	30	22	24	F	0	0	0	0
	2B	28	22	22	25	F	0	0	0	X
WS	1B	43	52	44	46	D	0	0	X	0
	3B	38	25	30	33	F	0	X	0	X
	2A0.33	21	42	24	26	D	0	0	X	0
	2B0.33	21	26	24	26	D	0	0	X	X
	2A	21	34	22	23	D	0	0	X	0
	2B	21	22	22	23	F	0	0	X	X
	5B0.25	43	52	54	55	D	0	X	X	X
	5B	38	52	42	43	D	0	0	X	0
	6A0.33	21	52	31	32	D	0	0	X	0
	6A0.25	21	52	27	30	F	0	0	X	0
	6B0.25	21	34	27	28	D	0	0	X	0
	6A	20	32	20	22	F	0	0	0	0
	6B	20	20	20	22	F	0	0	0	X
	7B	21	52	30	31	D	0	0	X	X
	8B	20	30	26	26	D	0	0	X	X

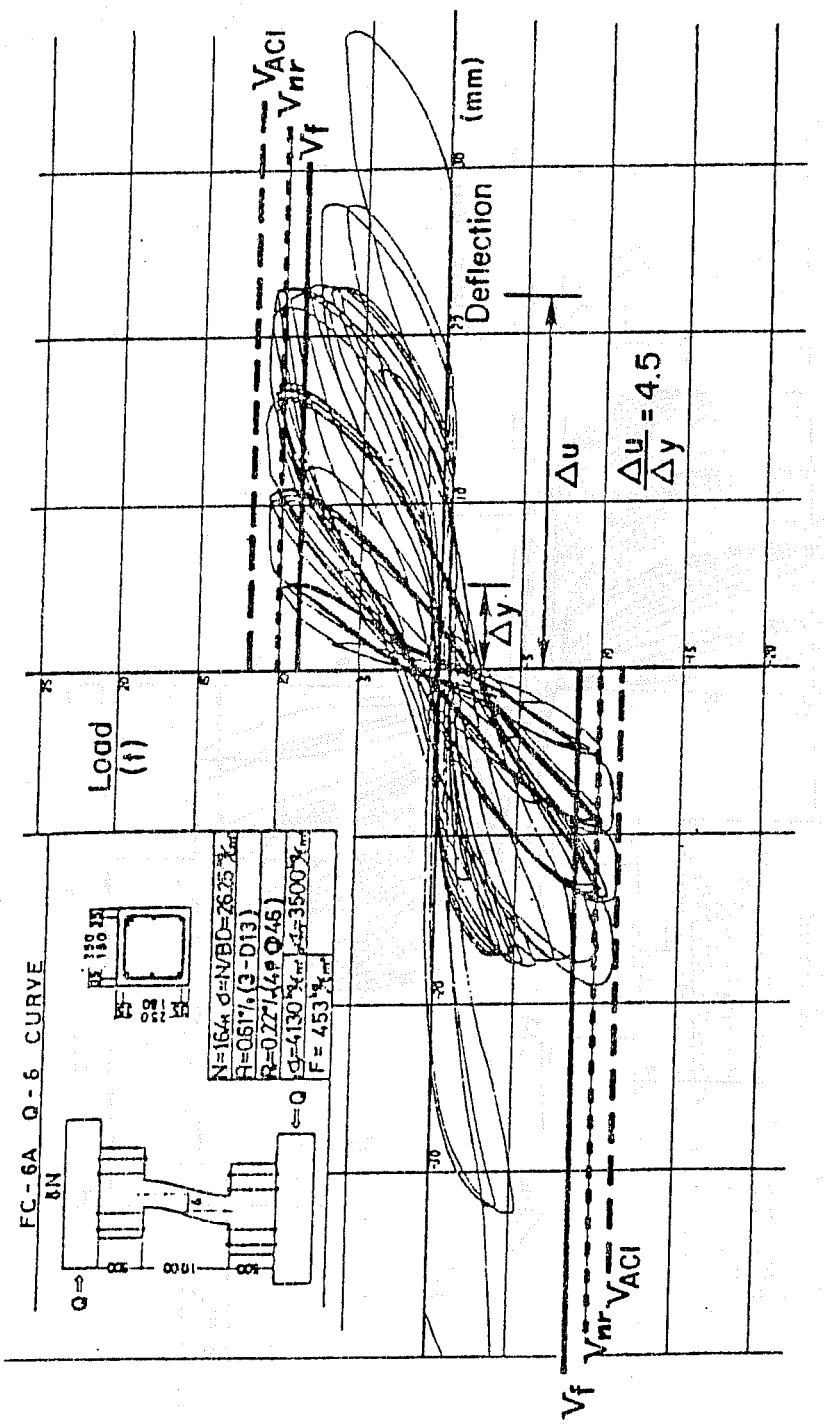

Fig. 8.3 Flexural behavior

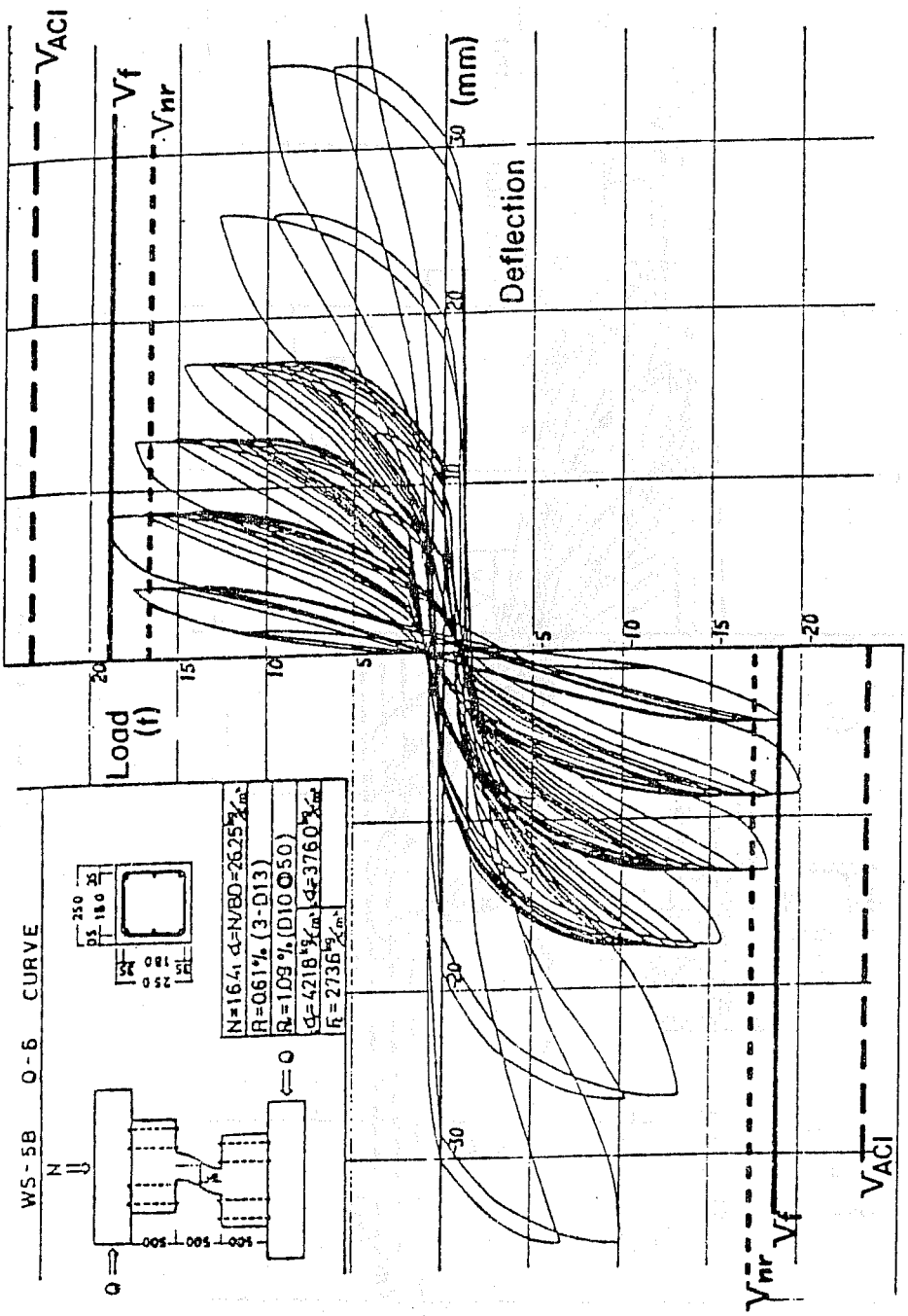

Fig. 8.4 Shear deterioration

Whenever V_{nr} was less than V_f, the observed behavior was shear degrading (sixty-seven of the eighty-one columns). In fourteen columns the observed response was flexural, however, V_{nr} was less than V_f. In no case did a specimen exhibit a shear mode when V_{nr} exceeded V_f. The results show that had the short columns been proportioned so that V_{nr} was greater than V_f, it is likely that the behavior would have been dominated by flexure.

Although the proposed equation does not include the effect of the transverse reinforcement, there are valid reasons for including some minimum transverse reinforcement in the column. First, the transverse reinforcement does carry a part of the shear force even if it is not included and, therefore, increases the margin against failure. In addition, transverse reinforcement helps confine the core and maintain the flexural capacity of column hinging regions, when flexural ductility is required. In Sec. 6.5 it was observed that increased amounts of transverse reinforcement did not improve the rate of deterioration after the maximum load was reached, but did improve the ability of the specimen to withstand large deformations.

To meet these requirements, it is recommended that in the design of short columns the minimum diameter and the maximum spacing of transverse reinforcement should be specified. It is reasonable to require that at least #3 bars at a maximum spacing of $d^*/4$ should be required. Such a requirement is nearly identical to that in Appendix A of the ACI Building Code.[25] When large cross sections are chosen for a short column, a minimum amount of transverse reinforcement may be necessary. In the thirty specimens tested in Japan in which V_{nr} was greater than V_f and whose behavior was dominated by flexure, the amount of transverse reinforcement varied widely. The range of $A_v f_{ys} d^*/s_h$ was from 0.12 V_{nr} to 2.8V_{nr}. Therefore, it may be reasonable to require that the transverse reinforcement meet the following requirement:

$$\frac{A_v f_{ys} d^*}{s_h} = 0.12 V_{nr} \tag{8.7}$$

In terms of a ratio of transverse reinforcement, ρ_h the minimum becomes

$$\rho_h \geq \frac{0.12 V_{nr}}{b d^* f_y} \tag{8.8}$$

where

$$\rho_h = \frac{A_v}{b s_h}$$

8.4 Procedure to Control the Performance

Figure 8.5 shows a flow chart of the proposed procedure to control the performance for short columns with $1 \leq a/d^* \leq 2.5$ using the equation V_{nr} (Eq. (8.6)). First, factored external shear to the frame is estimated and external shear to each column V_u is calculated using any appropriate analytical techniques. Second, the column cross section is selected and nominal flexural capacity $V_f = M_n/a$ is calculated. Third, the values of V_u and φV_f (φ is the strength reduction factor for flexure) are compared. If φV_f is less than V_u, the cross section must be revised, and V_f is calculated for the revised section. When φV_f is greater than V_u, the nominal shear capacity based on the proposed equation V_{nr} can be calculated. Fourth, both the values of V_f and V_{nr} and the values of φV_{nr} (φ is the strength reduction factor for shear) and V_u are compared. If V_f is less than V_{nr} and V_u is less than φV_{nr}, the transverse reinforcement is detailed to satisfy minimum requirements. Otherwise, the cross section must be revised.

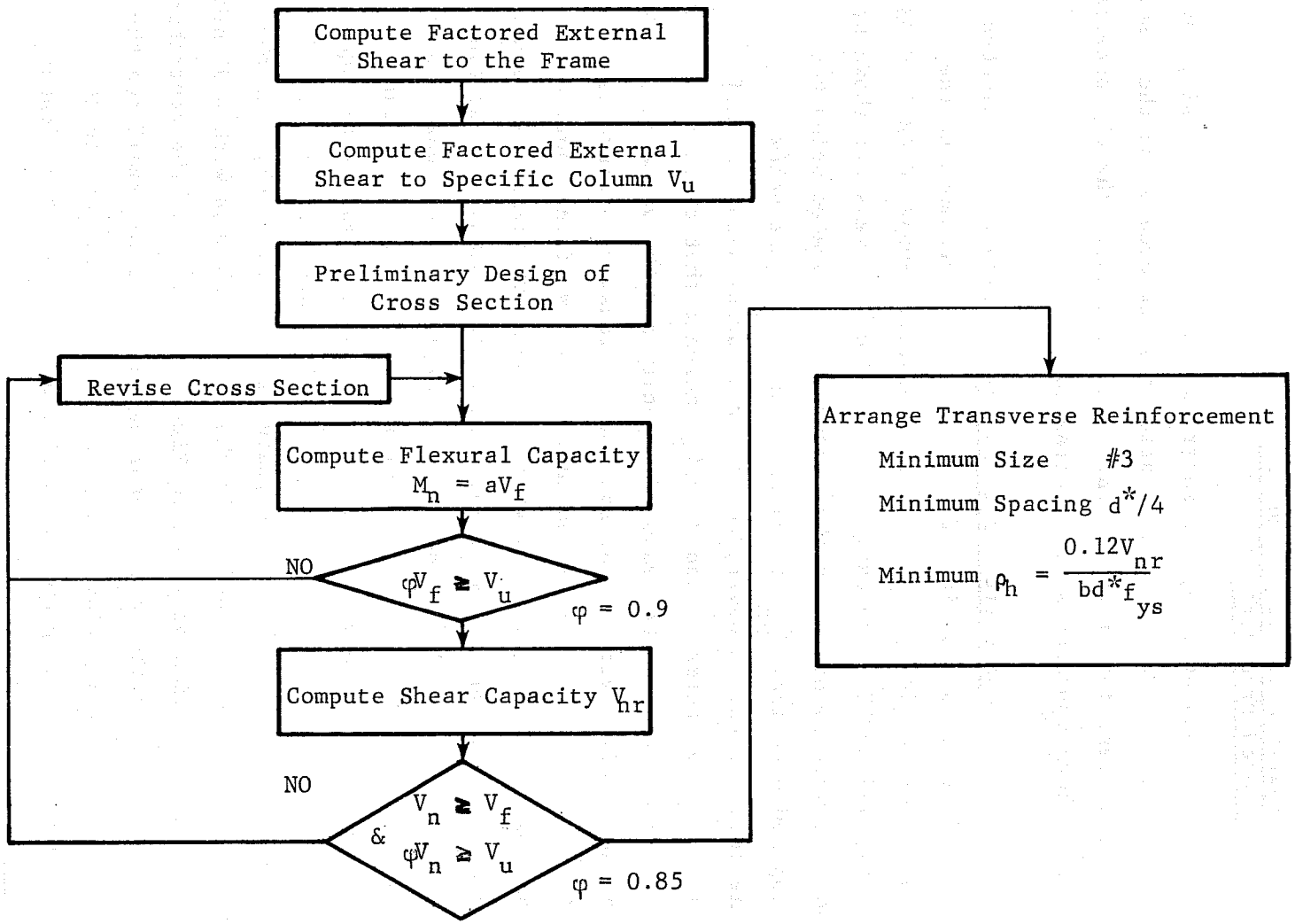

Fig. 8.5 Flow chart of proposed procedure ($1 \leq a/d^* \leq 2.5$)

8.5 Comparison of ACI Design and Proposed Procedure

In this section, the shear capacity calculated using the ACI method and the proposed equation are compared using the results of the current investigation and Japanese tests. The characteristics of both approaches are contrasted.

8.5.1 University of Texas Tests. Figure 8.1 indicates the effect of the spacing of transverse reinforcement to the shear capacity in the square short columns, C-DB32, C-DB21, C-DB, C-DB9, and C-DB3. The data of these five specimens are shown by solid square points. The shear capacity calculated using the proposed equation, V_{nr}, is shown by the line just below the test values. However, the shear capacity using the ACI Building Code terms V_c and $V_c + V_s$ indicate that there is a large difference between the measured capacity and the value of $V_c + V_s$ in the specimen with 12 in. spacing of transverse reinforcement. It is clear that the measured shear capacity of the short column does not vary significantly with the amount of transverse reinforcement. The ACI equations do not reflect this behavior, but the proposed equation indicates a fairly high constant shear capacity with increase in transverse reinforcement. Figures 8.6 through 8.9 (repeated from Chapter 6) are interaction diagrams for the square and rectangular columns. All figures indicate that the proposed equation provides a better estimate of the shear capacities than the ACI equations. However, in the case of columns with a/d^* near 2.5 (east direction strength in Figs. 8.8 and 8.9), the contribution of the concrete to the shear capacity becomes small and the proposed equation yields nearly the same capacity as the ACI equation. The beam geometry is approaching that of a slender beam.

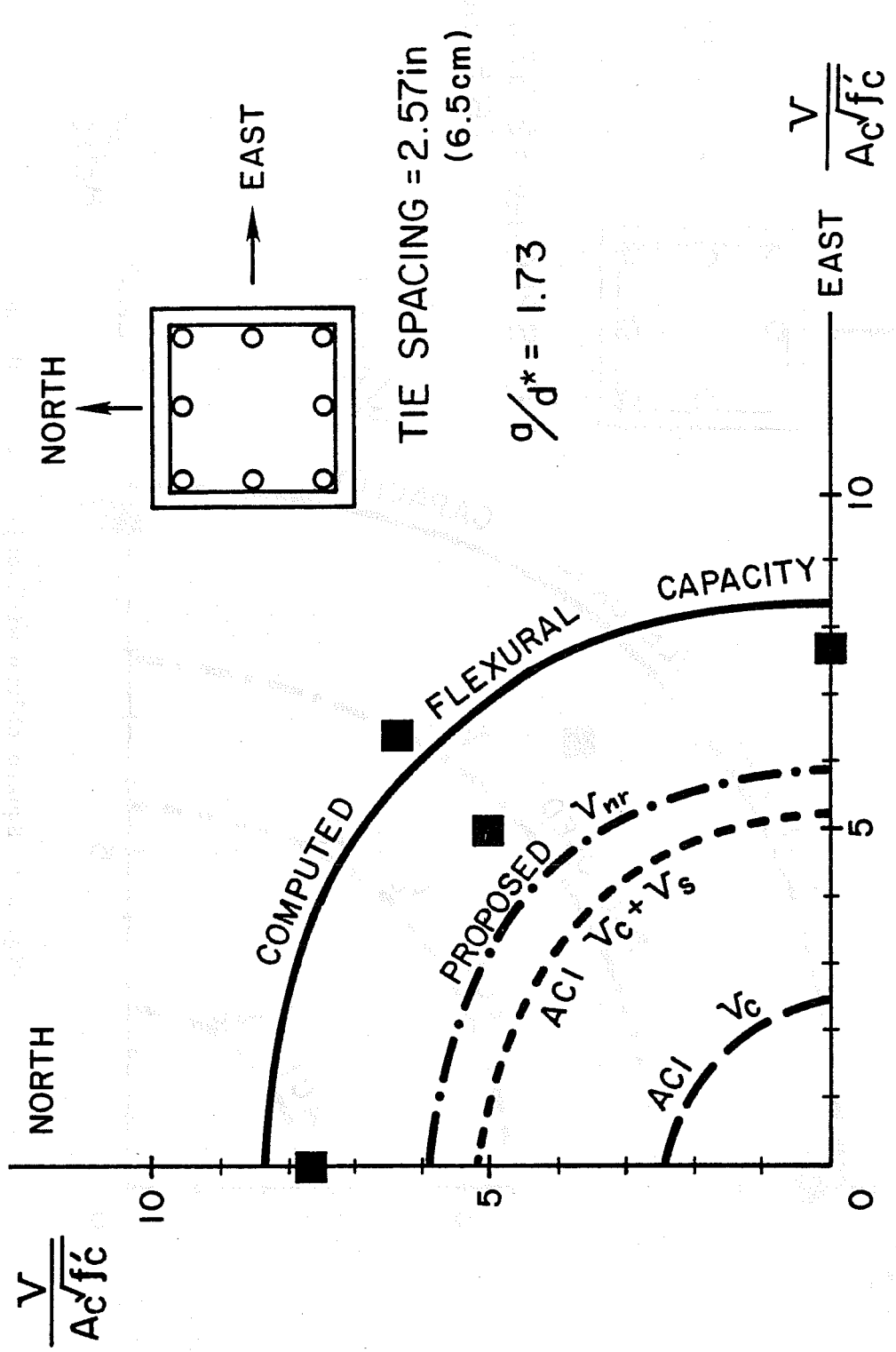

Fig. 8.6 Square column without axial load

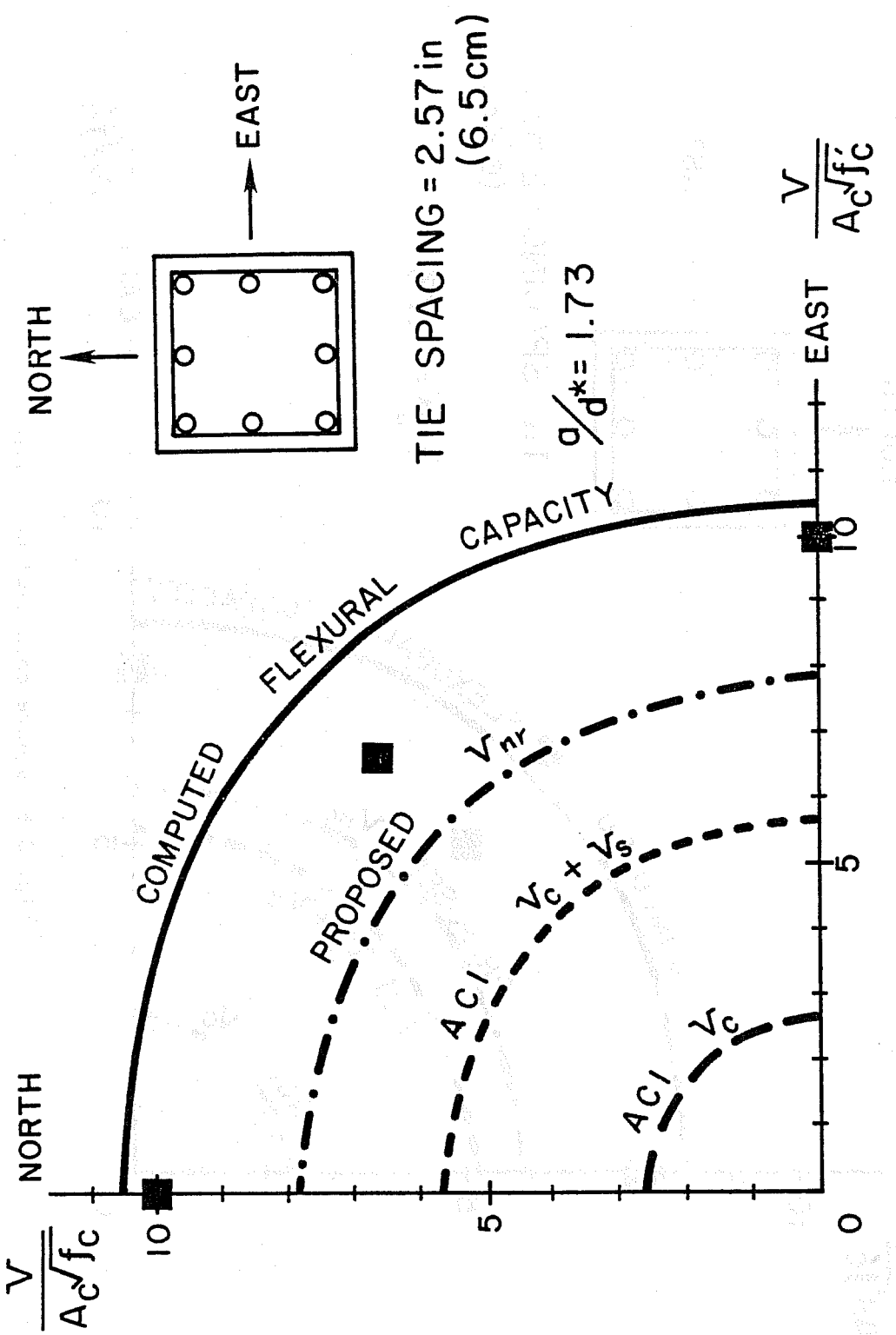

Fig. 8.7 Square column with axial load (120 kips)

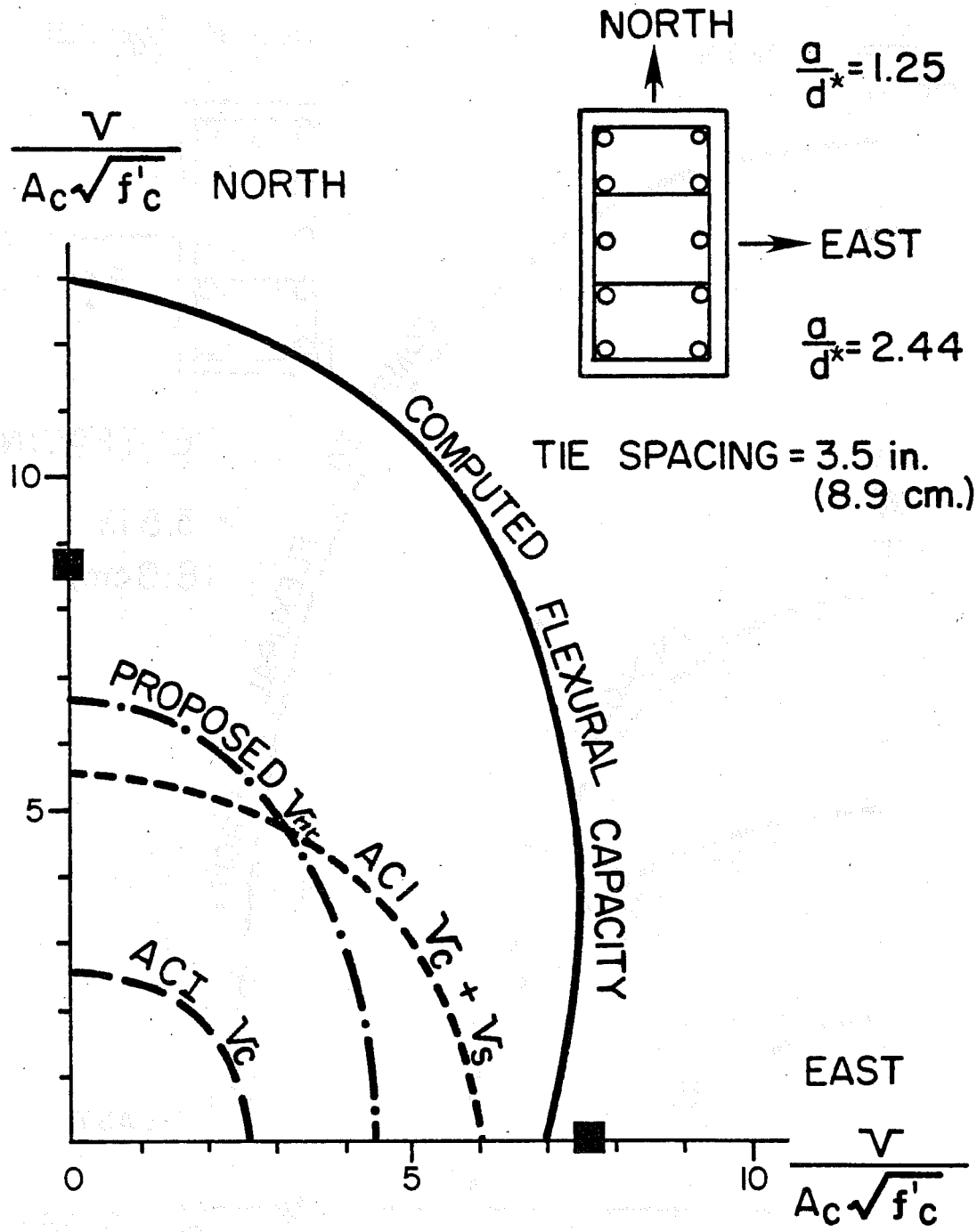

Fig. 8.8 Rectangular column without axial load

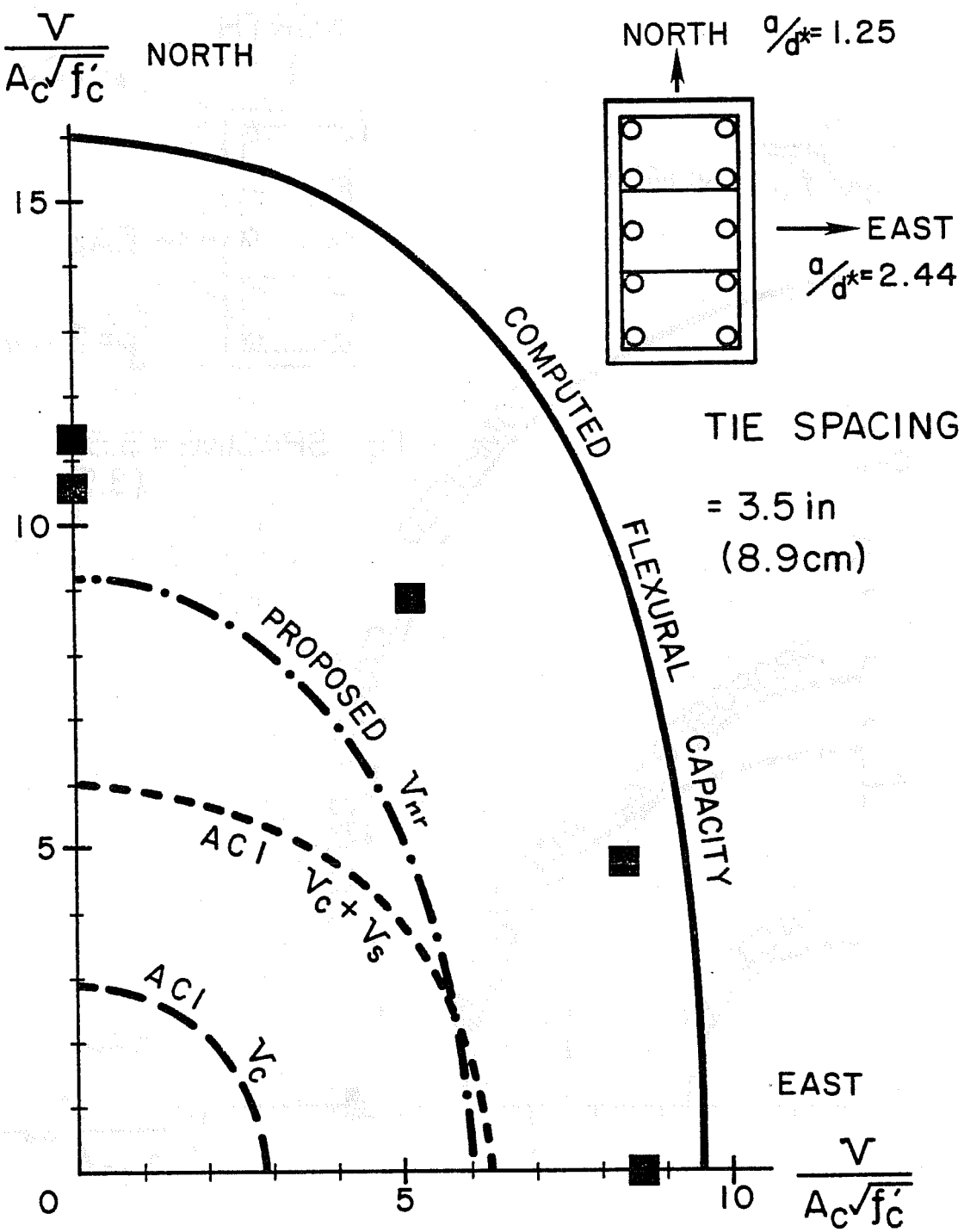

Fig. 8.9 Rectangular column with axial load (120 kips)

8.5.2 Japanese Tests. In Table 8.2 measured maximum capacities were compared with calculated values of shear and flexure for one-hundred eleven short columns tested in Japan. Seventy-four specimens meet ACI Building Code requirements for size and spacing of transverse reinforcement and the calculated flexure is greater than the shear capacity using ACI procedures. However, of the seventy-four specimens, forty-five specimens failed in a shear degrading made after reaching maximum load. Figure 8.4 showed an example of a specimen exhibiting shear deterioration even though it met all ACI Building Code requirements. However, using the proposed equation, in all cases in which the calculated shear capacity was greater than calculated flexural capacity, the behavior of the column was governed by flexure (Fig. 8.3).

8.5.3 A Comparison of ACI and Proposed Procedure. The proposed procedure appears to ensure better performance than ACI design requirements. Figure 8.10 shows a comparison of the longitudinal reinforcement ratio (total longitudinal reinforcement divided by the area of the cross section) for the case of V_{nr} (proposed equation) $\geq V_f$ and the case of V_n(ACI) $\geq V_f$. Three levels of transverse reinforcement were used to calculate V_n. $V_n = V_c + 8\sqrt{f'_c}\, bd^*$ ($V_c = 2(1 + 0.0005N/A_g)\sqrt{f'_c}\, bd^*$) indicates the maximum value of V_n, and $V_n = V_c + 50bd^*$ indicates the minimum. $V_n = V_c + 4\sqrt{f'_c}\, bd^*$ is chosen at the mid-range of transverse reinforcement. To determine the limits of ρ_g for which the $V_{nr} \geq V_f$ or the $V_n \geq V_f$ criterion will be met, the flexural (V_f) and shear capacities (V_{nr} or V_n) were computed in terms of ρ_g, substituted into $V_{nr} \geq V_f$ or $V_n \geq V_f$, and the equation was solved for ρ_g for different a/d^* ratios. Two limiting cases were considered; $\rho^* = \rho_g/2$ and $\rho^* = \rho_g/4$. In most cases the ratio of longitudinal reinforcement in the extreme tension zone will range from a maximum of $\rho_g/2$ to a minimum $\rho_g/4$ as shown in Fig. 8.10. Assuming a square column with $f'_c = 5$ ksi, $f_y = 60$ ksi and axial compressive stress

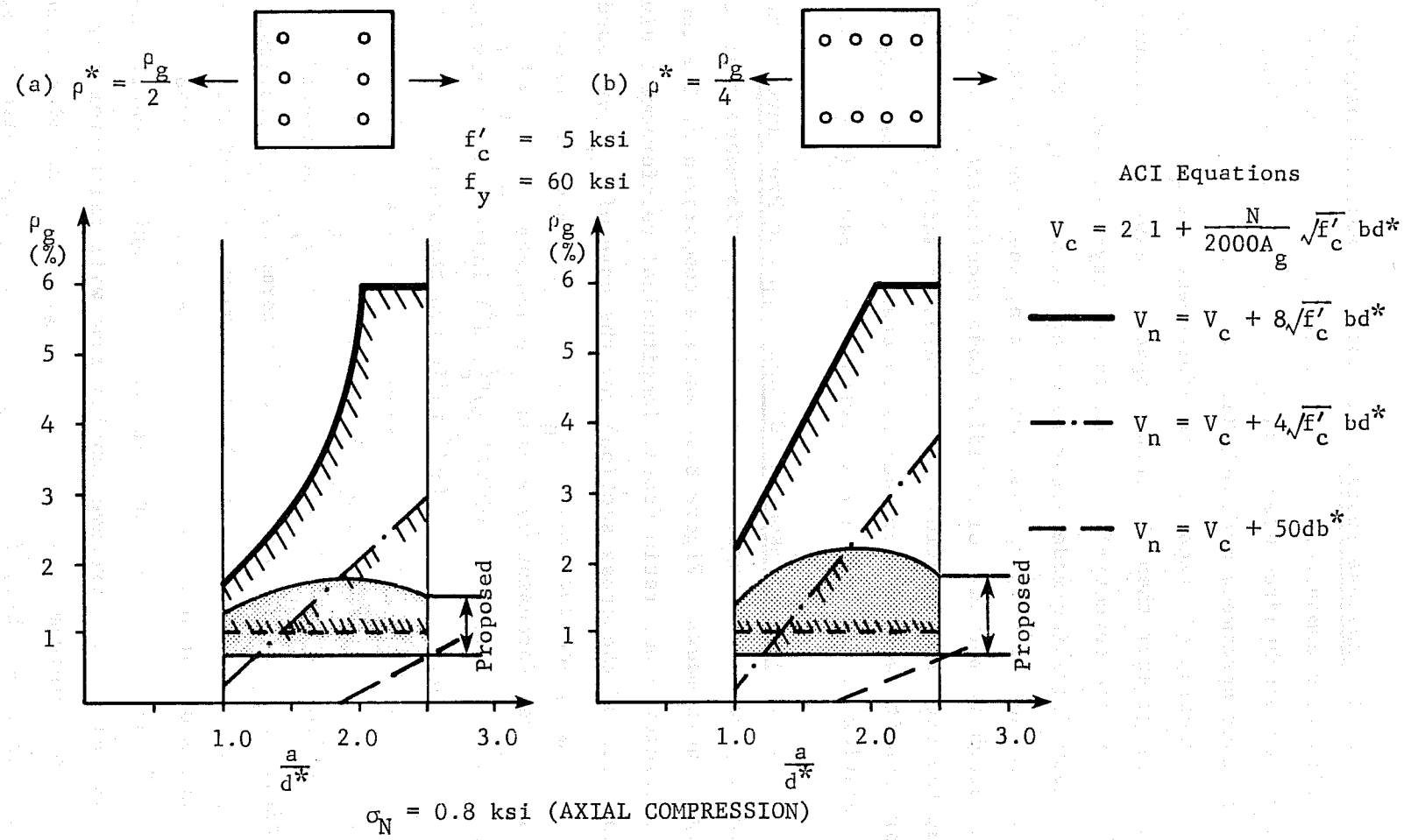

Fig. 8.10 Characteristics of ACI and proposed procedure

σ_N = 0.8 ksi (the maximum axial load to be used in Eq. (8.6)), V_{nr}, V_n and V_f were calculated. Figure 8.10(a) ($\rho^* = \rho_g/2$) indicates that the maximum ρ_g for $V_{nr} \geq V_f$ is about 1.8 percent and Fig. 8.10(b) ($\rho^* = \rho_g/4$) indicates that it is around 2.4 percent. Minimum ρ_g is determined as $400/f_y$ which is 1.0 percent for Grade 40 and 0.67 percent for Grade 60. The minimum ρ_g is determined from Eq. (10.3) of the ACI Building Code[25] by setting $\rho_g/2 = 200/f_y$. In the case of V_n, Figs. 8.10(a) and (b) show that it is impossible to design short columns using high longitudinal reinforcement ratio with decreasing a/d^* ratio. Some short columns which satisfied the relation $V_n \geq V_f$ and did not satisfy the relation $V_{nr} \geq V_f$ (the region between the line $V_n = V_c + 8\sqrt{f'_c}\, bd^*$ and V_{nr}) may exhibit shear deterioration. For a given a/d^* ratio, columns with ρ_g falling within the shaded zone ($V_{nr} \geq V_f$) would be expected to perform satisfactorily with regard to shear deterioration and the ability to dissipate energy.

It is interesting to note that using the ACI Code for short columns, a designer could choose a small cross section with substantial amounts of longitudinal and transverse reinforcement. Short columns proportioned by the proposed method would tend to have large cross sections, fairly small areas of longitudinal reinforcement and transverse reinforcement governed by minimum requirements.

The ACI Code does not specifically refer to short columns subjected to cyclic reversed loading. The proposed procedure was very effective in evaluating the Japanese data on short columns under unidirectional reversed loading. Therefore, the procedure can be considered acceptable for the short column under static and unidirectional reversed loading. Although there are not sufficient data to verify the procedure for short columns under any pattern of bidirectional reversed loading, it is likely that the procedure will provide sections that perform in a satisfactory

manner. Some tests indicate that large deformations in one direction may be detrimental to the response in the other direction. However, the proposed procedure may be applied to bidirectional loading with much greater confidence than existing ACI procedures.

8.6 Summary

The proposed procedure for the shear capacity of short columns has several significant characteristics. The transverse reinforcement does not contribute directly to the shear capacity. The prime variables are the concrete strength, the a/d^* ratio and the level of axial compression. Transverse reinforcement is necessary only for maintaining the integrity (confining) of the concrete core. Using the proposed procedure, shear degradation under static and unidirectional reversed loading is avoided while columns designed using the ACI Code may exhibit severe reduction of energy dissipating capacity under load reversals.

CHAPTER 9

SUMMARY AND CONCLUSIONS

9.1 Summary of the Investigation

The objective of the study was to develop a design procedure for reinforced concrete short columns subjected to cyclic lateral deformations which would provide adequate strength and maintain that strength through cyclic reversals of deformation. An experimental investigation of a series of short columns provides a basis for evaluating various design approaches.

9.1.1 Experimental Investigation. Ten rectangular short columns were tested in the current investigation. The columns were subjected to slowly applied cyclic deformations at the upper end of the column relative to the bottom end to simulate the action of a column between stiff floors subjected to lateral deformations. Loading direction, loading history, and axial compression were the prime variables. The behavior of the rectangular columns was compared with the behavior of square columns tested earlier.

9.1.1.1 Test Specimen. The test specimen was a 2/3-scale model of a prototype column. The test specimen had a 9x16 in. rectangular section with ten #6 (19 mm) longitudinal bars, 6 mm closed stirrups at 3.5 in. (87 mm) as transverse reinforcement and 1 in. (25 mm) cover. The specimens were tested to simulate a short column between stiff floors.

9.1.1.2 Test Schedule. Four specimens were deformed in the strong direction. In three of the four, unidirectional reversed loading and zero, 120 kips, or 240 kips axial compression

were applied. Axial compression was constant throughout the test. Monotonic loading with 120 kips axial compression was imposed on the fourth test.

Two specimens with zero and 120 kips axial compression were deformed in the weak direction. One specimen had bidirectional reversed loading along both strong and weak axes. The remaining three specimens were deformed diagonally; two had unidirectional reversed loading 30^{o} from the strong axis, and 30^{o} from the weak axis, respectively. The other had bidirectional reversed loading applied 30^{o} from the strong and 30^{o} from the weak axis.

The lateral load was controlled by deformation. Three cycles of reversed deflection were applied at each deflection limit and the deflection limit was incrementally increased.

In each specimen the applied forces, lateral deformation, strain in longitudinal and transverse reinforcements and rotations of the column ends were measured. Cracks were marked at every peak deflection limit. Experimental data from square columns tested in earlier investigations at the University of Texas were used for comparison with the results for rectangular column tests.

9.1.2 Conclusion from Test Results

9.1.2.1 Crack Pattern

(1) The angle of shear cracks is often assumed at 45^{o} in design, but even if initial cracks opened at an angle of 45^{o}, the angle with respect to the column vertical axis of the shear cracks at failure was less than 45^{o} in the short columns. This phenomenon was especially noticeable as the shear span to effective depth ratio was reduced.

(2) The crack pattern under diagonal loading was similar to that under loading in the principal direction. Especially in rectangular columns the crack pattern under diagonal loading is affected primarily by the deformation in the strong direction.

9.1.2.2 Strain Distribution

(1) Along the longitudinal reinforcement, the strain gradient is greater with axial compression.

(2) The strain distributions in the longitudinal and transverse reinforcement are not affected by the loading history (unidirectional or bidirectional) until the maximum load is reached in any direction.

9.1.2.3 Deterioration

(1) Axial compressive load produced an increase in the capacities, but more rapid deterioration of strength.

(2) The maximum load in the column under bidirectional loading reached almost the same value as that under unidirectional loading. However, after the deflection at the maximum load under unidirectional loading was reached in columns under bidirectional loading, the strength began to drop in both directions.

(3) The slope of the descending part of curves indicated that there were no differences between the columns with the unidirectional and bidirectional loading.

(4) As shear span to effective depth ratio decreased, the maximum load in the column increased, but after it was reached, deterioration of strength occurred rapidly.

(5) Increased amounts of transverse reinforcement added somewhat to shear strength and improved the ability of the specimen to withstand large deformations, but did not improve the rate of deterioration after the maximum load was reached.

9.1.2.4 Lateral Load Capacity. The maximum capacities of the columns with diagonal unidirectional loading could be estimated by an interaction line (circle or ellipse) connecting the maximum capacities of the columns under unidirectional loading along the principal axis.

9.2 Evaluation of Lateral Load Capacity

Measured shear capacity was compared with calculated flexural capacity and shear capacity using the ACI 318-77 approach, formulations based on plasticity theory (Thürlimann and Nielsen), and equations proposed by Zsutty. These methods did not accurately estimate shear capacity for the following reasons: (1) In most cases, shear capacity of short columns increases after first shear cracking because of some type of arch or strut action in the concrete; (2) The loading and deflection of the short columns is not the same as that of simply supported beams on which most methods are based, but is similar to that of continuous beams; (3) Short columns for which the calculated shear capacity using existing approaches is greater than flexural capacity may exhibit loss of energy dissipating capacity. Therefore, the equation to calculate the shear strength of short columns was developed using regression analysis based on data from continuous beams with $1 \leq a/d^* \leq 2.5$ which failed in shear. Measured shear capacities were compared with calculated shear capacities based on this equation and it was shown that this equation was acceptable.

9.3 Proposed Approach

An equation to control the performance of short columns was developed by simplifying the equation derived from the data of continuous beams failing in shear. The equation has the following form:

$$V_{nr} = (11 - 3\frac{a}{d^*}) A_c\sqrt{f'_c} + \frac{0.2N}{\frac{a}{d^*}}$$

$$\frac{0.2N}{\frac{a}{d^*}} \leq \frac{160A_g}{\frac{a}{d^*}}$$

$$1 \leq \frac{a}{d^*} \leq 2.5$$

In this simplification, the contribution of the transverse reinforcement is ignored because the results of short column tests indicate that the contribution of concrete was at least 70 to 80 percent of the total shear capacity. The equation is a function of the shear span to depth ratio (a/d^*), the concrete strength (f'_c), and the level of axial compression (N). Transverse reinforcement is necessary only for confinement of the concrete core.

Short columns designed using Appendix A of the ACI Code may degrade rapidly in shear after maximum load is reached. However, short columns designed by the proposed procedure would be expected to maintain energy dissipating characteristics under static or unidirectional reversed loading. A short column loaded in any direction can be designed or evaluated by this procedure. In general, the procedure will result in columns with large concrete cross sections and low percentages of longitudinal reinforcement. Based on comparisons with all data available,

the proposed procedure represents a considerable improvement over existing ACI and other approaches for designing or evaluating the strength of short columns.

9.4 Recommendations for Future Work

The following studies are suggested for future research based on the results of the current investigation.

9.4.1 Axial Compression. The effect of much higher axial compression (more than the axial load at balanced strain condition) on the hysteretic behavior of short columns needs study. Axial compression may cause a much more severe shear deterioration of the section. Such studies may help define the limit on the contribution of axial compression in the proposed equation and provide data for a more accurate expression for the shear capacity of short columns.

9.4.2 Bidirectional Loading. There are limited data on which to verify that short columns meeting the requirements of the proposed procedure will perform satisfactorily under any bidirectional loading pattern. The proposed equation was verified using tests of columns loaded unidirectionally and further research on bidirectional loading needs to be conducted.

A P P E N D I X A

SECOND ORDER EFFECTS—AXIAL COMPRESSION

Figure A.1 shows the free body diagram of a column specimen under applied loads and also shows the related equilibrium equations. These equations were derived by Ramirez.[23] The application of lateral deformations through the loading frame causes the axial load to be inclined. Second order effects are induced which increase the applied shear with respect to that measured.

The applied shear is given by the first equilibrium equation shown in Fig. A.1. Considering that Δ_v and Δ are small compared with the dimensions of the loading frame, the following simplification can be made:

$$V_a = V + \frac{N\Delta}{66.25} \quad \text{or} \quad V_a = (1 + \frac{e_v}{100})V$$

where V is measured shear and $e_v = 1.51N\Delta/V$ represents the percent error in assuming the measured shear is equal to the total applied shear force. The simplifications assumed in the formula for V_a are satisfactory because the errors computed without the simplifications are very near those computed with the simplifications.

Table A.1 presents the computed error in the maximum capacity for rectangular columns. The maximum error is only 1.6 percent for the specimen 2CUS. It is clear that the error is not significant and no modifications in shear due to second order effects are needed.

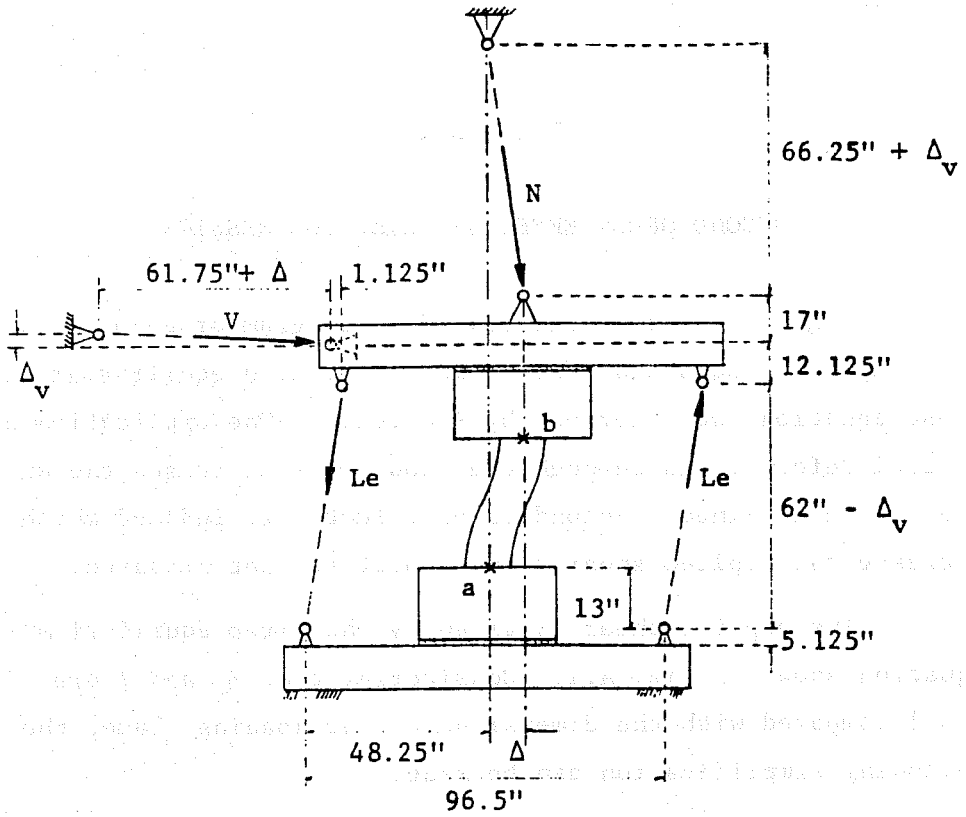

Equilibrium Equations:

$$V_a = \frac{61.75 + \Delta}{\sqrt{(61.75 + \Delta)^2 + \Delta_v^2}} V + \frac{\Delta}{\sqrt{(66.25 + \Delta_v)^2 + \Delta^2}} N$$

$$N_a = \frac{\Delta_v}{\sqrt{(61.75 + \Delta)^2 + \Delta_v^2}} V + \frac{66.25 + \Delta_v}{\sqrt{(66.25 + \Delta_v)^2 + \Delta^2}} N$$

$$M_a = \frac{(61.75 + \Delta)(61.125 - \Delta_v) - \Delta_v(49.375 - \Delta)}{\sqrt{(61.75 + \Delta)^2 + \Delta_v^2}} V +$$

$$\frac{\Delta(78.125 - \Delta_v) + (66.25 + \Delta_v)\Delta}{\sqrt{(66.25 + \Delta_v)^2 + \Delta^2}} N - \frac{(62 - \Delta_v)96.5}{\sqrt{(62 - \Delta_v)^2 + \Delta^2}} Le$$

Fig. A.1 Free body diagram of the specimen and equilibrium equations

TABLE A.1 P - Δ EFFECT

Specimen Name	N kips	V_m kips	Δ_m in.	e_v %
CMS	120	86	0.48	1.0
CUS	120	74	0.40	1.0
CUW	120	60	0.48	1.4
2CUS	240	91	0.40	1.6
CDS30	120	80	0.46	1.0
CDW30	120	74	0.37	0.9
(s) CBSW	120	69	0.40	1.1
(w)	120	52	0.32	1.1
(s) CDSW30	120	62	0.23	0.7
(w)	120	57	0.37	1.2

$$e_v = 1.51\ N\Delta_m\ /\ V_m$$

$$V'_m = (1 + e_v/100)\ V_m$$

APPENDIX B

GEOMETRY CORRECTION

The deflection measuring devices (potentiometers) monitor the movement of the specimen along the north-south, east-west, and vertical axes of the specimen. The orientation of the potentiometers does not vary during the test. The load cells, however, are attached to the rams so that they measure load along the axes of the rams. During movement to the diagonal direction in the specimen, the axes of the rams also move. Thus the load values read from the load cells are not oriented along axes coincident with the axes of deflection measurement. In order to have values of load which act along the axes of deflection measurement, the load cell readings are adjusted to account for the geometry change of the loading system. The method is simply to break the load cell reading into components along the desired axes and then sum the components in each direction to obtain the corrected value of load.

The correction equations were derived by Woodward.[24] Figure B.1 shows a coordinate system in which the original position of the specimen is shown as point O. A movement of the specimen shifts its position to point O'. The components of deflection are Δ_S along the north-south axis, Δ_E along the east-west axis, and Δ_V along the vertical axis. Figure B.2 shows the components of load for each of the load cells. The values of load as measured by load cells are denoted by N_M, H_{SM}, and H_{EM} for the axial load cell, south lateral ram load cell, and east lateral ram load cell, respectively. The components of load for each load cell are shown as well as the original length of

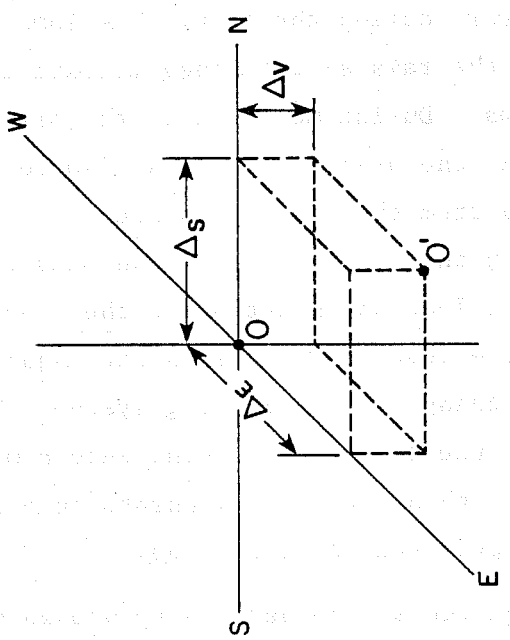

Fig. B.1 Coordinate system

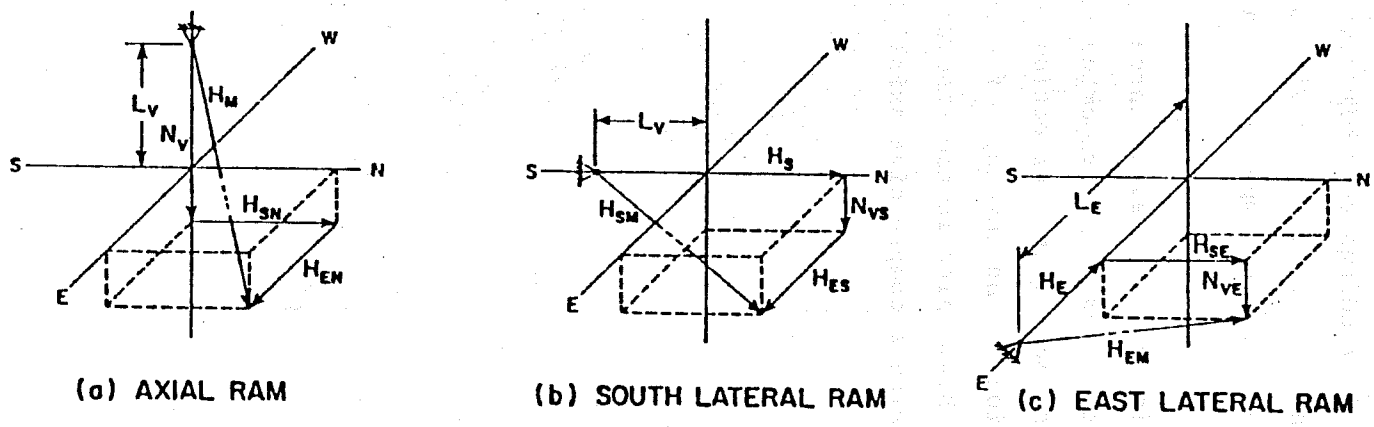

Fig. B.2 Load components

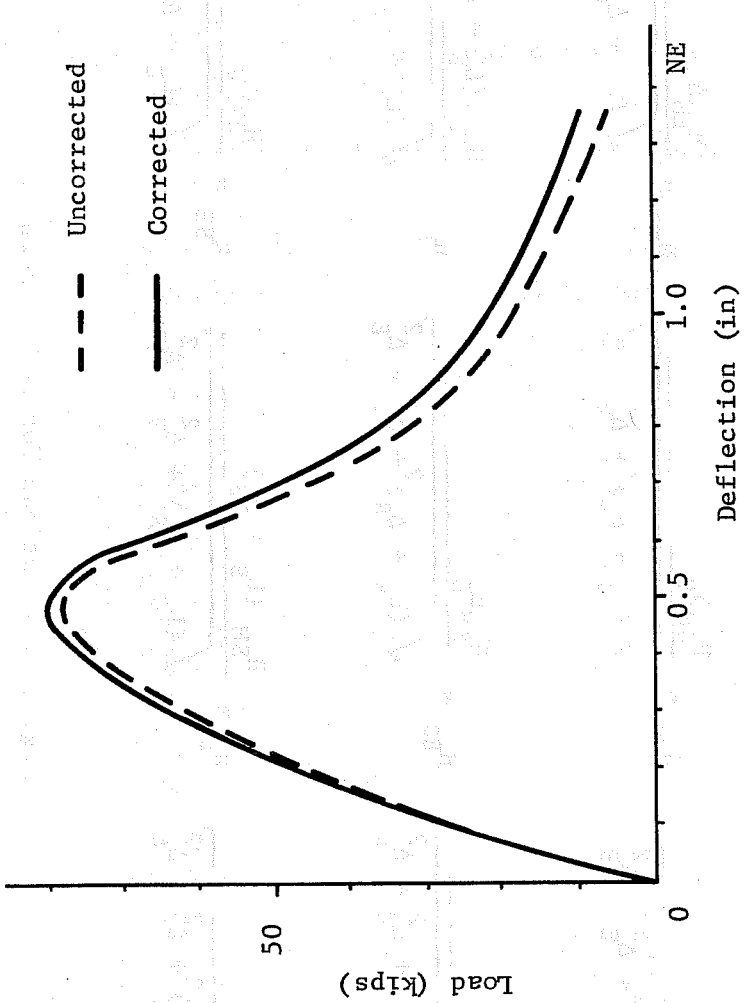

Fig. B.4 Effect of geometry correction

REFERENCES

1. Aoyama, H., et al., "A Study on the Cause of Damage to the Hachinohe Technical College due to 1968 Tokachi-Oki Earthquake (Part 1)," Proceedings of the U.S.-Japan Seminar on School Buildings, Sendai, Japan, September 1970, The Japan Earthquake Engineering Promotion Society, Tokyo, Japan, 1971, pp. 172-189.

2. Nielsen, N. N., and Nakagawa, K., "The Tokachi-Oki Earthquake, Japan, May 16, 1968: A Preliminary Report on Damage to Structures," International Institute of Seismology and Earthquake Engineering, Report No. 2, Tokyo Japan, June 1968.

3. Lew, H. S., Leyendecker, E. V., and Dikkers, R. D., "Engineering Aspects of the 1971 San Fernando Earthquake, "Building Science Series 40, National Bureau of Standards, U. S. Department of Commerce, December 1971.

4. Okada, T., et al., "Analysis of the Hachinohe Library Damage by 1968 Tokachi-Oki Earthquake," Proceedings, U.S.-Japan Seminar on Earthquake Engineering with Emphasis on Safety of School Buildings, Sendai, Japan, September 1970, pp. 172-189.

5. Selna, L. G., Morrill, K. B., and Ersoy, O. K., "Shear Collapse, Elastic and Inelastic Biaxial Studies of the Olive View Hospital Psychiatric Day Clinic," Proceedings, U.S.-Japan Seminar on Earthquake Engineering, Berkeley, 1973.

6. Mahin, S. A., Bertero, V. V., Chopra, A. K., Collins, R. G., "Response of the Olive View Hospital Main Building During the San Fernando Earthquake," Report No. EERC76-22, Earthquake Engineering Research Center, University of California, Berkeley, October 1976.

7. Aoyama, H., et al., "A Study on the Earthquake Resistant Design of Reinforced Concrete School Building," Proceedings of the U.S.-Japan Seminar on Earthquake Engineering with Emphasis on the Safety of Reinforced Concrete Structures, Berkeley, California, September 1973.

8. Sozen, M. A., et al., "Engineering Report on the Managua Earthquake of 23 December 1972," prepared for the Committee on Natural Disasters, National Academy of Sciences, Washington, D.C. 1975.

9. Anicic, D., et al., "Reconnaissance Report: Montenegro, Yugoslavia Earthquake April 15, 1979," Earthquake Engineering Research Institute, November 1980.

10. Blume, J. A., et al., "Reconnaissance Report: Miyagi-ken-Oki, Japan Earthquake, June 12, 1978," Earthquake Engineering Research Institute, December 1978.

11. Park, R., and Paulay, T., Reinforced Concrete Structures, John Wiley and Sons, New York, 1975, pp. 254-258.

12. Aktan, A. E., and Pecknold, D. A., "Response of a Reinforced Concrete Section to Two-Dimentional Curvature Histories," ACI Journal, Proceedings, V. 71, No. 4, May 1974, pp. 246-250.

13. Aktan, A. E., Pecknold, D. A., and Sozen, M. A., "Effect of Two-Dimensional Earthquake Motion on a Reinforced Concrete Column," Structural Research Series No. 399, Civil Engineering Studies, University of Illinois at Urbana, May 1973.

14. Takizawa, H., and Aoyama, H., "Biaxial Effects in Modeling Earthquake Response of R/C Structures," Earthquake Engineering and Structural Dynamics, Vol. 4, 1976, pp. 523-552.

15. Takizawa, H., "Biaxial and Gravity Effects in Modeling Strong-Motion Response of R/C Structures," Proceedings, Sixth World Conference on Earthquake Engineering, New Delhi, 1977, Paper No. 3-9, pp. 49-54.

16. Takiguchi, K., et al., "Response of R/C Column to Horizontal Bidirectional Deflection History," Proceedings, Seventh World Conference on Earthquake Engineering, Ankara, Turkey, 1980, Vol. 6, pp. 525-532.

17. Kokusho, S., Takiguchi, K., Kobayashi, K., "Analysis of Reinforced Concrete Sections under Biaxial Bending Moment," Transaction of the Japan Concrete Institute, Vol. 2, 1980, pp. 343-350.

18. Okada, T., and Seki, M., "A Simulation of Earthquake Response of R/C Buildings," Proceedings, Sixth World Conference on Earthquake Engineering, New Delhi, 1977, Vol. 9, pp. 25-30.

19. ACI-ASCE Committee 426, "The Shear Strength of Reinforced Concrete Members," Journal of the Structural Division, ASCE, Vol. 99, No. ST6, Proc. Paper 9791, June 1973, pp. 1091-1187.

20. A List of Experimental Results on Deformation Ability of Reinforced Concrete Columns under Large Deflection (No. 3) (in Japanese), Building Research Institute, Ministry of Construction, Japan, February 1978.

21. The Establishment of Detailing Practice for Current Building Design in Japan--Papers about the Ductility of Reinforced Concrete Columns under Large Deflections (in Japanese), Building Research Institute, Ministry of Construction, Japan, March 1974.

22. Maruyama, K., and Jirsa, J. O., "Shear Behavior of Reinforced Concrete Members under Bidirectional Reversed Lateral Loading," CESRL Report No. 79-1, The University of Texas at Austin, August 1979.

23. Ramirez, H., and Jirsa, J. O., "Effect of Axial Load on Shear Behavior of Short RC Columns under Cyclic Lateral Deformations," PMFSEL Report No. 80-1, The University of Texas at Austin, June 1980.

24. Woodward, K. A., and Jirsa, J. O., "Behavior Classification of Short Reinforced Concrete Columns Subjected to Cyclic Deformations," PMFSEL Report No. 80-2, The University of Texas at Austin, July 1980.

25. ACI Committee 318, Building Code Requirements for Reinforced Concrete (ACI 318-77) American Concrete Institute, Detroit, 1977.

26. Kent, D., and Park, R., "Flexural Members with Confined Concrete," Journal of the Structural Division, ASCE, Vol. 97, No. ST7, July 1971, pp. 1969-1990.

27. Thürlimann, B., and Grob, J., "Ultimate Strength and Design of Reinforced Concrete Beams under Bending and Shear," Publication, IABSE, Vol. 36-II, pp. 105-120, 1976.

28. Thürlimann, B., "Plastic Analysis of Reinforced Concrete Beams," Introductory Report of IABSE Colloquium, Kopenhagan 1979, Plasticity in Reinforced Concrete, 1979, pp. 71-90.

29. Thürlimann, B., "Shear Strength of Reinforced and Prestressed Concrete Beams--CEB Approach," ACI Symposium, 1976, Philadelphia.

30. Nielsen, M. P., Braestrup, M. W., "Plastic Shear Strength of Reinforced Concrete Beams," Structural Research Laboratory Technical University of Denmark, Report No. R73, 1976, translated from Byginingsstatiske Meddelelser, Vol. 46, No. 3, September 1975, pp. 61-99.

31. Nielsen, M. P., Braestrup, M. W., and Bach, F., "Rational Analysis of Shear in Reinforced Concrete Beams," IABSE Periodical, No. 2, May 1978, IABSE Proceedings P-15/78.

32. Nielsen, M. P., and Braestrup, M. W., "Shear Strength of Prestressed Concrete Beams without Web Reinforcement," Magazine of Concrete Research, Vol. 30, No. 104, September 1978, pp. 119-128.

33. Zsutty, T., "Beam Shear Strength Prediction by Analysis of Existing Data," Journal of the American Concrete Institute, Proc. V. 65, No. 11, November 1968, pp. 943-951.

34. Zsutty, T., "Shear Strength Prediction for Separate Categories of Simple Beam Tests," Journal of the American Concrete Institute, Proc. V. 68, No. 2, February 1971, pp. 138-143.

35. Statistical Computer Program for Stepwise Multiple Regression, Center for Highway Research, The University of Texas at Austin, October 1968.

36. Moody, K. G., Viest, I. M., Elstner, R. C., and Hognestad, E., "Shear Strength of Reinforced Concrete Beams. Parts 1 and 2," Journal of the American Concrete Institute, Proc. V. 51, No. 4, December 1954, pp. 317-332; No. 5, January 1955, pp. 417-434.

37. Morrow, J., and Viest, I. M., "Shear Strength of Reinforced Concrete Frame Members without Web Reinforcement," Journal of the American Concrete Institute, Proc. V. 53, No. 9, March 1957, pp. 833-869.

38. Baldwin, Jr., J. W., and Viest, I. M., "Effect of Axial Compression on Shear Strength of Reinforced Concrete Frame Members," Journal of the American Concrete Institute, Proc. V. 55, No. 5, November 1958, pp. 635-654.

39. Diaz de Cossio, and Siess, C. P., "Behavior and Strength in Shear of Beams and Frames without Web Reinforcement," Journal of the American Concrete Institute, Proc. V. 56, No. 8, February 1960, pp. 695-735.

40. Bower, J. E., and Viest, I. M., "Shear Strength of Restrained Concrete Beams without Web Reinforcement," Journal of the American Concrete Institute, Proc. V. 57, No. 1, July 1960, pp. 73-98.

41. Rodriguez, J. J., Bianchini, A. C., Viest, I. M., and Kesler, C. E., "Shear Strength of Two-Span Continuous Reinforced Concrete Beams," Journal of the American Concrete Institute, Proc. V. 55, No. 10, April 1959, pp. 1089-1130.

42. Watstein, D., and Mathey, R. G., "Strains in Beams Having Diagonal Cracks," Journal of the American Concrete Institute, Proc. V. 55, No. 6, December 1958, pp. 717-728.

43. Chang, T. S., and Kesler, C. E., "Static and Fatigue Strength in Shear of Beams with Tensile Reinforcement," Journal of the American Concrete Institute, Proc. V. 29, No. 12, June 1958, pp. 1033-1057.

44. Taub, J., and Neville, A. M., "Resistance to Shear of Reinforced Concrete Beams, Part 1, Beams without Vertical Stirrups," Journal of the American Concrete Institute, Proc. V. 32, No. 2, August 1960, pp. 193-220.

45. Krefeld, W. J., and Thurston, C. W., "Studies of the Shear and Diagonal Tension Strength of Simply Supported Reinforced Concrete Beams," Journal of the American Concrete Institute, Proc. V. 63, No. 4, April 1966, pp. 451-476.

46. Mathey, R. G., and Watstein, D., "Shear Strength of Beams without Reinforcement Containing Deformed Bars of Different Yield Strength," Journal of the American Concrete Institute, Proc. V. 60, No. 2, February 1963, pp. 183-208.

47. Acharya, D. N., and Kemp, K. O., "Significance of Dowel Forces on the Shear Failure of Rectangular Reinforced Concrete Beams without Web Reinforcement," Journal of the American Concrete Institute, Proc. V. 62, No. 10, October 1965, pp. 1265-1280.

48. Guralnick, S. A., "High Strength Deformed Steel Bars for Concrete Reinforcement," Journal of the American Concrete Institute, Proc. V. 57, No. 3, September 1960, pp. 241-282.

49. Moretto, O., "An Investigation of the Strength of Welded Stirrups in Reinforced Concrete Beams," Journal of the American Concrete Institute, Proc. V. 17, No. 2, November 1945, pp. 141-162.

50. Clark, A. P., "Diagonal Tension in Reinforced Concrete Beams," Journal of the American Concrete Institute, Proc. V. 23, No. 2, October 1951, pp. 145-156.

51. DePaiva, Rawdon, and Siess, C. P., "Strength and Behavior of Deep Beams in Shear," Journal of the Structural Division, ASCE, Vol. 91, No. ST5, October 1965, pp. 19-41.

52. Hedman, O., and Losberg, A., "Design of Concrete Structures with Regard to Shear Forces," CEB Bulletin D'Information No. 126, June 1978, pp. 183-209.

53. SEAOC, "Recommended Lateral Force Requirements and Commentary," Seismology Committee, Structural Engineers Association of California, San Francisco, 1973, pp. 146.

54. Collins, M. P., and Mitchell, D., "Shear and Torsion Design of Prestressed and Non-Prestressed Concrete Beams," Journal of the Prestressed Concrete Institute, Vol. 25, No. 5, Sept./Oct. 1980, pp. 32-100.